UNIVERSIDAD COMPLUTENSE DE MADRID
FACULTAD DE FARMACIA

TESIS DOCTORAL

Lipoxidación de vimentina y su interacción con zinc

Lipoxidation of vimentin and its interplay with zinc

MEMORIA PARA OPTAR AL GRADO DE DOCTOR

PRESENTADA POR

Andreia Marina de Oliveira Mónico

Directora

María Dolores Pérez-Sala Gozalo

Madrid

UNIVERSIDAD COMPLUTENSE DE MADRID

FACULTAD DE FARMACIA

Departamento de Bioquímica y Biología Molecular

TESIS DOCTORAL

Lipoxidación de vimentina y su interacción con zinc

Lipoxidation of vimentin and its interplay with zinc

MEMORIA PARA OPTAR AL GRADO DE DOCTOR

PRESENTADA POR

ANDREIA MARINA DE OLIVEIRA MÓNICO

Directora

María Dolores Pérez-Sala Gozalo

Madrid, 2019

UNIVERSIDAD COMPLUTENSE DE MADRID

CENTRO DE INVESTIGACIONES BIOLÓGICAS (CSIC)

Lipoxidación de vimentina y su interacción con zinc

Lipoxidation of vimentin and its interplay with zinc

By

Andreia Marina de Oliveira Mónico

A thesis

in Biochemistry, Molecular Biology and Biomedicine

Submitted to

Universidad Complutense de Madrid

in fulfillment of the requirements for the degree of

Doctor in Philosophy

Tutor

Mª Dolores Pérez-Sala Gozalo

Centro de Investigaciones Biológicas, CSIC

Madrid, 2019

UNIVERSIDAD COMPLUTENSE MADRID

DECLARACIÓN DE AUTORÍA Y ORIGINALIDAD DE LA TESIS PRESENTADA PARA OBTENER EL TÍTULO DE DOCTOR

D./Dña. Andreia Marina de Oliveira Mónico,
estudiante en el Programa de Doctorado Bioquímica, Biología Molecular y Biomedicina,
de la Facultad de Farmacia de la Universidad Complutense de Madrid, como autor/a de la tesis presentada para la obtención del título de Doctor y titulada:

Lipoxidación de vimentina y su interacción con zinc. Lipoxidation of vimentin and its interplay with zinc

y dirigida por: María Dolores Pérez-Sala Gozalo

DECLARO QUE:

La tesis es una obra original que no infringe los derechos de propiedad intelectual ni los derechos de propiedad industrial u otros, de acuerdo con el ordenamiento jurídico vigente, en particular, la Ley de Propiedad Intelectual (R.D. legislativo 1/1996, de 12 de abril, por el que se aprueba el texto refundido de la Ley de Propiedad Intelectual, modificado por la Ley 2/2019, de 1 de marzo, regularizando, aclarando y armonizando las disposiciones legales vigentes sobre la materia), en particular, las disposiciones referidas al derecho de cita.

Del mismo modo, asumo frente a la Universidad cualquier responsabilidad que pudiera derivarse de la autoría o falta de originalidad del contenido de la tesis presentada de conformidad con el ordenamiento jurídico vigente.

En Madrid, a 27 de agosto de 2019

Fdo.: Andreia Mónico

Esta DECLARACIÓN DE AUTORÍA Y ORIGINALIDAD debe ser insertada en la primera página de la tesis presentada para la obtención del título de Doctor.

ACKNOWLEDGEMENTS

This work was supported by the European Union's Horizon 2020 research and innovation program under the Marie Sklodowska-Curie Grant agreement no 675132 “Masstrplan”. Funding from MINECO/FEDER within the framework of grant SAF2015-68590-R, from MCIU/AEI/FEDER, UE, grant RTI2018-097624-B-I00 and from Instituto de Salud Carlos III/FEDER, RETIC Aradyal RD16/0006/0021 is also acknowledged. Feedback from COST Action CA15214 “EuroCellNet” is gratefully acknowledged.

The most special thanks go to Dr. Dolores Pérez-Sala. Your immense knowledge and enthusiasm for science as well as your infinite patience will always be an inspiration. Thank you for your endless support and kindness. I could not have imagined having a better advisor and mentor for my PhD studies.

I would also like to thank Dr. María Pajares for sharing with me your keenness for science. Thank you for all the good conversations that help me to improve as a researcher and as a person. Thanks to María Jesús Carrasco for your constant help and for your supporting words.

I would especially like to thank all my colleagues at the lab for your help and for all the good moments. In particular, I would like to thank Sofia for being my partner and for listening, understanding and supporting me in all the moments throughout these three years. One of the best things that I have won during my PhD was definitely you as a friend. Thanks to Álvaro for teaching me and for your ceaseless assistance. Your joy is contagious and has turned my PhD life much easier and fun.

My sincere thanks also go to Prof. Germán Rivas and to Dr. Silvia Zorrilla for their guidance and encouragement. I wish to thank to Prof. F. Javier Cañada and to Dr. Sonsoles Martín Santamaría for the important collaborations that allowed improving the outcome of my research project.

Special thanks are given to the Masstrplan network, to all the fantastic and brilliant people that I had the chance to meet and for all the remarkable opportunities given to me. In particular, I would like to thank Prof. Corinne Spickett, for being an enthusiastic coordinator, and to Debbie Toomeoks, who managed exceptionally the Masstrplan project details. Additionally, I would like to thank to Dr. Maria Fedorova, Prof. Rosário Domingues and Prof. Giancarlo Aldini, who provided me an opportunity to join their lab groups, as part of my secondments, and who supported me to conduct my research.

The help of many people at the Centro de Investigaciones Biológicas (CIB) is gratefully appreciated, specifically that of Maite Seisdedos and Gema Elvira at the confocal imaging. I am indebted to Dr. Rafael Núñez, Dr. Begoña Pou and Dr. Fernando Escolar for valuable help with electron microscopy.

I would like to thank the most important people in my life, my parents. Thank you mother for being an amazing and strong woman, for taking care of all difficulties and turn them into lessons, for teaching me to never give up and to always see the brightness in every situation. Thank you father for being the greatest example of resilience and for your endless love and kindness. Thank both you for your infinite support, and I hope to make you proud as you make me.

I would like to specially thank Tiago for being by my side throughout this PhD. You always know to choose the perfect words to calm me and to turn everything easier. Your support was crucial and I will always be in debt to you.

Lastly, I would like to thank my incredible friends, Vânia, Jacinta and Sabrina. Your friendship and support were uniquely important and I could not be more grateful to have you in my life.

ABBREVIATIONS

15d-PGJ_2	15-deoxy-$\Delta^{12,14}$-prostaglandin J_2
ACR	Acrolein
AD	Alzheimer's disease
AE	Acrodermatitis enteropathica
AKT	Protein kinase B
ATP	Adenosine triphosphate
BMH	1,6-bismaleimidohexane
BSA	Bovine serum albumin
CD	Circular dichroism
CID	Collision-induced dissociation
COX-2	Cyclooxygenase-2
cyPG	Cyclopentenone prostaglandins
DAPI	Diamidino-2-phenylindole
DAVID	Database for Annotation, Visualization and Integrated Discovery
DBB	Dibromobimane
DMEM	Dulbecco's Modified Eagle Medium
DMSO	Dimethylsulfoxide
DST	Disuccinimidyl tartrate
DTT	1,4-Dithiothreitol
EDTA	Ethylenediaminetetraacetic acid
EM	Electron microscopy
EMT	Epithelial-mesenchymal transition
ETD	Electron-transfer dissociation
FASP	Filter aided sample preparation
FCCP	Carbonyl cyanide 4-(trifluoromethoxy)phenylhydrazone)
FRAP	Fluorescence recovery after photobleaching
GFAP	Glial fibrillary acidic protein
GFP	Green fluorescent protein
GPx	Glutathione peroxidase
GSH	Reduced glutathione
GSSG	Oxidized glutathione

GTP	Guanosine triphosphate
HHE	4-hydroxyhexenal
HIV	Human immunodeficiency virus
HNE	4-hydroxynonenal
HRP	Horseradish peroxidase
HSF	Heat shock factor
Iac	Iodoacetamide
IF	Intermediate filament
LC	Liquid chromatography
iNOS	Inducible Nitric oxide synthase
Keap1	Kelch-like ECH-associated protein 1
KEGG	Kyoto Encyclopedia of Genes and Genomes
MALDI	Matrix-assisted laser desorption/ionization
MD	Molecular dynamics
MDA	Malondialdehyde
MS	Mass spectrometry
MT	Metallothionein
MTF-1	Metal transcription factor 1
NADPH	Nicotinamide adenine dinucleotide phosphate
NF-H	Neurofilament heavy chain
NF-L	Neurofilament light chain
NF-M	Neurofilament middle chain
NMR	Nuclear magnetic resonance
NF-κB	Nuclear factor kappa-light-chain-enhancer of activated B cells
Nrf2	Nuclear factor erythroid 2-related factor 2
O-GlcNac	O-linked β-N-acetylglusosamine
PAGE	Polyacrylamide gel electrophoresis
PAR	4-(2-pyridylazo)-resorcinol
PIPES	Piperazine-N,N′-bis(2-ethanesulfonic acid)
PBS	Phosphate-Buffered Saline
PDB	Protein Data Bank
PGA_1	Prostaglandin A_1
PMSF	Phenylmethylsulfonyl fluoride

PPARγ	Peroxisome proliferator-activated gamma
PTM	Post-translational modification
PUFA	Polyunsaturated fatty acid
Rac1	Ras-related C3 botulinum toxin substrate 1
RFP	Red fluorescent protein
SDS	Sodium dodecyl sulfate
SEM	Standard error of mean
SOD	Superoxide dismutase
SRP	Signal recognition particle
STEM	Scanning transmission electron microscopy
TGF-β	Transforming growth factor β
TMEA	Tris(2-maleimidoethyl)amine
TNZD	Transient neonatal zinc deficiency
TOF	Time-of-flight
TPEN	N, N, N', N' Tetrakis (2-pyridylmethyl) ethylenediamine
TRIS	Tris(hydroxymethyl)aminomethane
ULF	Unit-length filament
UPLC	Ultra performance liquid chromatography
WB	Western blot
WT	Wild-type
ZNF	Zinc finger motifs

Other abbreviations not shown here follow IUPAC nomenclature.

TABLE OF CONTENTS

LIST OF FIGURES

LIST OF TABLES

SUMMARY IN ENGLISH

Vimentin is a type III intermediate filament protein commonly found in fibroblasts, leukocytes, other cells of mesenchymal origin and in the eye lens. Over the years, vimentin has been described to play diverse roles across a great variety of cell and tissue functions and to be involved in the pathogenic mechanisms of several diseases [1].

In cells, vimentin builds an extended and actively dynamic network of filaments that spans the cytoplasm, and undergoes constant and relatively rapid alterations of shape and localization in response to post-translational modifications and to biochemical and/or mechanical stress [2].

Vimentin is a key sensor for oxidative or nitrosative stress, and it is the target for lipoxidation by several electrophilic lipids, which induce a marked remodeling of its filamentous network, as observed in work derived from this Thesis [3] and in previous works [4]. Furthermore, vimentin organization and function can be modulated by the ionic strength and by the presence of divalent cations, such as zinc [5, 6]. Indeed, previous work unveiled that vimentin strongly binds zinc, in vitro, and its function is importantly modulated by zinc availability, in cells [4, 7].

Remarkably, the highly conserved cysteine residue, C328, is important for the effect of oxidants on the assembly and on the morphology of vimentin filaments in vitro [8], and for vimentin remodeling in response to electrophilic attack in cells. Moreover, mutation of this cysteine residue alters filament assembly and/or properties in cellular models [4].

Nevertheless, the mechanisms underlying the effect of lipoxidation on vimentin organization as well as the structural and functional consequences of the vimentin-zinc interplay and its impact on the vimentin response against lipoxidative stress have not been totally elucidated. Therefore, an integrative approach was designed in order to characterize vimentin as a target for lipoxidation and to explore the interaction between vimentin and zinc, paying special attention to the cysteine residue as a hinge influencing vimentin responses to different stimuli.

In vitro assays were the first approach used to study vimentin oligomerization and modification by different electrophilic agents. Since the objective of this work was the study of the effect of micromolar concentrations of divalent cations and reactive agents on vimentin structure and function, first, a

procedure was set up to ensure the functional reconstitution of the protein, in the absence of metal chelators, in particular EDTA, which could interfere with the results.

The efficiency of the removal of EDTA was monitored both by a colorimetric assay, using the zinc binding compound PAR, and by NMR, taking advantage of the ability of EDTA to complex zinc. Moreover, ultrafiltration is revealed to be a good choice for efficient removal of EDTA, suitable for small sample volumes, and that, when followed by dialysis, allows the functional refolding of vimentin.

The in vitro modification by structurally diverse compounds was explored using this highly pure vimentin preparation. The structural and chemical properties of oxidants and electrophilic lipids, referred here as lipoxidants, markedly influence the functional outcome, which include morphological alterations such as aggregation, increased filament diameter, heterogeneity and/or bundling. Remarkably, the lipoxidant-induced alterations are attenuated in the C328S vimentin mutant, as well as in preformed filaments, highlighting the importance of the cysteine residue and the polymerization state of the protein in the vimentin response to lipoxidative modifications.

In cells, the presence of the cysteine residue and the dynamic exchange between polymerized and non-polymerized vimentin are crucial for the network reorganization induced by oxidation or lipoxidaton, referred here as (lip)oxidation. Indeed, cysteine crosslinking and inhibition of mitochondrial oxidative phosphorylation, two strategies used to minimize vimentin dynamics, protect the vimentin network from disruption by diamide. Thus, (lip)oxidation of soluble vimentin appears to impair normal assembly.

Interestingly, vimentin (lip)oxidation can also be modulated by context factors, including the levels of antioxidant defenses and certain divalent cations. Indeed, the results obtained indicate that zinc binds to the thiolate form of C328 and is able to prevent modification of vimentin by several electrophiles and cysteine crosslinkers, in vitro. In addition, micromolar concentrations of zinc are able to promote vimentin oligomerization and induce morphological changes in vimentin organization, which depend on the support used and whether vimentin is in its soluble or previously assembled form.

In cells, zinc availability seems to play a protective role against the disruption of the vimentin network induced by several electrophilic agents.

Taken together, these results substantiate vimentin as target for several electrophilic compounds and highlight the single cysteine residue, C328, and filament dynamics as critical factors for electrophile-induced network disruption. Moreover, the interplay between vimentin and zinc has a strong impact on the organization and on the assembly properties of vimentin and modulates its response to (lip)oxidation.

SUMMARY IN SPANISH

La vimentina es una proteína perteneciente a la familia de filamentos intermedios de tipo III que se encuentra comúnmente en fibroblastos, leucocitos, otras células de origen mesenquimatoso y en cristalino. A lo largo de los años, se ha descrito que la vimentina participa en una gran variedad de funciones celulares y tisulares y está involucrada en los mecanismos patogénicos de varias enfermedades [1].

En células, la vimentina forma una extensa y dinámica trama de filamentos que se extiende por todo el citoplasma, y sufre alteraciones constantes y relativamente rápidas de su organización y localización en respuesta a modificaciones postraduccionales y a estrés bioquímico y / o mecánico [2].

La vimentina es un sensor clave para el estrés oxidativo o nitrosativo, y es diana de lipoxidación de varios lípidos electrófilos, que normalmente inducen una remodelación marcada de su red de filamentos [3, 4]. Además, la organización y función de la vimentina pueden ser moduladas por la fuerza iónica y por la presencia de cationes divalentes [5, 6] Estudios previos han revelado que la vimentina se une a zinc, in vitro y que su función está sujeta a una estrecha regulación por la disponibilidad de zinc en células [4, 7].

Es importante destacar que el único residuo de cisteína de la vimentina, la cisteína 328, que se encuentra altamente conservada, es crucial para el efecto de los oxidantes en el ensamblaje y en la morfología de los filamentos in vitro [8], y para la remodelación de la vimentina en respuesta a agentes electrófilos en células. Además, la mutación de la cisteína 328 altera el ensamblaje de los filamentos de vimentina y / o sus propiedades en modelos celulares [4].

Sin embargo, los mecanismos subyacentes al efecto de la lipoxidación de vimentina, así como las consecuencias estructurales y funcionales de la interacción vimentina-zinc y su impacto en la respuesta de vimentina frente al estrés lipoxidativo no han sido totalmente aclarados. Por lo tanto, en este trabajo se elaboró una estrategia para caracterizar la vimentina como diana de lipoxidación y para explorar la interacción entre la vimentina y el zinc, prestando especial atención a su único residuo de cisteína como un factor importante en la respuesta de la vimentina frente a diferentes estímulos.

En primer lugar empleamos ensayos in vitro para estudiar la oligomerización de vimentina y su alteración por diferentes agentes electrofílicos. Dado que nuestro objetivo implicaba el estudio del efecto de concentraciones micromolares de cationes divalentes y compuestos reactivos sobre la estructura y función de la vimentina, se diseñó un procedimiento para asegurar la reconstitución funcional de la proteína recombinante libre de quelantes de metales, que podían interferir con los resultados de nuestros ensayos.

En particular, se emplearon métodos para eliminar el EDTA. La eficacia de la eliminación del quelante de metales se controló tanto mediante un ensayo colorimétrico, utilizando el compuesto capaz de unir zinc, PAR, como mediante RMN, aprovechando la capacidad del EDTA para formar complejos con zinc. Además, la ultrafiltración reveló ser una buena opción para la eliminación eficaz de EDTA, adecuada para pequeños volúmenes de muestra, y que en combinación con diálisis, permite el plegamiento funcional de la vimentina.

Los ensayos in vitro han demostrado que la vimentina es susceptible de modificación covalente por compuestos estructuralmente diversos. Las propiedades estructurales y químicas de los oxidantes y lípidos electrofílicos, denominados lipoxidantes en este trabajo, influyen notablemente en el resultado funcional de la modificación, que incluye alteraciones morfológicas como agregación, aumento del diámetro del filamento, heterogeneidad y / o asociación lateral de los filamentos.

Se ha observado que tanto el mutante vimentina C328S, como los filamentos previamente ensamblados presentan una respuesta atenuada a los compuestos electrófilos. Estas observaciones destacan la importancia del residuo de cisteína y del estado de polimerización de la proteína en la respuesta de la vimentina frente a la modificación lipoxidativa.

En células, la presencia del residuo de cisteína y el intercambio dinámico de subunidades entre vimentina polimerizada y no polimerizada parecen ser cruciales para la reorganización de la red de filamentos inducida por oxidación o lipoxidación, procesos que se incluyen en el término (lip)oxidación. De hecho, el *crosslinking* de cisteína y la inhibición de la fosforilación oxidativa mitocondrial, dos estrategias que minimizan la dinámica de vimentina, protegen los filamentos de vimentina de la fragmentación provocada por diamida. Por lo

tanto, la lipoxidación de la vimentina soluble parece afectar a ensamblaje normal.

Curiosamente, la (lip)oxidación de la vimentina también puede ser modulada por otros factores, como por ejemplo los niveles de las defensas antioxidantes celulares y de ciertos cationes divalentes. De hecho, los resultados indican que el zinc se coordina con la forma tiolato de la C328, y puede prevenir la modificación in vitro de la vimentina por varios agentes electrófilos y *crosslinkers* de cisteínas. Además, concentraciones micromolares de zinc pueden promover la oligomerización de vimentina e inducir cambios morfológicos en la organización de la proteína, que son variables según el soporte utilizado y dependen de si la vimentina es soluble o se ha ensamblado previamente.

En células, la disponibilidad de zinc parece tener un papel protector contra la alteración de la trama de filamentos de vimentina inducida por varios agentes electrófilos.

En conjunto, los resultados identifican la vimentina como diana de varios compuestos electrófilos y resaltan la presencia de la C328 y la dinámica de los filamentos como factores críticos para la alteración de la trama de filamentos inducida por estos agentes. Además, la interacción entre vimentina y zinc tiene un fuerte impacto en la organización de esta proteína y modula su respuesta frente a la (lip)oxidación.

INTRODUCTION

1. Cytoskeletal proteins

Cell integrity is supported by a complex and dynamic network of filaments known as the cytoskeleton. Cytoskeletal proteins not only contribute to maintain cell shape, but also participate in the correct positioning of organelles, provide tracks for the transport of vesicles and enable cells to carry out essential functions like division and movement [9, 10].

The eukaryotic cytoskeleton is constituted by three principal networks of filaments or fibers that differ in size and protein composition. Two of them are well-characterized: microtubules, which are composed of tubulin subunits, and actin microfilaments. Intermediate filaments (IFs) constitute the third cytoskeletal component, they are ubiquitously found in virtually all cells and are present both in the cytoplasm and in the nucleus.

Microtubules are the thickest of the three types of cytoskeletal fibers, with a diameter of about 25 nm. The building block of a microtubule is a dimer of homologous α- and β-tubulin subunits, which associate end-to-end to form protofilaments that run along the length of cylindrical microtubules, under requirement of the nucleotide GTP. These long polymers form a network radiating from the juxtanuclear centrosome or microtubule-organizing center to the cell periphery, enabling the transport of cargo through the cell and acting as compression-bearing mechanical elements [11].

Actin microfilaments display a diameter of approximately 7 nm. Individual actin monomers are globular proteins, G-actin, which interact head-to-tail with two other actin monomers to form actin filaments, F-actin. Within cells, actin filaments localize at the periphery of the cell, in the cortex underlying the plasma membrane, and in bundles called stress fibers. The microfilament system is required for cell contraction and to form protrusions like lamellipodia, filopodia and pseudopodia [12].

Lastly, intermediate filaments comprehend a group of fibrillary structures of variable size, ranging from 3-4 nm to approximately 12 nm. Cytoplasmic IFs create an extensive network of filaments from the perinuclear region towards the cell surface, while nuclear lamins constitute a filamentous layer located

between the inner nuclear membrane and the peripheral heterochromatin [13], and both contribute considerably to cell mechanics.

1.1 Intermediate filaments

Intermediate filaments establish a sophisticated and dynamic network that can be found in nearly all differentiated cells. They work as an interconnected system, interacting closely with the other cytoskeletal components. IFs differ from actin and tubulin in their diverse primary structure, their relative insolubility, their particular nonpolar architecture and their apparently nucleotide-independent dynamics [13, 14].

Within the human genome, IFs are encoded by over 70 functional genes and can be grouped into six distinct classes based on their sequence homology, encoding gene structure, charge, assembly mechanism and expression pattern [15], as summarized in table 1.

Table 1: Classification of intermediate filaments (IFs)

Class	Proteins	Size (kd)	Typical Localization
I	Acidic keratins	40-64	Epithelial cells
II	Neutral-basic keratins	52-68	Epithelial cells
III	Vimentin	55	Mesenchymal cells
	GFAP	52	Glial cells
	Desmin	53	Muscle
	Peripherin	54	Neurons
	Syncoilin	54	Muscle
IV	Neurofilaments -L, -M, -H	61-110	Neurons
	α-Internexin	61	Neurons
	Nestin	240	Stem cells
	Synemin	150-180	Muscle
V	Lamins (A, B, C)	62-78	Cell nucleus
Orphans (VI)	Filensin	83	Lens cells
	Phakinin	46	Lens cells

Types I and II are the largest group, composed by acidic and neutral-basic keratins typically found in epithelial cells. Vimentin, desmin, peripherin and glial fibrillary acidic protein (GFAP) integrate the type III IFs group. Vimentin is the most broadly distributed IF protein, characteristically expressed in cells of mesenchymal origin. Desmin is specifically expressed in muscle cells, whereas GFAP is expressed in glial cells, and peripherin is expressed in neurons of the peripheral nervous system. Type IV comprises neurofilaments (NF) NF-L, NF-M and NF-H, nestin, synemin and syncoilin, while the nuclear lamins (lamins A and C, B_1 and B_2) constitute the type V IF class. Filensin and phakinin are intermediate filament proteins expressed during differentiation of the lens epithelium, but they are not classified into any of the five types described, due to different features of its α-helical rod domain [16, 17].

1.1.1 Intermediate filament architecture and assembly

IF proteins share an analogous tripartite structure consisting of a central α-helical rod domain, and poorly ordered N-terminal head and C-terminal tail domains, the size and sequence of which vary among the different classes of IFs [13]. The conserved rod domain is the “signature” feature of the IF family and point mutations at the beginning or end of the rod strongly alter IF organization and dynamics [18]. Secondary structure prediction based on IF’s sequence reveals that the rod domain contains three α-helical regions of largely conserved length, termed coils 1A, 1B and 2, interconnected by non-helical linkers L1 an L12 (fig. 1).

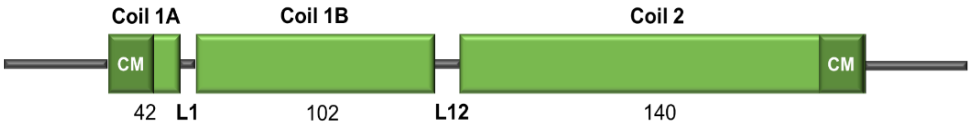

Figure 1. Structural organization of the IF monomer.
Helical segments are nominated “coil” and represented as boxes; the corresponding number of amino acids is detailed below each segment. “CM” designates conserved amino acid sequence motifs that occur at the amino-terminal and carboxy-terminal ends of the rod. Intrinsically disordered linker segments connecting the different helices are shown as L1 and L12.

The rod domain plays an important role in the interaction between IF monomers, which assemble to form a parallel coiled-coil homo- or heterodimers, depending on the type of fibrillary protein. Parallel dimers gather to form non-polar tetramers, adopting an antiparallel and half-staggered configuration, which further laterally associate to give origin to unit length filaments (ULFs) of about 60 nm length. Longitudinal association of ULFs and subsequent radial compaction result in extended filaments, as explained below for vimentin (fig. 2) [13]. The IF assembly process does not require cofactors in vitro, and apparently, is nucleotide-independent.

1.1.2 Pathophysiological relevance of intermediate filaments

Cytoplasmic IF expression and composition varies according to the cell-type. They participate in a wide scope of biological functions. Their intrinsic viscoelastic properties and their ability to build an extended network through the cell cytoplasm turn IFs into key regulators of cell shape and cell mechanics as well as controllers of the correct localization of organelles within the cell [2, 14]. In addition, IF dynamics actively influence the cell behavior in response to distinct environmental signals, which may include the regulation of key signaling pathways that control cell division, cell death or cell migration [16].

Contribution of IFs to human diseases may occur at different levels. Mutations in genes encoding IF proteins may be involved in pathogenesis, and IF variants may either predispose to or protect from disease. As summarized in table 2, more than 30 diseases are related to mutations of IF genes and the majority of them are considered rare (disease affecting less than 1 in 2000 citizens, in Europe, EURORDIS-Rare Diseases Europe, www.eurordis.org). Briefly, keratin mutations contribute to several diseases of skin and hair [19], myopathies and lens disorders are caused by genetic abnormalities of desmin, vimentin, filensin and phakinin [20], mutations of GFAP and neurofilaments are reported to be involved in neurodegenerative pathologies [21] and finally, lamin mutations induce several disorders, known as laminopathies, including premature aging syndromes, muscular dystrophy, lipodystrophy and neuropathy [22].

Table 2: Examples of diseases related to mutations in genes encoding IFs.

Data obtained from The Human Intermediate Filament Database [23]

Intermediate filament	Disease
Type I and II	
Acidic and neutral-basic keratins	▪ Epidermolysis bullosa simplex ▪ Epidermolytic hyperkeratosis ▪ Meesman corneal dystrophy ▪ Keratodermas
Type III	
Desmin	▪ Desmin-related myopathy ▪ Dilated cardiomyopathy 1A ▪ Distal myopathy
GFAP	▪ Alexander disease
Peripherin	▪ Amyotrophic lateral sclerosis 1
Vimentin	▪ Dominant cataract
Type IV	
Neurofilaments (NF-L, -M, -H)	▪ Parkinson disease ▪ Amyotrophic lateral sclerosis 1 ▪ Neuronal IF inclusion disease
Type V	
A-type lamins	▪ Hutchinson-Gilford progeria syndrome ▪ Restrictive dermopathy ▪ Charcot-Marie-Tooth disorder type 2B1 ▪ Familial partial lipodystrophy ▪ Limb-girdle muscular dystrophy
B-type lamins	▪ Acquired partial lipodystrophy ▪ Adult-onset leukodystrophy
Type VI	
Bfsp1 (filensin) Bfsp2 (phakinin)	▪ Autosomal-dominant cataract

In many of these diseases, alterations of IF proteins may lead to the appearance of IF-containing inclusion bodies. This is the case for Mallory-Denk bodies constituted by keratins in alcoholic and non-alcoholic steatohepatitis [24], Rosenthal fibers formed by GFAP in Alexander disease [25] and formation of desmin bodies in myopathies [26].

Lastly, IF proteins may be clinically relevant as diagnostic markers for disease. Identification and analysis of IF proteins in tissues, in blood or in cerebrospinal fluids may help to diagnose poorly differentiated tumors and to evaluate tissue injury [27].

In summary, IFs comprehend a large family of proteins, the expression and regulation of which are cell-type dependent. Their unique mechanical characteristics and their dynamics allow them to fulfil a wide array of biological

functions, ranging from supporting cell architecture to participating in cell survival, migration and division. This significant contribution of IFs to maintain cell and tissue homeostasis is reflected in their involvement in several pathologies, either by representing putative therapeutic targets or by acting as disease biomarkers.

1.2 Vimentin

Vimentin is a type III intermediate filament protein and it is the most widely distributed of the all IF proteins [1]. The sequence of vimentin is highly conserved across species, ranging from zebrafish to humans, which unveils an evolutionary role of vimentin in the physiological context [28, 29]. Over the years, vimentin has been described to play diverse roles in a great variety of cell and tissue functions and to be involved in the pathogenesis of diseases, such as cataracts, cancer, Chron's disease and HIV infection [30-33]. Moreover, our group previously identified vimentin as a target for reactive inflammatory mediators, potentially mediating cytoskeletal rearrangement [34].

1.2.1 Structure

The complete sequence of human vimentin, first described in 1988, codes for a protein of 466 amino acids, with a molecular weight (M_w) of 53 x 10^3 g/mol (UniProtKB; P08670 VIME) [35].

As reported for IFs, the vimentin monomer entails a tripartite structure comprising an α-helical rod of 310 amino acids, a poorly ordered "head" constituted by 95 amino acids at the N-terminal end and a likely disordered "tail" with a 61 amino acid-long sequence at the C-terminal end [36]. The rod domain is mostly arranged as a left-handed coiled-coil, consistent with its sequence organization into repeats of seven amino acids (heptads), where a hydrophobic residue is found at the first and fourth positions of the repeats [37]. The rod domain is segmented into three regions, as the result of the interruption of the heptad repetition in two conserved places that are described as flexible linkers, the 8-amino acid long linker L1 within coil 1 and the 16-amino acid long non-α-helical linker L12 between coil 1 and 2, similar to that illustrated in figure 1. At

the beginning of coil 2, the amino acid sequence presents a different hydrophobic pattern of 11-residue-long repeats (hendecads). Likewise, at position 350 of coil 2 there is a brief disruption in the heptad pattern by a single hendecad repeat that is referred to as “stutter”, and divides coil 2 into two segments as coil 2A and coil 2B [36].

Establishment of the molecular organization of full-length vimentin has been revealed to be very challenging due to its intrinsic capacity to self-assemble into flexible filaments which may prevent protein crystallization [38]. Therefore, a “divide-and-conquer” approach based on preparing multiple recombinant fragments of vimentin, preferably comprising 60 to 100 residues, has been proposed to study vimentin at the atomic level [39].

So far, several crystal structures of vimentin fragments have been achieved, corresponding to coil 1A as a monomer and as a dimer [40, 41], to coil 1B, from monomer up to its tetramer configuration [42] and to coil 2, at different low order assembly states [43, 44]. Recently, the first crystal structure of a high-order filamentous state of vimentin coil 1B was successfully achieved [45]. Superimposition of crystal structures of several overlapping segments of vimentin in combination with molecular dynamics simulations yielded a model of the complete rod domain [46]. Meanwhile, the N-terminal head and C-terminal tail domains have not been resolved yet, due to lack of a defined structure.

1.2.2 Assembly in vitro

Vimentin is highly insoluble in physiological buffers but under conditions of very low ionic strength or in the presence of chaotropic substances, such as urea or guanidinium hydrochloride, it is possible to find vimentin as a soluble form. In the presence of concentrations of urea above 8 M, vimentin exists mainly in the monomeric form. Decreasing urea concentration down to 6 M triggers the multi-step mechanism of vimentin assembly (fig. 2). The first event corresponds to the formation of a 46-nm-long dimer by the parallel alignment of the rod domains of two different vimentin polypeptides [41, 47]. Further dialysis into 5 M urea promotes the lateral association of two of these dimers to give origin to an antiparallel and, approximately, half-staggered tetramer, which constitutes the smallest soluble oligomeric form that occurs in low-salt buffer,

e.g. 5 mM Pipes-Na, pH 7.0 [48]. Under the electron microscope, these tetramers typically appear as rod-like structures, with a diameter of approximately 2-3 nm and 65 nm in length [49].

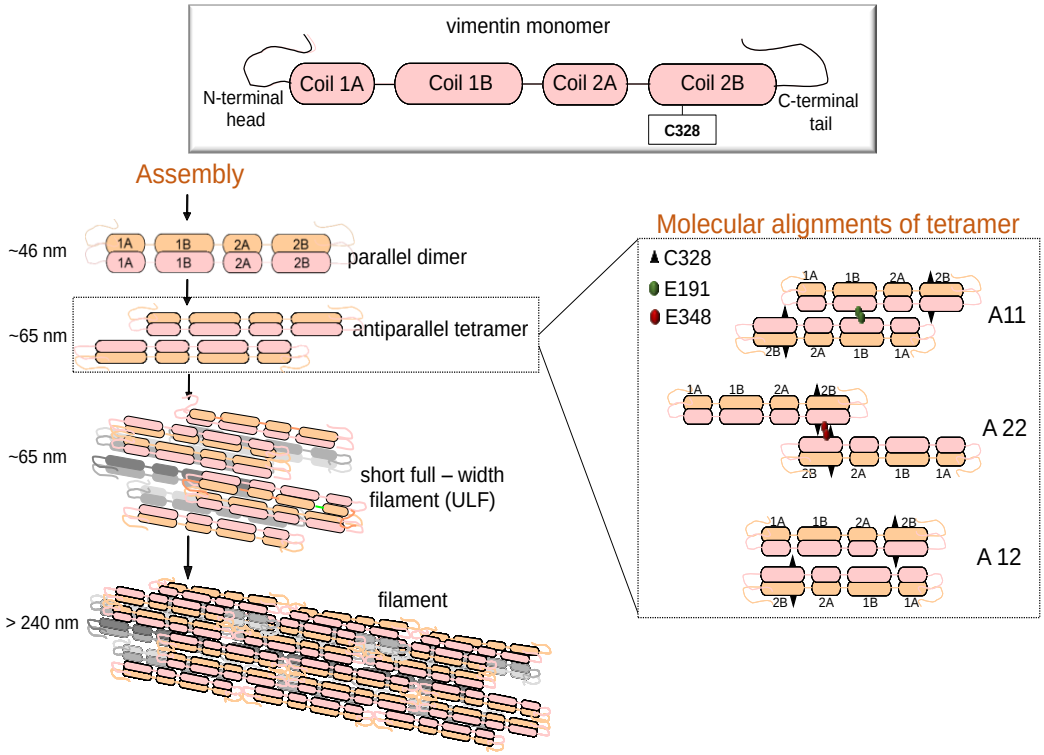

Figure 2: Schematic representation of the assembly of vimentin.
Vimentin comprises a central alfa-helical rod domain, an amino-terminal head and carboxy-terminal tail domains. The assembly process starts with the formation of a ~46nm-long parallel dimer, which further assembles into an anti-parallel tetramer of approximately 65 nm in length. These anti-parallel tetramers laterally assemble into unit-length filaments (ULFs), with ~65 nm in length, that longitudinally anneal and radially compact to give origin to long filaments (> 240 nm). Vimentin dimers can adopt different molecular alignments within tetramers (right panel): A11, A22, and A12, organized as illustrated.

Earlier in vitro studies using lysine-specific crosslinkers suggested three different alignments of the dimers within the tetramer: A11 and A22, in which the dimers are staggered in a way to bring either their 1B or 2B rod domain segments, respectively, into register; and A12 in which the two dimers are nearly overlapped [8, 50, 51].

Additionally, exploring the architecture of the dimer-dimer interaction has shown that glutamic acid residues at position 191 and position 348 correspond to points of overlap between adjacent dimers, consistent with the A11 and A22

alignments, respectively [47, 52]. At the same time, the formation of a correctly aligned tetramer that is competent to further assembly into filaments is mediated by the disordered head domain, involving basic residues responsible to attract the acidic residues existing in the rod domain of the second dimer [51, 53, 54]. Moreover, there is a complementarity in the charge distribution on adjacent surfaces, within the tetramer, important for the assembly of vimentin [41].

Once the ionic strength is raised, the highly charged rod-like tetrameric complexes assemble into 32-meric complexes known as unit-length filaments (ULFs) of roughly 60 nm in length and up to 20 nm in width [54]. The increase of the ionic strength relieves the basic head domain from intra-tetrameric interactions to form new contacts that engage two tetramers together. Such inter-tetrameric association is reinforced by the close interaction between the adjacent coiled-coils of the segments 1A and 2A. Successive cross-coiling of the coil 1A and coil 2A segments originating from different tetramers induces lateral association, enabling the oligomer to grow, in a roughly circular fashion, into octamers, 16-mers, and finally into ULFs [53, 55]. Interestingly, crosslinking studies using a temperature-sensitive mutant, vimentin K139C, unveiled that ULFs are predominantly assembled from A11 type tetramers and A22 and A12 configurations typically occur in the compacted filaments [51].

The ULF formation is termed as “phase 1” of IF assembly, and it is so fast that A11 tetramers are all consumed within milliseconds, as determined by an “stopped-flow” approach in combination with static light-scattering measurements [56].

The elongation process corresponds to the second step of vimentin assembly and it occurs within the first minutes after addition of assembly buffer, as followed by time-resolved static and dynamic light scattering [57] and by observation under electron microscopy of different time point preparations [38, 49, 58, 59]. In this assembly step, ULFs longitudinally anneal end-to-end into immature filaments. Consecutive ULF addition increases vimentin IF length till several microns [59]. Elongation stabilizes after 1 h, though it slowly continues through longitudinal annealing of long filaments, as verified by total internal reflection fluorescence microscopy of fluorescently labeled vimentin [60].

The third and last step of the assembly process consists in the radial compaction of protofibrils into mature filaments. Vimentin IFs radially compact from around 18 nm of diameter, at ten seconds, to approximately 13 nm after 1 h, as determined by EM [54]. Results from several studies indicate that the vimentin C-terminal tail domain plays an important role in width control during IF assembly [48].

Mass measurements with scanning transmission electron microscopy (STEM) are consistent with a typical average of 32 vimentin molecules (8 tetramers) per filament cross section [13]. Nevertheless, vimentin IFs display a high level of polymorphism, reflected in a heterogeneous mass per length (MPL) distribution along the different assembly stages. Correspondingly, vimentin ULFs may vary between 32 till 45 monomers per cross section, after two seconds of being challenged by a high-salt buffer, and vimentin mature IFs may contain from 30 to 44 monomers per filament cross section, after 1 h of polymerization [54].

Moreover, vimentin IF polymorphism strongly depends on the assembly conditions. As such, vimentin filaments formed by slow dialysis present a more regular and homogenous morphology, compared to those formed by dilution of vimentin into assembly buffer, which induces an abrupt increase of the ionic strength, causing a more heterogeneous rearrangement of tetramers [13, 54]. Similarly, salt concentration, temperature and the presence of divalent cations influence filament morphology, IF formation kinetics and mass per length composition along vimentin IFs, as reflected, for instance, by the increase in the number of subunits up to 56 or 84 upon assembly in the presence of 2.5 mM $MgCl_2$ [6, 54, 61, 62].

Summing up, vimentin filaments result from coiled-coil multi-domain amino acid sequences that are stabilized and linked by hydrophobic and ionic interactions, to form the fibrous protein structure. Morphology of the different assembly intermediates as well as IF formation kinetics can be followed by different techniques, which unveiled important context factors that may influence the assembly behavior of vimentin.

1.2.3 Assembly in cells

In cells, vimentin builds an extended and dynamic filamentous network which undergoes through constant and relatively rapid alterations of shape and localization. Cryo-electron tomography of ultrathin cryo-sections of cell cytoplasm showed vimentin filaments with an average diameter of roughly 12.5-13.5 nm [58].

Within the cell environment, vimentin exists both as soluble tetrameric complexes and polymerized forms, which are continuously exchanging subunits. Successful works using cell fusion, photobleaching and photoactivation strategies revealed that vimentin filament turnover, essential to maintain its structural integrity, occurs either by constant severing and reannealing at filament ends or by swapping units along the filament length [63].

In addition, vimentin assembly dynamics is regulated by post-translational modifications, such as phosphorylation, and requires ATP [3, 64, 65]. Accordingly, phosphorylation of several residues in the N-terminal head domain is important for the integrity and dynamics of the filamentous network. Particularly, phosphorylation of S55 promotes vimentin disassembly necessary for cells to undergo mitosis [66]. Recently, our group has demonstrated that C-terminal domain is fundamental for an extended vimentin IF network and for the cortical association of vimentin filaments in mitosis [67].

1.2.4 Function

In 1990s, studies with vimentin knockout mice originally pointed to a very mild phenotype, with mice being able to develop and reproduce without apparent defects [68, 69]. However, further detailed analyses of vimentin -/- mice have unveiled that loss of vimentin elicits marked cellular alterations with important pathophysiological implications. Indeed, vimentin deficiency is associated with cell morphological changes, impaired wound healing and reduction in cell adhesion, migration and stiffness [70-73]. Consequently, these reported phenotypes have unveiled various functional roles for vimentin within physiological systems, ranging from cell architecture to signaling, which may be translated either in the maintenance of cell and tissue homeostasis or be related

to the occurrence of pathologies. The main functions of vimentin are briefly summarized in table 3.

Table 3: **Biological functions of vimentin**

Function	Description	Reference
Cell architecture and intracellular organization	Vimentin builds an extended and dynamic network important for cell shape and organelle position, by: • regulating the location and motility of mitochondria, Golgi complex and lysosomes; • surrounding lipid droplets or misfolded proteins, forming cage-like structures and routing them to their fate; • accumulating at the nuclear periphery, stabilizing nucleus shape and position.	• [4, 74-76] • [77-79] • [80]
Cell mechanics	Vimentin IFs create particular viscoelastic properties important to: • maintain cell integrity in response to compressive stress; • provide mechanical flexibility required for cell contraction, migration and proliferation.	• [81]
Cell motility	Vimentin stimulates cell migration by: • restricting actin flow and aligning traction forces; • interacting with tubulin and actin to maintain cell polarity; • supporting the development of membrane protrusions, as lamellipodia and filopodia.	• [82]
Epithelial-Mesenchymal transition (EMT)	Vimentin is both a marker and effector for EMT by regulating cell motility required for the mesenchymal phenotype. • EMT is a biological process essential to embryonic development, wound healing and to cancer metastases formation, characterized by induction of cell motility, changes in gene expression and increased survival.	• [83] [84]
Cell adhesion	Vimentin is important for the cell-cell and cell-extracellular matrix contacts by: • promoting the stability and shape of focal adhesions, through interaction with integrins; • interacting with focal-adhesion intermediates, like plectin and with actin-crosslinking proteins, as filamin A and fimbrin; • protecting cell-matrix adhesions from shear stress and regulating the size of focal adhesions.	• [85-87] • [88] [89] [90] • [91]

Continuation of table 3: Biological functions of vimentin

Function	Description	Reference
Cell signaling	Vimentin IF network is enrolled in several intracellular signaling processes. Such as: • Signaling pathways requiring the 14-3-3 proteins, in a phosphorylation-dependent manner; • TGF-β-Slug signaling process, orchestrating fibroblast proliferation and keratinocyte activation, in wound healing; • AKT dependent signaling pathway, inhibiting autophagy and contributing to tumor progression.	• [92] • [71] • [93]
Cell division	Vimentin network undergoes a drastic remodeling during cell division: • vimentin filaments can be either solubilized or redistributed towards the cell cortex, depending on the cell type. • Interference with these processes leads to mitotic abnormalities.	• [67] • [30]

1.2.5 Vimentin related to disease

Vimentin biological functions are important for tissue and cell homeostasis. Nevertheless, such roles may contribute to the appearance of certain diseases, which turn vimentin as a putative drug target and an important diagnostic biomarker [1].

In the eye lens epithelium, the missense mutation E151K in coil 1B of vimentin provokes its misfolding and aggregation. Such incidence leads to opacification of the eye lens characteristically occurring in cataracts [94].

Due to its involvement in EMT, vimentin has been extensively reported as a key component of cancer progression and frequently described as a prognostic factor for poor survival in lung, breast, prostate, gastrointestinal cancers and malignant melanoma [95-100].

In addition to cancer, EMT is also involved in other pathological processes. EMT is related to the invasive properties of cells and to the development of intestinal fibrosis in Crohn's disease [101]. In rheumatoid arthritis, EMT induces hyperplasia of the tissues surrounding the synovial membrane and promotes cell invasion [102]. A similar phenomenon called

endothelial-to-mesenchymal transition is observed in atherosclerotic lesions [103]. Finally, vimentin overexpression is also considered a pathogenic factor in lung fibrosis [104].

During infection, vimentin mediates pathogen-host cell interaction and it has been reported to control the replication of HIV in the human T cell line MT4 [33, 105].

Vimentin may also behave as antigen in autoimmune diseases. Post-translational modification of vimentin creates antigenic epitopes, and consequently leads to the synthesis of antibodies. For instance, citrullinated, carbamylated and acetylated forms of vimentin function as antigens in rheumatoid arthritis and antibodies against them serve as diagnostic markers of the disease [106, 107].

Finally, vimentin is also related to aging and cell senescence. Proteomic studies have identified vimentin oxidatively modified by malondialdehyde (MDA) at the surface of senescent primary human fibroblasts. Moreover, secreted MDA-modified vimentin was detected in the plasma of aged senescence-accelerated mice, which have deregulated redox metabolism and accelerated aging [108]. Additionally, glycation of vimentin was found in skin fibroblasts of elderly donors and lack of serine phosphorylation during mitosis is associated to impaired cytokinesis and therefore, increased senescence [30, 109].

As a general overview, the type III IF vimentin is an important component of the cytoskeleton. Vimentin structural plasticity is reflected in the variety of its biological functions. This functional diversity is not only involved in physiological conditions but it may also participate in the pathogenesis of several diseases, which make vimentin a putative drug target and a relevant clinical biomarker.

1.2.6 Post-translational modifications (PTMs) of vimentin

Vimentin PTM is a critical mechanism for the regulation of network organization and remodeling in a broad range of physiological and pathological contexts.

Phosphorylation has been the primary covalent PTM regulator of IF dynamics studied over the years. Vimentin phosphorylation is tightly regulated by a broad group of coordinated kinases and phosphatases [65, 110-112].

Briefly, reversible phosphorylation and dephosphorylation of serine or threonine residues, particularly located in the head and tail domains, dynamically control vimentin assembly and disassembly, which are crucial for mitosis and maintenance of cell structural integrity [113-115]. In addition, vimentin phosphorylation mediates binding to other proteins, such as 14-3-3 proteins, regulating cell signaling and cell cycle control [92, 116]. Lastly, vimentin phosphorylation influences processes underlying cell motility of both normal and cancer cells, and mediates interaction with integrins important for cell adhesion [117-119].

Sumoylation, ubiquitination and acetylation have also been reported to regulate vimentin properties, commonly associated to pathological situations, as cancer [119-121]. For instance, increased levels of acetylated-vimentin are reported to be involved in Sirtuin 5-mediated hepatocellular carcinoma migration, whereas decreased levels of ubiquitinated vimentin are associated to its up-regulation in gastric cancer cells, promoting its aggressiveness.

Furthermore, vimentin is a target for advanced glycation end products, mainly through Maillard reaction, and it is also enzymatically modified by O-linked β-N-acetylglusosamine (O-GlcNac), known as *O*-GlcNAcylation. Glycation induces vimentin network remodeling into aggresomes in human skin cells, whereas O-glycosylation is required for host IF cytoskeleton-intracellular pathogen interaction during infection [105, 109].

Vimentin can also be modified by a broad range of oxidants and electrophilic lipids, which generally induces an extensive IF network organization [4]. Such oxidative and lipoxidative modifications are going to be the main topic of this thesis, thus a detailed description of their impact on vimentin is given later in this work.

The crosstalk between PTMs represents an additional level of cell regulation and signaling complexity. One of the best established examples of IF PTM cross-talk is the inverse correlation between phosphorylation and glycosylation. Typically, *O*-GlcNAcylation occurs on the same, or adjacent to phosphorylatable serine/threonine residues, which may compete with phosphorylation, stimulating or preventing it [122, 123].

Recently, we have demonstrated a putative interplay between vimentin phosphorylation and the impact of oxidative and lipoxidative modifications.

Vimentin hyperphosphorylation caused by phosphatase inhibitors, such as calyculin A, intensified the network fragmentation by diamide and potentiated vimentin IF juxtanuclear condensation and loss of peripheral filaments induced by 15-deoxy-$\Delta^{12,14}$-prostaglandin J_2 (15d-PGJ_2). On the other hand, a phosphorylation-deficient vimentin "SA mutant", in which 11 phosphorylatable serine residues present in the N-terminal head have been replaced by alanines, showed an attenuated IF network remodeling in the presence of the above mentioned compounds [3].

As a general overview, there are a broad range of PTMs that may target vimentin, contributing and modulating its structural and functional properties in a cell-type dependent manner. Accordingly, vimentin PTMs are essential to preserve cellular and tissue homeostasis and their abnormal regulation may lead to the appearance of diseases [119, 124].

2. Redox imbalance and protein lipoxidation

Cells are constantly exposed to oxidant species, arising from endogenous cellular metabolism or by exposure to environmental oxidants. The cellular concentration of such oxidative species is controlled by an elaborate antioxidant defense system, comprising antioxidant enzymes as superoxide dismutase (SOD) and glutathione peroxidase (GPx), and low-molecular-weight scavengers, such as glutathione and ascorbic acid [125].

Imbalance between oxidants and antioxidants in favor of the former leads to oxidative stress. The level of oxidative stress determines its physiological implications or pathological consequences, meaning that while low-level oxidant generation is involved in redox signaling, a high production of oxidative species may cause cell damage [126].

The cellular response to oxidative stimuli is mediated through an integrated system of thiol sensors, which work as molecular redox switches within redox signaling pathways with the main objective of conserving redox homeostasis [127].

The oxidant species are able to react with several biomolecules, unsaturated lipids present in membrane bilayers being a common target giving

rise to electrophilic species. Consecutively, some of these lipid oxidation products are able to react with proteins, a phenomenon that is known as lipoxidation [128].

Lipid species involved in lipoxidation include a wide variety of oxidized, nitrated and chlorinated products of phospholipid oxidation and metabolism, which are able to react with nucleophilic moieties, such as lysine, arginine, histidine and cysteine residues of proteins [129-131].

These lipoxidative PTMs may be implicated in the pathogenesis of cardiovascular diseases, cancer immunity and brain aging and neurodegeneration [132-135]. For many years, covalent addition of electrophilic lipids to proteins has been considered as an injurious consequence of oxidative stress, but now, protein lipoxidation is being recognized as well as a new mechanism of cell signaling relevant to redox homeostasis, adaptive response and inflammatory resolution [136, 137].

Notably, under oxidative stress, both oxidants and electrophiles coexist and therefore, proteins can suffer combinations of oxidative and lipoxidative modifications that can affect the same protein/residues in variable proportions. To refer to these potentially diverse modifications, consisting in oxidation or lipoxidation, we will use the term (lip)oxidation.

2.1 Electrophilic lipids and their involvement in protein modification

Polyunsaturated fatty acids (PUFAs), constituents of membrane phospholipids or lipoproteins, are susceptible to enzymatic and non-enzymatic lipid peroxidation which generates a remarkable structural diversity of reactive breakdown products [138].

Non-enzymatic phospholipid peroxidation is a radical-initiated and autocatalytic mechanism. It consists of the abstraction of the bis-allylic methylene hydrogen by other radical species followed by capture of oxygen atoms, originating lipid hydroperoxides. Such lipid hydroperoxides undergo rearrangement and cleavage reactions which result in the generation of lipid oxidation end products. On the other hand, cytochrome P450 enzymes, lipoxygenases and cyclooxygenases are also able to enzymatically produce oxidized fatty acids and phospholipids [139, 140].

These reactive lipid products possess electrophilic properties due to the presence of carbonyl groups (aldehydes or ketones) or α,β-unsaturated moieties and they can be classified in five principal categories: alkanals (and hydroxyalkanals), 2-alkenals, 4-hydroxy–2-alkenals, keto-alkenals, and alkanedials (dialdehydes). Malondialdehyde (MDA), acrolein (ACR), 4-hydroxyhexenal (HHE) and 4-hydroxynonenal (HNE) are the most abundant, active and studied electrophilic lipids [138]. Moreover, enzymatic and non-enzymatic transformations of arachidonic acid give origin to electrophilic eicosanoids, as cyclopentenone prostaglandins (cyPG) and isoprostanes [141].

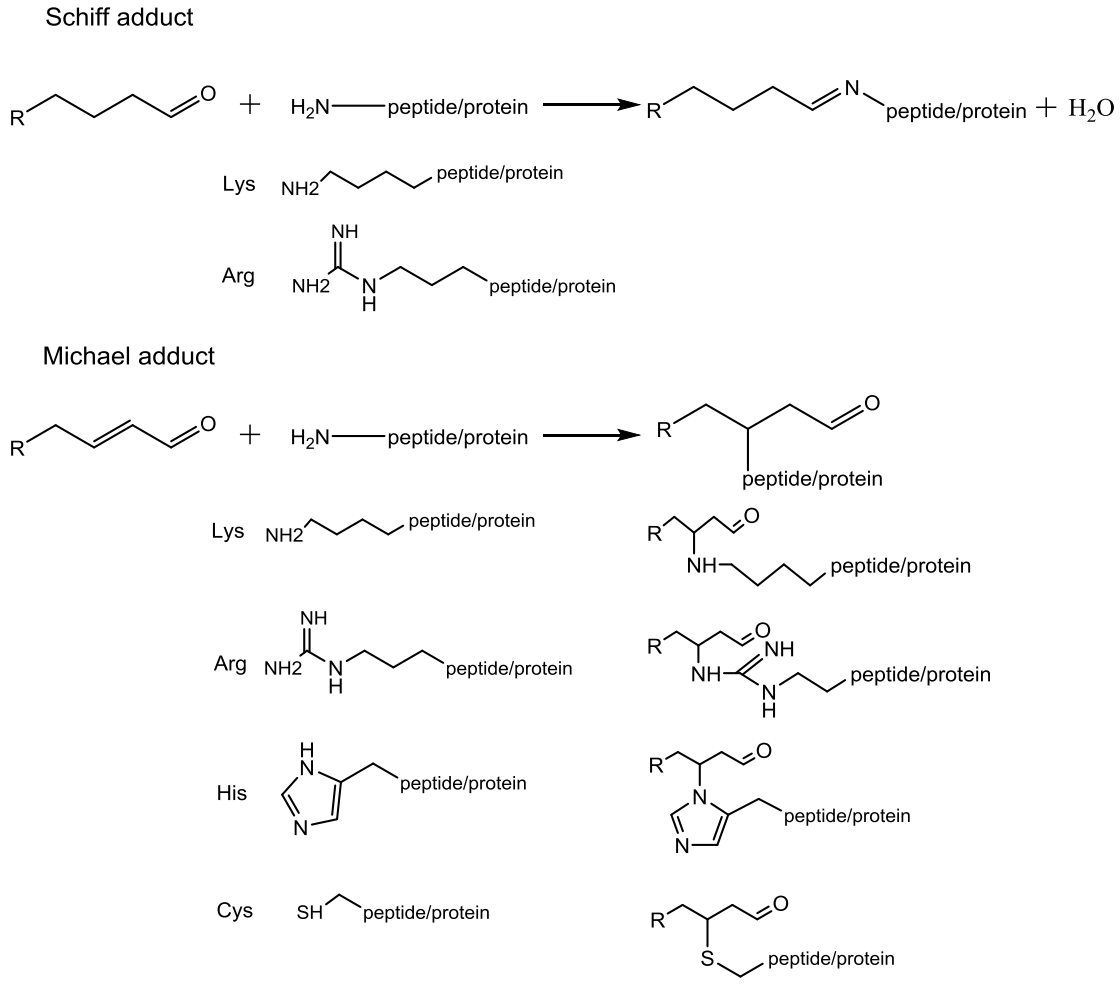

Figure 3. Main types of adducts formed between electrophilic lipids and proteins. Schiff adducts are exemplified for alkanals and lysine and arginine residues of peptides. Michael adducts are illustrated for alkenals and lysine, arginine, histidine and cysteine residues of peptides. This image was adapted from [128].

The type of interaction between proteins and the reactive lipid oxidation products depends on the chemical reactivities of the electrophile and of the nucleophilic site in the protein, determined by its pKa, surface accessibility and the pH of the intracellular compartment. Electrophilic lipids can mainly form Schiff adducts and/or Michael adducts with nucleophilic groups in peptides and proteins, specifically with the free amine group of lysine, the imidazole of histidine, the guanidine of arginine and the sulfhydryl group of cysteine (fig. 3). Although both Michael and Schiff adducts are reversible, the Schiff adducts are generally more unstable whereas Michael addition is almost irreversible due to the low rate of the reverse reaction [142].

2.2 Biological significance of lipoxidative PTMs

Development and improvement of specific and more sensitive methodology expanded the evidence for the occurrence of lipoxidation in vivo, in both healthy and damaged tissues. Proteins targeted by reactive lipid oxidation products may suffer changes in its conformation and its assembly properties, and interact differently with small ligands, cofactors, other proteins and cellular compartments [143]. In many cases, lipoxidized proteins may have impaired function contributing to pathological consequences [132]. On the other hand, lipoxidation of proteins may also have important physiological roles, by being involved in signaling pathways and triggering adaptive responses to stress conditions (fig. 4) [136].

The antioxidant response pathway via Keap1-Nrf2 and the heat shock response through HSF transcription factors, which have cytoprotective, proteostatic and anti-inflammatory functions, are examples of stress-activated pathways regulated by lipoxidation [136]. For instance, 4-hydroxynonenal (HNE) is reported to target the Keap1-Nrf2 pathway [144].

Adducts formed between prostaglandins and peptides/proteins have also significant biological effects. Cyclopentenone prostaglandins (cyPG) are endogenous lipid mediators and they have shown protective effects in cellular and animal models of inflammation and tissue injury, revealing to be potential therapeutic agents, due to their anti-inflammatory, antiproliferative, antiviral and antitumoral activity [145]. Additionally, cyPG are able to form covalent adducts

with diverse proteins along the activation pathway of the proinflammatory transcription factor NF-κB, with the transcription factor PPARγ and with proteins involved in the control of cellular redox status, such as thioredoxin and thioredoxin reductase. These modifications are responsible for their anti-inflammatory effects, their capacity to regulate lipid metabolism, adipocyte differentiation and to control the cellular redox status [146-148].

Chronic inflammatory processes induce oxidative/nitrosative stress and consequently, they are associated with high levels of lipid peroxidation products and protein lipoxidation. In turn, the resulting electrophilic lipids can alter the functions of proteins involved in inflammation, such as the nuclear transcription factor NF-κB and enzymes as iNOS and COX-2 [149, 150], and modulate the immune system by originating lipoxidized proteins highly immunogenic and leading to the generation of antibodies against them [134, 151].

In cancer, lipoxidation may have divergent results, either by triggering mechanisms associated with cancer progression, increasing the grade of malignancy, or by having anti-carcinogenic effects through induction of cell cycle arrest and apoptosis in cancer cells [134]. HNE is a clear example of the dual effect of lipoxidation in cancer. While HNE contributes to cancer cell survival by forming potentially mutagenic DNA-adducts or by negatively regulating proteins involved in DNA repair, HNE is also able to induce adaptive responses, through activation of autophagy or by causing cell cycle arrest, in order to eliminate damaged molecules and prevent further aggravation and deleterious consequences [144]. Interestingly, electrophilic prostaglandins, namely 15d-PGJ_2, covalently binds to glutathione S-transferase P1, an enzyme related to tumor chemoresistance, unveiling a potential application of electrophilic lipids to overcome the resistance of certain tumors to chemotherapy and radiation [152, 153].

The brain tissue is highly rich in PUFA-containing membrane compartments, which combined with the high abundance of redox transition metals and intense oxygen consumption turn it into an important source of reactive electrophilic species. In fact, lipoxidation processes are frequently associated with neurodegenerative disorders [154]. Proteomic studies have demonstrated increased lipid peroxidation in the brain of patients with Alzheimer disease (AD), by measuring the levels of free and protein-bound HNE,

malondialdehyde and acrolein, and they have identified lipoxidized proteins, which are consistent with the biochemical and cognitive dysfunction described in AD [154]. In addition, recent studies have reported that lipoxidative modifications of the cysteine residue at position 294 of the type III IF protein GFAP could contribute to its disruption and aggregation, and they could potentially be associated with astrocyte dysfunction and neurological disease [155].

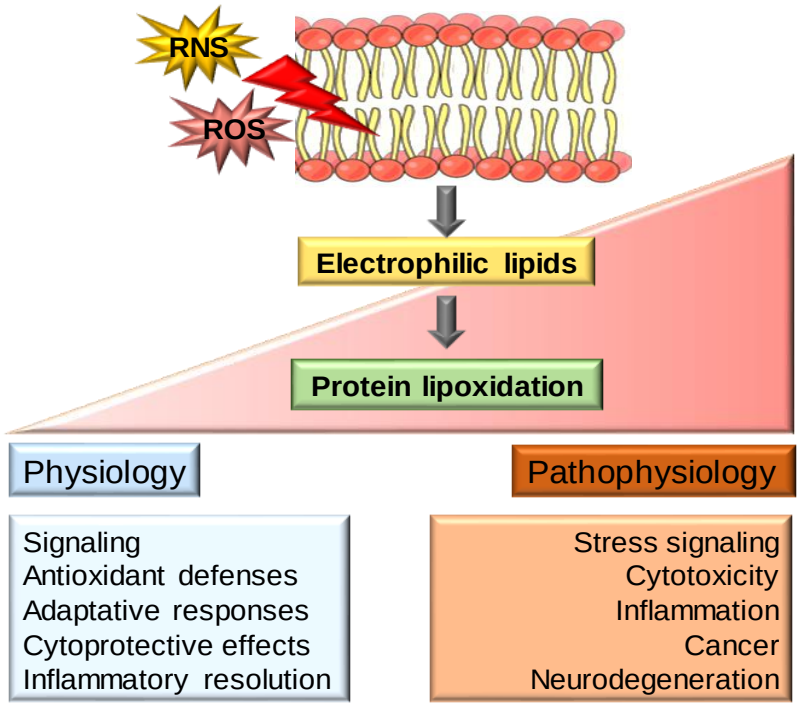

Figure 4. Protein lipoxidation in pathophysiology.
The generation of electrophilic lipids, during stress conditions, triggers the formation of covalent adducts with proteins (lipoxidation). Functional consequences in physiology (left box) or pathophysiology (right box), dependent on the levels of protein lipoxidation, are outlined. ROS, reactive oxygen species; RNS, reactive nitrogen species.

2.3 Biological relevance of lipoxidation adducts in cytoskeletal proteins

The above mentioned lipoxidative modification of GFAP illustrates the importance of cytoskeletal proteins as common targets for lipoxidation, which may have physiological or pathological relevance in oxidative stress, cellular senescence and age-related diseases [135, 156]. In fact, a lipidomic study focused on the mechanisms underlying the preservation or deterioration of

neurons and cerebral functions has identified several cytoskeletal proteins, such as actin, dynamin 1, GFAP, spectrin, tubulin and vimentin, as important targets for lipoxidative damage, putatively contributing to neuronal aging [135]. Moreover, previous studies have detected neurofilaments as targets for modification by HNE in the nervous system of mice. The levels of HNE-modified neurofilaments were surprisingly found constant through the life span of the mice, indicating a putative physiological role of HNE adduction related to the protection of neurons from carbonyl-mediated stress [157].

Additionally, proteins involved in cytoskeletal organization, including tubulin, actin, tropomyosin and vimentin are covalently modified by electrophilic lipids, including HNE and 15d-PGJ_2, which in all cases leads to cytoskeletal derangement, the intensity of the effect observed probably depending on the proportion of protein modified [34, 158, 159]. Actin, in particular, has been the subject of extensive investigation and proposed to serve as a potential marker for carbonylation damage and to act as a carbonyl scavenger [160].

2.3.1 Lipoxidative post-translational modifications of vimentin

A high number of reactive species, generated during stress conditions, can reversibly and irreversibly react with vimentin through nitrosative, lipoxidative or oxidative mechanisms [3, 161]. (Lip)oxidation refers here to both oxidative and lipoxidative modifications of vimentin.

Multiple amino acid residues may be targeted by (lip)oxidative modifications. Previous works reported vimentin sole cysteine at position 328 as highly susceptible for oxidation and a common site for electrophilic addition [4]. Cysteine modifications are often involved in redox sensing via disulfide formation, sulfenylation, S-glutathionylation or S-nitrosylation [162]. In fact, in vitro incubation of vimentin with H_2O_2 and $CuCl_2$ induces oxidative crosslinking, through disulfide formation [8, 163] and cell treatment with strong thiol oxidants, as diamide, induces extensive fragmentation of the vimentin IF network [3, 4]

Moreover, reactive species bearing unsaturated carbonyl moieties, including cyclopentenone prostaglandins (cyPG) and aldehydic compounds, as HNE, are able to react with recombinant vimentin, mainly through Michael addition or via Schiff base formation [3, 34, 164]. Within the cell environment,

such reactive compounds induce strong bundling and/or juxtanuclear condensation of vimentin filaments, which in some cases display characteristics of aggresomes [3, 4]. The biological relevance of this network remodeling is not completely understood. Vimentin may be both a mediator of cell damage or play a protective role as scavenger of electrophilic and oxidant compounds, preventing them from damaging other proteins and cellular components [165]. Moreover, aggresome formation by vimentin in response to electrophilic attack may play a cytoprotective role helping to isolate potentially toxic damaged/misfolded proteins and facilitating their clearance by autophagy [78]. On the other hand, cells containing (lip)oxidatively remodeled vimentin IF network may present mitotic abnormalities [67, 166]. Table 4 illustrates some examples of lipoxidant agents reported in the literature to target vimentin.

Table 4: Oxidants and electrophiles reported to modify vimentin

Lipoxidant agent	Residue	Species	Reference
H_2O_2	C328	Human	[163]
H_2O_2 + $CuCl_2$	C328	Human	[8]
Diamide	C328	Human	[4]; [3]
HNE	C328	Human	[167]; [3]
PGA_1	C328	Syrian Hamster	[164]
15d-PGJ_2	C328	Human	[34]; [3]
MDA	C328	Human	[108]
MDA	R122, R440, R450	Human	[168]
2-nonenal	K235	Human	[169]
Oxopentanal	H437, K439	Rat	[170]
Oxobutanal	K292, R158, R155	Rat	[170]
Oxooctanoic acid	R155	Rat	[170]

In summary, lipoxidative modification of cytoskeletal proteins may have direct or indirect functional consequences which could contribute either to maintenance of cell homeostasis or to cell damage and consequent development of pathologies. Besides, from a functional point of view, oxidized lipids bind to many targets in the cell proteome and their effects arise from interplay of the diverse modifications, which complicates the interpretation of the structural and functional outcomes. Consequently, attribution of functional roles to lipoxidation of proteins should be addressed with prudence and the use of sensitive and complementary methods to assess protein lipoxidation are extremely necessary.

2.4 Methods for the detection of protein–lipid adducts

Given the importance of lipoxidation in pathophysiology, important efforts have been concentrated in the development of highly sensitive methods to unequivocally determine and characterize this modification, both in healthy and damaged tissues [171].

Mass spectrometry (MS) provides state of the art approaches for the identification and characterization of lipoxidized proteins/residues as well as the modifying agents. MS-based analytical strategies permit the highly sensitive detection of compounds, fast scan rates suitable for high throughput sample screening and structural information at a molecular level, providing structural characterization of protein-lipid adducts in vitro and ex vivo settings. In the mass spectrum, peptide-lipid adducts are commonly determined on the basis of the mass shift against the unmodified peptide, which gives a clue on the reactive moiety attached to the peptide [171, 172].

The low abundance of lipoxidation adducts, together with the high complexity of biological samples, represent a great challenge for their detection. Therefore, identification of protein lipoxidation adducts typically involves enrichment methods, chemical labelling approaches and bottom-up strategies combining enzymatic digestion, chromatography methods and analysis by MS. These methods are commonly used to enhance sensitivity and selectivity, improving the structural interpretation [173]. The most popular chemical labels used for derivatization of the free carbonyl groups present in Michael adducts are biotin based hydrazide-functionalized reagents, Girard P reagents and aldehyde reactive probes. Lipid–protein Schiff adducts cannot be derivatized by this approach, unless the electrophilic lipid is a di-aldehyde [171].

MS-based approaches combined with enrichment procedures using biotin are increasingly being used to identify site-specific modifications of proteins in complex proteomes [142]. For instance, in the case of vimentin, introduction of an avidin chromatography step after tryptic digestion allowed enrichment of the vimentin peptide modified by PGA_1-B, thus making possible the identification of C328 as the site of modification by MALDI-TOF MS/MS analysis [164]. Another example is the identification of Rac1 as a target for modification by the biotinylated analog of 15d-PGJ_2, in vitro, by LC-MS/MS, and

in endothelial cells, by biotin affinity precipitation followed by western blot analysis with streptavidin [174]. The latter example demonstrates that other non-MS methods can be used to detect protein-lipid adducts, such as the combination of labelling techniques or enrichment procedures with SDS-PAGE followed by immunoblotting [155].

Alternatively, there are several antibodies available that directly recognize protein adducts of lipid peroxidation products, which can be applied to western blot, immunocytochemistry and immunohistochemistry [128 170]. These comprise antibodies against various types of HNE-, acrolein- and MDA-lysine adducts [175-177]. In general, immunostaining methods have good sensitivity, though additional methods are required to identify the proteins modified and the sites of modification.

Unquestionably, the identification and structural characterization of adducts formed between the oxidized lipids and proteins by the above mentioned methodology is critical to elucidate the impact of lipoxidation in cell biology [142]. Nevertheless, interpretation of functional consequences of protein lipoxidation is more complex to address. Therefore, insights into the functional consequences of protein lipoxidation requires interdisciplinary and integrative approaches involving additional biochemical and biophysical techniques associated with cell culture, purified systems, cytomimetic platforms and in vivo models.

For instance, lipoxidation can promote protein polymerization or aggregation and associations into hetero-complexes that can be analyzed by light scattering, fluorescence anisotropy and ultracentrifugation techniques [178]. Besides, with the increasing size of the protein associations, electron microscopy becomes suitable for the observation of lipoxidation-induced protein assemblies. EM allows measurements of changes in the dimensions of proteins at nanometer scale and in combination with tagged electrophilic lipids permits the detection of adducted moieties by recognition with gold-labeled tools, for example [179, 180].

Lastly, immunofluorescence of the proteins of interest or the use of different tags on lipoxidized macromolecules or their precursors can be used to analyze lipoxidation-induced morphological changes by means of fluorescence microscopy or to explore the protein-protein interactions by assessment of

colocalization rates using confocal or superresolution microscopy [4, 67, 181]. For instance, incubation of biological samples with lipid peroxidation substrate arachidonic acid or 15d-PGJ_2, tagged with either biotin or the fluorophore BODIPY, was used to assess their incorporation into cellular structures and their subcellular localization [182].

In sum, the structural and functional study of protein lipoxidation represents a complex task due to the high reactivity of the electrophilic species, the possible occurrence of simultaneous modifications, like various types of oxidations, and the crosstalk between these PTMs. Thus, combined tools are required to overcome limitations inherent to each individual technique. Therefore, interdisciplinary approaches will be applied here to study the effect of lipoxidation on the structure and function of vimentin, the putative mechanisms of electrophilic modification involved and its modulation by context factors, for instance, the presence of certain divalent cations such as zinc.

3. Zinc

Zinc is the second most abundant trace element, only behind iron, and participates in diverse protein functions that are essential for life. Bioinformatic scanning of the human genome sequence estimated the remarkable number of over three thousand proteins with potential zinc-binding sites, which represents 10% of the human proteome [183]. Functional annotation of the human proteome suggests that the majority of zinc-binding proteins are implicated in the regulation of gene expression, including DNA-binding transcription factors and members of the general transcription machinery [184]. The remaining zinc-binding proteome is mostly composed by enzymes, such as oxidoreductases, transferases, hydrolases, and proteins involved in ion transport [185].

The adult human body contains approximately 2-3 g of zinc, which is distributed through all organs, tissues and secretions of the organism. Measurements of metal composition estimated that 60% of zinc is stored in skeletal muscle, 30% in bone, 5% in the liver and skin, and the remaining 2-3% in other tissues (fig. 5) [186]. The concentration in plasma is relatively low, accounting for 0.1% of the total zinc present in the human body, 80% of which

is loosely bound to albumin and 20% is strongly bound to α2-macroglobulin [187].

In cells, the total zinc concentration can vary between tens and hundreds of micromolar, where 50% of zinc is distributed in the cytoplasm, 30-40% in the nucleus and 10% in the cell membrane [187]. Nevertheless, zinc can be bound to several proteins and stored into organelles and vesicles, meaning that the "free" cytosolic concentration is very low, ranging between picomolar and low nanomolar, while inside the zinc-containing vesicles, such as the synaptic vesicles in the hippocampus, it can reach concentrations in the hundreds of micromolar [188, 189].

Importantly, the biological activity of zinc depends on whether it is bound to a specific protein or present as free divalent ion. Therefore, regulation of intracellular free zinc concentration is strictly regulated, generally through two main mechanisms: zinc-transporting proteins and zinc-buffering systems [190].

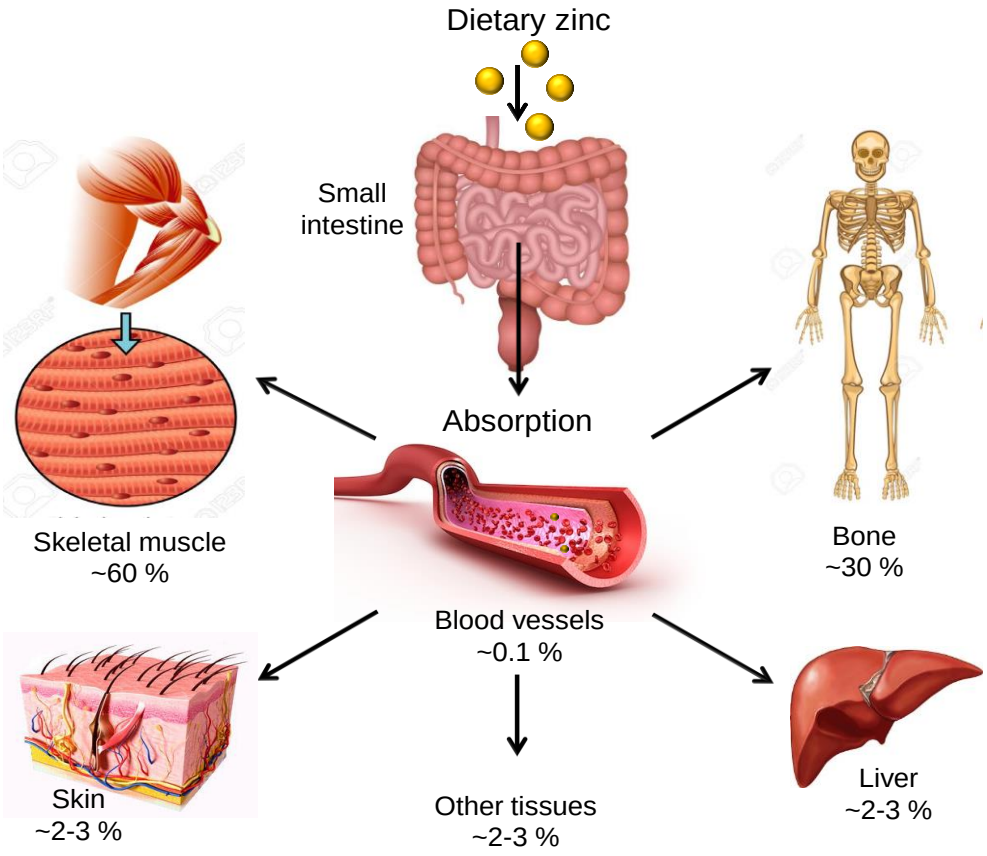

Figure 5: Distribution and storage of zinc in the human body.
Dietary zinc is absorbed in the small intestine and distributed to the peripheral tissues, including skeletal muscle (60%), bone (30%), skin and liver (5%), and other tissues (5%).

3.1 Zinc biochemistry and cellular functions

Under physiological conditions, zinc exists as a divalent cation (Zn^{2+}) and it is redox inert, meaning that it can neither oxidize nor reduce another substance [191]. Nevertheless, zinc is reactive as a Lewis acid in biological reactions, explaining its involvement in several physiological roles [192].

Within proteins, zinc can be coordinated by nitrogen from histidine, sulfur from cysteine and oxygen from aspartate or glutamate. Zinc binding to protein ligands adopts typically a tetrahedral geometry and can have different coordination numbers. Therefore, proteins are able to modulate the properties of zinc affinity by using variable combinations of ligands, and consequently, are capable to regulate the function of the zinc binding site [193]. Due to these particular features, zinc can play critical roles as a structural, catalytic and signaling element.

Proteins containing zinc finger motifs (ZNFs) constitute the most abundant class of structural zinc-binding proteins. Zinc contributes to the stability of these protein domains, characteristically comprised of four cysteine or two cysteines and two histidine residues. Given the wide variety of ZNFs, they are implicated in several cellular processes, such as nucleic acid replication, repair, transcription and translation [194].

Beyond its structural roles, zinc is known to facilitate catalytic transformations. Due to its strong Lewis acid property, zinc is able to stabilize the negative charges and consequently activate substrates in enzymes [195]. The first evidence of the catalytic role of zinc was obtained in 1939, when the erythrocyte carbonic anhydrase was found to contain stoichiometric amounts of zinc essential for its enzymatic activity [196]. Later, the presence of zinc has been documented in many enzymes in all six classes defined in the Enzyme Commission system, namely oxidoreductase, transferase, hydrolase, lyase, isomerase and ligase enzyme classes [197].

Additionally, biological regulation can be achieved by fluctuations of “free” zinc ion concentrations, which turns zinc into a signaling mediator in the transmission of information within cells and in the communication between cells [190].

The extracellular release of zinc acts as a signaling mediator in endocrine, paracrine and autocrine systems, and in the nervous system it modulates synaptic transmission by binding to several transporters and receptor channels on postsynaptic neurons [198].

In the cytosol, zinc influx can arise from extracellular sources, from intracellular organelles, such as the endoplasmic reticulum, and from redox-sensitive cytosolic proteins, as metallothioneins [199]. Intracellular zinc signaling can be mediated through changes in gene expression and can require biosynthesis of proteins to control cytosolic zinc concentration. Additionally, zinc targets a diverse number of phosphatases and kinases, involved in cellular signaling [190].

3.2 Interaction of cytoskeletal proteins with zinc

Among the roles of zinc within the cell cytoplasm, this transition metal is also able to interact with cytoskeletal proteins, mediating their structural stability or inducing polymorphic assemblies putatively deleterious for the cell.

Zinc interacts with tubulin in vitro and in vivo. At low concentrations (1.6-fold molar excess of zinc), zinc directly binds to tubulin and induces its assembly, in the absence of associated proteins [200]. At higher concentrations (20-fold molar excess of zinc) and longer periods of incubation, addition of zinc to polymerized tubulin in vitro results in the loss of microtubules and the formation of wide sheets [200]. Similar observations on the effect of zinc on tubulin assembly were found in vivo by implanting zinc wires into the brains of Lewis rats [201]. More recently, it was reported that zinc supplementation induced an increase of β-tubulin content in dendrites, indicating a putative involvement of this transition metal in microtubule stability within the dendritic cytoskeleton from hippocampal neurons [202].

Additionally, zinc is also able to interact with actin and alter the organization of its microfilament system. For instance, in cells of Madin-Darbin canine kidney, zinc exposure led to the loss of the stress fibers associated to the appearance of actin-rich plaques at the cell periphery. This was related to a reduction in cell adhesion and loss of junctional integrity, suggesting a

hypothetical negative effect of zinc in epithelial function, affecting the ability of the epithelium to act as a selective permeable barrier [203].

Several studies have also evidenced zinc interactions with intermediate filaments. Zinc has been reported to induce neurofilament phosphorylation in a mouse neuroblastoma cell line, suggesting a possible link between zinc and the phosphorylated heavy and medium subunits of neurofilaments commonly found in the neurofibrillary tangles in Alzheimer's disease [204].

Interestingly, zinc may affect motility and invasiveness of malignant colonic cells SW480, by acting on several components of the cytoskeleton, such as E-cadherin, β-catenin, vimentin, α-tubulin and actin. Indeed, zinc depleted E-cadherin and vimentin pools and promoted the remodeling and subsequent loss of tubulin and F-actin, in invasive colon cancer cells [205].

Our group has previously demonstrated the interaction of zinc with vimentin, both in vitro and in cells. In vitro, vimentin-zinc interaction protects the protein from alkylation, and micromolar concentrations of zinc induce the formation of large assemblies of vimentin, as observed by staining with zinquin, a zinc-probe, followed by fluorescence microscopy [4]. In cells, vimentin function is influenced by zinc availability. In the adrenal carcinoma cell line SW13, zinc chelation and subsequent supplementation induced disassembly and reassembly of GFP-vimentin short filaments, respectively. Moreover, in a cellular model of genetic zinc deficiency, a lower proportion of polymerized vimentin, thinner appearance of filaments, and an increased susceptibility of the vimentin network to oxidative stress were observed, that were attenuated by zinc supplementation [4]. This evidence led us to hypothesize a reciprocal outcome of the vimentin-zinc interaction, that is, zinc may regulate vimentin, and vimentin could also play a crucial role in cellular zinc homeostasis [7]. This led us to further explore the structural and functional consequences of the vimentin-zinc interplay and its impact on the vimentin response against (lip)oxidative stress.

3.3 Zinc and redox biology

As mentioned above, zinc stably remains in the Zn(II) valence state and does not directly undergo redox reactions. Paradoxically, zinc ions have an important function in the regulation of redox metabolism [191]. Such role can be related to the ability of zinc to interact with the sulfur (thiolate) donor ligand of cysteine, giving origin to zinc thiolate coordination environments that can be redox-active [206]. Interestingly, zinc binding can be modulated by oxidoreduction, explaining how bound zinc can be released, distributed and regulated [207].

In redox biology, zinc can support both pro-antioxidant and pro-oxidative processes. On one hand, this dual role arises from ability of the zinc to participate in the antioxidant system as a co-factor of various antioxidant enzymes. On the other hand, cellular oxidative stress can be caused by zinc deficiency or excess [208]. Consequently, it is important to be aware of zinc availability and concentration as a critical factor influencing its effects on the redox metabolism (fig. 6).

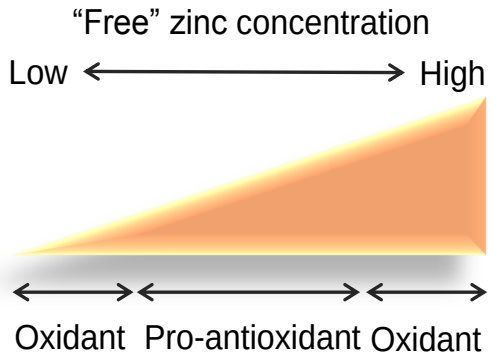

Figure 6. Relationship between the cellular concentration of “free” zinc and its effects on the redox metabolism.
Both deficiency and overload of zinc can contribute to induction of oxidative stress. The intermediate range of physiological concentrations of zinc supports “pro-antioxidant” processes. Adapted from [195].

3.3.1 Pro-antioxidant effects of zinc

The pro-antioxidant effects of zinc can be explained by three mechanisms, as detailed in figure 7: 1) induction of the antioxidant system, by supporting the activity of antioxidant enzymes and through upregulation of

transcription factors involved in the antioxidant response; 2) protection of free sulfhydryl groups; and 3) competition with redox-active ions [191].

Zinc is a structural component of the enzyme superoxide dismutase, which is present in the cytoplasm of cells and it is responsible for the conversion of the highly reactive superoxide radical to less reactive hydrogen peroxide and molecular oxygen, thus decreasing the toxicity of the reactive species [209], and act as cofactor of glutathione peroxidase [210].

Additionally, zinc modulates the antioxidant system by regulation of two important transcription factors, namely the nuclear factor Nrf2 and the responsive metal transcription factor 1 (MTF-1). In a zinc-dependent pathway, both transcription factors are part of the stress response to heavy metals, hypoxia and oxidative stress, which induce gene expression of several constituents involved in redox metabolism, as enzymes involved in glutathione biosynthesis, such as glutamate-cysteine ligase, and antioxidant enzymes, such as glutathione peroxidase, thioredoxin and thioredoxin reductase. Thus, zinc is able to modulate glutathione concentration and to neutralize free radicals [211, 212].

Zinc strongly induces metallothionein, which is a low-molecular weight cysteine-rich protein involved in zinc homeostasis and redox metabolism, through coordination of up to seven zinc atoms per molecule [213]. The cysteine thiolates of metallothionein react with oxidants and electrophiles with concomitant release of zinc. This effect may have a two-fold consequence in redox cellular state by working as an electrophile/oxidant scavenger or through antioxidant activity promoted by the release of physiological concentrations of zinc [213].

Lastly, zinc can compete with iron and copper at the binding sites in the cell membrane, owing to the similarities in their coordination chemistry, and thereby suppress their ability to catalyze the production of radicals from lipid peroxides. For example, competition of zinc with iron and copper leads to inhibition of the NADPH oxidase enzyme, another source of superoxide radicals [210].

In summary, physiological concentrations of zinc participate in the control of the production and elimination of reactive species and contribute to the proper functioning of the antioxidant defense system.

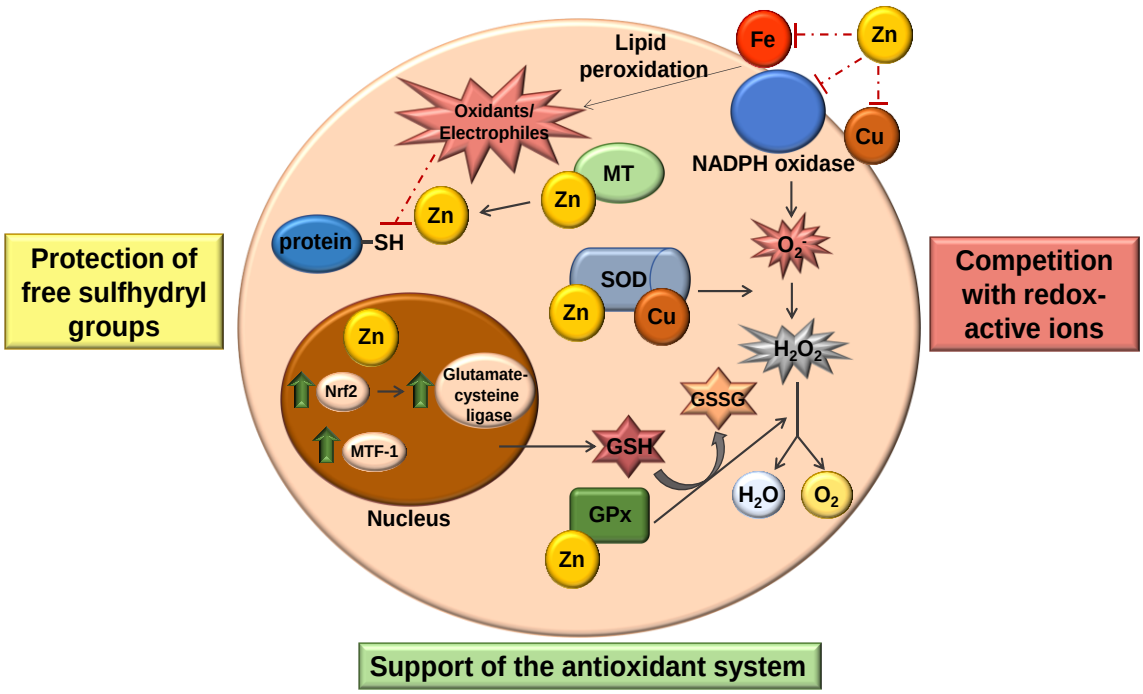

Figure 7. "Pro-antioxidant" mechanisms of zinc action.
Zinc supports the activity of antioxidant enzymes, such as superoxide dismutase (SOD) and glutathione peroxidase (GPx). Zinc regulates the expression of transcription factors MTF-1 and Nrf-2, inducing the gene expression of several constituents involved in redox metabolism, such as glutamate-cysteine ligase, therefore controlling the cellular concentration of glutathione (GSH) Moreover, zinc induces metallothionein (MT), an electrophile scavenger, and protects the sulfhydryl groups (-SH) from electrophilic attack. Lastly, zinc competes with redox-active ions, as iron (Fe) and copper (Cu), and inhibits NADPH oxidase, preventing the production of superoxide radicals (O_2^-) and reactive species from lipid peroxides. Adapted from [210]

3.3.2 Pro-oxidant effects of zinc

Zinc elicits oxidative stress above and below its physiological concentrations, generally resulting in cytotoxic, proinflammatory and pro-apoptotic outcomes [191].

Overall, zinc deficiency limits the efficiency of the antioxidant defense system, induces a global change in gene expression and leads to membrane damage in isolated organelles, protein and DNA, due to loss of protection from lipid peroxidation and response to stress [184, 214, 215].

Conversely, the perturbation of zinc homeostasis can lead to release of zinc above the physiological concentrations, which may have cytotoxic

consequences [216]. The “free” zinc increases uncontrolled interactions with proteins that can cause protein misfolding and aggregation, and the inherent pathological outcomes [217]. In addition, supraphysiological zinc levels can activate an inflammatory response, leading to production of reactive species and concomitant alterations of glutathione concentrations. Moreover, cellular accumulation of zinc is accompanied by homeostatic changes of other ions, such as potassium and calcium, which can induce mitochondrial and lysosomal dysfunction, interfering with energy metabolism and with signal transduction pathways that determine cell fate [218-220].

In summary, the cellular redox and zinc states are dynamic and strikingly connected, as zinc deficiency causes oxidative stress and oxidative stress affects cellular zinc metabolism. The interplay between redox and zinc biology has deep implications for physiology and for nearly all diseases associated with oxidative stress.

3.4 Pathophysiological implications of zinc

Zinc essentiality was established in 1961 for humans, when a zinc deficient dietary uptake was associated with a clinical syndrome consisting of growth retardation, anemia, hypogonadism and mental lethargy and subsequent amelioration of the symptoms was achieved with zinc supplementation [221]

Zinc is crucial in countless physiologic processes: zinc is essential in growth, brain development, immune function, tissue maintenance and wound healing [222].

Impairment of physical growth and development is one of the most studied clinical manifestations related to zinc deficiency. The underlying mechanisms are still not well understood, however its effect is significantly important during the periods of rapid growth such as embryonic development, infancy and puberty, during which, zinc requirements are the highest [223].

In the central nervous system, zinc plays essential roles in brain function either by regulating transcription factors and key enzymes involved in neuronal metabolism or by modulating the synaptic activity and neuronal plasticity. Therefore, chronic perturbations of brain zinc homeostasis have been related to the development of neurodegenerative diseases, such as Alzheimer’s disease,

Parkinson's disease and amyotrophic lateral sclerosis, and implicated in neuronal damage associated to traumatic brain injury. Zinc deficiency has been often associated with impaired cognitive function, behavioral problems and learning disability [224].

The immune system is highly proliferative, and therefore particularly vulnerable to zinc availability. Zinc affects cells involved in both innate and adaptive immunity, including monocytes, polymorphonuclear-, natural killer-, T- and B-cells. While acute zinc deficiency impairs the immune response, correlating with a higher risk of infections, chronic deficiency increases the production of pro-inflammatory cytokines and consequently, influences the outcome of several inflammatory diseases [225].

Additionally, the prostate, mammary and pancreatic glands are secretory tissues that have unique zinc requirements. These tissues store zinc in secretory vesicles and control its secretion in order to guarantee the amount of zinc necessary for biological processes. Therefore, abnormal zinc metabolism in these organs is associated with disorders such as diabetes, infertility and cancer [222, 226]. Moreover, a putative association between the altered expression of zinc transporters and cancer progression and metastatic phenotypes has been suggested, thus they have emerged as possible new targets for cancer therapy [187].

3.5 Causes of zinc deficiency

Zinc homeostasis is primarily regulated via the gastrointestinal system, by carrier-mediated absorption of exogenous zinc in the small intestine and by gastrointestinal secretion and excretion of endogenous zinc [227]. Nevertheless, zinc deficiency can be caused by different conditions, which include inadequate dietary intake, malabsorption syndromes and inflammatory diseases of the bowel, resulting in poor absorption and increased losses of zinc [222]. The prevalence of insufficient dietary zinc uptake is very high in developing countries, as well as in the elderly, even in industrialized countries [222].

Additionally, genetic zinc deficiency, which rarely occurs, is found during the infant stage and early childhood. In particular, genetic studies have

identified mutations in genes encoding zinc transporters that lead to zinc deficiency disorders, namely acrodermatitis enteropathica (AE) and transient neonatal zinc deficiency (TNZD) [228].

AE is an autosomal recessive disorder caused by mutations of the ZIP4 gene, resulting in an impaired absorption of zinc primarily in the small intestine, which leads to lower levels of zinc in plasma. In addition, as several cells in the body express ZIP4, impaired zinc availability can occur at the cellular level in various tissues. Given the diverse physiologic functions of zinc, AE presents multiple signs and symptoms. The classic clinical manifestations of AE are characterized by the appearance of skin lesions around the body orifices and on the extremities, alopecia and diarrhea, and other gastrointestinal dysfunctions. In advanced stages of the disease, patients may also experience growth delay, impaired wound healing, mental lethargy, anemia and hypogonadism [229]. Besides, zinc deficiency alters immunity, contributing to a higher predisposition to fungal and bacterial infection, which can further trigger severe systemic scenarios [230].

AE is fatal if zinc is not supplied, therefore zinc replacement therapy should be implemented and serum/plasma zinc levels should be periodically monitored. Theoretically, in the absence of a functional zinc transporter in the enterocytes, zinc supplementation will promote increased paracellular zinc absorption. Normally, clinical improvement is observed very rapidly, within days to weeks after starting the zinc therapy [229, 231].

Due to the characteristics of this zinc deficiency disease, cells from AE patients, which display decreased zinc uptake and content [232], can be used as a pathophysiological model to explore the importance of zinc availability in cell responses to (lip)oxidative stress. The fact that vimentin is expressed in different cell types in which a zinc-vimentin interaction could be pathophysiologically important, such as immune, neuronal and endothelial cells, makes the study of the interplay between zinc availability and the function of vimentin, a highly relevant objective.

AIMS AND OBJECTIVES

Vimentin is an intermediate filament protein typically expressed in mesenchymal cells, where it plays an important role in cell structure, division and response to injury and inflammation. Moreover, vimentin is a key sensor for oxidative or nitrosative stress, and is the target for lipoxidation by several electrophilic lipids.

Importantly, vimentin organization and function can be modulated by context factors, as the presence of certain divalent cations. Among them, zinc may interact with proteins, either by inducing specific conformations, supporting catalytic activity or stabilizing oligomeric associations. Earlier investigation performed by our group, unveiled a robust interaction between vimentin and zinc, both in vitro and in the cell environment.

Nevertheless, the mechanisms underlying the effect of lipoxidation on the organization of vimentin as well as the structural and functional consequences of the vimentin-zinc interplay and its impact on the response of vimentin to (lip)oxidative stress have not been totally elucidated.

Therefore, the following objectives were proposed:

- To set up reproducible refolding procedures yielding functionally competent vimentin preparations, suitable for the study of the effect of micromolar concentrations of electrophilic compounds and divalent cations.
- To explore the effect of the modification of vimentin by several lipoxidants in vitro, and its impact on assembly behavior and on the morphology of preformed filaments.
- To identify and characterize the mechanisms underlying the disruption of the vimentin network by electrophilic compounds in cells.
- To address the role of zinc on the assembly and organization of vimentin in vitro.
- To study the interplay between vimentin and zinc availability and its impact on the response of vimentin to (lip)oxidation in cells.

MATERIALS AND METHODS

1. Materials

Amicon ultrafiltration devices (10K cut-off) were from Millipore. PD-SpinTrap G-25 columns were from GE Healthcare. Slide-A-Lyzer MINI Dialysis devices (20K cut-off) were from Thermo. 96-well plates were from Falcon. Carbon support grids, MESH CF 400 CU UL, used for electron microscopy were from Aname. High precision cells made of Quartz SUPRASIL, 1 mm and 10 mm path length, used for circular dichroism (CD) and for turbidity experiments, respectively, were purchased from Hellma.

1.1 General reagents

1.1.1 Electrophoresis and Western Blotting reagents

Electrophoresis purity grade acrylamide, N,N'-methylenebisacrylamide, ammonium persulfate, N,N,N',N'-tetramethylethylenediamine, sodium dodecyl sulfate (SDS) and glycine were purchased from Bio-Rad. Tris(hydroxymethyl)aminomethane was from Merck. Sypro-Ruby used for total protein staining was obtained from Bio-Rad. Polyvinylidene fluoride Immobilon-P membranes were from Millipore. The enhanced chemiluminescence detection system was from Amersham Biosciences.

1.1.2 Cell culture reagents

Cell culture medium DMEM, DMEM without glucose, OPTIMEM used for cell transient transfections, as well as trypsin-EDTA were from Gibco Life Technologies. Fetal bovine serum was from Sigma or Biowest. Penicillin, streptomycin and geneticin G-418 antibiotics were from Invitrogen. Sterile plastic material for cell culture was acquired from Falcon (Corning). 35-mm glass bottom dishes (p35) for imaging of live cells were from MatTek Corp.

1.1.3 Other reagents

Recombinant hamster vimentin was from Cytoskeleton, Inc. Buffers, high purity salts and other reagents used for preparing solutions were mainly from Sigma and Merck. Milli-Q distilled water was obtained through a Millipore system. Lipofectamine 2000 was from Life Technologies. The bicinchoninic acid (BCA) Protein Assay Kit for measuring protein concentration in cell lysates was from Pierce. The polar extract of *E. coli* phospholipids was from Avanti Polar Lipids. Electrophilic lipids 15-deoxy-$\Delta^{12,14}$-prostaglandin J_2 (15d-PGJ_2) and its biotinylated analog, and 4-hydroxynonenal (HNE), were from Cayman Chemical. Hydroxynonenal-dimethyl acetate, sodium azide, dibromobimane (DBB), dimethylsulfoxide (DMSO), diamide and zinc chloride ($ZnCl_2$) were from Sigma. Biotin polyethyleneoxide iodoacetamide (Iac-B) was from Sigma or from Santa Cruz Biotechnology. Carbonyl cyanide 4-(trifluoromethoxy)phenylhydrazone (FCCP) and disuccinimidyl tartrate (DST) were from Santa Cruz Biotechnology. 1,6-bismaleimidohexane (BMH) and tris(2-maleimidoethyl)amine (TMEA) were purchased from Thermo Scientific. The reducing agent 1,4-Dithiothreitol (DTT) was obtained from Invitrogen Life Technologies. The luminescent ATP detection assay used to measure steady-state ATP concentrations was from Abcam.

1.2 Antibodies and reagents for protein labelling

Alexa Fluor 488 carboxylic acid succinimidyl ester dye used for protein labelling, as well as Phalloidin-Alexa 568 used for F-actin staining were from Molecular Probes, Invitrogen. Anti-vimentin antibodies used were mouse monoclonal V9 clone (sc-6260) and its Alexa 488 and agarose conjugates from Santa Cruz Biotechnology. Anti-actin and diamidino-2-phenylindole (DAPI) were from Sigma. Anti-HNE adducts antibody was from Calbiochem. Secondary antibodies, namely anti-mouse and anti-rabbit immunoglobulins conjugated to horseradish peroxidase (HRP) were from DAKO. Streptavidin-HRP was from GE Healthcare Life Sciences.

1.3 Previously generated plasmids

The GFP-vimentin wt and C328S constructs used for performing FRAP assays were previously generated and described in publications from the Pérez-Sala laboratory [34]. Briefly, full-length human cDNA vimentin (Origene) was cloned into the EcoRI, SmaI sites of pEGFP-C1 vector (Clontech) to obtain GFP-vimentin wt. Cysteine 328 was mutated to serine using the Quickchange XL site-directed mutagenesis kit from Stratagene and primers, forward 5'-GGTGCAGTCCCTCACC**TCT**GAAGTGGATGCCC-3' and reverse, 5'-GGGCAT CCACTTC**AGA**G GTGAGGGACTGCACC-3' to obtain GFP-vimentin-C328S.

For cell experiments, we have used SW13/cl.2 cells stably transfected with RFP//vimentin wt or RFP//vimentin C328S. These constructs were also generated before by Pérez-Sala's group [4]. From the above described plasmids, vimentin wt and C328S were subcloned into the EcoRI and BamHI sites of pIRES2-AcGFP1 and pIRES2 DsRed-Express2 bicistronic plasmids, obtained from Clontech, to yield constructs that express the fluorescent protein and untagged vimentin as separate proteins. This strategy allows monitoring cells expressing transfected vimentin.

2. Methods

2.1 Protein preparation and in vitro reconstitution

Recombinant human vimentin wt and C328S were purchased from Biomedal. This company performed a custom expression and purification procedure, based on solubilization from bacterial inclusion bodies by combined anion and cation-exchange chromatography, as described by Herrmann and colleagues [233]. After a two-step purification procedure, vimentin was obtained in 8 M urea, 5 mM Tris-HCl, pH 7.6, 1 mM EDTA, 10 mM β-mercaptoethanol, 0.4 mM PMSF. Protein concentration was estimated from its A_{280} nm, using an extinction coefficient of 22450 $M^{-1}cm^{-1}$.

Aliquots of the protein were kept at - 80ºC. In experimental descriptions, amino acid numbering for vimentin includes the initial methionine.

2.1.1 Protein dialysis

Dialysis of vimentin followed the standard refolding protocol [233]. Briefly, the human recombinant protein at 1 mg/ml in 5 mM Tris-HCl, pH 7.6, containing 8 M urea, 1 mM EDTA, 10 mM β-mercaptoethanol, 0.4 mM phenylmethylsulfonyl fluoride and approximately 150 mM KCl, was subjected to step-wise dialysis against 5 mM Pipes-Na pH 7.0, 1 mM DTT, containing 6 M urea, then 4 M urea, 2 M urea and no urea at r.t., for 1 h each, and finally, to two additional steps against 5 mM Pipes-Na, pH 7.0, 0.25 mM DTT, the last one for 16 h at 16ºC.

Bovine serum albumin (BSA) at 1 mg/ml in 5 mM Pipes-Na, pH 7.0 containing 1 mM EDTA was dialyzed against 5 mM Pipes-Na, 1 mM DTT, pH 7.0, with four buffer changes, for 1 h each, and, subsequently, into 5 mM Pipes-Na, 0.25 mM DTT, pH 7.0, with two changes.

2.1.2 Spin-column gel filtration and ultrafiltration

Gel filtration was performed using PD SpinTrap G-25 1 ml columns equilibrated with 5 mM Pipes-Na, 0.1 mM DTT, pH 7.0, before loading 140 μl samples of vimentin or BSA and eluting by centrifugation at 800 x g, according to the instructions of the manufacturer.

For ultrafiltration, BSA or vimentin samples (250 μl) containing 1 mM EDTA were diluted 10-fold with EDTA-free buffer, applied to Millipore Amicon Ultra filter units (10 K pore size) and centrifuged at 3000 x g for 15 min at 16ºC, which concentrated the samples down to their original volume. Then, samples were diluted again 10-fold with buffer without EDTA and the procedure was repeated.

2.2 Colorimetric estimation of EDTA concentration

The concentration of EDTA in the protein solutions was estimated through a colorimetric assay by monitoring its competition with 4-(2-pyridylazo)-resorcinol (PAR) for zinc binding. The binding of zinc to PAR forms a colored complex with absorbance at 492 nm. The effective dissociation constant (K_d) of

the $Zn(PAR)_2$ complex is 2.1 x 10^{-12} M^2 , at pH 7.0 [234, 235] . Since EDTA complexes zinc with higher affinity (K_d of 2.3 x 10^{-14} M at pH 7.4, [236]), its presence decreases the formation of $Zn(PAR)_2$ complex, thus decreasing the absorbance at 492 nm. A calibration curve was obtained by mixing samples containing 100 µM PAR and 10 µM $ZnCl_2$ with known concentrations of EDTA and measuring the absorbance at 492 nm, using a Varioskan Flash (Thermo) microplate reader. The amount of EDTA in the protein preparations was determined from their absorbance at 492 nm after incubation with 100 µM PAR and 10 µM $ZnCl_2$, and extrapolation using the calibration curve. Sample volumes of 1 to 10 µl were used in a typical total assay volume of 100 µl. Measurements were performed 5 min after mixing the reagents.

2.3 NMR analysis

NMR studies were performed with the help of The Nuclear Magnetic Resonance and Molecular Recognition group led by Professor F. Javier Cañada, mainly by Eva Martínez-Senra.

NMR spectra were acquired in a 500 MHz Bruker AVANCE NMR spectrometer equipped with a SEF 19F-1H probe or a 600 MHz Bruker AVANCE NMR spectrometer equipped with a cryogenic triple resonance TXI probe. For samples dissolved in deuterated buffer (20 mM deuterated Tris, Cambridge Isotope), spectra were acquired with a simple 90º pulse sequence (zg Bruker pulse sequence) and with 32 K data points and 2 second recovery delay and 10 ppm of spectral width centered at 4.7 ppm (chemical shift of residual deuterated water signal). For samples dissolved in non-deuterated buffers, a 10% (v/v) final concentration of deuterated water was added for locking the deuterium signal and the standard Bruker pulse sequence “zgesgp”, using excitation sculpting gradients for water signal suppression, was used. The spectra were acquired at 25ºC with 32 K points, 2 second recovery delay and 14 ppm of spectral width centered at 4.7 ppm (chemical shift of water). The spectra were acquired using from 8 to 2048 scans depending on the sample concentration; no line broadening was applied in the processing. Bruker TOPSPIN software was used for acquisition and processing of the spectra. For testing the pH dependence of the chemical shift signals of EDTA, samples of 1

to 3 mM EDTA, with and without cation (Ca^{2+}, Zn^{2+}, Mg^{2+} or La^{3+}), in 20 mM deuterated Tris were prepared at different pH (between 5 and 9) by acidification with deuterated hydrochloric acid. The actual pH was measured after the addition of the corresponding dichloride salt of each cation. EDTA and $ZnCl_2$ solutions were prepared in deuterated water.

2.4 Vimentin polymerization assay

Vimentin wt at 3.8 µM in 5 mM Pipes-Na, pH 7.0, was incubated with 150 mM NaCl, for 15 min at 37ºC or with the indicated concentrations of $ZnCl_2$ or $MgCl_2$ for 1 h at room temperature (r.t.). All samples were submitted to ultracentrifugation at 55000 rpm for 30 min at 4ºC. Aliquots of supernatants, containing soluble vimentin, and of the pellets with polymerized vimentin resuspended in Laemmli buffer, were analysed by SDS-PAGE, followed by total protein staining with Sypro Ruby and ultraviolet (UV) light detection.

2.5 In vitro modification of vimentin by oxidants and electrophiles

Modification of vimentin was assessed by gel-based assays. Briefly, vimentin at 3.8 µM in 5 mM Pipes-Na, pH 7.0, was incubated for 60 min at r.t. in the presence of the indicated compounds. DTT final concentration was kept below 0.2 mM. Incorporation of biotinylated prostaglandins was analyzed by SDS-PAGE followed by blot and biotin detection with HRP-streptavidin. HNE adduct formation was estimated by immunochemistry after SDS-PAGE and WB with an anti-HNE adducts antibody. The effects of diamide and of DMSO were assessed by electrophoresis under non-reducing conditions followed by protein staining with Sypro Ruby or by western blot (WB) with anti-vimentin antibody.

2.6 In vitro crosslinking assays of vimentin

Modification of vimentin by different crosslinkers was assessed by gel-based techniques. Vimentin at concentrations between 3 and 5 µM in 5 mM Pipes-Na, pH 7.0, 0.2 mM DTT, was incubated during 60 min, at r. t., in the presence of the indicated compounds. To evaluate the protective effect of the

different salts on vimentin crosslinking, the recombinant protein was preincubated with increasing concentrations of $ZnCl_2$, $MgCl_2$ or NaCl, as indicated in the figures, and then submitted to crosslinking with the different reagents. Equal volumes of the samples were run on 7.5% SDS-polyacrylamide electrophoresis gels and fixed with a solution of 40% (v/v) methanol/ 10% (v/v) acetic acid in H_2O, during 60 min. The gels were incubated with Sypro Ruby stain overnight with gentle agitation, protected from light. After washing with a solution of 10% (v/v) methanol, 6% (v/v) acetic acid in H_2O, the gels were visualized under UV light on a Gel-Doc XR Imaging System (Bio-Rad).

2.7 Electrophoresis and Western blotting

Incubation mixtures were denatured at 95ºC for 5 min in Laemmli sample buffer (80 mM Tris-HCl, pH 6.8; 2% (w/v) SDS, 10% (v/v) glycerol, 5% (v/v) β-mercaptoethanol and 0.15% (w/v) bromophenol blue) and were separated on 7.5 or 10% SDS-polyacrylamide electrophoresis gels and transferred to Immobilon-P membranes using a Bio-Rad Blot Semi-dry Transfer system and a Whatman filter-based method. Blots were blocked with 2% (w/v) non-fat dried milk and incubated with primary antibodies, typically at 1:500 dilution, and with HRP-conjugated secondary antibodies, at 1:2000 dilution, as described in [3, 4]. In all cases, the signal was obtained with the enhanced chemiluminiscence system (ECL), upon exposure of the blots to Agfa Curix film. Blots were quantified using Scion Image software (Scion Corporation MD, Frederick MD, USA).

2.8 Electron microscopy

For EM inspection of soluble oligomeric species, vimentin was prepared at 0.2 mg/ml in 5 mM Pipes-Na, pH 7.0, in the presence of DTT. Soluble vimentin samples were fixed by addition of 0.1% (v/v) glutaraldehyde, final concentration.

For EM observation of filaments, vimentin polymerization was induced by incubation with 150 mM NaCl, at 37°C. Time-dependent assembly of vimentin

was followed by fixing the mixtures at 5, 10, 60 and 120 min after addition of the polymerizing buffer.

Assessment of the effect of electrophilic compounds or divalent cations on vimentin assembly or preformed filaments was done by inducing vimentin polymerization by incubation with 150 mM NaCl for 1 h at 37ºC before or after treatment with electrophilic compounds or divalent cations for 1 h at 37ºC or r.t., as indicated. Assays were repeated at least three times and all incubation mixtures were processed in duplicate.

Drops of incubation mixtures were applied onto carbon support grids (MESH CF 400 CU UL, Aname), which were subsequently washed with water and stained with 2 % (w/v) uranyl acetate (Merck). Grids were inspected on a JEOL transmission electron microscope JEM-1230, equipped with a digital camera CMOS TVIPS TemCam-F416. EM images were processed with FIJI software for the measurement of width and length of vimentin oligomeric species and filaments. Filament width was determined using the “plot profile” plugin of straightened filaments. On average, 50 vimentin species were measured per experimental condition.

2.9 Circular dichroism

Far-UV CD spectra of vimentin wt at 5 µM in 5 mM Pipes-Na, pH 7.0, 0.2 mM DTT, were recorded in a JASCO J-810 spectropolarimeter equipped with a Peltier type cell holder (Jasco Corp.) in 0.1 cm path length cells. Ellipticities corrected for buffer contribution were converted to mean residue ellipticities using a mean molecular mass per residue of 113.

2.10 Turbidity experiments

Turbidity of solutions containing 5 µM vimentin wt or C328S in the presence of the indicated compounds was determined by measuring the absorbance at 350 nm, at r.t, using an Agilent Cary 60 UV-Vis spectrophotometer. Incubation mixtures (70 µl) were placed in Hellma absorption cuvettes and increasing amounts of $ZnCl_2$, $MgCl_2$ or NaCl were sequentially added to the mixture to achieve the indicated final concentrations,

and the absorbance was immediately measured. In the graphics, absorbance values corresponding to control (vimentin without $ZnCl_2$) were subtracted and were corrected accordingly to vimentin concentration and volume of the mixtures. For time-lapse monitoring, turbidity of vimentin was measured every 2 min, for a total of 26 min in the analysis of the reversibility of the effect of $ZnCl_2$, and for 16 min in the analysis of the effect of incubation with $ZnCl_2$ before or after addition of NaCl.

2.11 Protein labeling and fluorescence anisotropy

Vimentin wt and C328S were covalently labeled in the amino groups with a three-fold molar excess of Alexa Fluor 488 carboxylic acid succinimidyl ester dye [237]. After labelling, mixtures were loaded onto PD Minitrap G-25 columns in order to eliminate the free dye. The degree of labeling of vimentin, ranging between 0.2 and 0.9 moles of fluorophore per mole of protein, was estimated from the molar absorption coefficients of 22450 $M^{-1}cm^{-1}$ and of 71000 $M^{-1}cm^{-1}$, at 280 nm, for vimentin and for the dye, respectively. Aliquots of vimentin were stored at - 80°C, until assayed.

Unlabeled vimentin (1 µM) was mixed with a tracer amount of Alexa 488-labeled vimentin (50 nM) and were dispersed in Corning 96-well black microplates with different concentrations of $ZnCl_2$. Fluorescence anisotropy was monitored using a POLARstar Galaxy plate reader, at λ_{exc} = 485 nm and λ_{em} = 520 nm, at 26^{o}C.

2.12 Effect of zinc on the morphology of vimentin assemblies on different supports

For visualization on glass slides, a 5 µl aliquot of vimentin at 5 µM in 5 mM Pipes-Na (pH 7.0), 0.2 mM DTT, was placed on a glass slide, and 5 µl of vehicle, 200 µM, 500 µM or 2.5 mM $ZnCl_2$ (final concentrations) were added to the solution and gently mixed with the pipette tip. Next, a coverslip was placed on top of the mixtures and samples were visualized on a Leica SP2 confocal microscope using the differential interference contrast mode for image acquisition. For zinc detection, Zinquin, a fluorescent probe to detect both free

and protein-bound zinc, was added to the mixtures at 1 mM (final concentration). Zinquin fluorescence was detected by excitation with an ultraviolet laser at 351 and 364 nm, and emission between 450 and 520 nm was acquired.

For monitoring vimentin assemblies formed in solution, 80 µl aliquots of vimentin at 5 µM were incubated with different concentrations of $ZnCl_2$, in a flat-bottom microplate. The solutions were observed under a Zeiss optical inverted microscope coupled to an Axiocam ERc 5s camera, after 20, 40 and 60 min of incubation.

For observation of vimentin in microdroplets stabilized by *Escherichia coli* polar extract, phospholipids were dissolved in spectroscopic grade chloroform and kept at −20°C. Before use, a lipid film made by evaporating the chloroform under a nitrogen stream was resuspended in mineral oil to the final concentration by two cycles of vigorous vortexing plus 15 min sonication in a water bath. The solution containing a mixture of unlabeled vimentin wt (4 µM) and vimentin wt labeled with Alexa 488 (1 µM), in the absence or in the presence of 200 µM $ZnCl_2$, was vigorously mixed with *E. coli* lipids. The emulsions containing *E.* coli stabilized microdroplets surrounding the protein solution were applied on a glass slide and observed on a Leica SP2 confocal microscope.

2.13 Computational studies

The computational studies were performed by Joan Guzmán-Caldentey at the group of Computational Chemical Biology led by Dr. Sonsoles Martín-Santamaría.

2.13.1 Building of the vimentin models

PyMol software was used to build the 3D models from the vimentin X-ray structures available at the Protein Data Bank (PDB IDs 3KLT and 1GK4). PDBs 3KLT and 1GK4 structures share seven amino acids of its sequence, where C328 is located. One monomer of each PDB structure was kept and superimposed to the dimer from the other PDB by the overlapping region. Thus,

two vimentin dimer models comprising the region between D264 and G406, differing in the geometry, were constructed: 1GK4 superimposed to 3KLT model (model A) and 3KLT superimposed to 1GK4 model (model B). These starting vimentin dimers were subsequently used to build other models. All the studied models were submitted to molecular dynamics (MD) simulations.

2.13.2 Protein-protein docking

The two models of vimentin dimer from the Molecular Dynamics (MD) simulations were submitted to servers HADDOCK and ZDOCK to perform protein-protein docking. Several tetramers were obtained (as dimers of dimers), studied and submitted to MD simulations.

2.13.3 Molecular Dynamics simulations

MD simulations were carried out using Amber14. Eight steps of preparation were performed before running MDs. The first one consisted of 1000 steps of steepest descent algorithm followed by 7000 steps of conjugate gradient algorithm; a 100 $kcal \cdot mol^{-1} \cdot A^{-2}$ harmonic potential constraint was applied on the proteins and the ligand. In the four subsequent steps, the harmonic potential was gradually lowered respectively to 10, 5, and 2.5 $kcal \cdot mol^{-1} \cdot A^{-2}$ for 600 steps of conjugate gradient algorithm each time, and then the whole system was minimized uniformly. In the following step the system was heated from 0 to 100 K using the Langevin thermostat in the canonical ensemble while applying a 20 $kcal \cdot mol^{-1} \cdot A^{-2}$ harmonic potential restraint on the proteins and the ligand. The next step heated up the system from 100 to 300 K in the isothermal−isobaric ensemble under the same restraint condition as before. In the last step the same parameters were used to simulate the system for 100 ps but no harmonic restraint was applied. At this point the system was ready for the production run, which was performed using the Langevin thermostat under NPT ensemble, at a 2 fs time step. All production runs were performed for 100 or 150 ns. Zinc atoms were added to the system using Leap.

2.14 Cell culture

The following cell lines were used throughout this work and cultured as follows:

SW13/cl.2 human adrenal carcinoma vimentin-deficient cells were the generous gift of Dr. A. Sarriá (University of Zaragoza, Spain) [238]. SW13/cl.2 cells stably transfected with RFP//vimentin wt or RFP//vimentin C328S (RFP//vimentin wt and C328S cells, respectively) have been previously reported [4]. Cells were cultured in DMEM supplemented with 10% (v/v) fetal bovine serum and antibiotics (100 U/ml penicillin plus 100 μg/ml streptomycin). For maintenance of stably transfected cells, G-418 at 500 μg/ml final concentration was added to the culture medium.

Primary human fibroblasts from a control subject (AG10803) and from a patient with acrodermatitis enteropathica (AE) (ONIM entry 201100, cell line GM02814A) were obtained from the National Institute of General Medical Sciences (NIGMS) Human Genetic Cell Repository at the Coriell Institute for Medical Research (Candem, NJ), and were manipulated according to the instructions of the supplier. Cells were cultured in DMEM supplemented with 10% (v/v) fetal bovine serum and antibiotics (100 U/ml penicillin plus 100 μg/ml streptomycin).

2.15 Cell treatments

For immunofluorescence, SW13/cl.2 cells stably transfected with RFP//vimentin wt or RFP//vimentin C328S, grown on glass coverslips, were treated with vehicle or diamide, at 1 mM final concentration, for 5 or 15 min, as indicated, in the absence of serum. For glucose depletion, cells were washed with DMEM without glucose and cultured in this medium. In protection assays, cells were preincubated with DBB at 100 μM for 15 min, with 20 mM sodium azide for 15 min, 10 μM FCCP for 20 min, or 30 μM or 200 μM $ZnCl_2$ for 1 h, prior to the addition of 1 mM diamide.

Primary control fibroblasts (AG10803 cells) and primary fibroblasts from an AE patient (GM02814A cells), grown on glass coverslips, were preincubated

with H_2O or with 30 µM $ZnCl_2$ for 30 min, after which they were treated with vehicle (DMSO) or 10 µM HNE, for 2 h 30 min, in the absence of serum. At the end of the treatments, cells were washed with cold PBS, fixed and processed as detailed below.

2.16 Immunofluorescence

Cells were fixed with 4% (w/v) paraformaldehyde, permeabilized with 0.1% (v/v) Triton X-100, blocked with 1% (w/v) BSA in PBS and incubated with anti-vimentin-Alexa 488 at 1:200 dilution. After washing, cells were incubated with Phalloidin-Alexa 568 (Molecular Probes) for filamentous actin (F-actin) staining. All the procedure was carried out at r.t. Coverslips were mounted on glass slides with Fluorsave (Calbiochem). Images shown were acquired on Leica SP2, SP5 or AF6000 LX microscopes. Image analysis was performed with software from Leica (LasX) or from FIJI.

2.17 Transient transfection

Transient cell transfection was carried out at 80% cell confluence, using Lipofectamine 2000, following the instructions of the manufacturer. Briefly, 1 µg of total DNA, comprising RFP//vimentin wt (0.8 µg) plus GFP-vimentin wt (0.2 µg), and 3 µl of Lipofectamine, dissolved in OPTIMEM, were added to p35 dishes containing 1 ml of DMEM. Cells were incubated with this mixture for 5 h, after which, they were allowed to recover for 48 h in complete medium before performing FRAP assays.

2.18 FRAP assays

For fluorescence recovery after photobleaching (FRAP) assays, SW13/cl.2 cells cultured on p35 glass bottom dishes, transiently transfected with RFP//vimentin wt plus GFP-vimentin wt, as detailed above, were placed on a thermostatized chamber for observation on a Leica SP5 microscope, essentially as described previously [4] . Briefly, a pre-bleach image was taken,

after which, an area of 18 x 1.5 μm was bleached by three pulses of 488 nm laser power. Post-bleach single section images were acquired every 3 s for 5 min. Fluorescence recovery was registered and plotted in recovery graphs. A minimum of twenty FRAP assays were carried out per experimental condition.

2.19 Vimentin solubility experiments

The proportion of soluble and insoluble vimentin in cells was determined using a previously established protocol [239]. RFP//vimentin wt cells were treated with the indicated agents. At the end of the treatment, cells were lysed in 20 mM Tris-HCl, pH 7.4, 600 mM NaCl, 0.5 % (v/v) Triton X-100, 0.1 mM sodium orthovanadate and protease inhibitors (2 μg/ml each of leupeptin, aprotinin and trypsin inhibitor, and 1.3 mM Pefablock). Lysates were centrifuged at 12000 x g for 10 min at 4ºC. Aliquots from pellet (30 μl, insoluble vimentin) and supernatant (15 μl, soluble vimentin) fractions were separated by SDS-PAGE and vimentin content was assessed by western blot.

2.20 ATP measurements

The luminescent ATP detection assay (Abcam) was used to measure steady-state ATP concentrations. RFP//vimentin wt cells were seeded onto 96 well glass bottom plates (150 x 10^4 cells/well) and grown for 48 hours. Cells were treated with inhibitors of oxidative phosphorylation (20 mM NaN_3 for 15 min or 10 μM FCCP for 20 min), in the absence of glucose. ATP concentrations were determined in triplicate by luminescence measurement using a Varioskan Flash (Thermo) microplate reader according to the manufacturer's instructions.

2.21 Proteomic studies

Primary human fibroblasts from a control subject (AG10803 cells) and primary fibroblasts from an acrodermatitis enteropathica (AE) patient (GM02814A cells), grown on p100 dishes, were preincubated with H_2O or with 30 μM $ZnCl_2$ for 30 min, after which they were treated with vehicle (DMSO) or 10 μM HNE, for 1 h, in the absence of serum. At the end of treatments cells

were washed with cold PBS. Next, 1 ml PBS was added to each p100 dish and cells were scraped and transferred to an eppendorff tube. This procedure was repeated twice and cells were centrifuged at 1000 x g, 5 min at 4 °C. The supernatant was discarded and the pellets were kept at – 80 °C until assayed.

The proteomic analysis of control and zinc-deficient fibroblasts was performed in the University of Leipzig, as part of my secondment, in collaboration with the group of Dr. Maria Fedorova.

2.21.1 Protein extraction

Cell pellets were resuspended in lysis buffer (7 M urea, 2 M thiourea, 1 % (w/v) Na-deoxycholate in 50 mM Tris-HCl, pH 7.5). Samples were sonicated on ice using a Vibra-Cell tip sonicator (20 kHz, 1 min with on/off pulses of 5 s each, 40% amplitude; Sonics & Materials, Inc., Newtown, CT, USA) and centrifuged (20 min, 10,000 × g, 4 °C). Supernatants were collected and protein concentrations were determined by the Bradford assay, as described in the literature [240].

2.21.2 FASP digestion

Samples were processed by filter aided sample preparation (FASP) procedure using 30 K Microcon filtration devices (Millipore). Briefly, 50 µl aliquots of the total protein extracts were incubated with 100 mM DTT, during 1 h at 37ºC. The samples were loaded into the filtration device and centrifuged at 14000 x g for 30 min. The concentrates were diluted in the devices with 0.2 ml of urea solution (8 M urea, 0.1 M Tris-HCl, pH 8.5) and centrifuged again. After centrifugation, the concentrates were mixed with 0.1 ml of 50 mM iodoacetamide in urea solution and incubated in darkness at r.t. for 20 min, followed by centrifugation for 10 min. Then, the concentrate was sequentially diluted with 0.1 ml of urea solution and 0.1 ml of 0.05 M NH_4HCO_3 and concentrated again. The resulting concentrate of the total protein extract was incubated overnight at 37ºC with 1.2 µg of trypsin. Following digestion, peptides were collected in the filtrate by centrifugation for 10 min at 14000 x g at r.t and

diluted with 0.05 M NH_4HCO_3. Peptides from total protein extracts were diluted 1:2.5 in 3 % (v/v) aqueous acetonitrile.

2.21.3 LC-MS/MS

A nano-Acquity UPLC (Waters GmbH) was coupled online to a Linear Trap Quadrupole Orbitrap XL ETD mass spectrometer equipped with a nano-electrospray ionization source (Thermo Fischer Scientific). The precursor ion survey scans were acquired at an orbitrap (resolution of 60,000 at *m/z* 400) for an *m/z* range from 400 to 2000. CID-tandem mass spectra (isolation width 2, activation Q 0.25, normalized collision energy 35%, activation time 30 ms) were recorded in the linear ion trap by data-dependent acquisition for the top six most abundant ions in each survey scan, with dynamic exclusion for 60 s, using Xcalibur software (version 2.0.7).

2.21.4 Database search

The acquired tandem mass spectra were searched against the Uniprot *Human reviewed* database using Sequest search engine (Proteome Discoverer 1.4 and 2.2, Thermo Scientific), allowing up to two missed cleavages and a mass tolerance of 10 ppm for precursor ions and 0.8 Da for product ions. Oxidation of methionine and carbamidomethylation of cysteine were used as variable modifications. Only protein identifications with a protein score ≥ 10 and a minimum of 3 peptides per protein with peptides ranked on position 1 and charge-dependent scores (Xcorr ≥ 2.0, 2.25, 2.5, and 2.75 for charge states 2, 3, 4, and 5) were considered.

2.21.5 Label-free relative quantification

Label-free relative quantification was performed using Progenesis QI for proteomics (Nonlinear Dynamics), using LC-MS data from three biological replicates analyzed in three technical replicates. Only peptides showing regulation with p-value < 0.05, by the one-way analysis of variance (ANOVA), were considered for further analysis. As control and zinc-deficient fibroblasts

were obtained from individuals with different age, namely 22 years and 6 months-old, respectively, the protein levels were compared individually within each cell model and no comparisons were made between models.

2.22 Statistical analysis

All experiments were performed at least three times. Unless indicated, results are presented as average values ± standard error of mean (SEM). Statistical analyses were carried out using GraphPad Prism 5. For comparisons of different sets of values the Student's *t*-test was used. Differences were considered significant for $p<0.05$. For comparison of multiple data sets ANOVA followed by Tukey's post-test was used. Whenever a statistically significant difference was found, it is indicated on the graphs. Although these types of statistical analyses are not commonly applied to biophysical techniques, we have used them for consistency of the interpretation of the results.

RESULTS

1. Refolding and validation of vimentin functionality

Vimentin is a key sensor for oxidative or nitrosative stress, and is the target for lipoxidation by several electrophilic lipids. Cysteine 328 represents a common site for electrophile addition and it can work as a modulator of vimentin assembly properties and behavior towards (lip)oxidative stress. Therefore, vimentin assembly, the effect of (lip)oxidation and the importance of C328 will be addressed in this study.

Consequently, parallel experiments were executed with wild-type vimentin (vimentin wt) and a vimentin mutant with cysteine 328 substituted by a serine residue (vimentin C328S), which demanded careful and reproducible preparation techniques for both protein forms. Moreover, in order to explore the interaction with divalent cations, appropriate methods had to be set up to remove metal chelators, in order to ensure the accurate interpretation of the results.

1.1 Detection of EDTA in protein samples by NMR

In order to study the effect of micromolar concentrations of divalent cations on vimentin behavior, it was necessary to assess the presence of metal chelators, such as EDTA, used during purification of the protein.

NMR methods have been employed to detect EDTA and quantitate metals in human blood [241, 242]. Similarly, we set up a procedure using ^{1}H NMR to analyze the presence of EDTA, using zinc to generate a diagnostic complex, in vimentin samples, commercial lyophilized vimentin and dialyzed vimentin. Upper panel of figure 8 shows a 500 MHz 1D-^{1}H NMR spectrum of a commercial sample of vimentin. Commercial vimentin is a lyophilized preparation and it needs to be reconstituted in water. Analysis of reconstituted vimentin ^{1}H NMR spectrum revealed the presence of a substantial amount of EDTA, assigned as the chelate formed between EDTA and 150 µM $ZnCl_2$, together with signals corresponding to sucrose, a stabilizer present in the sample, and to Pipes-Na buffer. Corroborating the presence of EDTA complexed with Zn^{2+} in vimentin samples, the middle panel of figure 8 shows

the reference proton spectrum of this complex, where the two coupled doublets at 3.25 and 3.32 ppm (2JHH = 17.3 Hz) correspond to the AB spin system of the methylene protons of the four acetyl groups, non-equivalent due to the structure of the metal chelate, and the singlet at 2.79 ppm corresponds to the four equivalent protons of the ethylenediamine moiety. As presented in the lower panel of figure 8, free EDTA gives two singlet peaks, the one at low field corresponding to the 8 methylene protons of acetyl moieties and the one at high field to the 4 protons of the ethylenediamide moiety. These free EDTA peaks are strongly dependent on the pH of the sample, whereas the peaks of the EDTA-zinc complex do not change [243]. Therefore, we have considered the characteristic pattern of the shifts of the signals given by the EDTA-zinc complexes as the most reliable and specific way of detection of this metal chelator in protein samples.

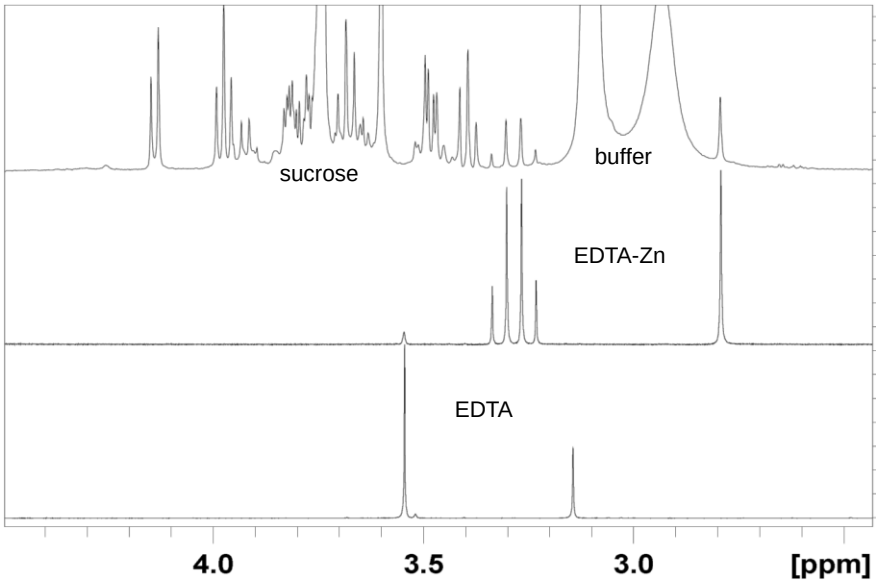

Figure 8. Detection of EDTA by NMR analysis.
Upper panel: 500 MHz 1D-^{1}H NMR spectrum of a commercial sample of vimentin (0.7 µM) with 150 µM $ZnCl_2$. Sucrose and Pipes-Na buffer proton signals are identified. The ^{1}H-NMR spectrum also displays an additional singlet at 2.79 ppm and two coupled doublets at 3.25 and 3.32 ppm. Middle panel: reference proton spectrum of EDTA complexed with Zn^{2+}, which is detailed in the text. Lower panel: reference proton spectrum of EDTA at pH 7.2.

1.2 Design of a colorimetric procedure to quantitate EDTA

In order to confirm the presence of EDTA and quantitate its levels in protein samples after dialysis, a colorimetric assay as described in Methods was designed, taking advantage of the ability of EDTA to compete with 4-(2-pyridylazo)-resorcinol (PAR) for zinc binding. This competition allows performing a titration to obtain the EDTA concentration in the dialysates (fig. 9)

This method demonstrated that samples of vimentin or bovine serum albumin (BSA) initially containing 1 mM EDTA still retained ~ 450 µM EDTA after dialysis, corroborating the values determined by NMR. Not discarding the possible competition of PAR with other metal-binding biomolecules, this technique was revealed to be an easy and convenient method for EDTA determination in protein preparations.

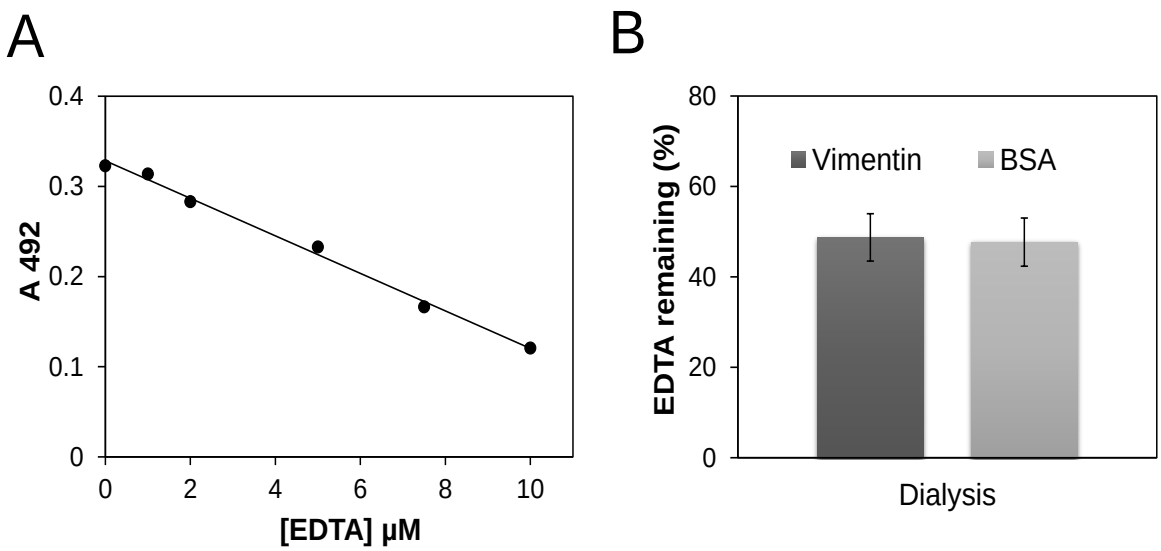

Figure 9. Colorimetric assay to quantitate EDTA in protein samples.
(A) Calibration curve obtained by the absorbance values at 492 nm of mixtures containing EDTA, at the indicated concentrations, with 100 µM PAR and 10 µM $ZnCl_2$. (B) Determination of EDTA remaining after dialysis of vimentin and BSA, using the calibration curve. The initial EDTA concentration in both samples was 1 mM. Results are mean values ± standard deviation of 4 assays.

1.3 Procedures to remove EDTA from protein preparations

After optimizing and validating this EDTA detection method, we applied it to search for an efficient procedure to remove EDTA from vimentin. As detailed

in figure 10A, we assessed the presence of EDTA in BSA and vimentin preparations after dialysis followed by gel filtration, ultrafiltration, or ultrafiltration plus dialysis. As shown in the bar graph, protein dialysis followed by spin-column gel filtration was insufficient, since ~ 200 µM EDTA still remained in the preparations.

Ultrafiltration allowed the repetitive dilution of the protein samples with EDTA-free buffers, followed by centrifugation which permitted controlling protein concentration. This method used alone was able to reduce EDTA concentration below 10 µM, as determined by the PAR competition assay, and below the detection limits of NMR (fig. 10B). Ultrafiltration followed by dialysis turned out to be even more efficient, allowing EDTA removal to concentrations below 5 µM. These virtually undetectable EDTA levels remaining in vimentin preparations allowed the execution of the intended assays in the presence of micromolar concentrations of divalent cations.

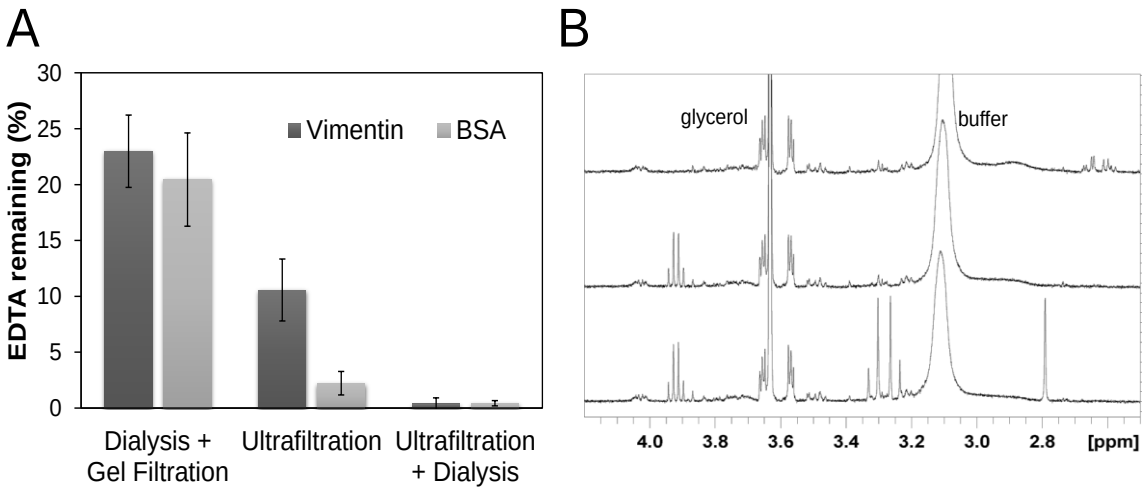

Figure 10. Efficiency of different methods to remove EDTA.

(A) Colorimetric detection of EDTA present in protein samples after diverse purification procedures using the PAR competition assay. Results shown are mean ± standard deviation of 4 (dialysis plus gel filtration), 2 to 7 (ultrafiltration), or 3 to 7 (ultrafiltration plus dialysis) assays.

(B) NMR analysis. Upper panel: 600 MHz 1D-^{1}H NMR spectrum of an ultrafiltrated vimentin sample (1.8 µM final concentration). Signals of buffer and additives used in the purification (glycerol, from the ultrafiltration filters) are observed. Middle panel: The same sample analyzed was monitored again after addition of 150 µM of $ZnCl_2$. A quadruplet that appears at 3.92 ppm corresponds to trifluoroethanol added as reference. Lower panel: NMR analysis of the sample after addition of 20 µM EDTA. The signal pattern of the AB system at 3.32 and 3.25 ppm and the singlet at 2.79 ppm corresponding to the Zn^{2+}-EDTA chelate are clearly visible.

1.4 In vitro reconstitution of vimentin

Both preparations of vimentin wt and C328S were obtained in 8 M urea, 5 mM Tris-HCl, pH 7.6, 1 mM EDTA, 10 mM β-mercaptoethanol, 0.4 mM PMSF. In such conditions, vimentin is mostly present in the soluble and unfolded form. Therefore, we focused in designing an effective method to refold vimentin into a functional protein, which required eliminating EDTA and gradually removing urea. Taking into account that ultrafiltration followed by dialysis was found to be the most effective method to remove EDTA, we employed the procedure summarized in figure 11 [243].

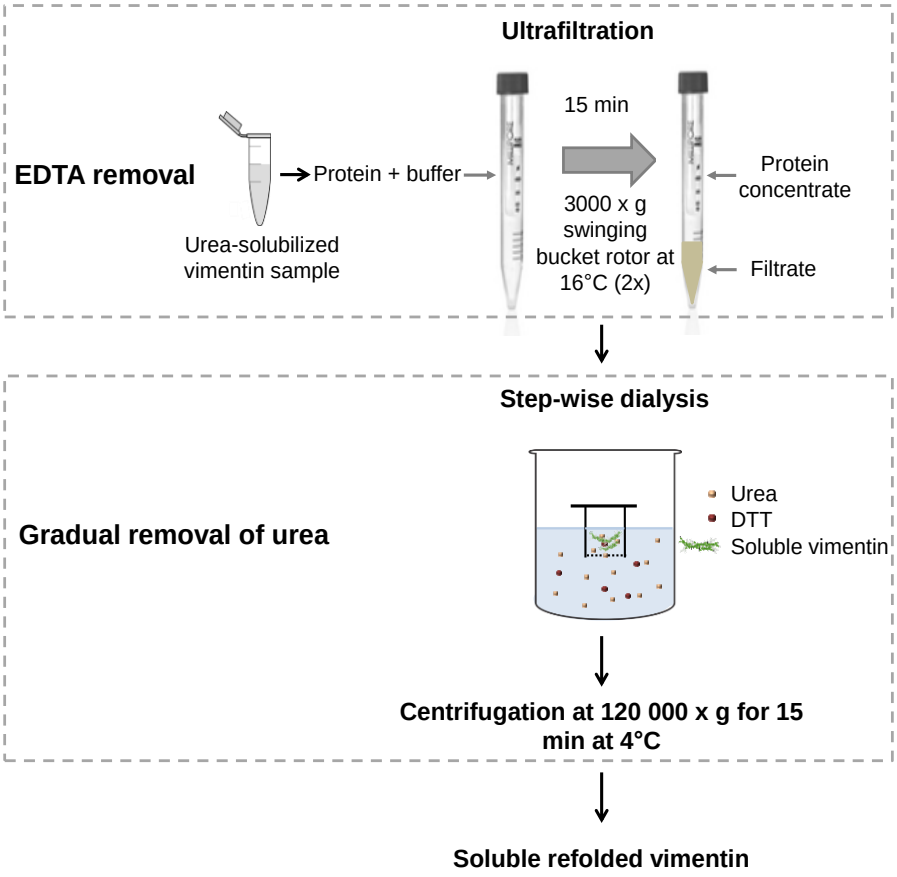

Figure 11. Procedures for in vitro refolding of vimentin.
Urea-solubilized vimentin was diluted with EDTA-free buffer, applied to Millipore Amicon Ultra filter units (10 K pore size) and centrifuged at 3000 x g for 15 min at 16°C, for concentration to its original volume. Then, samples were diluted again 10-fold with EDTA-free buffer and the procedure was repeated. The retained volume of vimentin sample was transferred to Slide-A-Lyzer MINI Dialysis devices (20 K cut-off) and submitted to six steps of dialysis gradually decreasing urea concentrations, as described in Methods. Finally, the resulting vimentin preparation was centrifuged at 120000 x g for 15 min at 4°C, and the supernatant containing soluble refolded vimentin was stored at -80°C.

1.5 In vitro validation of vimentin functionality

Validation of the structure and function of the vimentin preparation resulting from the above procedures is a critical point before starting the planned experiments (fig. 12).

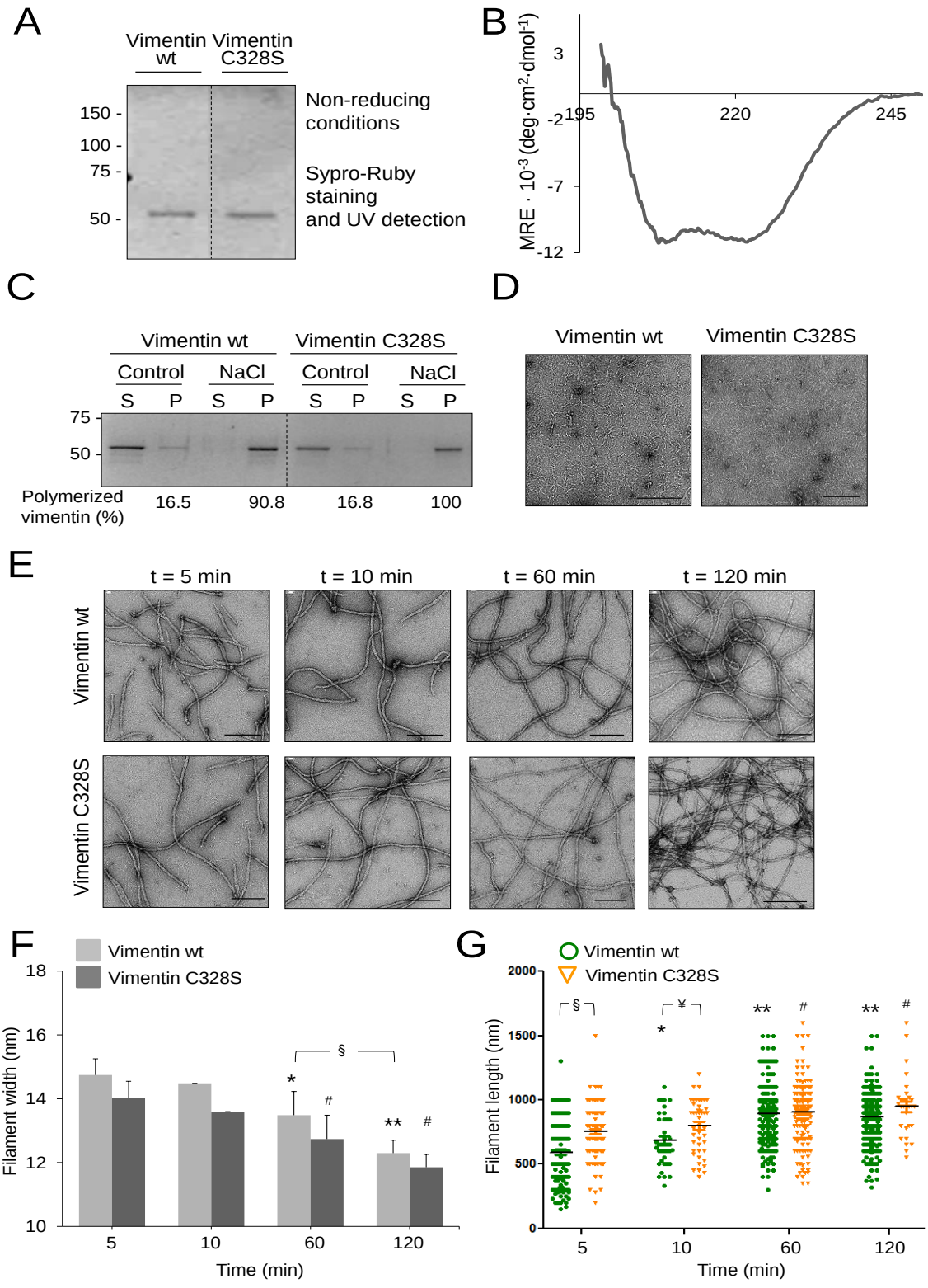

Figure 12. In vitro validation of vimentin functionality.
(A) Vimentin wt and C328S analysis by SDS-PAGE under non-reducing conditions followed by total protein staining with Sypro Ruby. (B) Far-UV CD spectrum of vimentin wt in 5 mM Pipes-Na, pH 7.0, approximately 0.2 mM DTT. (C) Polymerization assay performed by incubation of vimentin wt or C328S at 3.8 µM in the presence of 150 mM NaCl during 15 min at 37ºC, in 5 mM Pipes-Na, pH 7.0, 0.2 mM DTT. All samples were submitted to ultracentrifugation, after which, supernatant (S) and pellet (P) containing soluble and polymerized vimentin, respectively, were assessed by SDS-PAGE. The proportion of polymerized vimentin was determined by image scanning and is displayed below the plots. Results are representative of five assays. (D) Analysis of vimentin structures by electron microscopy (EM). Soluble vimentin WT or C328S were processed and visualized by EM at 50000-fold magnification. (E) EM inspection of vimentin filaments obtained by incubation with 150 mM NaCl for different times, as specified. Filament width (F) and length (G) were measured using FIJI software. It is important to clarify that measurement of filament length was limited by the EM field; although some filaments can reach longer lengths, the values registered in the graph correspond to the length observed in a single field. Results shown are mean ± SEM of 50 to 200 filaments per condition (F): *p<0.05 and **p<0.001 vs vimentin wt at 5 min, #p<0.05 vs vimentin C328S at 5 min, §p<0.05 as indicated); (G): *p<0.05 and **p<0.0001 vs vimentin wt at 5 min, #p<0.05 vs vimentin C328S at 5 min, §p<0.0001 and ¥ p<0.05 as indicated, by unpaired Student's *t*-test). Scale bars are 200 nm.

Vimentin wt and vimentin C328S were first assessed by gel-based techniques (fig. 12A). Total protein staining with Sypro-Ruby revealed a band with an electrophoretical mobility of approximately 53 kDa, suggesting that both forms of vimentin exist as monomers, under denaturing conditions. In non-reducing conditions, we appreciated the absence of other oligomeric species which pointed out that the presence of the reducing agent dithiothreitol (DTT), at a concentration at or below 0.2 mM, was sufficient to prevent the formation of the typical oxidative dimer resulting from the disulfide bond of the cysteine residues, described previously [8], thus preserving this residue in its reduced form when stored at -80°C.

Circular dichroism (CD) spectroscopy of the far- and near-UV regions has been used in studies exploring the assembly mechanism and the structural integrity of type III intermediate filaments [244, 245]. Thus, we recorded the near-UV CD signals of soluble vimentin wt in 5 mM Pipes-Na, pH 7.0, 0.2 mM DTT, where it is expected to exist as a mixture of oligomeric species (fig. 12B) [48, 51]. The CD spectrum revealed one broad negative band, which is characteristically given by the significant intertyrosine coupling between

tyrosines and phenylalanines that are predicted to be in the position “a” and “d” of the heptad repeat of the rod domain coiled-coil of vimentin [246]. This confirms that after refolding procedures, ultrafiltrated and dialyzed vimentin is mostly organized as a coiled-coil alpha-helical structure, which is in good agreement with what was previously described [244, 247].

In low ionic strength buffer, vimentin exists as soluble oligomeric species and these complexes form bona fide IFs when the ionic strength is increased [48]. Vimentin filaments are readily pelletable by ultracentrifugation. As demonstrated in figure 12C, both vimentin wt and C328S polymerized upon addition of 150 mM NaCl, and more than 90 % of the total protein was recovered in the pellet under the polymerization conditions, while, in the hypotonic buffer, the proportion of polymerized protein was approximately 16 % of the total protein.

Inspection of negatively stained vimentin structures by electron microscopy (EM) revealed that soluble vimentin appeared in a homogeneous pattern of small rod-like structures of 2-5 nm width and variable length, together with fibrils and occasionally, some protein aggregates (fig. 12D). The vimentin rod-like structures likely correspond to the first stable soluble oligomers found in vitro after reconstitution in a urea-free buffer, which are mostly vimentin tetramers, as previously described [51, 248].

Time-dependent assembly of vimentin was followed at 5 min, 10 min, 60 min and 120 min after addition of 150 mM NaCl by EM (fig. 12E). As described earlier, vimentin assembly occurs in three steps: within the first seconds, soluble vimentin tetramers laterally associate to form unit-length filaments (ULFs); between the first and fifth minute of assembly, ULFs longitudinally anneal to form loosely packed filaments which finally undergo a radial compaction process to form IFs of width around 12-13 nm [59]. Therefore, EM images illustrated in figure 12E depict vimentin structures corresponding to the longitudinal annealing phase and to the time dependent radial IF compaction process.

At early polymerization time points (5 min), both vimentin wt and C328S formed filaments of nearly normal appearance, of approximately 14 nm of width and mean filament length of 500 nm and 700 nm, respectively. At later polymerization times, filament width suffered a gradual and time-dependent

decrease while filament length increased, consistent with the elongation and radial compaction phases. At all time points monitored by EM, vimentin wt filaments showed a slightly wider diameter compared to vimentin C328S filaments, reaching 12.3 and 11.8 nm of diameter, respectively. Regarding the elongation process, vimentin C328S filaments were significantly longer than wt at 5 and 10 min, suggesting a faster assembly and highlighting a role of the residue at the 328 position in the assembly process.

In summary, combination of these distinct techniques validated the ultrafiltration process followed by dialysis as an effective method to remove EDTA and to renature vimentin in a functional state able to form structures consistent with those reported in the literature. Additionally, our results revealed for the first time subtle differences between the polymerization behavior of vimentin wt and C328S that should be the object of future studies.

2. Characterization of vimentin as target for lipoxidation and oxidation

As mentioned before, vimentin is a target for modification by several oxidants and electrophiles, a phenomenon referred here as (lip)oxidation, which induces an intense remodeling of its cellular network. Nevertheless, information on the impact of (lip)oxidation on filament assembly and structure is scarce. Once reproducible refolding methods had been set up yielding functionally competent vimentin, the morphological variations and putative mechanisms of its modification by various lipoxidants in vitro and in cells could be addressed.

2.1 In vitro modification of vimentin by oxidants and electrophiles

Vimentin modification by several electrophiles and oxidants (fig. 13A) was first assessed in vitro. The cysteine residue at position 328 is highly susceptible to oxidation and a common site for electrophile addition. Therefore, we have explored the role of this residue in the impact of vimentin (lip)oxidation by performing parallel experiments in vimentin wt and C328S (fig. 13).

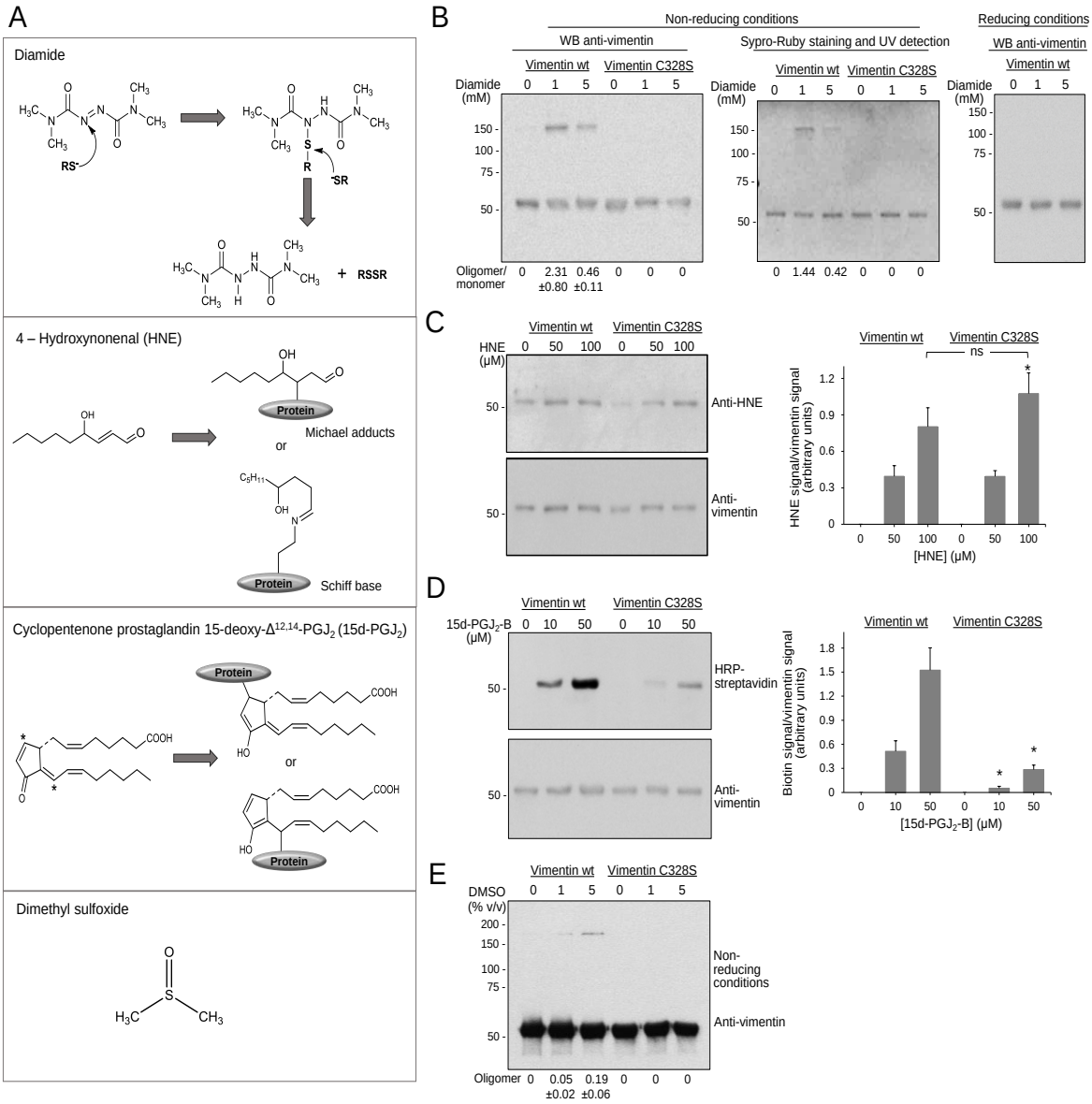

Figure 13 Lipoxidants induce in vitro modification of vimentin.

(A) Structures of the electrophilic compounds (lipoxidants) used and their mechanisms of reaction with proteins. Diamide reacts with thiol groups of proteins through its diazenecarbonyl moiety, a two-step reaction between thiolate anion and the diazene double bond yielding a disulfide and a hydrazine. 4-Hydroxynonenal (HNE) modifies proteins through two mechanisms: via Michael addition to a nucleophile by the active alkene bond or through Schiff's base formation by reaction of the aldehydic group with an amino group of the protein. The cyclopentenone prostaglandin 15-deoxy-$\Delta^{12,14}$-PGJ_2 (15d-PGJ_2) reacts with proteins by forming Michael adducts through its electrophilic carbon atoms, marked with asterisks. The structure of DMSO is represented. (B) Diamide promotes disulfide-crosslinked oligomers of vimentin. Purified vimentin wt or C328S (3.8 μM), as indicated, was incubated in the presence of 1 or 5 mM diamide for 1 h at r.t. Incubation mixtures were subjected to SDS-PAGE under non-reducing or reducing conditions and vimentin oligomeric species were inspected either by Sypro-Ruby staining followed by UV detection or by western blot (WB). The proportion of oligomer versus monomer was determined by image scanning.

(C) Modification of vimentin by HNE. Purified vimentin wt or C328S was incubated with vehicle (DMSO, 5 % v/v) or HNE at 50 or 100 μM for 1 h. Western blot with an anti-HNE adducts and vimentin antibodies was performed to estimate the levels of HNE adduction and vimentin, respectively. The signal from the anti-HNE antibody after subtraction of the background value (vehicle), was corrected by the vimentin level. (D) Modification of vimentin by biotinylated 15d-PGJ_2. Vimentin wt or C328S was incubated in the presence of vehicle (DMSO, 5 % v/v) or the biotinylated analog of 15d-PGJ_2 (15d-PGJ_2-B) at 10 or 50 μM for 1 h. Incorporation of 15d-PGJ_2-B was assessed by detection of the biotin signal on blots with HRP-conjugated streptavidin. Vimentin levels were monitored by western blot. (E) Vimentin wt or C328S was incubated in the presence of the indicated concentrations of DMSO (v/v), for 1 h and the formation of disulfide-bonded oligomeric species was monitored by SDS-PAGE under non-reducing conditions and western blot. The levels of oligomer were estimated in overexposed films by image scanning. The size of the molecular weight standards used (in kDa) is given at the left of the blots. All experiments were executed at least three times and average values of the determinations ± SEM are shown either in the graphs or below the blots. (*$p<0.05$ vs the indicated conditions in panel C or vs the same condition for vimentin wt in panel D by Student's t-test).

Diamide is an oxidant able to promote disulfide bond formation between thiol groups of cysteine residues (fig. 13A) [249]. Treatment of vimentin wt with diamide induced the formation of an oxidative dimer of an apparent molecular weight of 150 kDa, as revealed by SDS-PAGE under non-reducing conditions, followed by either western blot with anti-vimentin antibodies or total protein staining with Sypro-Ruby. As reported previously by Rogers and colleagues, this dimer also occurs upon cysteine crosslinking and it has a particularly low electrophoretical mobility due to the presence of an elevated percentage of α-helix within the protein [8]. On the other hand, this oxidative dimer was not detected in vimentin C328S or under reducing conditions, indicating that it was due to disulfide crosslinking between the cysteines (fig. 13B).

HNE is able to react either through Michael addition with various nucleophilic residues or by Schiff base formation with amino groups (fig. 13A). In this experiment, HNE adducted to vimentin was detected by western blot using an anti-HNE adducts antibody [250]. As shown in figure 13C, both vimentin wt and C328S were similarly modified by HNE in a concentration-dependent manner, consistent with the fact that HNE is not a cysteine-specific lipoxidant.

The biotinylated derivative of the cyPG 15d-PGJ_2 (15d-PGJ_2-B) covalently binds vimentin, mainly through its cysteine residue (fig. 13A) [4]. Vimentin was treated with two different concentrations of 15d-PGJ_2-B, the incorporation of which was evaluated by SDS-PAGE followed by detection with HRP-streptavidin (fig. 13D). Monitoring the biotin signal showed a progressive modification of vimentin wt with increasing concentrations of this electrophilic prostaglandin. Likewise, vimentin C328S was modified when incubated in presence of 15d-PGJ_2-B, but to a lower extent. This might be due to the ability of these electrophilic prostaglandins to form adducts with residues other than cysteine, such as histidine, as reported previously for a structurally related Δ^{12}-PGJ_2 [251].

These electrophilic compounds, except diamide, were dissolved in dimethyl sulfoxide (DMSO), as vehicle. It is known that DMSO may interact with L-cysteine leading to the oxidative formation of an L-cystine [252]. Taking into account this report, we have also explored the effect of different concentrations of DMSO on vimentin oxidation (fig. 13E). Under non-reducing conditions, we observed the concentration-dependent appearance of a faint band at approximately 150 kDa. This oligomer was detected in vimentin wt, but it did not occur in vimentin C328S, which suggests that DMSO is able to induce oxidative cysteine crosslinking of vimentin.

Altogether, these results identify vimentin as target for several electrophilic compounds, which may result in the formation of adducts or oxidative cysteine-crosslinked dimers.

2.2 Effect of lipoxidation/oxidation on the assembly of vimentin in vitro

Electrophilic modification of vimentin may have functional consequences, for instance on its ability to properly assemble into long and well-compacted filaments. This possibility was explored by EM observation of vimentin preincubated with the indicated reactive compounds followed by polymerization with the assembly buffer (fig. 14).

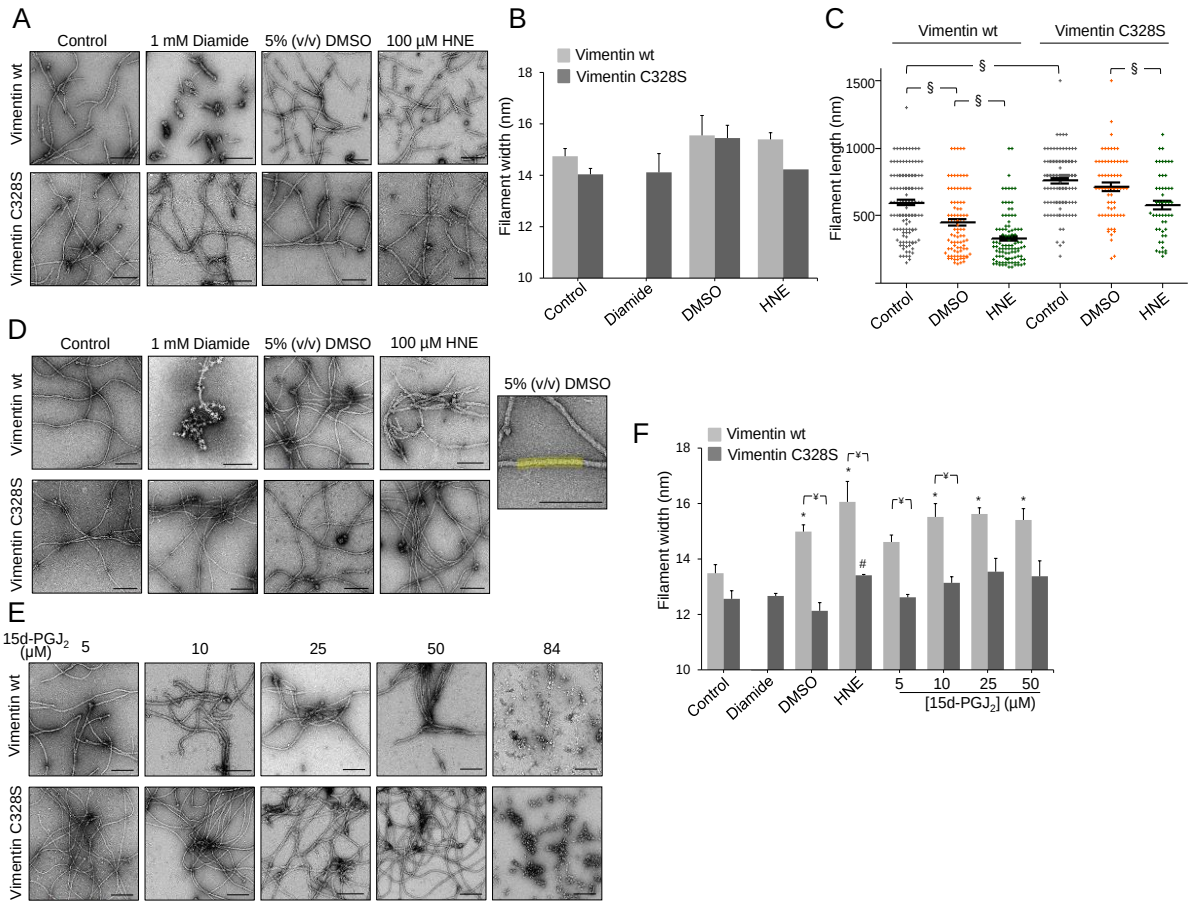

Figure 14. (Lip)oxidation effect on in vitro vimentin assembly.

Purified vimentin wt or C328S was preincubated with 1 mM Diamide, 5% (v/v) DMSO or 100 µM HNE for 60 minutes (A) and (D) or with increasing concentrations of 15d-PGJ_2 (E), after which, polymerization was promoted by incubation with 150 mM NaCl (final concentration), for 5 min (A) and for 60 min (D). Aliquots of the incubation mixtures were processed as detailed in Methods and filaments were visualized by EM. Images shown are representative of at least three independent assays with similar results. (B) Filament width was measured as the average thickness of segments of at least 100 nm, as illustrated in the right panel in D, and compiled in the graphs for 5 min (B) and for 60 min of polymerization (F). In (C), the length of filaments measured within the EM image field is represented in the scattered plot. A p value < 0.001 was obtained for comparison between all experimental conditions by ANOVA followed by Tukey's post-test, except for vimentin C328S control vs DMSO, and vimentin wt control vs vimentin C328S HNE (non significant). In the figure, only the differences between some of the conditions are marked for clarity (§ p<0.001). The results presented in (F) are average values from at least 60 individual filaments per experimental condition ± SEM (*p<0.05 vs control, # p<0.05 vs DMSO, ¥ p<0.05 vimentin wt vs vimentin C328S by unpaired Student's *t*-test). Scale bars are 200 nm for (A), (D) and (E) and 100 nm for the right panel in (D).

Under these conditions, 5 min after inducing polymerization, vimentin wt preincubated in hypotonic buffer formed filaments of normal appearance (fig. 14A). These filaments presented an average width of 14.7 ± 0.3 nm and a mean length of approximately 600 ± 21 nm, as quantitated in the graphs displayed in figure 14B and 14C, suggesting that at this time point, they were not completely elongated and compacted. In sharp contrast, preincubation with the oxidant diamide severely disrupted vimentin wt assembly (fig. 14A), leading to the formation of polymorphic aggregates and short incipient filaments.

DMSO was used as vehicle for lipid electrophiles. Since we have observed that DMSO is able to induce the formation of an oxidative dimer, we also explored its effect on vimentin assembly by EM (fig. 14A). At 5 min of polymerization in the presence of 5% DMSO (% v/v), vimentin wt was able to form filaments, although shorter and wider than control ones (average width ~15.5 nm). On the other hand, preincubation of vimentin wt with 100 µM HNE revealed it to be more deleterious than its vehicle (DMSO), since the mean length of HNE-pretreated filaments suffered a decrease of 27% compared to the length of DMSO-pretreated ones (fig. 14A). Taken together, these observations suggest that electrophilic compounds affect filament elongation or end-to-end annealing at early times of polymerization.

Remarkably, assembly of vimentin C328S was less susceptible to preincubation with electrophilic compounds (lower images in fig. 14A). In the control condition, vimentin C328S filaments displayed longer mean length and, in general, they presented a more compacted morphology, exhibiting an average width slightly thinner than vimentin wt filaments. Notably, the effect of diamide was absent in vimentin C328S, which polymerized into filaments with normal morphology. Moreover, the shortening effect of DMSO was nearly abolished in the vimentin mutant, which displayed a non-significant 6% length reduction. Finally, although HNE caused a 19% decrease in the average length of vimentin C328S filaments, this damaging effect was also attenuated in respect to wt.

Next, we evaluated the effect of preincubation with the same reactive compounds on filament assembly, after 1 h of polymerization (fig. 14D). At this time point, vimentin wt and C328S pretreated with vehicle were fully polymerized, appearing as long filaments spanning more than one micron of

length. Vimentin wt presented a mean width of 13.5 ± 0.3 nm, whereas vimentin C328S compacted reaching an average diameter of 12.6 ± 0.3 nm, as summarized in figure 14F.

At the end-point of polymerization, diamide-pretreated vimentin wt was not able to assemble into normal filaments, forming even bigger aggregates together with irregular filamentous structures (fig. 14D). Notably, vimentin C328S continued to be unaffected by this oxidant and polymerized properly into long and well compacted filaments.

In presence of DMSO, vimentin wt was able to fully elongate (fig. 14D). However, DMSO-pretreated filaments presented a more irregular morphology, with more variable width along the filament, and in general wider than control filaments (~ 15 nm). On the other hand, vimentin C328S preincubated with DMSO fully polymerized into apparently normal filaments.

After 1h of polymerization, filaments formed by HNE-pretreated vimentin wt were shorter, both ends being frequently visible in the same field at the magnification used (fig. 14D). Additionally, they displayed intense bundling and appeared as more irregular and disengaged filamentous structures. In this condition, filament width was markedly increased, reaching an average diameter of 16.9 ± 0.9 nm. Similarly to the early points of polymerization, the consequences of HNE pretreatment were mitigated in vimentin C328S. Nevertheless, the width of HNE-pretreated vimentin C328S filaments showed a significant increase compared to DMSO-preincubated ones, although the mean filament diameter was not wider than 14 nm.

The effect of different concentrations of the cyclopentenone 15d-PGJ_2 on vimentin assembly was also visualized under EM (fig. 14E). Increasing concentrations of this electrophilic prostaglandin slightly increased vimentin wt diameter in respect to DMSO vehicle (fig. 14F). Moreover, vimentin wt filaments preincubated with concentrations above 25 µM of 15d-PGJ_2 showed a rougher appearance and more frequent aggregates. According to the previous results with the other electrophiles, vimentin C328S formed more homogenous filaments. Nonetheless, at the highest concentration of 15d-PGJ_2 employed (84 µM), both vimentin wt and C328S failed to assemble as normal filaments.

In summary, these results show that lipoxidants disrupt vimentin assembly, inducing morphological alterations of filaments that adopt different

patterns depending on the structural properties of the various agents used. Moreover, the presence of the single cysteine residue of vimentin appears to be required for (lip)oxidation-induced alterations of assembly.

2.3 Susceptibility of polymerized vimentin to disruption by electrophilic agents

In cells, vimentin occurs in polymerized and non-polymerized states, which are continuously exchanging. Therefore, we next investigated whether electrophilic agents exerted differential effects in non-polymerized and polymerized vimentin (fig. 15). To this end, we examined the sample mixtures resulting from incubation of vimentin wt with the indicated compounds before and after inducing polymerization with 150 mM NaCl by EM (fig. 15A).

Interestingly, the first observation derived from these studies was that if assembly was induced just after thawing, vimentin formed filaments significantly narrower compared to the ones that were polymerized after preincubation in a hypotonic buffer, as displayed in the graph of figure 15A. This may reflect that soluble vimentin wt is sensitive even to environmental conditions. Notably, preformed filaments treated with diamide did not present any obvious alteration in filament morphology, in sharp contrast with the effect of diamide on soluble vimentin, which drastically disrupts subsequent assembly.

Even though treatment with DMSO of polymerized vimentin caused a significant increase of filament width up to 13.3 nm ± 0.3 nm, filaments were still markedly narrower than those formed by vimentin assembled after preincubation with DMSO. Likewise, preformed filaments treated with HNE presented attenuated alterations of filament morphology, and were visibly longer and significantly more compacted than those assembled after HNE pretreatement. Similarly, preformed filaments were less susceptible to variations of filament morphology induced by treatment with 15d-PGJ_2. Summarizing, EM observation revealed that vimentin wt preformed filaments were more resistant to the electrophilic treatment and presented, in general, a more homogenous appearance compared to the morphological alterations observed in filaments formed by electrophile-pretreated vimentin.

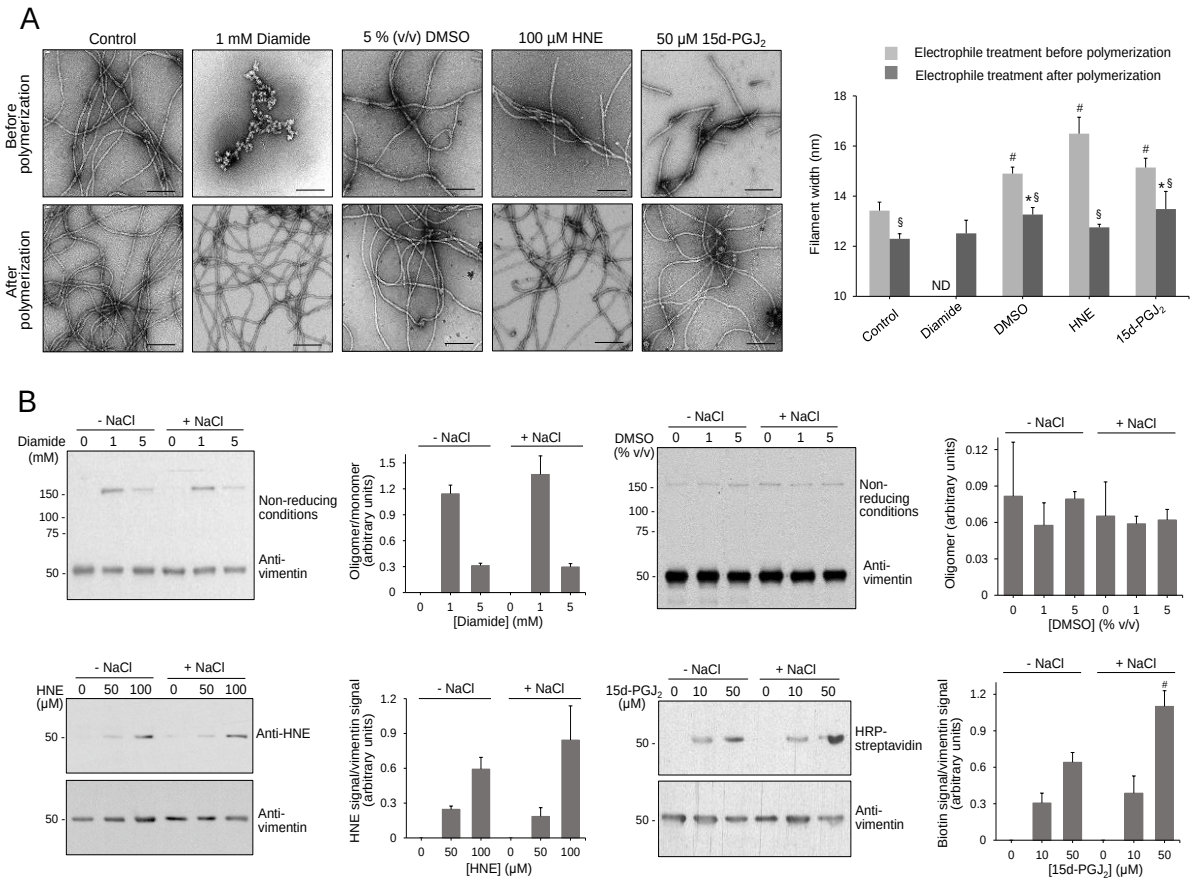

Figure 15. Impact of (lip)oxidation on filament formation and on preformed vimentin filaments.

(A) Inspection of filament morphology by EM. Purified vimentin wt was treated with the indicated oxidants or electrophilic lipids before (upper images) or after NaCl-induced polymerization (lower images). Scale bars, 200 nm. The histogram in the right panel shows filament width quantitated as in figure 14. Results represent average values ± SEM of 3 to 5 experiments totaling 50 filaments. (*p<0.05 vs control of polymerization followed by electrophile treatment; #p<0.05 vs control of electrophile treatment followed by polymerization; §<0.05 vs the same treatment before polymerization by unpaired Student's *t*-test). ND, not determined. (B) Vimentin was incubated for 1 h at r.t. in the absence (- NaCl) or presence of NaCl (+ NaCl), after which, it was incubated with the indicated oxidants or electrophilic lipids for an additional hour and the extent of modification was assessed as in figure 13. Results shown in graphs are average values ± SEM of three independent determinations (# p<0.05 vs - NaCl by paired Student's *t*-test).

In order to ascertain whether the attenuation of the effect of (lip)oxidation on preformed filament morphology was due to a lower extent of modification of polymerized vimentin, we have employed gel-based assays (fig. 15B). In these experiments, vimentin wt was initially preincubated in the absence or presence of 150 mM NaCl, followed by treatment with the indicated electrophilic compounds. As shown in the graphs, polymerized and non-polymerized

vimentin treated with diamide or DMSO, formed a similar amount of oxidative dimers. In the same way, the extent of adducts formed by HNE or 15d-PGJ_2-B and vimentin was similar or even larger at higher concentrations of the electrophilic agents, after prior polymerization with NaCl.

These results suggest that, even though the modification of non-polymerized and polymerized vimentin seems to occur to a similar extent, (lip)oxidation of vimentin is more detrimental for filament formation if it takes place prior to assembly. Nevertheless, we cannot exclude the possibility that the subunits modified in every situation are different; for instance, in polymerized vimentin, modification of accessible and peripheral subunits could have milder consequences on filament stability. Given the fact that, in cells, vimentin undergoes remodeling, we were interested in exploring this polymerization-dependent effect of (lip)oxidation in the cellular environment.

2.4 Impact of the oxidant diamide on vimentin organization in cells

In order to study the role of vimentin dynamics and the cysteine residue in the response of vimentin towards (lip)oxidative stress, we have used the adrenal carcinoma cell line SW13/cl.2 (SW13), devoid of cytosolic IFs. This cell model allows transfection with different vimentin constructs, such as vimentin wt or C328S, which can be studied without the interference of endogenous vimentin [4].

SW13 cells were stably transfected with bicistronic expression plasmids coding for untagged vimentin wt or C328S and DsRed-Express2 protein (RFP) as separate products (RFP//vimentin wt or C328S). Cells expressing either construct were subjected to treatment with diamide and its effect on the vimentin network was visualized by immunofluorescence (fig. 16A). In the control condition, both vimentin wt and C328S formed an extended network of filaments, spreading from the juxtanuclear region to the cell periphery.

Diamide is a chemical oxidizing agent, which was reported to decrease the concentration of glutathione in cells, indicating that this electrophilic agent is able to induce oxidative stress [253]. Treatment with 1 mM diamide for 15 min provoked an extensive remodeling of the vimentin network, which appeared as disperse dots in 85% of RFP//vimentin wt-expressing cells, as quantitated in

the graph of figure 16A. Strikingly, diamide-induced network reorganization was virtually abolished in cells expressing vimentin C328S.

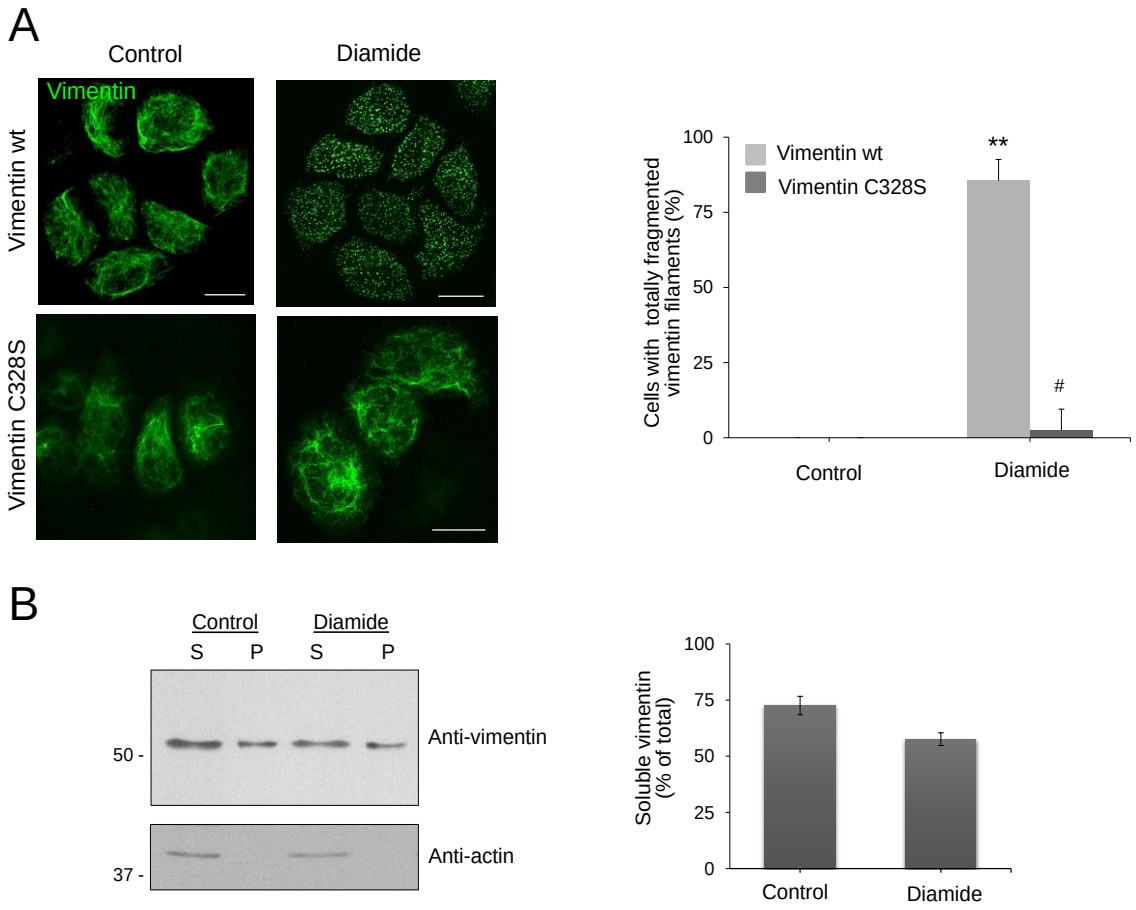

Figure 16. Vimentin network reorganization induced by diamide in cells.
(A) SW13/cl.2 cells stably transfected with RFP//vimentin wt or C328S were treated with vehicle (H_2O) or with 1 mM diamide for 15 min, after which, cells were fixed and the vimentin network was visualized by immunofluorescence. Scale bars, 20 μm. The graph depicts the proportion of cells with totally fragmented vimentin filaments in control or diamide treated cells (right panel) as average values ± SEM of three experiments totaling at least 150 cells (**p<0.01 vs wt-control; #p<0.05 vs wt-diamide by Student's *t*-test). (B) The solubility of vimentin wt upon treatment with diamide was monitored by cell fractionation and western blot of supernatant (S) and pellet (P) fractions with anti-vimentin antibody. As a control, blots were probed with anti-actin antibody. The proportion of soluble vimentin wt was estimated by image scanning and average values obtained from three experiments ± SEM are shown in the graph.

In order to explore if the deleterious effect of diamide was associated to changes in vimentin solubility, we estimated the proportion of soluble vimentin by means of a high-salt/Triton X-100-based fractionation protocol, as detailed in [239]. As illustrated in figure 16B, diamide treatment slightly decreased the

proportion of soluble vimentin. This effect could be due to an increase in either vimentin aggregation or cysteine crosslinking induced by this oxidant. Notably, no vimentin degradation was observed after diamide treatment, indicating that the marked reorganization was not due to loss of integrity of the protein. Actin was used as control of diamide specificity, and it remained mostly soluble in all conditions.

Taken together, these results show that the cysteine residue is required for vimentin network reorganization induced by diamide treatment. Additionally, vimentin disassembly or degradation do not seem to be associated with these morphological alterations.

2.5 Modulation of vimentin dynamics in SW13/cl.2 cells

The results presented above highlighted two critical points: preformed filaments are more resistant to (lip)oxidative treatments and diamide-induced remodeling was not caused by an increase of vimentin solubility. Therefore, we hypothesized that vimentin network disruption provoked by diamide would require active vimentin exchange of subunits, in a way that reincorporation of modified vimentin would cause anomalous filaments. Therefore, we first monitored vimentin filament dynamics in SW13/cl.2 cells, transiently transfected with a combination of untagged vimentin wt (80%) and GFP-vimentin wt (20%), by fluorescence recovery after photobleaching (FRAP) assays (fig. 17A). In the control situation, fluorescence reappearance was observed within the first seconds, as determined in the lower panel of figure 17A, indicating that this cell model has a high rate of subunit exchanging and consequently, very active vimentin dynamics. Nevertheless, this technique was not able to elucidate the nature or the oligomerization state of the fluorescent vimentin incorporated into the bleached filaments.

Further experiments were done to assess strategies to preclude vimentin dynamics. Dibromobiname (DBB) is a bifunctional reagent which irreversibly crosslinks vicinal thiol groups and has been proposed to stabilize the vimentin filamentous network [4]. Quantitative analysis of fluorescence recovery revealed that DBB efficiently blocks vimentin dynamics, since the recovery of fluorescence was nearly null (fig. 17A).

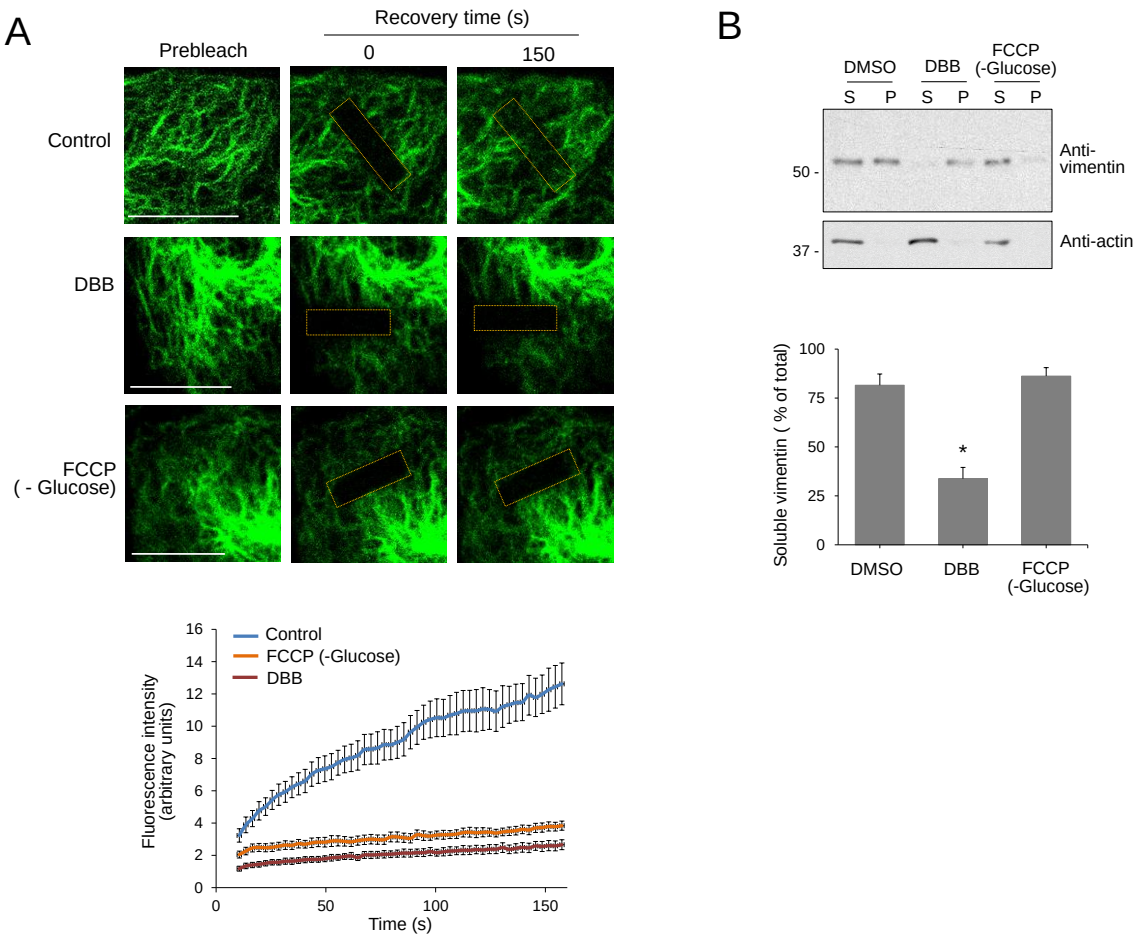

Figure 17. Modulation of vimentin dynamics in SW13/cl.2 cells.

(A) Assessment of vimentin dynamics by FRAP. SW13/cl.2 cells were transiently transfected with RFP//vimentin wt plus GFP-vimentin wt for live cell monitoring as detailed in Methods. FRAP assays were performed in cells treated with vehicle (control), 100 μM DBB or 10 μM FCCP in glucose-free medium for 10 to 30 min. Representative images acquired prior to (pre-bleach), immediately after (0 s) and 150 s after bleaching are shown. The bleached area is delimited by a dotted yellow rectangle. Scale bars, 10 μm. The graph shows measurements of the fluorescence intensity of the bleached area taken every 3 s. Results are average values of at least 20 determinations ± SEM. Differences between values from control and treated cells were statistically significant at all time points by Student's *t*-test. (B) Vimentin solubility under the conditions of the assays was determined as above. The graph depicts average values from 3 to 7 determinations ± SEM (*p<0.05 vs DMSO (vehicle) by unpaired Student's *t*-test).

Depletion of ATP was previously described to inhibit subunit exchange on vimentin filament precursors [64]. Thus, cells were treated with the ionophore carbonyl cyanide-4-(trifluoromethoxy) phenylhydrazone (FCCP), which prevents ATP production by dissipating the mitochondrial proton gradient [254]. This treatment was performed in absence of glucose to prevent ATP production by glycolysis [64]. The same procedure was applied and FRAP

determinations showed a clear reduction of the fluorescence recovery rate after treating cells with this inhibitor of oxidative phosphorylation, indicating a sharp inhibition of vimentin dynamics.

Potential alterations of vimentin solubility by these strategies were assessed as described in figure 16B and results are shown in figure 17B. Western blot analysis demonstrated that DBB treatment lowered the vimentin soluble pool by approximately 50%, consistent with the increase in cysteine crosslinking, which could lead to insoluble aggregates. In turn, the amount of soluble vimentin did not suffer changes when cells were treated with FCCP in the absence of glucose. In all situations, treatments had no effect on actin solubility (fig. 17B, lower blot).

2.6 Protective effect of minimizing vimentin dynamics on diamide-induced network disruption

After confirming the ability of cysteine crosslinking and depletion of ATP to minimize vimentin filament dynamics, we tested the protective potential of these strategies against disruption of vimentin filaments by diamide (fig. 18). Diamide induced a strong reorganization of vimentin network into dots in approximately 80% of cells after a 5 min treatment and in more than 90% of the cells after 15 min (fig 18A). The percentage of cells with totally fragmented vimentin is detailed in figure 18B. Pretreatment of cells with 100 µM of DBB for 15 minutes, fully protected the vimentin network from remodeling by subsequent diamide treatment for 15 min. However, vimentin showed a tendency to accumulate close to nucleus and F-actin was not protected from oxidative damage, appearing as a reticular pattern instead of as a homogeneous network. Likewise, FCCP also triggered vimentin juxtanuclear condensation, an effect that was also perceived on F-actin. This effect, which was beforehand reported to be independent from inhibition of oxidative phosphorylation by Maro and colleagues [255], precluded long-term treatment with this inhibitor, for which its protective potential effect was assessed by adding diamide for 5 min. Under these conditions, FCCP in glucose-free medium virtually abolished diamide-induced vimentin network disruption. We also observed a significant protection when cells were preincubated in glucose-free medium with sodium azide

(NaN_3), which reduces ATP production by inhibition of cytochrome C oxidase and disrupts the mitochondrial respiratory chain [256].

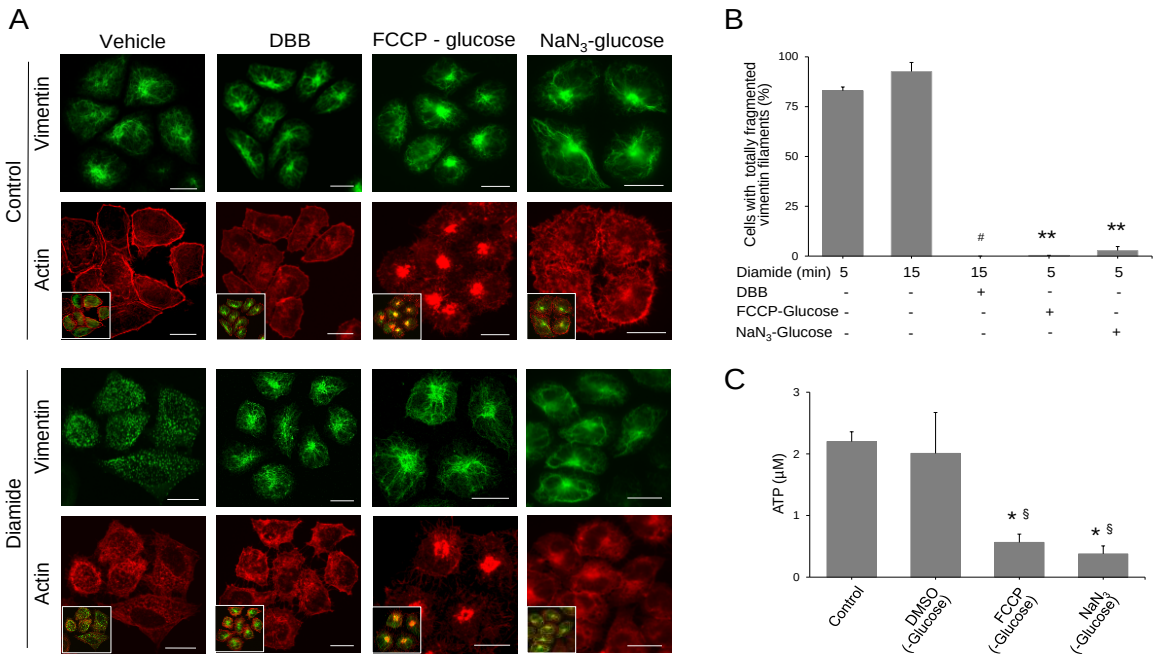

Figure 18. Protective effect of minimizing vimentin dynamics against diamide-induced network fragmentation.

(A) SW13/cl.2 cells stably transfected with RFP//vimentin wt were pretreated with 100 µM DBB in serum-free medium or with 20 mM NaN_3 or 10 µM FCCP for 15 or 20 min, respectively, in the absence of glucose, as indicated, before addition of vehicle (upper two rows) or 1 mM diamide (lower two rows) for 5 min in the case of FCCP or NaN_3-pretreated cells, or for 15 min in control and DBB pre-treated cells. Cells were fixed and vimentin distribution (green) was assessed by immunofluorescence and representative images of "fragmented" vimentin network are shown. F-actin distribution (red) was monitored by phalloidin staining. Overlay of vimentin and actin signals are presented in the insets. (B) Graph depicting the proportion of cells showing a completely fragmented vimentin network. In every experiment, at least 300 cells were monitored per experimental condition. Results are average values ± SEM of three experiments. (**p<0.0001 vs diamide 5 min, # p<0.05 vs diamide 15 min). (C) Steady-state ATP levels under the different experimental conditions were determined as detailed in Methods. Results are presented as mean values of three experiments performed in triplicate ± SEM (*p<0.05 vs control, § p<0.05 vs DMSO in glucose-free medium by unpaired Student's *t*-test).

Regarding the strategies used to block vimentin dynamics, cysteine crosslinking by DBB was revealed to be the most efficient one, preventing vimentin fragmentation even after longer treatments with diamide. In turn, the protective properties of ATP depletion induced by FCCP or sodium azide were gradually lower during longer treatments. Besides, these compounds were toxic

at higher concentrations, compromising their effect against diamide-induced reorganization of vimentin.

Steady-state levels of intracellular ATP under the conditions of these assays were determined and depicted in the graph in figure 18C. The inhibitors of oxidative phosphorylation, FCCP and NaN_3 in glucose free-medium, diminished effectively the concentrations of ATP by 75% and 83%, respectively.

In summary, these results show that the vimentin network is actively dynamic in SW13.cl2 cells. Nevertheless, vimentin subunit exchange can be prevented either by cysteine crosslinking or ATP depletion. Moreover, vimentin filament dynamics appears to be required for diamide-induced remodeling, as implied by the protective effect of strategies blocking vimentin subunit exchange, which suggests that vimentin network disruption occurs when modified vimentin “subunits” attempt to integrate into filaments.

3. Vimentin-zinc interplay and its relevance in pathophysiology

Previous chapters have highlighted the role of vimentin as a sensor of (lip)oxidation and the importance of C328 in these processes. Interestingly, vimentin (lip)oxidation can also be modulated by context factors, including the levels of antioxidant defenses and of certain divalent cations. Among them, zinc may interact with proteins, either by inducing specific conformations, supporting catalytic activity or stabilizing oligomeric associations [191]. Earlier investigation performed by our group, unveiled a robust interaction between vimentin and zinc, both in vitro and in the cell environment [4]. However, the structural features of vimentin-zinc interaction have not been elucidated. Thus, we designed a combination of experimental strategies to understand its role in the structural organization of vimentin in vitro and within the cellular context, assessing its importance in vimentin responsiveness to lipoxidation.

3.1 Effect of divalent cations on vimentin polymerization in vitro

The ability of zinc to induce vimentin polymerization was evaluated by incubation of vimentin wt or C328S with increasing concentrations of $ZnCl_2$, followed by ultracentrifugation and gel electrophoresis of supernatant (S) and pellet (P) fractions, corresponding to soluble and polymerized vimentin, respectively (fig. 19).

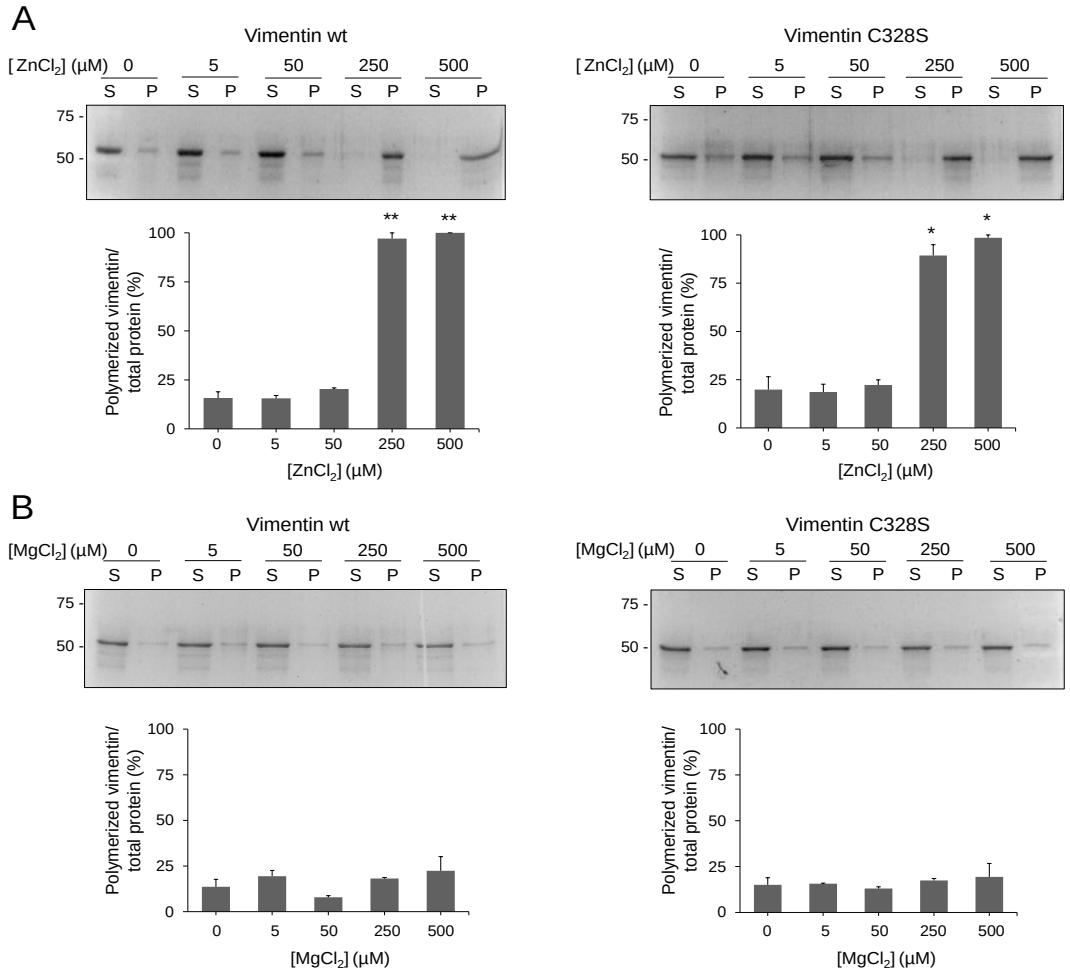

Figure 19. Polymerization assays of vimentin wt and C328S with divalent cations.
(A) Polymerization assays were performed by incubation of vimentin wt and C328S at 3.8 μM, in 5 mM Pipes-Na, pH 7.0, with increasing concentrations of $ZnCl_2$ during 1 h at r.t. All samples were subjected to ultracentrifugation, after which, supernatant (S) and pellet (P) fractions were analysed by SDS-PAGE. Total protein was stained with Sypro-Ruby and visualized by UV detection. The proportion of polymerized vimentin was determined by image scanning and displayed in the graphs. Results shown are mean ± SEM of three independent experiments, **p<0.0005; *p<0.05 vs 0 μM $ZnCl_2$ by Student's t-test. (B) Vimentin wt and C328S polymerization with increasing concentrations of $MgCl_2$. Samples were subjected to the same procedure described above. The proportion of polymerized vimentin was determined for two independent assays.

In low ionic strength buffer, such as 5 mM Pipes-Na, pH 7.0, 75-80% of both forms of vimentin, wild-type and C328S, occurred as soluble species. Low concentrations of zinc, up to 50 µM, did not alter the proportion of soluble vimentin, but concentrations at or above 250 µM induced polymerization of practically 100% of vimentin (fig.19A). Vimentin has also been reported to interact with magnesium ions [62], which, as zinc are redox inactive. However, incubation with $MgCl_2$ in the same concentration range did not elicit vimentin polymerization, as shown in figure 19B. Thus, at 500 µM $MgCl_2$, vimentin wt and C328S still appeared mostly in the soluble fraction. These results could suggest that micromolar concentrations of zinc induce structural rearrangements of vimentin that alter its solubility, which do not occur in presence of equivalent amounts of other divalent cations.

3.2 Turbidity and fluorescence anisotropy of zinc-induced vimentin polymerization

In order to explore the nature of the vimentin polymers formed by incubation with zinc, we applied additional biophysical techniques. Turbidity or light scattering, and fluorescence anisotropy measurements allowed monitoring vimentin oligomerization when incubated with different concentrations of zinc (fig. 20). We observed an increase in the turbidity of the solutions of vimentin wt with increasing concentrations of the divalent cation (fig. 20A). A significant increase in turbidity could be detected with 150 µM $ZnCl_2$. These results indicate the formation of bigger structures in the presence of zinc. Vimentin C328S displays a similar behavior, which suggests that the formation of zinc-induced structures can occur in vimentin bearing either a cysteine or a serine residue at position 328. In this method, zinc concentrations above 300 µM and turbidometric measurements longer than 20 min, were not taken into account, since we detected a decrease on the absorbance that might be compatible with sedimentation of large protein assemblies (data not shown).

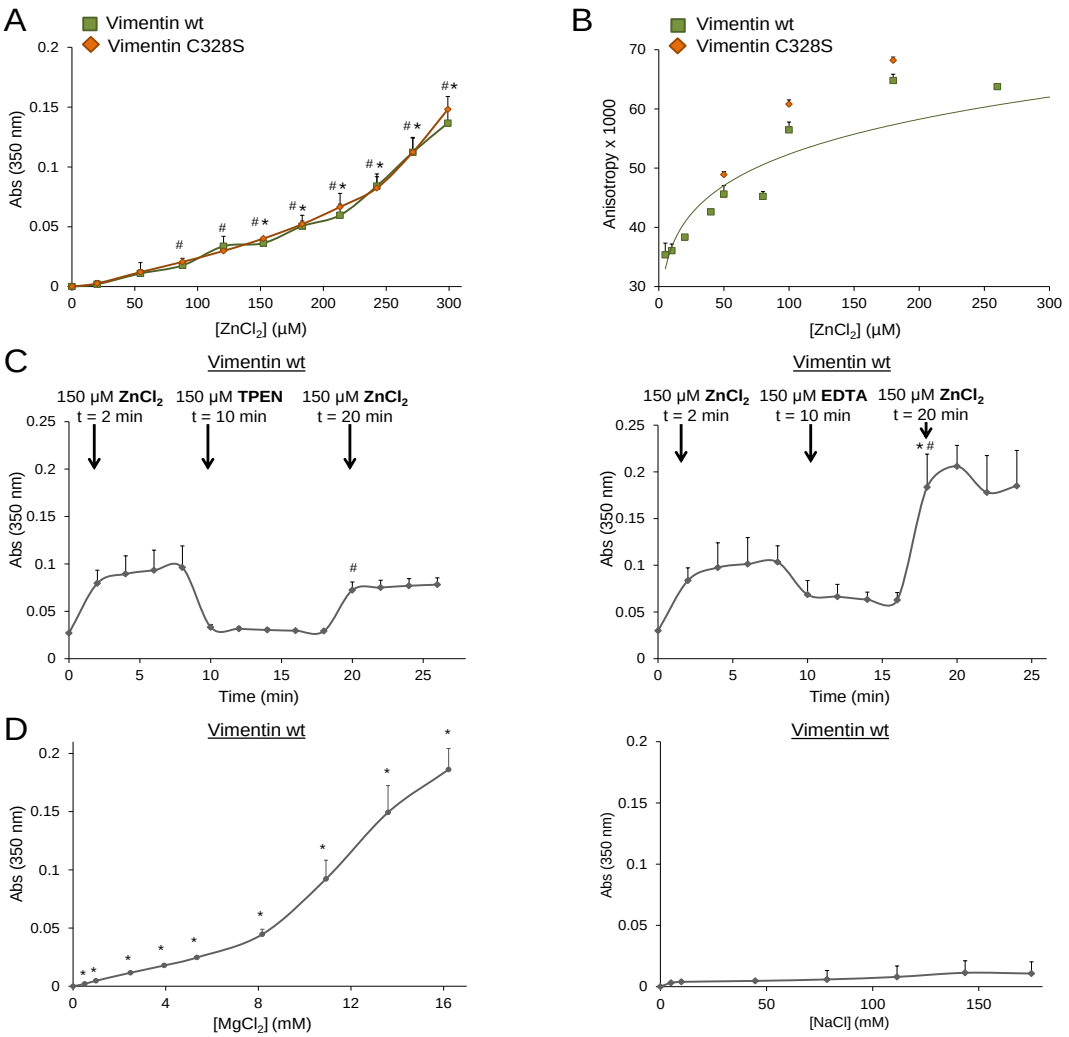

Figure 20. Monitoring vimentin polymerization by turbidity and fluorescence anisotropy experiments.

(A) Turbidity analysis of vimentin wt and C328S as a function of increasing concentrations of $ZnCl_2$. Solutions of vimentin wt and C328S (70 µl) were placed in Hellma absorption cuvettes. Increasing amounts of $ZnCl_2$ were sequentially added to the protein solution to achieve the indicated final concentrations. Absorbance values were immediately measured at 350 nm. At least three independent experiments were performed and mean values ± SEM are represented in the graphs. *p<0.05 vs 0 µM $ZnCl_2$ in vimentin wt; #p<0.05 vs 0 µM $ZnCl_2$ in vimentin C328S, by Student's t-test. (B) Steady-state fluorescence anisotropy of vimentin wt or C328S as a function of zinc concentration. Sample mixtures of unlabeled vimentin (1 µM) with vimentin labeled with Alexa 488 (50 nM) were incubated with different concentrations of $ZnCl_2$. Fluorescence anisotropy was monitored at λ_{exc} = 485 nm and λ_{em} = 520 nm, at 26 ^{o}C. Results presented are mean ± SEM of two (vimentin C328S) or eight replicates (vimentin wt). (C) Analysis of the reversibility of the effect of zinc on vimentin wt using TPEN (left panel) or EDTA (right panel). Turbidity changes were followed over time upon addition of $ZnCl_2$ and metal chelators, as detailed in the graph. Three independent experiments were performed for each condition. *p<0.05 vs t = 2 min; # p < 0.05 vs t = 10 min. (D) Turbidity measurements of vimentin wt incubated with increasing concentrations of $MgCl_2$ (left panel, n=3) and NaCl (right panel, n=2). *p<0.05 vs 0 µM $MgCl_2$.

Next, we used fluorescence anisotropy to complement our studies about the potential of zinc as a polymerizing agent. A mixture of unlabeled vimentin wt or C328S with the corresponding vimentin labeled with Alexa 488, as a tracer, was incubated with increasing concentrations of zinc and fluorescence was measured (fig. 20B). We observed a concentration-dependent increase in anisotropy that is compatible with the formation of larger protein species, which corroborated the ability of zinc to induce vimentin polymerization at micromolar concentrations. As observed above in the turbidity measurements, there were no significant differences in zinc-induced aggregation between vimentin wt and C328S.

In order to explore whether the effect of zinc on vimentin polymerization is reversible, we monitored turbidity upon subsequent addition of $ZnCl_2$ and two metal chelators, ethylenediaminetetraacetic acid (EDTA) and N, N, N', N' Tetrakis (2-pyridylmethyl) ethylenediamine (TPEN) (fig. 20C). Both TPEN and EDTA form a 1:1 complex with zinc; however TPEN has higher affinity for zinc than EDTA (K_d of 6.4 x 10^{-16} M and 6 x 10^{-14} M, for TPEN and EDTA, respectively [236]. Addition of 150 µM $ZnCl_2$ to the vimentin solution rapidly induced an increase in light scattering, according to previous assays. Subsequent addition of an equivalent concentration of zinc chelators elicited a fast decrease in absorbance, more marked in the case of TPEN. This decrease suggested disassembly of the zinc-induced polymers of vimentin upon chelation by TPEN or EDTA. Lastly, replenishment of 150 µM $ZnCl_2$, final concentration, restored the light scattering to the initial or even higher levels, in the case of the assay with EDTA. The observation that TPEN was more effective in reversing the effect of zinc is in good agreement with its higher chelating potential.

Finally, turbidity measurements were performed to explore the effect of other salts, such as $MgCl_2$ and NaCl, on vimentin polymerization (fig. 20D). We observed that concentrations of $MgCl_2$ at or above 500 µM induced a significant increase of light scattering. Moreover, millimolar concentrations of $MgCl_2$ were required to promote similar turbidity changes to the ones observed with $ZnCl_2$. In turn, incubation of vimentin with increasing concentrations of NaCl, up to 170 mM, did not result in a significant increase in turbidity.

As a conclusion of these experiments, we could propose that micromolar concentrations of $ZnCl_2$ act as a switch, reversibly inducing the formation of

high order oligomeric species of vimentin, as indicated by increased turbidity and fluorescence anisotropy. In sharp contrast, millimolar concentrations of $MgCl_2$ were required to induce similar changes. Moreover, millimolar concentrations of NaCl, sufficient to elicit the formation of vimentin filaments, do not increase turbidity, probably because of the different size and/or shape of filaments compared to zinc-induced vimentin oligomers.

3.3 Assessment of the morphology of zinc-induced vimentin structures on different supports

The techniques used above yielded valuable information on zinc-induced vimentin polymerization. However, they did not provide structural information on the polymers formed. Thus, we used optical and fluorescence microscopy to explore the morphology of vimentin oligomers formed on different supports (fig. 21). First, we applied mixtures of vimentin wt with different concentrations of $ZnCl_2$ on glass slides. Direct visualization by optical microscopy revealed the presence of long and thick filaments or filament bundles together with irregular aggregates, which displayed a larger size with increasing zinc concentrations (fig. 21A). Additionally, zinc-induced polymers were intensely stained by Zinquin, a fluorescent probe used to detect both free and protein-bound zinc [257], suggesting a robust binding of zinc to vimentin.

We next incubated a solution of vimentin in a flat-bottom microplate, in the absence and presence of $ZnCl_2$ as detailed in figure 21B. Vimentin assemblies formed in suspension were observed under an optical microscope at different time points (0, 20, 40 and 60 min). In the absence of zinc, occasional aggregates of vimentin were detected, appearing as disperse dots without any distinguishable structure. Incubation with 200 and 500 µM $ZnCl_2$ led to the formation of an array of garland-like structures that homogeneously distributed in the solution. This particular “beading” network of vimentin in solution became denser with time.

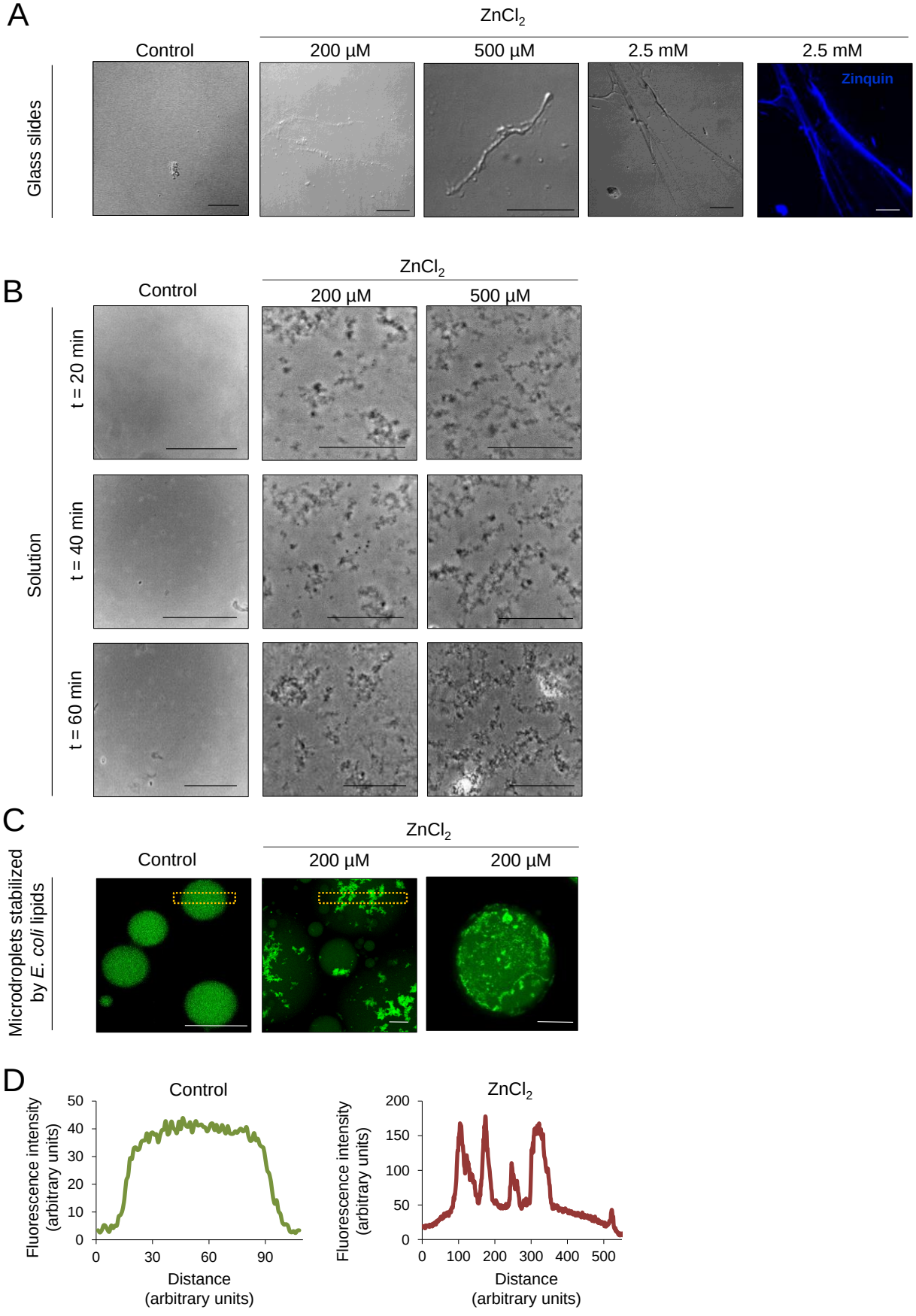
A
ZnCl2
Control
200 µM
500 µM
2.5 mM
2.5 mM
Zinquin
Glass slides
B
ZnCl2
Control
200 µM
500 µM
Solution
t = 20 min
t = 40 min
t = 60 min
C
ZnCl2
Control
200 µM
200 µM
Microdroplets stabilized by E. coli lipids
D
Control
ZnCl2
Fluorescence intensity (arbitrary units)
Distance (arbitrary units)
0
10
20
30
40
50
0
30
60
90
0
50
100
150
200
0
100
200
300
400
500

Figure 21. Effect of zinc on vimentin morphology on different supports.
(A) Vimentin at 5 µM in 5 mM Pipes-Na (pH 7.0) , 0.1 mM DTT, was placed on a glass slide, and mixed with vehicle, 200 µM, 500 µM or 2.5 mM $ZnCl_2$ (final concentrations) before visualization by differential interference contrast. In the right panel, $ZnCl_2$-induced vimentin filaments were labeled with Zinquin and visualized by fluorescence microscopy . Scale bar, 20 µm. (B) Aliquots of vimentin at 5 µM were incubated with different concentrations of $ZnCl_2$, in a flat-bottom microplate. The solutions were observed under the optical microscope after 20, 40 and 60 min of incubation. The experiments were performed in triplicate and representative results are shown. Scale bar, 25 µm. (C) Overall projections of representative confocal images of microdroplets containing a mixture of unlabeled and Alexa 488-labeled vimentin wt (4 and 1 µM, respectively), in the absence and presence of 200 µM $ZnCl_2$. Scale bar, 20 µm. (D) Fluorescence intensity was analyzed by image scanning and the profiles representative of the indicated areas are shown.

Vimentin was also encapsulated inside aqueous droplets stabilized in an oil phase by a lipid layer, to obtain picoliter-sized compartments. A mixture of unlabeled vimentin wt with vimentin wt labeled with Alexa 488 (4:1) was encapsulated inside the droplets with or without zinc. These microdoplets were observed under fluorescence microscopy and representative images are displayed in figure 21C. Without zinc, vimentin was homogenously dispersed inside the vesicle, as shown by the plot of the fluorescence intensity, which remained virtually constant inside the indicated area of the vesicle (fig. 21D). On the other hand, micromolar concentrations of zinc induced vimentin aggregates, as demonstrated by the variations in fluorescence intensity inside the vesicle (fig. 21D). Moreover, the structure of these zinc-induced vimentin aggregates recalled the “beading” distribution observed in suspension (fig. 21C). In summary, zinc was able to induce vimentin oligomerization, leading to structures morphologically dependent on the support used.

3.4 Electron microscopy of zinc-induced vimentin structures

We next inspected the vimentin wt and C328S species formed in the presence of different concentrations of zinc, under EM after negative staining (fig. 22).

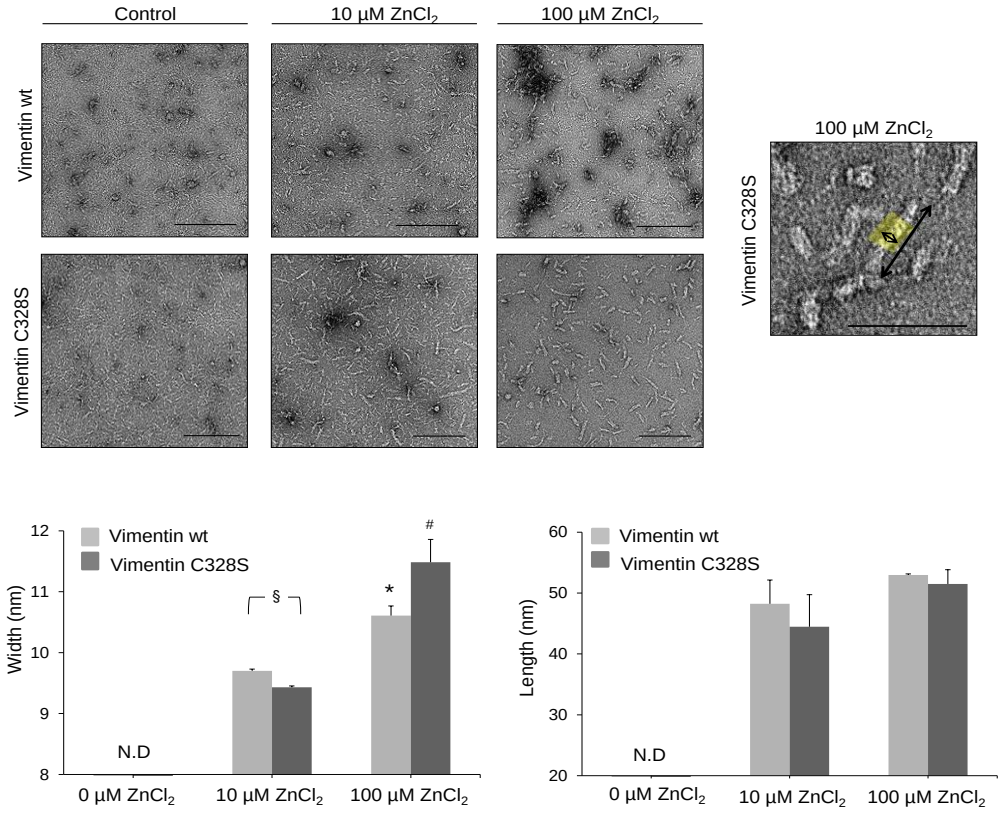

Figure 22. Morphology of zinc-induced vimentin structures monitored by electron microscopy.

Negatively stained vimentin wt or C328S species obtained after 1 h incubation with vehicle, 10 μM or 100 μM $ZnCl_2$ (final concentrations), at r.t, in 5 mM Pipes-Na, pH 7.0, 0.1 mM DTT. Graphs summarize the average values of width (left panel) and length (right panel) of zinc-induced vimentin assemblies. The width was measured using FIJI software as the average thickness of segments of at least 20 nm in length, as illustrated in the right panel. Results shown are mean values ± SEM of 50 "structures" per condition. §$p<0.05$ vimentin wt vs C328S, as indicated; *$p<0.05$ vs vimentin wt -10 μM $ZnCl_2$; # $p<0.05$ vs vimentin C328S-10 μM $ZnCl_2$ by unpaired Student's *t*-test. Scale bars, 200 nm and 100 nm for the right panel.

As described in the first chapter, vimentin in hypotonic buffer appeared mainly as small rod-like structures of 2-5 nm width and variable lengths, on average no longer than 40-50 nm. The dimensions of these oligomeric species were found to be very challenging to determine, due to the low contrast between their contour and the image background. In the presence of zinc,

vimentin formed assemblies with easily distinguishable features. The width of the rod-shaped particles markedly increased in the presence of 10 µM $ZnCl_2$, reaching 9.70 ± 0.03 nm and 9.43 ± 0.03 nm, in vimentin wt and C328S, respectively. Moreover, 100 µM $ZnCl_2$ further increased the diameter of vimentin structures, as depicted in the graphs. The length of the structures did not suffer a noticeable variation with increasing zinc concentrations and remained at 50 nm. Taken together, these observations suggest that zinc may promote lateral association of vimentin oligomers. This effect could be similar to that reported for millimolar concentrations of magnesium ions, which are described to accumulate in the outer regions of vimentin filaments and are able to crosslink different vimentin subunits, leading to appearance of thicker filaments [5, 258].

3.5 Impact of zinc on NaCl-induced vimentin assembly and on preformed filaments

The results shown indicate that zinc, at micromolar concentrations, can induce some kind of association between vimentin oligomers, under hypotonic conditions. Nevertheless, under physiological conditions, vimentin assembly takes place in the presence of 150 mM NaCl. Therefore, we were interested in exploring the effect of zinc on NaCl-induced vimentin assembly and on preformed filaments (fig. 23).

Thus, we first performed turbidity assays to assess the size of vimentin assemblies in presence of zinc, before and after polymerization with NaCl (fig. 23A). Soluble vimentin was first incubated with 150 µM $ZnCl_2$, which increased turbidity as previously described (fig. 20A). Subsequent addition of 150 mM NaCl induced an abrupt increment in light scattering. Interestingly, in the inverse approach, NaCl-induced polymerization of vimentin only increased absorbance slightly, and subsequent addition of zinc further increased the absorbance, although to lower values compared to adding zinc before NaCl. This outcome may suggest that in both situations higher order associations occur; however the features of those complexes could vary depending on whether zinc is added to soluble vimentin or to assembled vimentin.

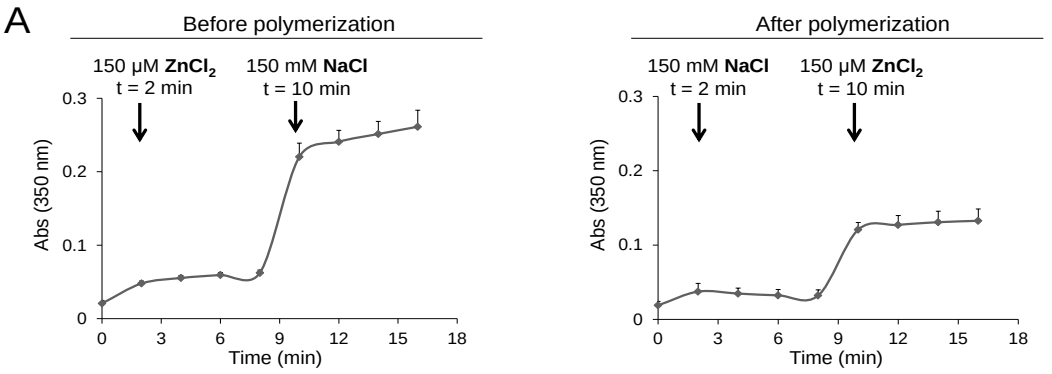
A
Before polymerization
150 µM ZnCl2
t = 2 min
150 mM NaCl
t = 10 min
Abs (350 nm)
Time (min)
After polymerization
150 mM NaCl
t = 2 min
150 µM ZnCl2
t = 10 min
Abs (350 nm)
Time (min)

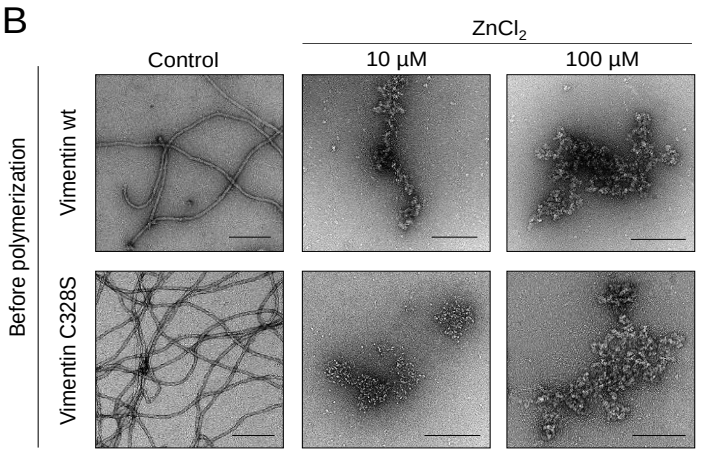
B
ZnCl2
Control
10 µM
100 µM
Before polymerization
Vimentin wt
Vimentin C328S

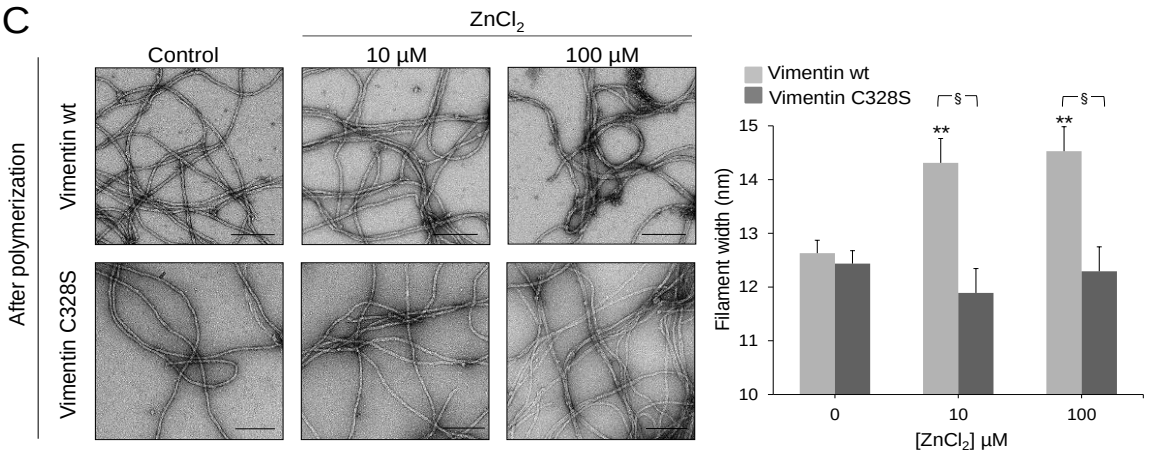
C
ZnCl2
Control
10 µM
100 µM
After polymerization
Vimentin wt
Vimentin C328S
Vimentin wt
Vimentin C328S
Filament width (nm)
[ZnCl2] µM

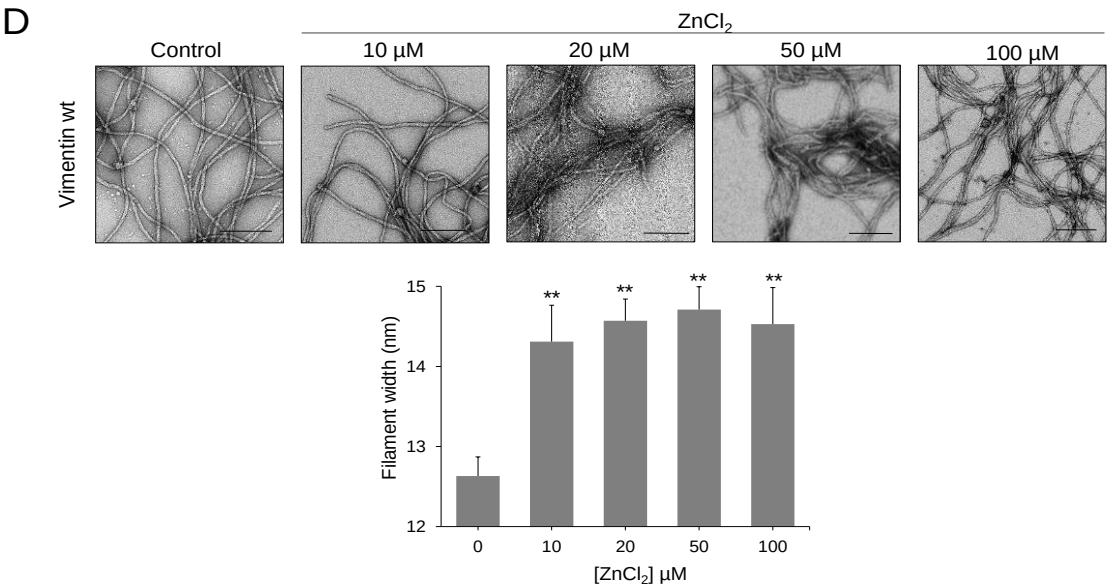
D
ZnCl2
Control
10 µM
20 µM
50 µM
100 µM
Vimentin wt
Filament width (nm)
[ZnCl2] µM

Figure 23. Impact of zinc on vimentin assembly and on preformed filaments.
(A) Turbidity measurements of vimentin wt were taken every 2 min during 16 min, at r.t, to monitor the effect of the order of addition of $ZnCl_2$ and NaCl, as indicated, on the oligomerization of the protein (B) EM observation of the effect of zinc on vimentin wt or C328S assemblies before polymerization with NaCl. Vimentin samples were incubated with vehicle, 10 or 100 µM $ZnCl_2$ for 1 h, at r.t, after which, they were incubated in the presence of 150 mM NaCl for an additional hour, at 37°C. (C) EM inspection of the effect of zinc on vimentin wt or C328S filament morphology after polymerization with NaCl. Vimentin wt or C328S was first polymerized with NaCl for 1 h at 37°C, and then, incubated with the indicated zinc concentrations. The right panel displays filament width as mean values ± SEM of 50 filaments per condition (**p<0.01 vs wt-control; §p<0.05 vimentin wt vs C328S by Student's *t*-test). (D) EM observation of the morphological changes of vimentin preformed filaments induced by increasing concentrations of $ZnCl_2$. Filament width measurements are presented in the graph as average values ± SEM of 50 filaments per condition. **p<0.005 vs control by Student's *t*-test. Images shown are representative of at least three independent assays with similar results. Scale bars, 200 nm.

To explore this possibility, the morphology of assemblies formed in both situations was explored by electron microscopy. Figure 23B displays representative images of vimentin wt or C328S incubated with 10 and 100 µM $ZnCl_2$ before assembly with 150 mM NaCl. As described previously, both vimentin wt and C328S form long filaments of approximately 12 nm of width, when incubated with assembly buffer, which is composed of 5 mM Pipes-Na, pH 7.0 and 150 mM NaCl. When 10 µM $ZnCl_2$ was added to soluble vimentin wt for 1 h at r.t. before polymerization, vimentin formed aggregates that tended to align but could not form filaments. After preincubation with 100 µM $ZnCl_2$, vimentin wt failed to assemble upon subsequent addition of NaCl, and formed larger irregular structures. A similar effect of zinc was observed in vimentin C328S, which did not assemble into filaments in either condition. Thus, the interaction of vimentin with zinc appears to preclude subsequent polymerization into "normal" filaments induced by physiological concentration of salt. Moreover, this effect of zinc on vimentin polymerization seems to be independent from the presence of cysteine in the position 328.

In contrast, when vimentin wt was fully polymerized, incubation in the presence of 10 and 100 µM $ZnCl_2$ caused both an increase in filament diameter and filament coalescence into bundles (fig. 23C). Determination of width revealed that 10 and 100 µM $ZnCl_2$ were able to significantly increase the average filament diameter by 12% and 15%, respectively. Filament bundling

was scarce at lower concentrations of zinc, but at 100 µM $ZnCl_2$, we observed a tighter union into intertwined filaments. In sharp contrast, vimentin C328S formed filaments with the typical morphology in presence of zinc, with no significant width alterations (fig. 23C). Nevertheless, at higher concentrations they also merged to form linear bundles, which seemed to be less intertwined and coiled than the ones observed in vimentin wt. These experiments corroborate that zinc is able to promote lateral association of vimentin filaments, and somehow it rearranges filament structure into a conformation that produces wider filaments, which is dependent on the presence of the cysteine residue.

Evaluation of concentration-dependence of zinc impact was performed as shown in figure 23D. The above described bundling effect was cumulative with increasing concentrations of zinc. Regarding vimentin filament diameter, it suffered an important increase at the lowest concentration of zinc assayed and it was roughly maintained around 14 nm at higher concentrations. In summary, zinc is able to promote vimentin association into aggregates or bundles, depending on the polymerization state of the protein.

3.6 Characterization of vimentin–zinc interaction by computational and crosslinking studies

The vimentin sequence possesses a high proportion of negative charges and potential sites for interaction with divalent cations [5]. In addition, the results presented increased our interest to investigate the possible binding spots for zinc in vimentin and the role of C328 in this interaction.

In collaboration with the group of Computational Chemical Biology led by Dr. Sonsoles Martin-Santamaria, a 3D structure of a putative vimentin dimer was modeled, comprising amino acids from D264 to G406, which corresponds to coil 2 of the rod-domain where the cysteine is located at position 328 (fig. 24A). Next, this dimer was used to explore the potential binding sites for zinc within this region (fig. 24A). Molecular dynamics (MD) simulations indicated that there exist 23 possible hot spots for zinc atoms within this modeled dimer of vimentin, in regions with predominant negative density charge. Moreover, stable interactions were observed between zinc atoms and residues D331 and E329, which are located in the region surrounding C328. Under physiological

conditions, the thiol group of C328 can exist either in its protonated or thiolate form. Interestingly, MD simulations showed that C328 in its thiolate form can directly participate in the coordination with zinc. Consequently, such outcome led us to infer that C328-zinc interaction could hypothetically protect this residue from modification by electrophilic agents.

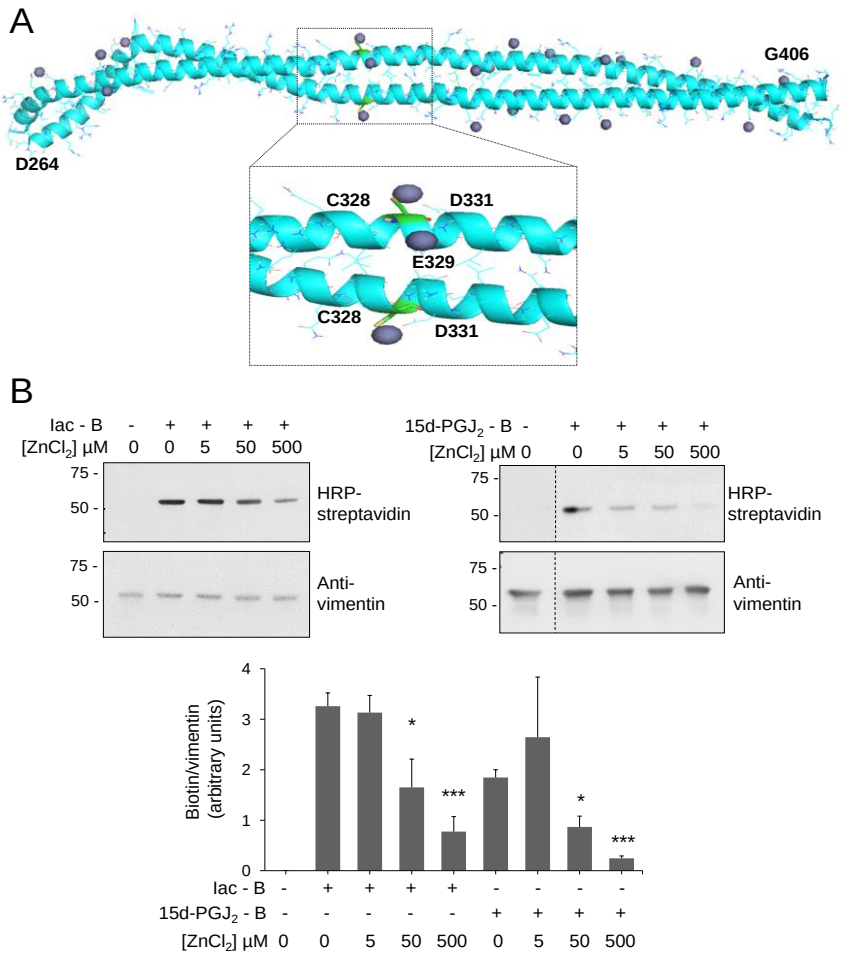

Figure 24. Characterization of the vimentin–zinc interaction by computational and chemical modification studies.

(A) Final structure of a putative dimer of the vimentin region comprising from D264 to G406, after 100 ns of MD simulation. Zinc atoms are shown in the proximity of vimentin C328, in its thiolate form. (B) Protective role of zinc against vimentin modification. Purified vimentin wt at 4.3 µM was preincubated with the indicated concentrations of $ZnCl_2$ for 1 h at r.t., after which, it was treated with vehicle, 10 µM of biotinylated iodoacetamide (Iac-B) or 1 µM biotinylated 15d-PGJ_2 (15d-PGJ_2-B), for an additional hour at 37°C. Incubation mixtures were subjected to SDS-PAGE and the incorporation of the indicated compounds was assessed by detection of the biotin signal on blots with HRP-conjugated streptavidin. Vimentin levels were monitored by western blot. Dotted lines indicate where lanes from the same gel have been cropped. The proportion of the biotin signal with respect to vimentin was summarized in the graph as means values ± SEM of four independent assays. * $p < 0.05$ vs Iac-B or 15d-PGJ_2-B at 0 µM $ZnCl_2$; *** $p < 0.0005$ Iac-B or 15d-PGJ_2-B at 0 µM Zn Cl_2 by Student's *t*-test.

Thus, in order to explore a putative protective role of zinc against cysteine modification of vimentin, we preincubated vimentin with increasing concentrations of $ZnCl_2$ followed by treatment with the biotinylated analogs of iodoacetamide or 15d-PGJ_2 (fig. 24B). The indicated biotinylated derivatives of electrophilic compounds covalently bound to vimentin, as previously described [3, 4]. Remarkably, analysis by SDS-PAGE and blotting for biotin detection showed that preincubation with 50 and 500 µM $ZnCl_2$ significantly decreased the incorporation of Iac-B by 50% and 75%, respectively. Likewise, 500 µM $ZnCl_2$ prevented the modification of vimentin wt by 15d-PGJ_2-B by approximately 90%.

Taken together, these results revealed important hot spots for zinc binding, emphasizing the potential coordination of zinc with the thiolate form of cysteine as a key interaction to prevent purified vimentin modification by cysteine-reactive agents.

3.7 Protective role of zinc against cysteine-crosslinking of vimentin

Previous studies have demonstrated that the single cysteine residue of vimentin participates in the formation of an oxidative dimer, resulting from a disulfide bond induced either by the oxidant diamide or by H_2O_2 [3, 8]. In addition, according to the model obtained, binding of zinc could not only protect vimentin from alkylation but also from crosslinking through disulfide bonds or by cysteine reagents. Therefore, we explored the chemical and oxidative crosslinking of vimentin and its potential protection by zinc (fig. 25).

The bifunctional cysteine crosslinker dibromobimane (DBB) irreversibly crosslinks vicinal cysteine groups within a distance of 3-6 Å [259], through a reaction mechanism depicted in figure 25A [260]. Analysis by SDS-PAGE showed that the cysteine-crosslinked product, resulting from treatment of vimentin with DBB, appears as one main band at ~150 kDa. This DBB-induced oligomer is similar to the ones formed through oxidative crosslinking induced by H_2O_2 or diamide (fig. 25B). Moreover, the formation of this crosslinked-dimer required the presence of the cysteine residue, as corroborated by the absence of the oligomer band in vimentin C328S (fig. 25C). Of note, cysteine residues are believed to be oriented outwards the dimer, which means that crosslinking

would only occur if the cysteines from different dimers fall within close distance in tetramers or in filaments.

In order to explore the ability of zinc to prevent oxidative or chemical cysteine crosslinking, we preincubated vimentin with increasing concentrations of this divalent cation before treatment with either the oxidant diamide (fig. 25D) or the cysteine crosslinker DBB (fig. 25E). Preincubation with micromolar concentrations of $ZnCl_2$ tended to preclude the formation of the oxidative dimer induced by diamide. Notably, 500 µM $ZnCl_2$ significantly decreased the appearance of the diamide-induced dimer by 65% (fig. 25D). Regarding DBB-crosslinking of vimentin, these experiments revealed that preincubation with 5 µM $ZnCl_2$ diminished the levels of cysteine-crosslinked dimer by approximately 42%. Moreover, concentrations at or above 20 µM $ZnCl_2$ significantly prevented vimentin crosslinking by DBB (fig. 25E).

The organization of vimentin tetramers within filaments is not completely understood. As shown in figure 25F, vimentin polymerization prior to crosslinking resulted in increased levels of oligomeric species, together with the appearance of extra bands with different electrophoretical mobilities. This result may imply that in filaments, vimentin rearranges into tetramer configurations where cysteines are closer or more prone to crosslink, than in soluble vimentin. Importantly, micromolar concentrations of zinc were capable of decreasing the formation of oligomers, both in soluble and assembled vimentin (fig. 25F). In contrast, millimolar concentrations of another divalent cation, namely magnesium, failed to prevent DBB-induced crosslinking (fig. 25G). In summary, vimentin is susceptible to both oxidative and chemical crosslinking, which results in the formation of a cysteine-crosslinked product. Remarkably, zinc is able to prevent vimentin crosslinking by different agents, an effect that is not mimicked by other divalent cations.

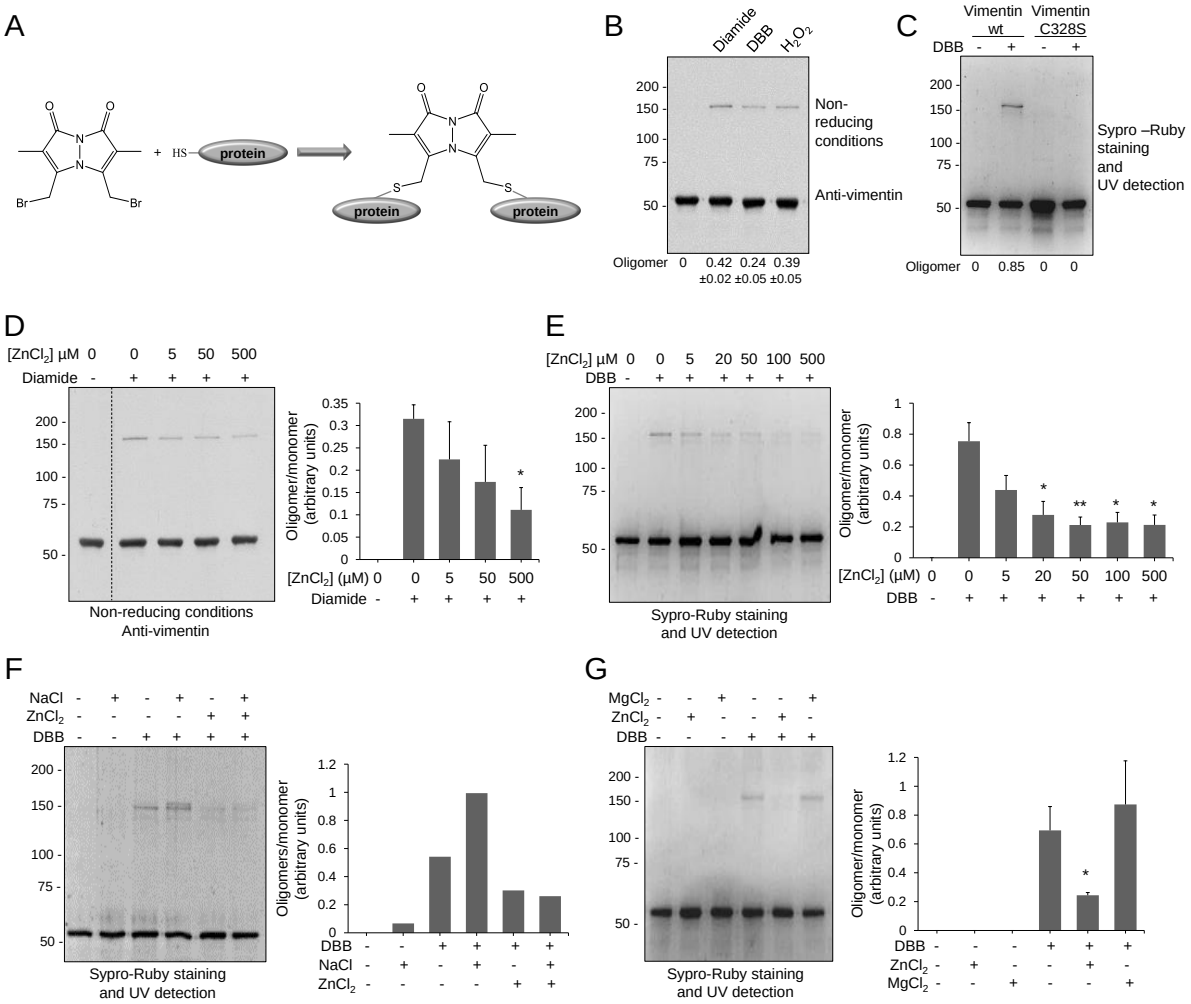

Figure 25. Protective role of zinc against cysteine-crosslinking.

(A) Dibromobimane (DBB) structure and its crosslinking mechanism of thiol-containing proteins. DBB reaction occurs by nucleophilic substitution (S_N2), where the bromide ion is displaced by the thiolate anion of a cysteine residue. DBB contains two electronegative bromine atoms which allow the reaction with two thiol groups of the same or different proteins, forming a 4.8 Å-long crosslink between them. (B) Cysteine-crosslinking of vimentin induced by several agents. Vimentin wt at 4.7 µM was incubated with vehicle, 1 mM diamide, 24 µM DBB or 1 mM H_2O_2 for 1 h at r.t. Incubation mixtures were subjected to SDS-PAGE under non-reducing conditions and vimentin levels were assessed by western blot. The amount of oligomer is displayed below the plot as average values ± SEM of three independent experiments. (C) Vimentin wt or C328S at 4.5 µM were incubated with 50 µM DBB for 1 h at r.t, and subjected to SDS-PAGE. Vimentin oligomeric species were visualized by Sypro-Ruby staining followed by UV detection. The formation of the cysteine-crosslinked oligomer was assessed by image scanning and values are presented below the plot. (D,E) Impairment of diamide or DBB-induced crosslinking of vimentin by preincubation with $ZnCl_2$. Vimentin wt at 4.3 µM was preincubated with vehicle or with increasing concentrations of $ZnCl_2$, as shown, during 1 h at r.t, and then, incubated for an additional hour with 1 mM diamide (D) or 24 µM DBB (E). In (D), samples were analyzed by non-reducing SDS-PAGE followed by western blot with anti-vimentin.

In (E), vimentin oligomers were detected by Sypro-Ruby staining followed by UV detection. The proportion of vimentin oligomer vs monomer was determined and average values ± SEM from three assays are depicted in the graphs. *p<0.05 vs diamide or DBB in the absence of $ZnCl_2$;**p<0.001 vs DBB in the absence of $ZnCl_2$, by unpaired Student's *t*-test. (F) DBB crosslinking of soluble and polymerized vimentin in the presence and absence $ZnCl_2$. Vimentin at 3.8 µM was first incubated with vehicle or 150 mM NaCl during 10 min at 37°C, after which, it was incubated for 1 h at r.t with 500 µM $ZnCl_2$, followed by an additional hour incubation with 24 µM DBB. Mixtures were processed as above and representative results are presented. (G) Vimentin crosslinking by DBB after preincubation with $ZnCl_2$ or $MgCl_2$. Vimentin wt at 4.3 µM was first incubated with vehicle, 500 µM $ZnCl_2$ or 500 µM $MgCl_2$ for 1 h, at r.t, after which, it was incubated with 45 µM DBB. At least three independent assays were performed and mean values ± SEM are shown. *p<0.05 vs DBB in the absence of salts, by unpaired Student's *t*-test.

3.8 The selective effect of zinc against crosslinking of vimentin

Further studies into the protective role of zinc against cysteine crosslinking were performed using other bifunctional cysteine crosslinkers with spacer arms of different lengths, as detailed in the table of figure 26A. Both tris(2-bismaleimidohexane)amine (TMEA) or bismaleimidohexane (BMH), which span 10.3 Å and 13.0 Å, respectively, gave rise to the appearance of vimentin crosslinking products compatible with vimentin dimers (fig. 26B). It should be noted that, although TMEA is a three-arm crosslinker, it apparently only gives rise to vimentin dimers. As shown before, we observed that zinc significantly reduced DBB-crosslinking. However, the presence of zinc was less efficient to preclude the crosslinking reaction by BMH or TMEA. Densitometric scanning of gels estimated that preincubation of vimentin with 500 µM $ZnCl_2$ diminished the TMEA-induced oligomer by 56%, while no significant decrease was observed for the BMH-induced oligomeric band (fig. 26B).

Earlier studies used the amino-crosslinker disuccinimidyl tartrate (DST) to propose several potential conformations of vimentin dimers in the tetramers [50]. Using the properties of this amino-crosslinker, we explored whether zinc could affect crosslinking through residues other than cysteine (fig. 26C). As observed in denaturing SDS-PAGE, DST induced the formation of two main bands, at ~140 kDa and ~150 kDa.

A

Compound	Structure	Spacer (Å)
Dibromobimane (DBB)	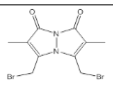	4.88
Tris(2-maleimidoethyl)amine (TMEA)	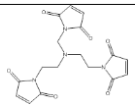	10.3
Bismaleimidohexane (BMH)	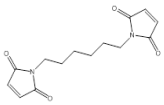	13.0

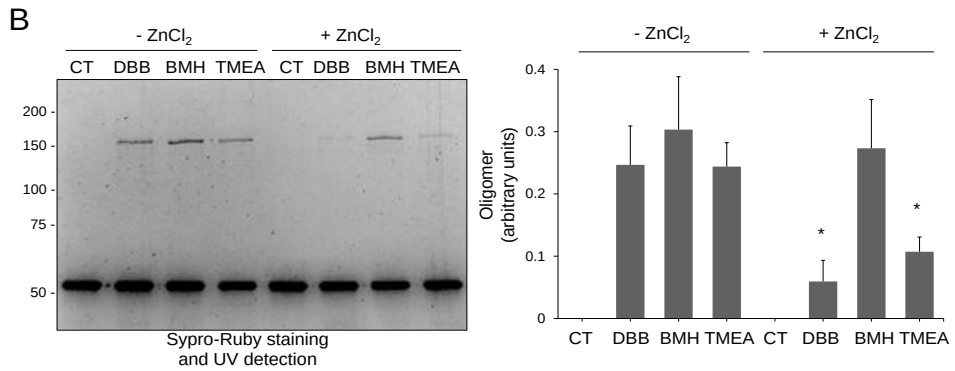

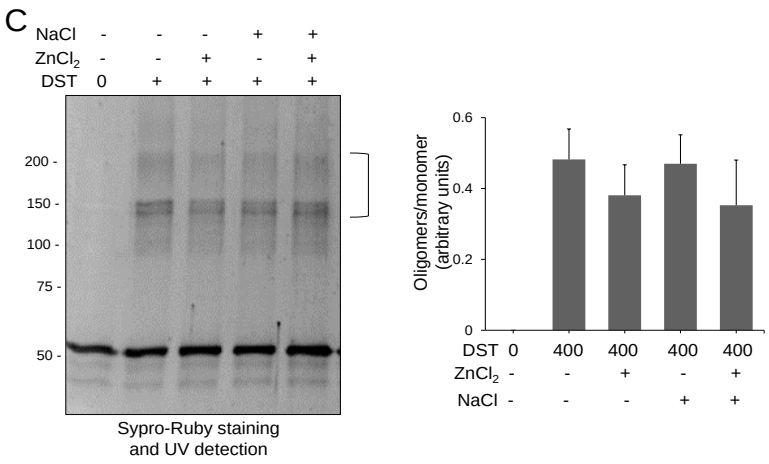

Figure 26. Selectivity of the protective effect of zinc on vimentin crosslinking.

(A) Structures and spacer arms of three cysteine-crosslinkers: dibromobimane (DBB), tris(2-maleimidoethyl)amine (TMEA) and bismaleimidohexane (BMH). (B) Vimentin wt at 4.3 µM was preincubated with vehicle (H_2O) or with 500 µM $ZnCl_2$ for 1 h at r.t, after which, it was incubated with vehicle (DMSO) or with 24 µM of the indicated cysteine-crosslinker. Incubation mixtures were subjected to SDS-PAGE, stained with Sypro-Ruby and detected under UV light. Oligomer formation was evaluated by image scanning and mean values ± SEM from three assays are represented in the graphs. *p<0.05, with respect to the reaction with the same crosslinker in the absence of $ZnCl_2$ by paired Student's *t*-test. (C) Zinc effect on amino-crosslinking of vimentin. Vimentin wt at 5.8 µM was incubated with vehicle (H_2O), 150 mM NaCl, or 500 µM $ZnCl_2$, as indicated. Then, incubation mixtures were treated with 400 µM disuccinimidyl tartrate (DST) for 1 h at 37°C. Samples were processed similarly as described above. The proportion of oligomeric species (bracket) vs monomer of three assays were determined and depicted in the graph. No significant differences were found by paired Student's *t*-test.

The previous reports assigned this particular electrophoretical mobility to a vimentin dimer. Smeared bands also appeared at higher molecular weights, suggesting the formation of tetramers or even higher oligomeric species, under our conditions. Previous polymerization with NaCl did not alter the pattern or intensity of the oligomeric species, whereas, preincubation with zinc slightly decreased, although non-significantly, DST-crosslinking, both in soluble and polymerized vimentin.

Taken together, our results indicate that preincubation with zinc selectively protects vimentin from cysteine crosslinking, and more specifically, from crosslinking by agents inducing a relatively short-distance linkage, from 2-3 Å, in the case of the disulfide bond, to 10 Å in the case of TMEA.

3.9 Influence of zinc on the response of vimentin to oxidative conditions in cells

In the cell environment, “free” zinc concentrations vary from picomolar to nanomolar in the cytoplasm, to millimolar levels in certain organelles such as lysosomes [188]. Moreover, zinc may serve regulatory and structural roles and support the activity of antioxidant enzymes. Based on the evidence obtained so far, an experimental approach to verify the protective role of zinc against the oxidative damage of the vimentin network in cells was set up (fig. 27).

Vimentin deficient SW13/cl.2 adrenal carcinoma cells, stably transfected with vimentin wt, were used first as a cell model for this experiment. In this type of cells, vimentin appears as an extended filamentous network, as visualized by immunofluorescence and described in Section 2 (fig. 27A). Incubation with $ZnCl_2$ induced vimentin reorganization into thicker filaments, appearing more condensed in the central region of the cell. Vimentin filament retraction was determined by measuring the area occupied by vimentin within the cell with respect to the area covered by F-actin, as represented in the upper graph of figure 27B. Although visually there appeared to be a difference in the vimentin network, no statistically significant difference was found.

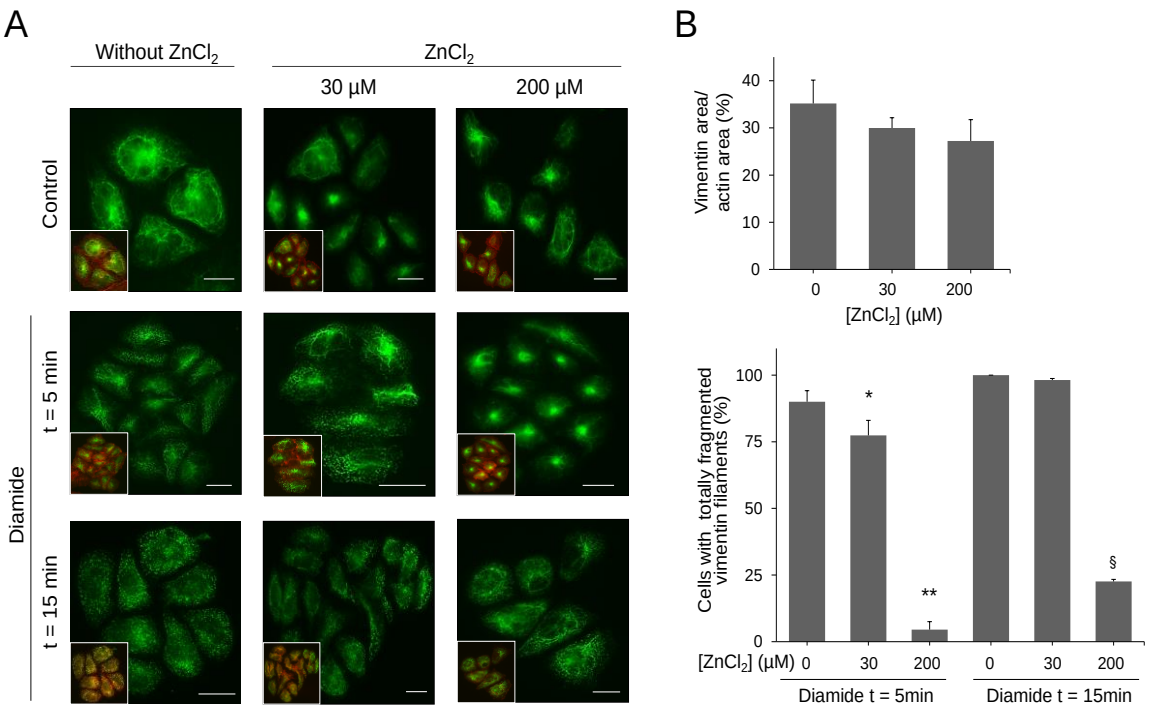

Figure 27. Influence of zinc on vimentin remodeling upon oxidative damage by diamide. (A) SW13/cl.2 cells stably transfected with RFP//vimentin wt were preincubated with vehicle (H_2O), 30 µM $ZnCl_2$ or 200 µM $ZnCl_2$ for 1 h. Then, cells were treated with 1 mM diamide for 5 or 15 min, as indicated. Cells were fixed and vimentin distribution (green) was evaluated by immunofluorescence. Phalloidin staining was used to monitor F-actin distribution (red). Insets display the overlay of vimentin and actin signals. Scale bars, 20 µm. (B) The upper graph shows the effect of zinc on the extension of the vimentin IF network, as the area occupied by vimentin vs that occupied by F-actin. The lower graph corresponds to the assessment of the protection exerted by zinc against the disruption of the vimentin IF network provoked by diamide. Accordingly, the proportion of cells with totally fragmented vimentin filaments was determined in the different conditions. Results are mean values ± SEM of three independent experiments. Regarding the upper graph, no significant differences were found by paired Student's *t*-test. In the lower graph, *p<0.05 vs diamide 5 min; **p<0.01 vs diamide 5 min; § p< 0.0001 vs diamide 15 min by paired Student's *t*-test.

As an oxidant agent for these assays, we chose diamide due to the short incubation time necessary for its effect and the clarity of the morphological changes induced, as shown before in Section 2: between 90% and 100% of the cells showed total reorganization of vimentin filaments into dots, after a 5 or 15 min incubation. Determination of the percentage of cells that presented punctuated vimentin, without any apparent filament, is depicted in the lower graph of figure 27B. Preincubation for 1 hour with 30 µM $ZnCl_2$ offered a partial protection against a 5 min diamide treatment. However, this $ZnCl_2$ concentration

was insufficient to prevent vimentin reorganization into dots after longer treatments with the oxidant. Notably, increasing the concentration of $ZnCl_2$ to 200 µM protected vimentin against diamide-induced reorganization more efficiently, thus, the percentage of cells with totally fragmented vimentin was significantly reduced to 5% and 20%, after 5 and 15 min diamide treatments, respectively.

Taken together, these results show that zinc induces a mild reorganization of the vimentin network in cells, but exerts a significant protective effect against the drastic disruption of vimentin filaments elicited by the oxidant diamide.

3.10 Importance of zinc availability in a pathophysiological model

Further studies were done to substantiate the vimentin-zinc interaction and its role in a pathophysiologically relevant model (fig. 28). For this, we used primary human fibroblasts from a control subject (AG10803 cells), and primary fibroblasts from an acrodermatitis enteropathica (AE) patient (GM02814A cells), which have a deficiency in zinc uptake and content [232]. Using this model, a protective effect of zinc supplementation on diamide-induced filament fragmentation has been previously reported [4]. Therefore, we have explored a potential protective role of zinc on HNE-induced cell damage. As detailed in the scheme represented in figure 28A, both cell types were preincubated with H_2O or with 30 µM $ZnCl_2$ for 30 min, after which, they were treated with vehicle (DMSO) or 10 µM HNE, for 1 h or 2 h 30 min.

As described previously by our group [4], control fibroblasts displayed a robust filamentous network of vimentin, where filaments were found uniformly and longitudinally distributed along the cell (fig. 28B, left panels). In turn, zinc-deficient fibroblasts appeared with a more elongated shape, in which vimentin filaments presented a more variable orientation and thinner diameter (fig. 28B, right panels).

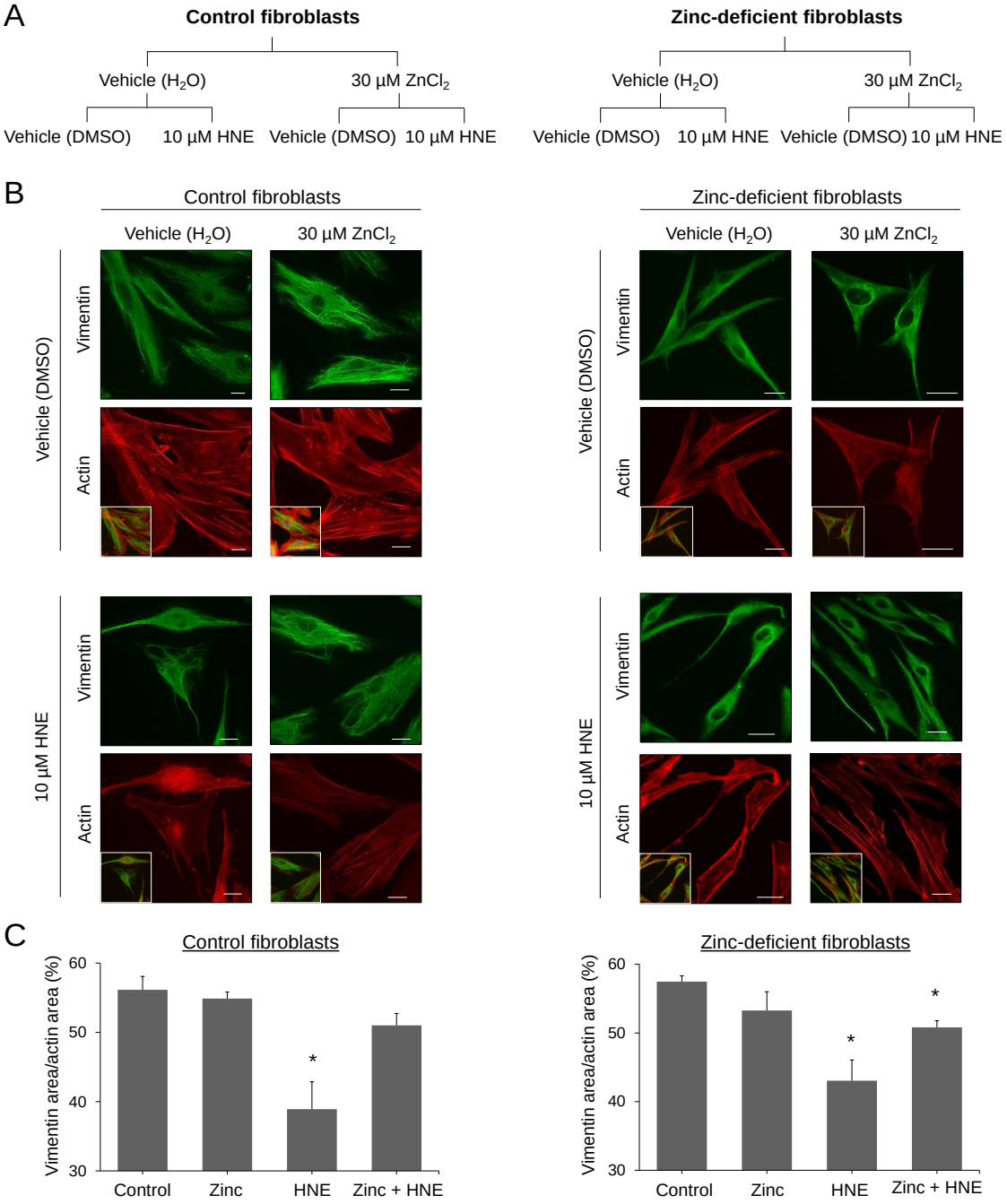

Figure 28. Importance of zinc availability in a pathophysiological model.

(A) Scheme outlining the experimental procedure. Primary human fibroblasts (AG10803 cells) as control, and primary fibroblasts from an acrodermatitis enteropathica (AE) patient (GM02814A cells) were preincubated with H_2O or with 30 µM $ZnCl_2$ for 30 min, after which, they were treated with vehicle (DMSO) or 10 µM HNE, for 2 h 30 min. (B) Representative fluorescence microscopy images of four independent experiments with similar results are displayed. Vimentin (green) and actin (red) were visualized by immunofluorescence and Phalloidin-Alexa 568 staining, respectively. Insets show the overlay of vimentin and actin signals. Scale bars, 20 µm. (C) Measurements of vimentin area vs actin area from four independent assays, in each of which, an average of 15 cells per condition were measured. Results are mean values ± SEM. *p<0.05 vs control by paired Student's *t*-test. No comparisons were made between control and zinc-deficient fibroblasts.

In both cell types, HNE treatment induced vimentin reorganization into thicker filaments in the perinuclear area. To support this evidence, the area occupied by vimentin within the cell was determined (fig. 28C). In the control situations, vimentin immunostaining occupied 50-60% of the cell area in both normal and zinc-deficient fibroblasts. Supplementation with 30 µM $ZnCl_2$ did not induce significant changes in the extension of the vimentin filamentous network. Filaments appear to be thicker, which is in good agreement with zinc ability to favor lateral association of vimentin, as previously reported in [4] and with the induction of vimentin bundling by zinc, observed by EM (fig. 23). In turn, HNE induced filament condensation and significantly reduced the area occupied by vimentin by 30% and 25%, in control and zinc-deficient fibroblasts, respectively (fig. 28C). Cell supplementation with zinc prior to HNE treatment appeared to attenuate HNE-induced retraction of vimentin filaments, although changes were not statistically significant.

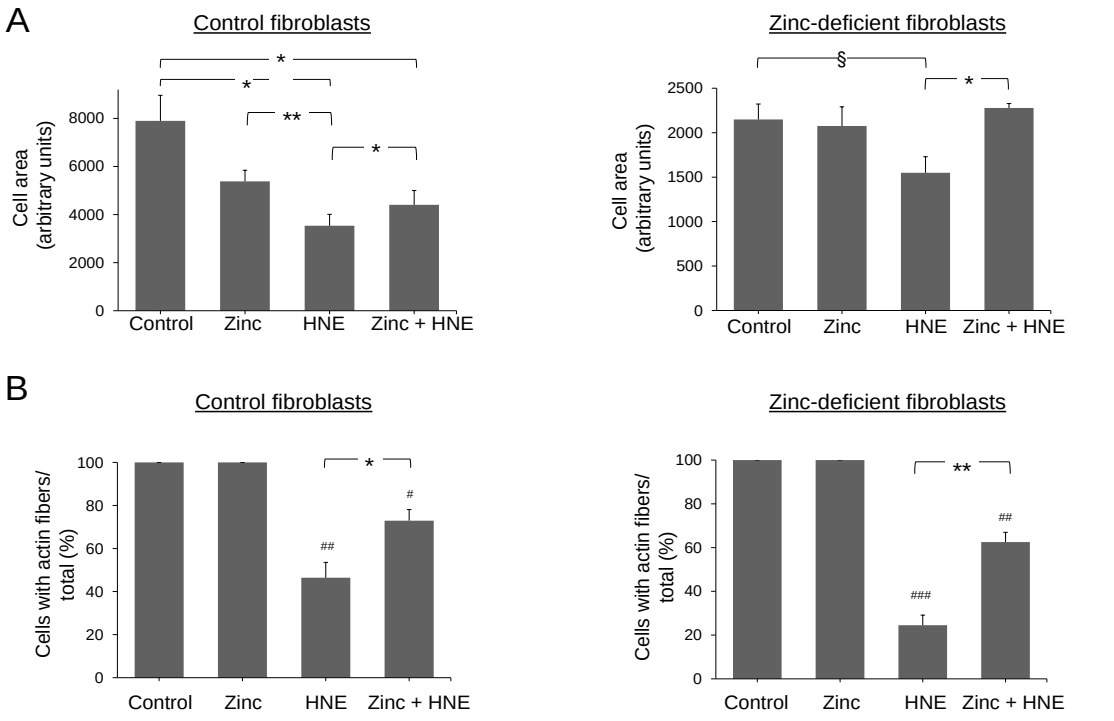

Figure 29. Effect of zinc availability and HNE on control and zinc-deficient fibroblasts.
(A) Effect of zinc and HNE on the cell size estimated by measuring the area covered by F-actin. The results are mean values ± SEM of four independent assays in each of which, an average of 15 cells per condition were measured. *p<0.05; **p<0.0005, §p< 0.01 as indicated, by paired Student's *t*-test. (B) Assessment of the protection exerted by zinc against the disruption of the actin network provoked by HNE. The proportion of cells displaying stress fibers was determined in the different conditions. Results are mean values ± SEM of four independent experiments with an average of 20 determinations each. *p<0.05; **p<0.005, as indicated, #p<0.05, ##p<0.005, ###p<0.0005 vs control by paired Student's *t*-test.

Moreover, treatment with HNE and/or zinc not only affected vimentin organization but also other cellular features, namely the cell size (fig. 28). Therefore, we determined the cell size by measuring the area occupied by F-actin and the results are summarized in figure 29.

As described above, control and zinc-deficient fibroblasts are morphologically different and they displayed considerably distinct sizes, with the control fibroblasts 3.7-fold larger than the AE fibroblasts.

In control fibroblasts, zinc supplementation caused a moderate, although non-significant, decrease of the cell size; whereas in zinc-deficient fibroblasts, zinc did not induce a noticeable change in the cell area (fig. 29A). Remarkably, HNE reduced the cell area by 56% and 28%, in control and zinc-deficient fibroblasts, respectively. Interestingly, the effect of HNE on the cell area was attenuated when both cell types were previously supplemented with zinc.

Additionally, HNE treatment drastically disrupted the actin cytoskeleton (fig. 28). Under control and zinc supplementation conditions, actin predominantly formed stress fibers, which were longitudinally distributed along the cell cytoplasm, and actin was well defined at the edges of the cell. However, in HNE-treated fibroblasts, actin suffered an intense remodeling into a diffuse and dotted pattern in the cytoplasm, and into an irregular and scalloped edge at the cell periphery. Determination of the proportion of cells displaying stress fibers showed disruption of these structures by HNE treatment in more than 50% and 75% of the cells, in control and zinc-deficient fibroblasts, respectively (fig. 29B). Remarkably, zinc supplementation exerted a clear protection on the actin cytoskeleton, since only 27-37% of the cells suffered stress fiber disruption upon subsequent treatment with HNE. Therefore, besides the partial protection of the vimentin network observed, zinc also played a protective role on actin, preserving the stress fibers upon lipoxidative attack. Together with previous evidence, these results suggest the importance of zinc availability on the structure of the vimentin network under pathophysiological conditions. Likewise, they unveil a more general protective role of zinc against the cytoskeletal reorganization induced by HNE.

3.11 Proteomic study of the effects of zinc and 4-hydroxynonenal in control and zinc-deficient fibroblasts

In order to obtain a more comprehensive view of the cellular effects of zinc availability and HNE treatment, we performed analysis of the cellular proteome using a bottom-up proteomic approach. The effects of HNE in fibroblasts with or without zinc supplementation were studied proteome-wide by relative label-free quantification (tables 5 and 6).

Table 5. Functional annotation of proteins differentially regulated in control fibroblasts treated with vehicle, zinc, HNE and zinc plus HNE (ANOVA $p < 0.05$). Fold changes in protein levels are shown relative to a control sample. Fold changes lower or equal to 0.7 and higher or equal to 1.5 have been highlighted, as potentially more relevant.

Fibroblasts control

			Fold change		
Proteins	**Acession UniProt**	**Molecular function**	**Zinc**	**HNE**	**Zinc + HNE**
Zinc binding proteins					
Zinc finger protein 613	Q6PF04	Transcriptional regulation;	10.5	9.4	4.5
Synaptic vesicle membrane protein VAT-1 homolog	Q99536	Oxidoreductase activity;	1.3	1.2	1.1
Transcription intermediary factor 1-beta	Q13263	Chromatin binding, DNA binding;	1.2	1.2	1.3
Ectonucleotide pyrophosphatase/phosphodiesterase family member 1	P22413	ATP metabolic process;	0.8	0.7	0.7
Actin regulation					
Myosin light chain kinase, smooth muscle	Q15746	Actin binding; ATP binding; Calmodulin binding;	1.0	0.9	0.7
Actin-related protein 2/3 complex subunit 4	P59998	Actin binding; Structural constituent of cytoskeleton;	1.5	1.7	1.5

Considering the four experimental treatments, assigned as control, zinc, HNE, and zinc plus HNE, only 6 proteins were up or downregulated in the fibroblasts from the healthy subject with respect to the control condition (ANOVA $p < 0.05$) (table 5). Zinc finger protein 613 was remarkably up-regulated in cells supplemented with zinc (10.5-fold), treated with HNE (9.4-fold), and preincubated with zinc and treated with HNE (4.5-fold). Other proteins able to bind zinc were weakly up-regulated, such as synaptic vesicle membrane protein VAT-1 homolog and transcription intermediary factor 1-beta. Moreover, variations in abundance were observed in other cytoskeletal proteins, including

actin-related protein 2/3 complex subunit 4 and myosin light chain kinase, under some of the conditions.

In turn, in zinc-deficient fibroblasts, a higher number of proteins were significantly up- or downregulated across the different experimental conditions, summing a total of 55 proteins differentially regulated compared to the control (ANOVA $p < 0.05$). Analysis using DAVID functional annotation tool [261, 262] did not demonstrate a significant enrichment of any KEGG pathway. Nevertheless, up- and downregulated proteins were attributed to three different groups, based on their biological functions provided by UniProtKB, as summarized in table 6. Thus, proteins were grouped as being involved in cell adhesion/junction, SRP-dependent cotranslational protein targeting to membrane/ ribosomal proteins and in protein transport.

Supplementation with zinc promoted a slight downregulation of 16 proteins, out of the 29 proteins gathered in table 6, through the different biological function groups. Interestingly, HNE treatment and the combination of zinc plus HNE slightly stimulated the expression of proteins involved in cell adhesion and junction. This is the case of annexin, catenin alpha-1, catenin delta-1 and fermitin, which have been reported to bind cadherin or modulate actin cytoskeleton dynamics [263, 264]. Nevertheless, the potential role of these proteins in the cytoskeletal alterations observed under confocal microscopy needs further study (fig. 28). Notably, levels of several ribosomal proteins that might be involved in signal recognition particle SRP-dependent cotranslational protein targeting to membrane were increased by HNE, suggesting a stimulation of protein biogenesis in response to lipoxidation. These analyses will be complemented using additional bioinformatics tools as wells as validation strategies in future studies.

Overall, evaluation of differentially regulated proteins between all experimental conditions suggest a higher susceptibility of fibroblasts with lower zinc content to HNE treatment and zinc supplementation. Although statistically significant, the magnitude of many of the changes observed is small. Therefore, interpretation of these proteomic data should be done cautiously, bearing in mind the possibility of false positives in large datasets and the limitations of small number of replicates.

Table 6. Functional annotation of proteins differentially regulated in zinc-deficient fibroblasts treated with vehicle, zinc, HNE and zinc plus HNE (ANOVA $p < 0.05$). Fold changes in protein levels are shown relative to a control sample. Fold changes lower or equal to 0.7 and equal or higher than 1.5 were highlighted, as potentially more relevant.

Zinc-deficient fibroblasts

			Fold change		
Proteins	**Acession UniProt**	**Molecular function**	**Zinc**	**HNE**	**Zinc + HNE**
Cell-cell adhesion/ junction/stress fiber					
Annexin A2	P07355	Cytoskeletal protein and cadherin binding	0.8	1.1	1.1
Calponin-2	Q99439	Actin, cadherin and calmodulin binding	0.7	1.0	1.0
Calreticulin	P27797	Chaperone, zinc ion binding	1.1	0.9	0.8
Catenin alpha-1	P35221	Actin-f, beta-catenin and cadherin binding	1.1	1.3	1.5
Catenin delta-1	O60716	Cadherin and protein kinase binding	1.1	1.1	1.2
Paxillin	P49023	Beta-catenin and integrin binding, metal ion binding	0.8	0.8	1.1
Integrin-linked protein kinase	Q13418	ATP binding, integrin binding, protein kinase binding	0.8	1.0	1.1
Fermitin family homolog 2	Q96AC1	Actin-f binding;	1.0	1.3	1.4
General vesicular transport factor p115	O60763	Cadherin binding	1.1	1.3	1.3
Staphylococcal nuclease domain-containing protein 1	Q7KZF4	Cadherin binding, endonuclease activity	1.1	1.2	1.2
Chloride intracellular channel protein 1	O00299	Cadherin binding, chloride channel activity	0.7	1.0	0.9
6-phosphofructokinase type C	Q01813	6-phosphofructokinase activity, ATP and cadherin binding	0.9	1.2	1.4
GTP-binding nuclear protein Ran	P62826	Cadherin and chromatin binding	0.8	1.1	1.0
SRP-dependent cotranslational protein targeting to membrane/ Ribosomal proteins					
60S ribosomal protein L7	P18124	DNA and mRNA binding, protein homodimerization	1.0	1.4	1.7
40S ribosomal protein S18	P62269	RNA binding, structural constituent of ribosome	1.1	1.7	1.7
60S ribosomal protein L10a	P62906	RNA binding, structural constituent of ribosome	0.8	1.3	1.3
Signal recognition particle receptor subunit alpha	P08240	GTPase activity, GTP and RNA binding, signal recognition particle binding	0.8	1.8	1.9
40S ribosomal protein S3	P23396	Class I DNA endonuclease activity; damaged DNA binding	0.9	1.3	1.5
40S ribosomal protein S5	P46782	mRNA binding, structural constituent of ribosome	0.6	1.1	1.3
40S ribosomal protein S25	P62851	RNA binding	0.9	1.4	1.4
40S ribosomal protein S4	P62701	RNA binding, structural constituent of ribosome	0.8	0.9	1.2
60S ribosomal protein L3	P39023	5S rRNA binding structural constituent of ribosome	1.1	0.9	1.1
60S ribosomal protein L12	P30050	Large ribosomal subunit, rRNA binding	0.6	1.1	1.2
40S ribosomal protein S15a	P62244	RNA binding, structural constituent of ribosome	0.9	1.4	1.4
Protein Transport					
Importin subunit beta-1	Q14974	Hsp90 protein binding, zinc ion binding	1.0	1.2	1.2
Nuclear transport factor 2	P61970	Protein transporter activity, constituent of nuclear pore	0.4	0.6	0.6
Mitochondrial import receptor subunit TOM22 homolog	Q9NS69	Protein transmembrane transporter activity	1.1	0.7	0.6
Leucine-rich PPR motif-containing protein, mitochondrial	P42704	Beta-tubulin binding	1.1	1.4	1.6
Spliceosome RNA helicase	Q13838	ATPase activity; ATP-dependent protein binding	1.1	1.2	1.3

Remarkably, no significant changes were found in vimentin expression. As a follow up of these results, further studies will be performed in vimentin immunoprecipitated from fibroblasts, to get insight into the possible post-translational modifications induced by HNE treatment in the absence and presence of zinc. This work will provide more information to substantiate the vimentin-zinc interaction and unveil the mechanisms underlying vimentin network remodeling in response to lipoxidation in pathophysiological models.

DISCUSSION

Vimentin is a highly dynamic protein that forms an extended network of filaments in cells, regulating a wide spectrum of cellular functions. Moreover, vimentin acts as mediator of cell responses to mechanical forces and/or biochemical stress [1]. The highly conserved cysteine residue, C328, arises not only as a fundamental key for the organization and function of vimentin, but also as an important regulator of its behavior in response to (lip)oxidative stress [4].

Although extensive work has been performed to explore vimentin features both in vitro and in cells, vimentin structure and the mechanisms underlying its assembly are not completely understood. Moreover, the remodeling under stress conditions as well as the influence of cellular context factors, such as the presence of divalent cations need further study. In this thesis, we have elaborated an integrative approach in order to explore the oligomerization of vimentin under different conditions and to characterize this protein as a target for lipoxidation, paying special attention to the cysteine residue as a hinge influencing vimentin response to different stimuli.

1. Refolding and validation of vimentin functionality

Vimentin morphology as well as its assembly properties are sensitive to different factors as the ionic strength, the presence of metals or the reaction with electrophilic compounds [4, 6].

In vitro assays were the first approach used to study vimentin oligomerization and modification by different electrophilic agents. To this end, we have used recombinant vimentin wild-type and vimentin mutated at the cysteine residue that was substituted by a serine residue. Purification of recombinant vimentin needs to be performed under denaturing conditions using high concentrations of urea [233]. In addition, metal chelators, such as EDTA, are generally used for inhibition of proteases during protein purification, to eliminate endotoxin or to prevent oxidation by metals in protein preparations [265-267].

Since the aim was to study the effect of micromolar concentrations of divalent cations on vimentin structure and function, a method to correctly refold vimentin into its functional form and to efficiently eliminate metal chelators and

other possible additives that could interfere with the interpretation of the results, was needed.

1.1 NMR and colorimetric assays demonstrate that EDTA can be carried on unnoticed during protein dialysis

Here, simple methods to interrogate the presence of EDTA, namely, NMR experiments and a complementary colorimetric assay to estimate the amount of EDTA present in the protein preparations (fig. 8-10) have been provided. Both detection methods use the ability of EDTA to chelate zinc, forming a 1:1 complex of extremely high affinity with a dissociation constant of 2.3×10^{-14} M at pH 7.4 [236]. In ^{1}H NMR experiments, the characteristic pattern of the shifts of the signals given by the EDTA-zinc complexes is considered the most reliable and specific way of detection of this metal chelator in protein samples (fig. 8). Such conclusion is supported by the fact that the peaks resulting from EDTA-zinc complex do not change through a wide pH range (from 5.9 to 8.2) [243], in sharp contrast with the free EDTA peaks which are strongly dependent on the pH of the sample.

Additionally, EDTA binds zinc ions much more tightly than the other common divalent metals such as magnesium and calcium ions, which have dissociation constants of approximately 10^{-9} M and 10^{-11} M, respectively [268]. Therefore, EDTA selectively chelates zinc present in a protein solution, even in the presence of high concentrations of the other divalent cations, which increases the sensitivity and reproducibility of the detection method.

Similarly, the colorimetric assay set up in this work also takes advantage of the high affinity of EDTA for zinc (fig. 9). In this technique, EDTA competes with the chromogenic compound 4-(2-pyridylazo)-resorcinol (PAR) for zinc binding, in such a way that the decrease in the absorbance at 492 nm, characteristic for the PAR-zinc complex, can be used to estimate the amount of EDTA present in the sample.

Both detection methods revealed to be easy and convenient ways to monitor the presence of EDTA in the vimentin preparation. Moreover, the colorimetric method does not require sophisticated equipment and can be carried out in any biochemistry laboratory. Nevertheless, we cannot discard the

presence of other metal-binding compounds or proteins in the sample that may also compete with the chelators for zinc binding; therefore a combination of different methods to detect EDTA is advisable.

1.2 Ultrafiltration followed by dialysis allows the efficient removal of EDTA and the functional refolding of vimentin

The application of the mentioned techniques to different protein preparations, initially containing 1 mM EDTA, demonstrated that EDTA can be carried on unnoticed during protein dialysis (fig. 30). The lack of effectiveness of dialysis could be explained by the capacity of EDTA to form supramolecular aggregates in solution and its ability to associate with proteins, which prevent its elimination through the dialysis devices with pore-sizes over a hundred times larger [269]. In addition, the efficacy of dialysis may vary with buffer composition. Indeed, our group tested the influence of the ionic strength in the performance of the dialysis procedure, and the results confirmed previous observations [270] showing that EDTA removal by dialysis is more effective when physiological concentrations of NaCl are added to the dialysis buffers [243].

The concentration of EDTA remaining after dialysis (~ 450 µM) probably does not affect the results of studies employing millimolar concentrations of divalent cations [271]. Nevertheless, additional care should be taken when performing assays with micromolar concentrations of metals. Moreover, the presence of EDTA can change several protein parameters, such as thermal denaturation [272], or promote pH alterations after addition of divalent cations [273]. Therefore, the concentration of EDTA present in the protein preparations should be carefully monitored and the complete removal of EDTA should be assessed by the methods described herein or by other techniques, like HPLC or spectrometric procedures [274, 275].

Although there are previous reports on the inefficiency of several procedures to remove EDTA [270, 272], the information is scarce and not readily found in bibliographic searches. Therefore, our observations call attention to the fact that EDTA is not thoroughly removed by dialysis procedures. Indeed, we have encountered that this problem affects commercial

protein preparations, which may contain considerable amounts of EDTA not listed in the buffer composition.

Besides dialysis, other procedures routinely used to separate macromolecules from small compounds were tested for reducing EDTA concentration, namely, spin column gel filtration and ultrafiltration (fig. 30). Size exclusion chromatography using spin desalting columns was less effective compared with ultrafiltration; however the use of longer columns with higher resolution may improve the efficacy of the procedure.

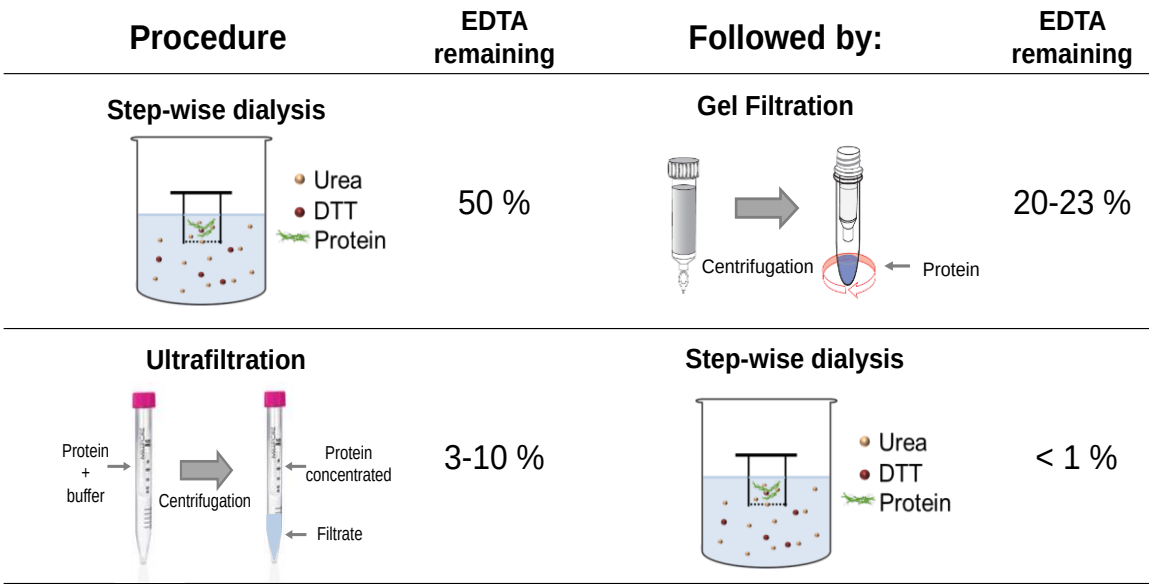

Figure 30. Efficiency of several procedures to remove EDTA.
Colorimetric determination of EDTA present in protein samples, initially containing 1 mM EDTA (100%), using the PAR competition assay, allowed the assessment of the efficacy of several purification procedures. Dialysis is the less effective method to eliminate EDTA from hypotonic protein solutions, as 50% of the EDTA remains in the dialyzed protein preparations; when followed by gel filtration, the EDTA amount is decreased down to ~20%. Ultrafiltration applied individually diminishes the EDTA concentration down to 3-10%; when combined with dialysis, the EDTA amount becomes virtually undetectable, therefore revealing to be the most efficient procedure to remove this metal chelator.

After testing several methods, we concluded that ultracentrifugation could be a good choice for efficient removal of EDTA, suitable for small sample volumes. Moreover, since vimentin requires dialysis to gradually remove urea as a part of the refolding protocol, we also tested the combination of both procedures and the results indicate that this approach efficiently eliminates EDTA from vimentin preparations (fig. 30). These results led us to establish the

ultrafiltration procedure prior to dialysis, detailed in the scheme of figure 11, as the most suitable method to reconstitute vimentin before performing the intended assays.

Beyond assessing the presence of putative additives that might interfere with the results, it is imperative to confirm that the techniques described above allow the correct refolding of vimentin into a functional protein. Therefore, biochemical and biophysical techniques associated to electron microscopy were applied to ensure the correct and functional reconstitution of both vimentin wt and C328S (fig. 12).

Analysis of ultrafiltrated and dialyzed preparations of vimentin by gel-based assays shows that both forms maintain a high level of purity after the refolding procedures, without apparent signals of degradation and/or cysteine oxidation (fig. 12A). Importantly, the tertiary structure of vimentin is functionally rescued after the refolding procedure, being mostly organized as a coiled-coil alpha-helical structure, as analyzed by CD (fig. 12B), and consistent with what is reported in the literature [244].

Further characterization of vimentin wt and C328S functionality involves the assessment of vimentin ability to polymerize when the ionic strength is raised up to physiological concentrations. Ultracentrifugation experiments show that both vimentin wt and C328S are able to polymerize into insoluble oligomers after addition of the polymerizing buffer, containing 150 mM NaCl (fig. 12C). Previous studies using analytical ultracentrifugation gave a detailed characterization of the vimentin species formed in hypotonic buffers [48, 51]. In fact, these studies also showed that the assembly process starts during renaturation of monomers by dialysis from 8 M urea into low ionic strength buffer, in which stable tetrameric assemblies are primarily formed.

Many available protocols recommend single-step polymerization and centrifugation procedures to confirm vimentin functionality. Nevertheless, confirmation of the formation of bona fide IFs is desirable, given the possibility that vimentin polymerizes into non-filamentous structures, as observed here with zinc (fig. 23). Under our conditions, EM inspection of non-polymerized vimentin wt and C328S morphology shows a homogeneous pattern of small rod-like structures. Moreover, raising the ionic strength gives origin to filaments with the typical morphology. This indicates that both vimentin wt and C328S

oligomeric species are assembled in a non-aggregated and functional fashion after ultrafiltration and dialysis (fig. 12D).

1.3 The substitution of C328 by serine appears to promote a faster assembly of vimentin

Our results indicate that both vimentin wt and C328S functionally undergo lateral assembly, elongation and compaction till filaments reach the typical width of nearly 12 nm and span, in some cases, several micrometers, at the end-point of polymerization.

Interestingly, determination of filament width and length show that vimentin C328S filaments present a diameter slightly narrower than those formed by vimentin wt, through all the different polymerization time points. In addition, at the earlier polymerization time points, vimentin C328S filaments are significantly longer than vimentin wt filaments, a tendency that is observed even at the end-point of assembly. The differences observed indicate that the highly conserved cysteine residue plays an important role in vimentin assembly and it influences the morphology of filaments. Indeed, the presence of cysteine seems to be related to a slower filament elongation and to the appearance of looser filaments with respect to vimentin mutant C328S, in the first stages of assembly. Substitution of cysteine by serine, on the other hand, could lead to tighter packing, due to its smaller size of the side chain and/or occurrence of different electrostatic interactions [276].

In fact, vimentin filaments are polymorphic and can comprise a variable number of tetramers per section, depending on the assembly conditions, the integrity of the protein, and the presence of certain divalent cations [55, 277]. The most accepted model comprises eight tetramers per section; however a higher number of subunits per filament cross-section has also been reported [54], which may result in a wider diameter.

Importantly, our results show that vimentin elongation and diameter are highly sensitive to oxidative modifications, a factor that had not been previously identified. In our conditions, preincubation of vimentin wt with electrophilic compounds prior to polymerization appears to delay filament elongation, an effect remarkably attenuated in vimentin C328S (fig. 14A) [3]. This outcome

could be related, at least in part, to oxidative modifications of the cysteine residue, and therefore, could contribute to explain the formation of longer filaments when the cysteine is not present. In sum, our results, summarized in figure 31, reveal for the first time subtle differences between the polymerization behavior of vimentin wt and C328S, which warrant further investigation.

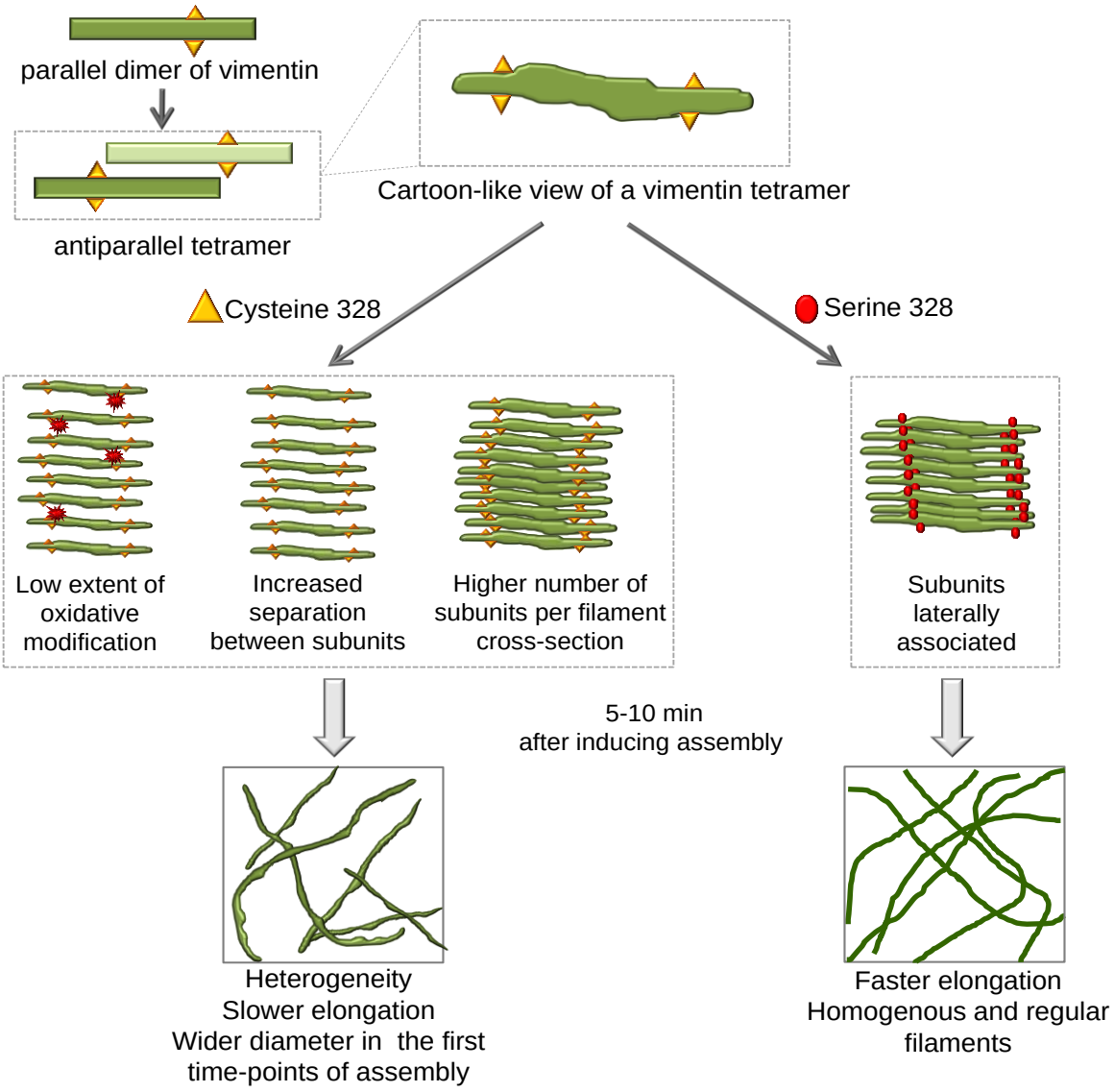

Figure 31. Influence of C328 on the first stages of vimentin polymerization.
The presence of the cysteine residue could induce variable conformations of the assembly intermediates, resulting in shorter, wider and more heterogeneous filaments, in the first 5 or 10 min of assembly. In turn, vimentin C328S assembles into more homogenous filaments, which suggests that the vimentin mutant is less vulnerable to conformational/morphological alterations

2. Characterization of vimentin as target for lipoxidation and oxidation

The unique biochemical and biophysical features of the vimentin structure together with the formation of an extensive and dynamic filamentous network confer vimentin an important role as a sensor of altered cell environment as well as a mediator of cell changes in response to mechanical and biochemical stress [1, 161, 278]. In fact, vimentin is a target for several oxidants and electrophilic lipids that, in general, lead to a marked vimentin network remodeling [4, 34]. Here, we have addressed the mechanisms underlying the effect of (lip)oxidative modifications of vimentin, both in vitro and in cells.

2.1 Vimentin is susceptible of modification by structurally diverse electrophilic compounds

Assessment of the in vitro modification of vimentin by different electrophilic species allowed the observation of distinct patterns depending on the reactivity of the modifying agents (fig. 13). Diamide induced the formation of a thiol-crosslinked product through disulfide bonding, therefore dependent on the presence of the single cysteine residue of vimentin, C328. A similar type of modification was detected upon incubation of vimentin wt with DMSO. DMSO is used as a solvent of both polar and hydrophobic compounds and it is frequently used as a vehicle for the storage and delivery of various molecules, both in vitro and in cell culture experiments [279, 280]. Although the effect of DMSO on oxidative modifications is rarely reported [281], our results indicate that even when used as vehicle, DMSO can induce a mild oxidation of vimentin.

In turn, HNE has a broader reactivity and its incorporation is detected in both vimentin wt and C328S mutant. Studies in biological systems reported that HNE primarily targets cysteine C328 in vimentin [167], however, our observations indicate that HNE can form adducts with other vimentin residues, when C328 is not present. Indeed, although cysteine residue is the most reactive to HNE if compared to histidine and lysine residues, the thiol adduct

has been reported to be less stable than histidine and lysine conjugates to HNE [282], which could explain the similar extent of HNE adduct formation in both vimentin wt and C328S. In contrast, the biotinylated analog of 15d-PGJ_2 shows a higher selectivity for the cysteine residue. This agrees with previous results in the literature, showing that cyclopentenone prostaglandins have selectivity for cysteine residues, as occurs for instance in the transcription factor NF-κB or in the Ras proteins [147].

Overall, these results indicate that the single cysteine residue of vimentin is particularly reactive, arising as an important hot spot for (lip)oxidative modifications. In fact, earlier experiments have reported that substitution of the cysteine residue by serine results in a vimentin mutant which is more resistant to the effect of treatment with electrophilic agents, in cells [4, 34, 164]. Moreover, the described observations are consistent with previous studies showing that cysteine C328 is a common target for several oxidative modifications besides lipoxidation, such as thiolation, glutathionylation and nitrosylation [283-285]. Indeed, proteomic studies have reported that the specific consensus sequence I/L-X-C-X_2-D/E directs the selective *S*-nitrosylation of cysteine in target proteins [285]. In vimentin, C328 is located within the L-T-C-E-V-D sequence that coincides with the required motif for *S*-nitrosylation. In this location, the cysteine residue is surrounded by acidic residues, glutamic acid, E329, and aspartic acid, D331, and by a hydrophobic residue, L326, which could increment cysteine nucleophilicity, and therefore could increase its susceptibility to post-translational modifications.

2.2 Morphological alterations of vimentin depend on the presence of C328 and on the properties of the lipoxidant agents

Vimentin is therefore susceptible to modification by structurally diverse compounds. Interestingly, the functional consequences of (lip)oxidation are dependent on the chemical structure and reactivity of the electrophilic compounds, as indicated by the variability of the electrophile-induced effects on vimentin assembly and on filament morphology (fig. 14). In vitro, diamide induces abnormal vimentin aggregation which drastically disrupts subsequent filament formation. This suggests that when a substantial proportion of vimentin

tetramers are linked by disulfide bonds, their conformation does not allow normal assembly or elongation. In contrast, preincubation with DMSO affects filament length and induces a marked increase of filament width. This effect is notably attenuated in vimentin C328S, suggesting that it could be partially caused by the formation of disulfide-bonded dimer observed in DMSO-treated vimentin wt. In turn, treatment with HNE has a stronger effect on filament length and width, inducing the formation of shorter and wider filaments of vimentin wt, at early and late time points of polymerization, respectively. This could be related to its ability to modify several residues. 15d-PGJ_2 induces various morphological alterations likely due to the disruption of assembly by the introduction of the bulky moiety of the prostaglandin.

It is worth noting that preincubation of vimentin wt in buffer before polymerization leads to the appearance of wider filaments compared to the ones assembled without delay. In addition to the herein reported evidence that vimentin C328S filaments are consistently thinner and longer, with respect to wild-type filaments, these observations suggest that oxidation occurring during preincubation, mainly affecting the cysteine residue, alters filament assembly through the putative cysteine-mediated mechanisms mentioned above. This possibility is further supported by the attenuation of the lipoxidant-induced morphological alterations in the vimentin C328S mutant. Therefore, the highly conserved cysteine residue is emerging not only as a hot spot for post-translational modification in vimentin, but also as a switch influencing its assembly properties and its behavior in response to electrophilic or oxidative stress.

2.3 The polymerization state of vimentin influences the functional outcome of the lipoxidative modification

The functional outcome caused by electrophilic modification is strikingly attenuated in preformed filaments of vimentin wt (fig. 15). However, gel-based assays confirm that the extent of (lip)oxidative modification is similar in both polymerized and non-polymerized vimentin, being in some cases higher in preformed filaments. This observation suggests that the nature or orientation of

the modified residues could be different in preformed filaments, which do neither interfere with the filament structure nor induce filament disruption.

Alternatively, previous incubation of soluble vimentin with (lip)oxidants could lead to the formation of bulky subunits, due to the adducted moiety, which would not be suitable for subsequent assembly. An additional possibility arises from potential conformational changes in the isolated subunits induced by the modification of C328, which putatively do not occur once incorporated in the filament. Inversely, C328 modification could impair the conformational rearrangements required for the formation of mature filaments.

As an overview, our in vitro results highlight vimentin as a target for several electrophilic agents. The structural and chemical properties of the lipoxidant agents markedly influence assembly, inducing morphological alterations such as aggregation, increased filament diameter, heterogeneity and/or bundling. Most importantly, the single cysteine residue arises as a critical modulator of vimentin behavior in response to (lip)oxidative stimuli and as a regulator of the intensity of the functional outcome. In addition, the impact of treatment with lipoxidants is strongly dependent on the polymerization state of vimentin, in such a way that modification of isolated subunits is more deleterious than that of preformed filaments. These observations are summarized in the scheme (fig. 32).

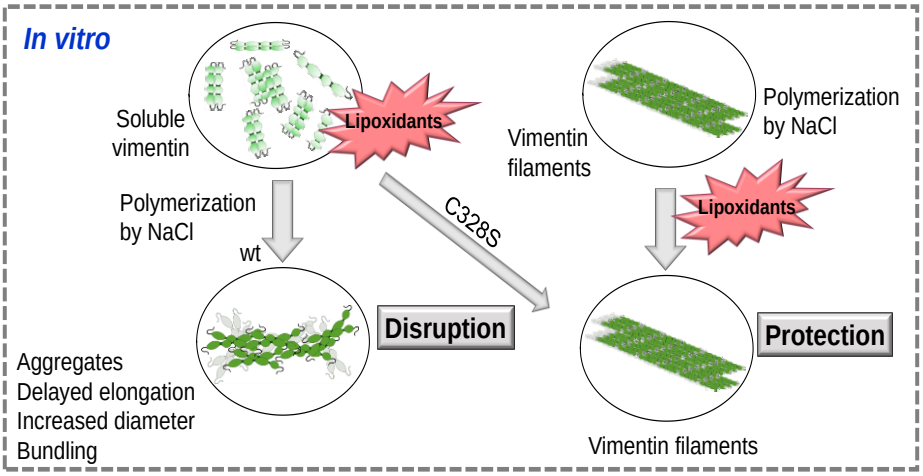

Figure 32. Relevance of the polymerization state of vimentin and the role of its single cysteine residue in the impact of (lip)oxidation.

In vitro, preincubation of soluble vimentin with electrophilic lipids and/or oxidants (lipoxidants) hampers subsequent filament formation induced by NaCl, leading to impaired elongation and/or aggregates, filaments of increased diameter or filament bundles, in a manner dependent on the presence of C328. In contrast, lipoxidation of preformed filaments does not severely alter filament morphology. Figure taken from [3].

2.4 In cells, diamide-induced disruption of the vimentin network requires active filament dynamics and the presence of C328

In cells, (lip)oxidation induces a noticeable reorganization of the vimentin network. In particular, cell treatment with the oxidant diamide intensely disrupts vimentin filaments, which is reliant on the presence of C328 (fig. 16). Although in vitro, diamide clearly induces the formation of a cysteine-crosslinked product, previous studies from our group did not detect this oxidative dimer in cells. In fact, diamide could induce the formation of mixed disulfides with other proteins or small molecules resulting in glutathionylation or cysteinylation [286, 287]. In addition, diamide is also able to decrease the concentration of glutathione [253], an essential thiol molecule for the regeneration of oxidized protein sulfhydryls, which in turn could increase vimentin susceptibility to lipoxidation. Lastly, diamide could indirectly promote the irreversible oxidation of the cysteine residue to sulfinic or sulfonic acids [288]. Such modifications may be involved in the disruption of vimentin network; nevertheless we cannot discard the possibility of diamide-induced oxidation of other cytoskeletal components or regulatory proteins that may indirectly affect the organization of the vimentin filamentous network [67, 289]. Therefore, the characterization of diamide-induced vimentin modification in cells requires further study.

In cells, vimentin exists both as soluble and polymerized forms, which are continuously exchanging subunits, therefore constituting a highly dynamic network [63]. In fact, our FRAP experiments show that after photobleaching, vimentin filaments are able to rapidly reincorporate “new subunits” and therefore, undergo a fluorescence recovery within seconds/minutes (fig. 17). Interestingly, there are several strategies, involving ATP depletion or cysteine crosslinking, which are able to minimize vimentin dynamics. The motile properties of vimentin have been reported to require ATP [290], and under our conditions, treatment with inhibitors of ATP synthesis, indeed blunted fluorescence recovery. However, the mechanism by which these compounds block vimentin dynamics is not completely understood. Previous studies suggest that ATP could either mediate the dissociation of vimentin tetramers from filaments, by regulating IF disassembly through phosphorylation, or preserve tetramer solubility by acting as a cofactor of chaperones [64].

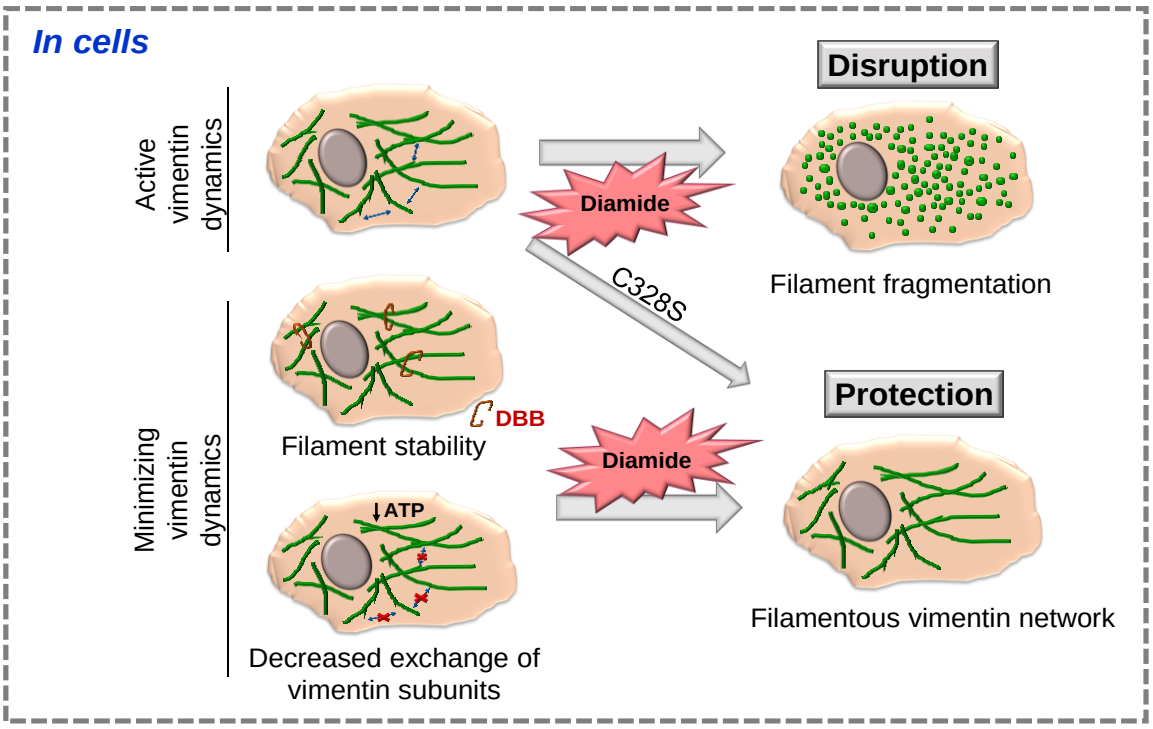

Figure 33. Importance of vimentin dynamics for the disruption of vimentin filaments induced by diamide.

In cells with active vimentin dynamics, diamide induced fragmentation of vimentin wt, but not C328S filaments. Minimizing vimentin dynamics protects the morphology of the vimentin wt network from diamide-induced disruption. Taken together these observations suggest that incorporation of modified vimentin subunits into filaments would be the process leading to network disruption. Figure taken from [3].

On the other hand, the cysteine crosslinker DBB could fix/stabilize the filament structure through direct or indirect mechanisms, preventing the exchange of vimentin subunits.

Remarkably, blocking vimentin dynamics protects its network against diamide-induced remodeling, indicating that the electrophilic disruption requires the active exchange of vimentin subunits (fig. 18). As observed in vitro, preformed filaments are more resistant to disruption. This leads us to propose a model according to which, modification of vimentin would occur in polymerized and soluble forms, but the disruption of the network would take place when soluble modified vimentin would be recruited into the filaments. Nevertheless, we should take into account other potential mechanisms. In the case of DBB, crosslinking of cysteine residues could directly protect this residue from other modifications. On the other hand, the protective effect of mitochondrial uncouplers could be the result of the alteration of other mitochondrial functions.

Lastly, both strategies used to minimize vimentin dynamics could act through indirect mechanisms that prevent vimentin disruption in response to diamide treatment.

Taken together, these results indicate that the vimentin network can be intensely remodeled by treatment with electrophilic compounds, an effect that requires an active vimentin dynamics and it is modulated by the presence of the single cysteine residue (fig. 33).

3. Vimentin-zinc interplay and its relevance in pathophysiology

The organization and function of the vimentin network can be modulated by several factors. Besides post-translational modifications, such as phosphorylation and the herein described lipoxidation, the ionic strength and the presence of divalent cations also play an important role in the regulation of vimentin behavior [5, 6]. Zinc is the second most abundant trace element and is essential for a wide range of biological functions [191]. Previous work unveiled that in vitro, vimentin binds zinc and its function is clearly modulated by zinc availability, in cells [4, 7]. Therefore, here we have addressed the structural and functional consequences of the vimentin-zinc interplay and its impact on the response of vimentin to (lip)oxidative stress.

3.1 Zinc reversibly induces the formation of large assemblies of both vimentin wt and C328S

In vitro studies performed with the wt and C328S forms of the protein unveil a similar behavior of both in presence of micromolar concentrations of zinc (fig. 19A). Likewise, turbidity and fluorescence anisotropy measurements show an analogous effect of increasing concentrations of zinc on the formation of larger assemblies, in both forms of vimentin (fig. 20A). In fact, within proteins, zinc coordinates mainly with cysteine, histidine, aspartate and glutamate residues [193]. Even though it is a rare situation, accounting for less than 1 % of all cases of zinc-ligand coordination, other amino acids, such as serine,

threonine or lysine, are also able to interact with zinc [291]. Therefore, zinc binding is not strictly dependent on the presence of the cysteine residue.

Interestingly, zinc has been reported to promote protein aggregation through various mechanisms. In the case of the transcription factor p53, zinc is able to bridge individual subunits, through coordination of different residues at protein-interface sites, consequently leading to the formation of larger assemblies [292]. Moreover, in vitro addition of an excess of zinc to polymerized tubulin results in the loss of microtubules and the formation of wide β-sheets [200]. Hypothetically, similar mechanisms could be involved in the formation of larger assemblies of vimentin in presence of this divalent cation. Therefore, the principle of zinc binding at protein-interface sites could be putatively involved in the formation of larger assemblies of vimentin. Alternatively, zinc could promote different vimentin subunit interactions favorable to the formation of β-sheets, instead of the typical α-helical organization, and consequently, induce vimentin associations more prone to oligomerization. Confirmation of these hypotheses would require further experimentation. However, zinc addition promoted the fast precipitation of vimentin on CD cuvettes, for which alternative strategies could be needed to address this point. Among them, thioflavin T, a probe used to explore the role of zinc binding in the formation of amyloid fibrils by Aβ11-28 [293], could be proposed.

Over the zinc proteome, proteins bind zinc with variable affinity. In the case of metallothioneins, these proteins bind zinc with an affinity constant ranging from nanomolar to picomolar order [294], whereas for tubulin, the zinc binding affinity is over the micromolar to millimolar ranges [295]. Our in vitro results suggest that vimentin binds zinc with an affinity in the micromolar range, therefore, similar to tubulin.

Remarkably, the action of zinc on vimentin polymerization/aggregation is fully reversed by the addition of metal chelators, EDTA or TPEN (fig. 20C and fig. 34). This is consistent with previous work reporting that zinc depletion induces reversible filament disassembly, in cells [4]. These observations are particularly relevant for the putative role of zinc in the regulation of vimentin dynamics, meaning that release of zinc into the cytoplasm as a response to extra- or intracellular stimuli, could contribute to rapid vimentin assembly/oligomerization that could be promptly reversed after restoring the

homeostatic concentrations of zinc [190]. Nevertheless, the possibility also exists that high concentrations of zinc could cause irreversible alterations of vimentin conformation.

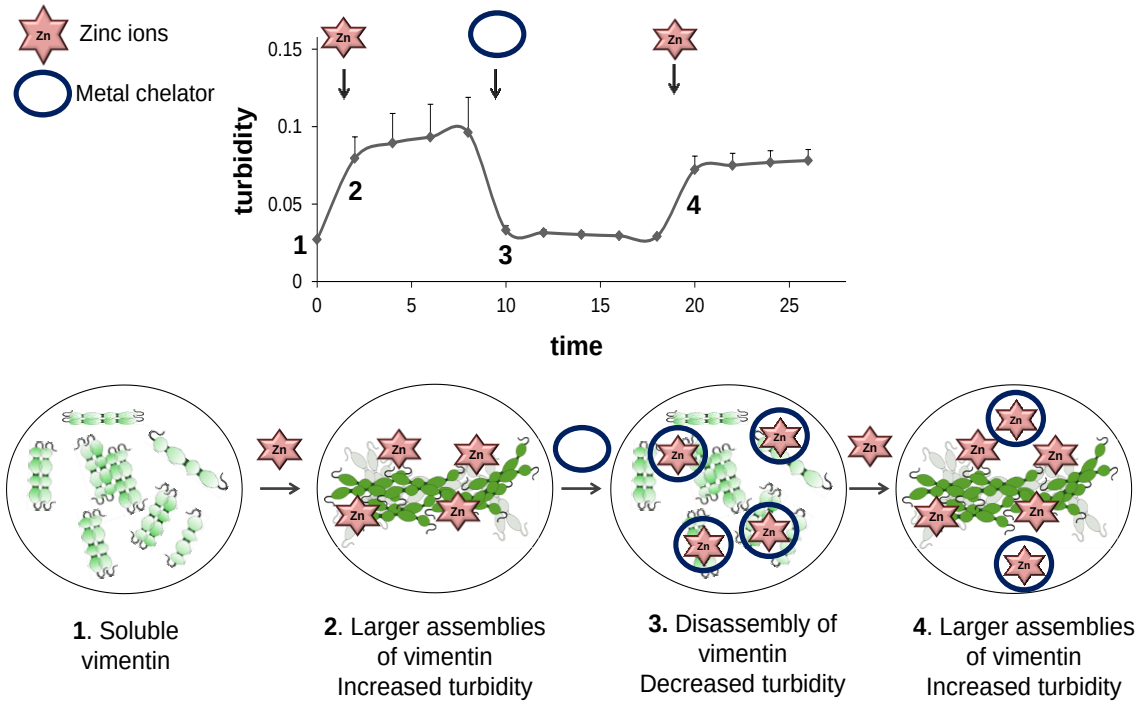

Figure 34. Reversible effect of zinc on vimentin polymerization.
Monitoring the turbidity changes shows that incubating vimentin with zinc induces the formation of larger assemblies, which are disassembled upon addition of an equivalent amount of a metal chelator, as suggested by the decrease of the solution turbidity. Subsequent addition of zinc restores the turbidity values indicating that larger aggregates of vimentin are being formed again.

Notably, the effect of zinc on vimentin polymerization, detected by turbidity assays, is not mimicked by the same concentration range of other divalent cations, such as $MgCl_2$, or monovalent salts, as NaCl. Although 150 mM NaCl is herein described to assemble vimentin into long 12 nm-wide filaments, it does not significantly increase vimentin turbidity, suggesting that zinc-induced structures are considerably larger and/or morphologically different. On the other hand, millimolar concentrations of $MgCl_2$ are required to induce changes similar to the ones observed with $ZnCl_2$. Even though our experiments could not ascertain the binding constants of these divalent cations to vimentin, it could be inferred that vimentin binds zinc with higher affinity than magnesium. Typically, magnesium cations bind to aspartate and glutamate residues, namely

through coordination with the oxygen atoms from their carboxyl or carbonyl groups [296], while zinc preferably coordinates with the sulfur atom of the cysteine residues [297]. These variations of metal coordination preferences within the protein could be related to the differences observed in the effect of the divalent cations on vimentin aggregation.

3.2 The effect of zinc on the morphology of vimentin assemblies is variable depending on the support used

The effect of zinc on the morphology of vimentin aggregates varies according to the support used for the incubation mixture, ranging from the appearance of a “beaded” network of protein, in solution, to the formation of robust cables, on glass slides (fig. 21). The morphological differences observed could putatively arise from changes in the conformation of the protein and/or in the overall charge of the molecule that occur on the distinct supports. Consequently, these variable factors could influence the nature of zinc interactions within the vimentin structure, which could lead to different subunit associations and consequently, could build morphologically distinct vimentin structures. Indeed, zinc coordination is dynamic, involving changes in geometry and/or coordination number and ionization of ligands [298]; therefore, zinc binding sites have plasticity and/or can adopt several structures, according to the features of the protein environment.

Importantly, vimentin can exist both in intra and extracellular spaces [1], being subjected to different environmental conditions that may promote different rearrangements of the vimentin structure. In diseases such as age-related macular degeneration, vimentin can be found in extracellular deposits, where micromolar to millimolar zinc concentrations have been measured and could be involved in vimentin aggregation [299, 300]. Taken together, these observations suggest that the functional outcome of exposure of vimentin to zinc can vary depending on its location and the concentration of zinc.

3.3 The functional outcome of zinc interaction with vimentin depends on the polymerization state of the protein

EM inspection of both vimentin wt and C328S structures formed in presence of zinc corroborate the results obtained in the turbidity and fluorescence anisotropy experiments, that this divalent cation is able to induce the formation of larger assemblies of vimentin (fig. 22). Determination of the dimensions of these vimentin structures indicates that width is the feature more affected by increasing concentrations of zinc, thus, it could be inferred that this divalent cation primarily induces lateral association of vimentin oligomers. Nevertheless, we cannot discard the possibility that zinc promotes vimentin elongation, at longer times of polymerization.

Turbidity experiments gave the first evidence that the polymerization state of vimentin could influence the functional outcome of the interaction with zinc, indicating that the size and/or shape of the zinc-induced structures are different if vimentin is soluble or previously assembled (fig. 23A). EM inspection of the morphological changes revealed that preincubation with zinc prior to assembly induces atypical protein aggregation that fails to further assemble into filaments upon addition of 150 mM of NaCl, in both vimentin wt and C328S. These observations suggest that zinc binding rearranges the structure of the soluble subunits of vimentin into non-functional assemblies that are incompetent to form filaments. Moreover, this suggests that this effect is due to the interaction of zinc with residues other than cysteine, most likely, carboxylic residues, which account for 18 % of vimentin sequence.

In contrast, zinc addition to preformed filaments of vimentin wt induces intense bundling and a marked increase of filament diameter. This effect could be due to filament reorganization into a looser configuration and/or to a higher level of polymorphism, as a result of lateral association of an unusual number of vimentin subunits, in presence of zinc. Notably, this effect does not occur in vimentin C328S filaments. Therefore, whereas zinc appears to alter the structure of both wt and C328S subunits, its effect on preformed filaments requires the presence of C328, which underlines the importance of this residue in vimentin structure and function.

3.4 Zinc coordinates with the thiolate form of C328 and protects vimentin from modification by different cysteine-reactive compounds in vitro

The relevance of the potential cysteine-zinc coordination is highlighted by the results obtained from the computational and crosslinking experiments (fig. 24). Besides the 23 possible hot-spots for zinc binding found within the modeled dimer of vimentin, MD simulations indicated that cysteine residue, C328, in its thiolate form, participates in the coordination with zinc. In nature, an important proportion of the cysteine residues occur in its thiolate form, where the thiol/thiolate proportion is dependent on the pKa and accessibility of the cysteine residue within the protein environment [301]. Our group was able to experimentally determine the pKa of C328, by setting up a procedure based on the modification of cysteine residues by the fluorescent compound monobromobimane (Mónico et al., manuscript in preparation). Interestingly, soluble vimentin presents two different pKa values, of approximately 4.6 and 7.4, possibly resulting from the existence of distinct oligomeric or conformational species in the protein preparation. Therefore, under physiological conditions, the cysteine residue will occur in both thiol and thiolate forms, and the interaction between the latter form and zinc may have important implications in the regulation of vimentin function within the cellular environment. This is strongly supported by the ability of zinc to prevent vimentin alkylation by cysteine-reactive agents (fig. 24B) and to preclude chemical and oxidative cysteine crosslinking in vitro (fig. 25). In particular, the protective role of zinc against vimentin modification by 15d-PGJ_2 and diamide, lipoxidant agents which, as described here, strongly affect vimentin functionality, could be highly relevant.

The disposition of the tetrameric units within the filaments is not completely understood. Nevertheless, it is currently accepted, that in dimers, cysteine residues are oriented outwards. In turn, dimers can adopt different alignments within tetramers, in which the distance between cysteines is variable [50, 51]. Indeed, cysteine crosslinking induced by DBB indicates that there are cysteines from distinct dimers that fall within close distance (3 to 6 Å), likely in adjacent tetramers or in filaments.

Remarkably, zinc selectively prevents DBB-induced cysteine crosslinking (fig. 25 and fig. 26). One putative explanation arises from the sterical hindering caused by the zinc coordination with the cysteine. Alternatively, zinc could bind to other sites of vimentin, rearranging its structure in such a manner that cysteines could no longer be at a distance amenable for DBB crosslinking, but still be at a distance adequate for crosslinking with longer space-arm crosslinkers, as bismaleimidohexane (BMH). These hypothetical mechanisms are summarized in the scheme of figure 35.

Even though the protective role of zinc towards cysteine modification in vitro is used here to support its interaction with the thiolate form of C328, it should be borne in mind that, some of these zinc-thiolate coordination environments, could be even more reactive and susceptible to modification, which is reliant on the affinity properties of the zinc binding sites within the protein [191].

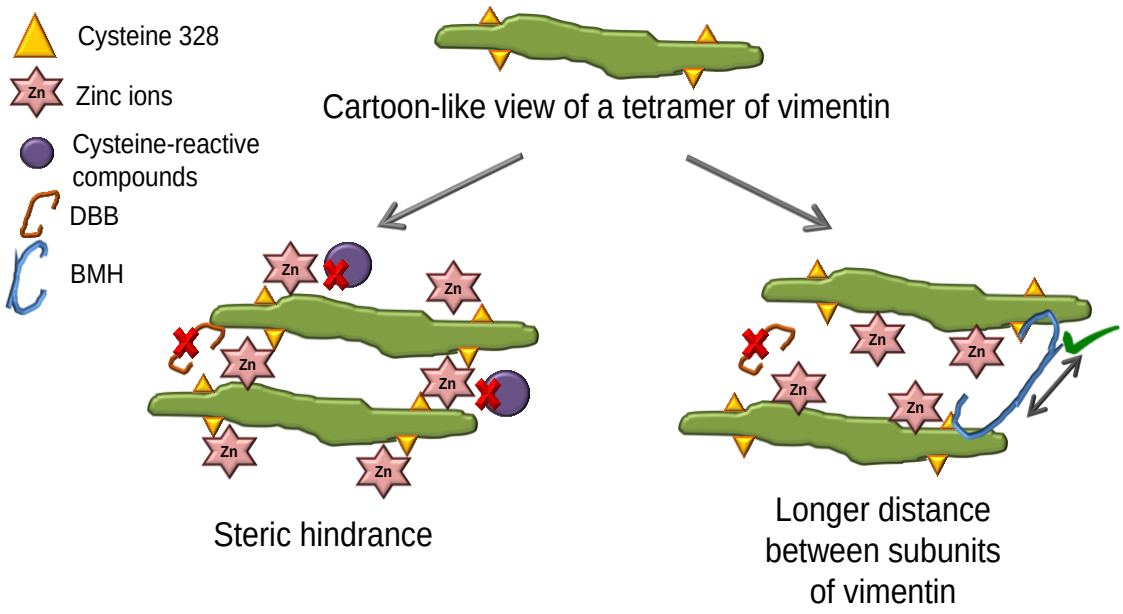

Figure 35. Hypothetical mechanisms for the protective role of zinc against cysteine modification of vimentin.

Interaction between zinc and vimentin subunits prevents cysteine modification by diverse reactive agents, in vitro. This protection could be due to direct steric hindrance through zinc coordination with C328, in the case of alkylating agents and crosslinkers (left panel), or to conformational changes that result in longer distance between vimentin subunits and preclude cysteine crosslinking by shorter crosslinkers, as DBB, but do not affect the crosslinking by longer space-arm crosslinkers, as BMH (right panel).

3.5 In cells, supplementation with zinc prevents diamide-induced disruption of the vimentin network

The effects of zinc on vimentin in vitro have a clear counterpart in cells. In fact, zinc treatment, at concentrations in the physiological range, shows a tendency to promote vimentin network reorganization into thicker filaments, in adrenal carcinoma cells and in fibroblasts (fig. 27A and fig. 28B). These alterations could be due to the capacity of zinc to induce lateral association and filament bundling, as observed in vitro.

Additionally, prior supplementation with zinc attenuates the network fragmentation induced by diamide, a protective role that is dependent on the concentration of zinc and on the time of exposure to the oxidant (fig. 27 and fig. 36). Based on the in vitro observations, this protection could be explained by the direct effect of zinc on vimentin, through mechanisms associated to thiolate-zinc coordination that precludes vimentin modification by diamide. However, within the cell environment, the interpretation is much more complex, since additional mechanisms could also be indirectly involved in the protective function of zinc. For instance, the “pro-antioxidant” effect of this divalent cation is well-recognized, by supporting the activity of several enzymes and regulating the concentration of important antioxidant molecules, such as glutathione, that are capable of scavenging reactive electrophilic compounds [210]. Therefore, zinc could decrease diamide availability through the antioxidant system, and thus mitigate its deleterious effect. Lastly, a decline in ATP production, via zinc inhibition of glyceraldehyde 3-phosphate dehydrogenase [302], could indirectly block vimentin dynamics, consequently preventing the oxidatively-modified isolated subunits to reincorporate into the filaments and subsequently disrupt the filamentous network of vimentin.

3.6 Zinc attenuates the effect of lipoxidation induced by HNE, in a pathophysiological model

The reported observations of zinc in the prevention of diamide-induced disruption of the vimentin network have extended our interest to explore this putative protective role in a relevant pathophysiological model. Genetic alteration of zinc availability has important consequences on vimentin functionality, as indicated by the observation of a basal alteration of the vimentin network, in acrodermatitis enteropathica (AE) fibroblasts, which after zinc addition rearranges to a morphology closer to the one observed in the control fibroblasts [4]. Therefore, we have used fibroblasts from AE patient, displaying low cellular zinc uptake and content, to address the interplay between zinc availability and vimentin function as well as its impact on the lipoxidation induced by HNE.

Supplementation with zinc and treatment with HNE have clear effects not only on the vimentin network but also in the overall state of the cell, namely on the cell size and on the actin microfilament system, in both control and zinc-deficient fibroblasts (fig. 28 and fig. 29).

Interestingly, the extent of the effects of HNE varies depending on the cell model and the feature under study. For instance, the effects of HNE on the retraction of vimentin appear to be similar in control and zinc-deficient cells, whereas the effect on cell shrinking is stronger in control and the effects on actin appear to be more marked in zinc-deficient fibroblasts. Nevertheless, differences between both cell types should be interpreted cautiously for the reasons given in the following section.

Remarkably, most of HNE-induced alterations are significantly attenuated by previous supplementation with zinc, both in control and zinc-deficient fibroblasts (fig. 28 and fig. 29). Therefore, these observations substantiate the protective role of this divalent cation against the cytoskeletal reorganization induced by (lip)oxidative stress (fig. 36).

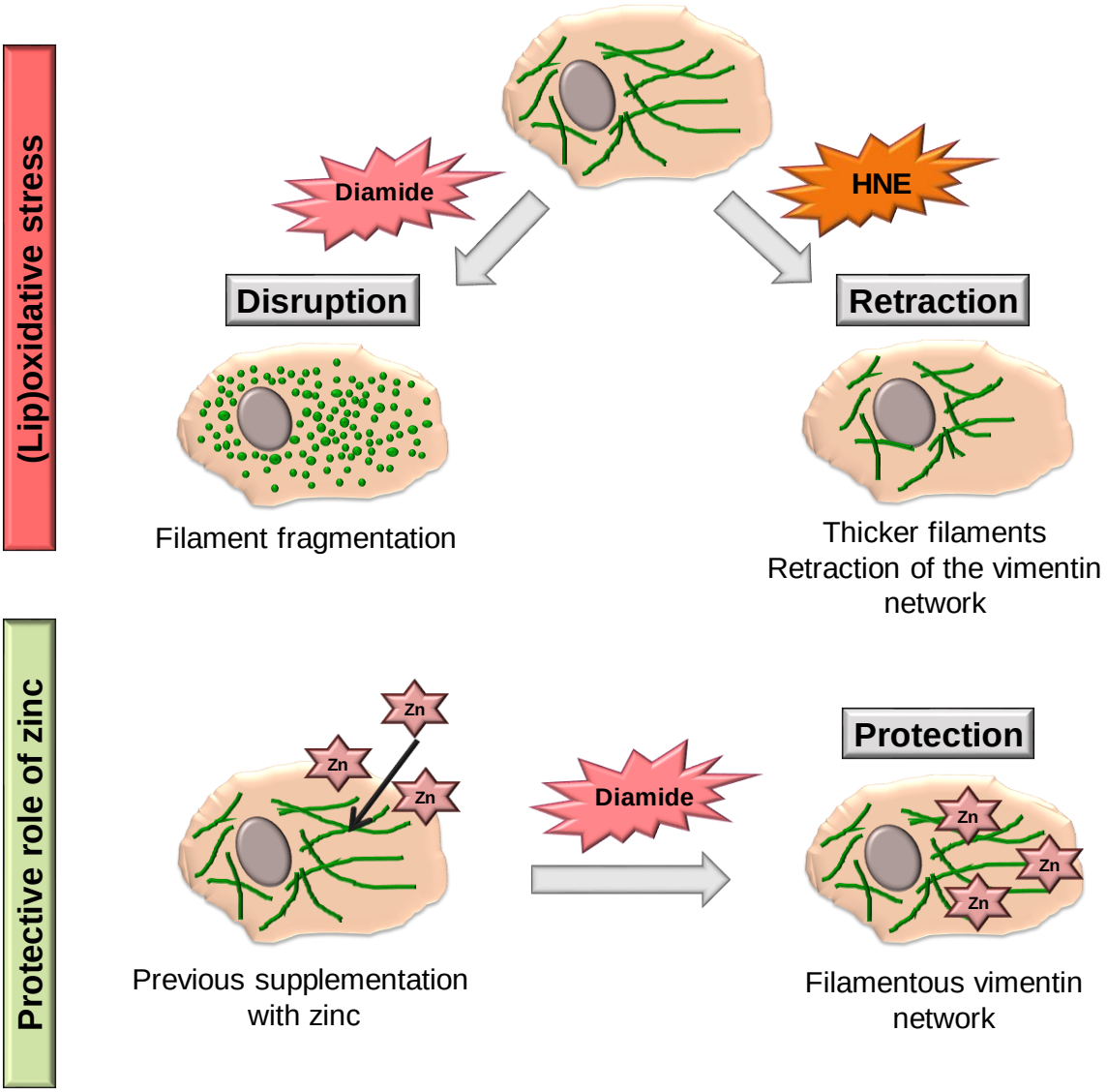

Figure 36. Importance of zinc availability in the response of vimentin to (lip)oxidative stress induced by diamide and HNE.

Cell treatment with diamide induces fragmentation of vimentin network, whereas HNE provokes reorganization of the network into thicker filaments, appearing closer to the perinuclear area of the cell. In stress conditions, prior supplementation with zinc attenuates the effects of diamide on the vimentin network.

3.7 Proteomic studies unveil effects of zinc and HNE on the abundance of proteins involved in cytoskeletal organization

Quantitative proteomics was used in an attempt to obtain a more systematic view of the changes in cellular homeostasis induced by HNE and zinc (tables 5 and 6). In control fibroblasts, only 6 proteins suffered significant changes across the different experimental conditions. In contrast, 55 proteins were differentially regulated in zinc-deficient fibroblasts, indicating a higher susceptibility to HNE and zinc treatment. Nevertheless, as control and AE fibroblasts were derived from individual donors, we will not attempt to make a direct comparison of their response to the different experimental conditions, since they could be influenced by factors as donor age or genetic background. For this, our aim is to compare the distinct conditions within each cell model, separately.

In control fibroblasts, functional analysis has demonstrated that the proteins which suffered the higher variation of its abundance are reported to bind zinc and to be involved in the reorganization of the cytoskeletal network. This is the case of the zinc-finger protein 613 (Q6PF04), a transcription factor belonging to the abundant family of zinc-finger proteins (ZNFs) [194]. Nevertheless, the function of this protein is still not well characterized. Other important examples are the myosin light chain kinase and the actin-related protein 2/3 complex subunit 4, which modulates the movement of actin filaments and regulates actin polymerization, respectively [303, 304]. Therefore, these proteins are important for actin-driven processes, such as the formation of filopodia, lamellipodia and stress fibers and consequently, important for cell migration, adhesion and shape [305]. Remarkably, there is a complex interplay between actin and vimentin, both in resting and in dividing cells [67, 306]. Indeed, plectin-mediated interaction between contractile actomyosin arcs and vimentin filaments controls the localization and dynamics of these two cytoskeletal systems and it is therefore important for cell morphogenesis [307]. Thus, we could assume that changes in the actin system may have putative functional outcomes in the vimentin network, and the other way around.

Regarding zinc-deficient fibroblasts, analysis of the biological function has shown that 13 of the proteins differentially regulated are intrinsically

associated to cell junction formation or to cell adhesion, thus being closely involved in the reorganization of the cytoskeletal network that is required for these cellular processes, although the amplitude of the changes observed in most proteins was limited. In particular, annexin A2, calponin-2, paxillin and integrin-linked protein kinase are reported to bind actin, inducing conformational changes and regulating its dynamics [263, 308]. Besides being involved in cell-adhesion processes, these proteins also play an important role in the transduction of extracellular signals into intracellular responses, and consequently they are significant mediators of the cell response to lipoxidative stress [309]. In particular, catenin alpha-1 and catenin delta-1 are moderately up-regulated in all conditions. These proteins are able to bind actin and to form a dynamic complex with cadherin, participating in the formation of adherens junctions, which are key contributors to tissue morphogenesis and homeostasis [264]. Nevertheless, the extent of the changes observed is in general small. Moreover, there do not seem to be changes elicited by HNE that are reverted in the zinc-supplemented cells. Indeed, in some cases, both zinc and HNE induce changes in protein abundance, that although small, go in the same direction.

Interesting studies have described that certain oxidized phospholipids exhibit potent barrier-protective effects in lung endothelial cell barrier dysfunction, putatively through enhancement of peripheral actin cytoskeleton, cell-cell and cell-substrate contacts [310, 311]. Thus, HNE- and zinc-mediated regulation of different classes of cell adhesive structures may have a prominent role in the cell response to lipoxidative stress. Nevertheless, the functional consequences warrant further investigation in order to understand whether this interaction is beneficial or detrimental for cell homeostasis.

Remarkably, HNE and zinc plus HNE treatments caused an increase of the levels of several ribosomal proteins involved in signal recognition particle SRP-dependent cotranslational protein targeting to membrane. These proteins constitute essential cellular machinery that mediates the proper localization of membrane and secretory proteins, ensuring the correct membrane protein biogenesis for cell structure and function, and contributing to the effectiveness of cellular adaptive responses to the stress caused by compromised protein biogenesis [312]. Moreover, the cotranslational protein translocation pathway could be coupled to the unfolded protein response in order to effectively

eliminate unfolded/damaged non-functional proteins [313]. Therefore, these observations suggest that HNE-induced lipoxidation and/or supplementation with zinc could trigger important cellular adaptive pathways in order to restore cell homeostasis, either by activating cell machinery involved in protein biogenesis, therefore contributing to protein turnover and guaranteeing the optimal protein functioning, or by up-regulating pathways responsible for the efficient elimination of damaged proteins.

Notably, no significant changes were observed in the levels of vimentin during the time frame of these treatments. Nevertheless, previous studies have reported an effect of zinc on vimentin levels in lung cancer cells [314] and in renal tubular epithelial cells [315]. Moreover, earlier proteomic studies, in several experimental models and in samples from patients, have identified HNE-adducts in vimentin, as well in other cytoskeletal proteins, such as tubulin and actin [167, 316]. Immunofluorescence studies, using anti-vimentin and anti-HNE adduct antibodies, have shown colocalization of HNE at the edges of the vimentin network where the intermediate filaments are less organized and do no reach the cell periphery, in senescent fibroblasts [316]. Thus, hypothetically, the changes observed in the vimentin network could be the direct result of the modification by HNE and/or interaction with zinc, or could arise from indirect effects occurring in other proteins or structures that affect vimentin organization. Future studies will focus on the PTMs of vimentin induced by HNE and zinc as well as in the development of models to elucidate the mechanisms underlying their functional consequences.

In summary, our results unveil novel features of vimentin assembly in vitro and in cells, highlighting the modulatory effect of (lip)oxidation and zinc availability. Moreover, they open novel perspectives for the study of other IF proteins as sensors for oxidants and electrophiles as well as their interplay with zinc.

CONCLUSIONS IN ENGLISH

As the result of the work presented in this thesis, in which the effect of lipoxidation on vimentin organization as well as the functional and structural consequences of the vimentin-zinc interaction were addressed, we have reached the following conclusions:

1. The chelator agent, EDTA, present in protein preparations, is often inefficiently removed by dialysis.
2. NMR detection of the complex formed between EDTA and zinc and the colorimetric assay monitoring the competition between EDTA and the zinc-binding compound PAR are adequate methods for an initial assessment of the presence of this chelator agent.
3. Ultrafiltration followed by dialysis achieve an efficient removal of EDTA from purified vimentin preparations, allowing the functional refolding of the protein, in the absence of metal chelators.

These results shed light on the importance of effective methods to detect and remove EDTA from protein preparations.

4. Vimentin is susceptible to modification by structurally diverse electrophilic compounds. The functional consequences of the modification depend on the reactivity and chemical structure of the modifying agents.
5. The single cysteine residue of vimentin, C328, is particularly reactive, arising as an important hot spot for (lip)oxidative modifications and as a hinge influencing the morphological changes in vimentin configuration in response to lipoxidation.
6. The impact of treatment with lipoxidants on vimentin organization is strongly dependent on its polymerization state, in such a way that modification of isolated subunits is more deleterious than that of preformed filaments.
7. In cells, the vimentin network can be intensely remodeled by treatment with electrophilic compounds. This effect requires an active dynamics/subunit exchange and is modulated by the presence of the single cysteine residue.

Taken together, these results unveil the role of the cysteine residue, C328, and filament dynamics in the functional outcome of vimentin lipoxidation

8. Zinc reversibly induces vimentin assembly into larger structures, possibly by inducing lateral association of vimentin oligomers. This outcome is not mimicked by other salts, such as $MgCl_2$ and NaCl.
9. The functional consequence of the exposure of vimentin to zinc and the morphology of the assemblies formed depend on the support used and on the polymerization state of the protein.
10. The cysteine residue, C328, is important for zinc-induced morphological alterations of vimentin preformed filaments.
11. Zinc protects vimentin from in vitro modification by various electrophilic compounds and crosslinkers targeting the cysteine residue.
12. In cells, prior supplementation with zinc attenuates the remodeling of the vimentin network induced by diamide and some of the morphological and cytoskeletal alterations provoked by HNE.

These results indicate that zinc induces vimentin polymerization and protects it from modification by electrophilic compounds in vitro, putatively through interaction with its cysteine residue. Zinc also exerts complex protective effects on (lip)oxidation-induced alterations in cells.

CONCLUSIONS IN SPANISH

Como resultado del trabajo presentado en esta Tesis, en la que se ha estudiado el efecto de la lipoxidación sobre la organización de la vimentina, así como las consecuencias funcionales y estructurales de la interacción vimentina-zinc, se han alcanzado las siguientes conclusiones:

1. El agente quelante, EDTA, presente en las preparaciones de proteínas, no se elimina de manera eficiente mediante diálisis.
2. La detección mediante RMN del complejo formado entre EDTA y zinc y el ensayo colorimétrico basado en la competición entre EDTA y el compuesto PAR, capaz de unir zinc, son métodos adecuados para una evaluación inicial de la presencia de este agente quelante en las preparaciones de proteínas.
3. La ultrafiltración seguida de diálisis logra una eliminación eficiente de EDTA de las preparaciones de vimentina, permitiendo el plegamiento funcional de la proteína, en ausencia de quelantes de metales.

Estos resultados destacan la importancia de utilizar métodos efectivos para detectar y eliminar el EDTA de las preparaciones de proteínas.

4. La vimentina es susceptible de modificación por compuestos electrófilos estructuralmente diversos. Las consecuencias funcionales de la modificación dependen de la reactividad y la estructura química de los agentes implicados.
5. El único residuo de cisteína de la vimentina, C328, es particularmente reactivo, y se destaca como una diana importante de modificaciones (lip)oxidativas e que influyen en los cambios morfológicos en la conformación de los filamentos de vimentina en respuesta a la lipoxidación.
6. El impacto del tratamiento con lipoxidantes en la organización de la vimentina depende en gran medida de su estado de polimerización, de tal manera que la modificación de las subunidades aisladas es más perjudicial que la de los filamentos preformados.
7. En las células, la trama de filamentos de la vimentina puede sufrir una intensa remodelación en respuesta al tratamiento con compuestos

electrófilos. Este efecto requiere un intercambio activo de subunidades y está modulado por la presencia del único residuo de cisteína, C328.

En conjunto, estos resultados revelan el papel del residuo de cisteína, C328, y la dinámica de los filamentos en las consecuencias funcionales de la lipoxidación de vimentina.

8. El zinc induce el ensamblaje de vimentina en estructuras de mayor tamaño de forma reversible, posiblemente favoreciendo la asociación lateral de oligómeros de vimentina. Este resultado no se observa tras la incubación de vimentina con otras sales, como MgCl2 y NaCl.
9. La consecuencia funcional de la exposición de vimentina al zinc y la morfología de los complejos formados dependen del soporte utilizado y del estado de polimerización de la proteína.
10. El residuo de cisteína, C328, es importante para las alteraciones morfológicas de los filamentos preformados de vimentina inducidas por zinc.
11. El zinc protege la vimentina de la modificación in vitro por diversos compuestos electrófilos y agentes de crosslinking dirigidos al residuo de cisteína.
12. En las células, el suplemento previo con zinc atenúa la remodelación de la trama de filamentos de vimentina inducida por diamida y algunas de las alteraciones provocadas por HNE en proteínas del citoesqueleto.

Estos resultados indican que el zinc induce la polimerización de vimentina y la protege de la modificación por compuestos electrófilos in vitro, potencialmente a través de la interacción con su residuo de cisteína. El zinc también ejerce efectos protectores complejos sobre las alteraciones inducidas por (lip)oxidación en las células.

REFERENCES

[1] F. Danielsson, M.K. Peterson, H. Caldeira Araujo, F. Lautenschlager, A.K.B. Gad, Vimentin Diversity in Health and Disease, Cells 7(10) (2018).

[2] J. Lowery, E.R. Kuczmarski, H. Herrmann, R.D. Goldman, Intermediate Filaments Play a Pivotal Role in Regulating Cell Architecture and Function, J Biol Chem 290(28) (2015) 17145-53.

[3] A. Monico, S. Duarte, M.A. Pajares, D. Perez-Sala, Vimentin disruption by lipoxidation and electrophiles: Role of the cysteine residue and filament dynamics, Redox Biol (2019) (doi: 10.1016/j.redox.2019.101098).

[4] D. Perez-Sala, C.L. Oeste, A.E. Martinez, M.J. Carrasco, B. Garzon, F.J. Canada, Vimentin filament organization and stress sensing depend on its single cysteine residue and zinc binding, Nat Commun 6:7287 (2015).

[5] Y.C. Lin, C.P. Broedersz, A.C. Rowat, T. Wedig, H. Herrmann, F.C. Mackintosh, D.A. Weitz, Divalent cations crosslink vimentin intermediate filament tail domains to regulate network mechanics, J Mol Biol 399(4) (2010) 637-44.

[6] G.L. C, O. Saldanha, A. Aufderhorst-Roberts, C. Martinez-Torres, M. Kuijs, G.H. Koenderink, S. Koster, K. Huber, Effect of ionic strength on the structure and elongational kinetics of vimentin filaments, Soft Matter 14(42) (2018) 8445-8454.

[7] D. Perez-Sala, C.L. Oeste, F.J. Sanchez-Gomez, Vimentin gets a new glow from zinc, Oncotarget 6(18) (2015) 15742-3.

[8] H.H. Rogers K., Franke W., Characterization of Disulfide Crosslink Formation of Human Vimentin at the Dimer, Tetramer, and Intermediate Filament Levels, J Struct Biol 117(1) (1996) 55-69.

[9] T.D. Pollard, R.D. Goldman, Overview of the Cytoskeleton from an Evolutionary Perspective, Cold Spring Harb Perspect Biol 10(7) (2018).

[10] A.F. Pegoraro, P. Janmey, D.A. Weitz, Mechanical Properties of the Cytoskeleton and Cells, Cold Spring Harb Perspect Biol 9(11) (2017).

[11] J. Roostalu, T. Surrey, Microtubule nucleation: beyond the template, Nat Rev Mol Cell Biol 18(11) (2017) 702-710.

[12] T. Svitkina, The Actin Cytoskeleton and Actin-Based Motility, Cold Spring Harb Perspect Biol 10(1) (2018).

[13] H. Herrmann, U. Aebi, Intermediate Filaments: Structure and Assembly, Cold Spring Harb Perspect Biol 8(11) (2016).

[14] W.H. Goldmann, Intermediate filaments and cellular mechanics, Cell Biol Int 42(2) (2018) 132-138.

[15] M. Hesse, T.M. Magin, K. Weber, Genes for intermediate filament proteins and the draft sequence of the human genome: novel keratin genes and a surprisingly high number of pseudogenes related to keratin genes 8 and 18, J Cell Sci 114(Pt 14) (2001) 2569-75.

[16] S. Etienne-Manneville, Cytoplasmic Intermediate Filaments in Cell Biology, Annu Rev Cell Dev Biol 34 (2018) 1-28.

[17] S. Kim, P.A. Coulombe, Intermediate filament scaffolds fulfill mechanical, organizational, and signaling functions in the cytoplasm, Genes Dev 21(13) (2007) 1581-97.

[18] A.A. Chernyatina, D. Guzenko, S.V. Strelkov, Intermediate filament structure: the bottom-up approach, Curr Opin Cell Biol 32 (2015) 65-72.

[19] M. Knobel, E.A. O'Toole, F.J. Smith, Keratins and skin disease, Cell Tissue Res 360(3) (2015) 583-9.

[20] S. Song, A. Landsbury, R. Dahm, Y. Liu, Q. Zhang, R.A. Quinlan, Functions of the intermediate filament cytoskeleton in the eye lens, J Clin Invest 119(7) (2009) 1837-48.

[21] P.S.J. Weston, T. Poole, N.S. Ryan, A. Nair, Y. Liang, K. Macpherson, R. Druyeh, I.B. Malone, R.L. Ahsan, H. Pemberton, J. Klimova, S. Mead, K. Blennow, M.N. Rossor, J.M. Schott, H. Zetterberg, N.C. Fox, Serum neurofilament light in familial Alzheimer disease: A marker of early neurodegeneration, Neurology 89(21) (2017) 2167-2175.

[22] S.M. Kang, M.H. Yoon, B.J. Park, Laminopathies; Mutations on single gene and various human genetic diseases, BMB Rep 51(7) (2018) 327-337.

[23] I. Szeverenyi, A.J. Cassidy, C.W. Chung, B.T. Lee, J.E. Common, S.C. Ogg, H. Chen, S.Y. Sim, W.L. Goh, K.W. Ng, J.A. Simpson, L.L. Chee, G.H. Eng, B. Li, D.P. Lunny, D. Chuon, A. Venkatesh, K.H. Khoo, W.H. McLean, Y.P. Lim, E.B. Lane, The

Human Intermediate Filament Database: comprehensive information on a gene family involved in many human diseases, Hum Mutat 29(3) (2008) 351-60.

[24] M.B. Omary, N.O. Ku, P. Strnad, S. Hanada, Toward unraveling the complexity of simple epithelial keratins in human disease, J Clin Invest 119(7) (2009) 1794-805.

[25] R.K. Liem, A. Messing, Dysfunctions of neuronal and glial intermediate filaments in disease, J Clin Invest 119(7) (2009) 1814-24.

[26] H.H. Goebel, A. Blaschek, Protein aggregation in congenital myopathies, Semin Pediatr Neurol 18(4) (2011) 272-6.

[27] J. Neradil, R. Veselska, Nestin as a marker of cancer stem cells, Cancer Sci 106(7) (2015) 803-11.

[28] H. Herrmann, B. Fouquet, W.W. Franke, Expression of intermediate filament proteins during development of Xenopus laevis. II. Identification and molecular characterization of desmin, Development 105(2) (1989) 299-307.

[29] M. Schaffeld, H. Herrmann, J. Schultess, J. Markl, Vimentin and desmin of a cartilaginous fish, the shark Scyliorhinus stellaris: sequence, expression patterns and in vitro assembly, Eur J Cell Biol 80(11) (2001) 692-702.

[30] M. Matsuyama, H. Tanaka, A. Inoko, H. Goto, S. Yonemura, K. Kobori, Y. Hayashi, E. Kondo, S. Itohara, I. Izawa, M. Inagaki, Defect of mitotic vimentin phosphorylation causes microophthalmia and cataract via aneuploidy and senescence in lens epithelial cells, J Biol Chem 288(50) (2013) 35626-35.

[31] A. Satelli, S. Li, Vimentin in cancer and its potential as a molecular target for cancer therapy, Cell Mol Life Sci 68(18) (2011) 3033-46.

[32] P. Henderson, D.C. Wilson, J. Satsangi, C. Stevens, A role for vimentin in Crohn disease, Autophagy 8(11) (2012) 1695-6.

[33] C. Fernandez-Ortega, A. Ramirez, D. Casillas, T. Paneque, R. Ubieta, M. Dubed, L. Navea, L. Castellanos-Serra, C. Duarte, V. Falcon, O. Reyes, H. Garay, E. Silva, E. Noa, Y. Ramos, V. Besada, L. Betancourt, Identification of Vimentin as a Potential Therapeutic Target against HIV Infection, Viruses 8(6) (2016).

[34] K. Stamatakis, F.J. Sanchez-Gomez, D. Perez-Sala, Identification of novel protein targets for modification by 15-deoxy-Delta12,14-prostaglandin J2 in mesangial cells

reveals multiple interactions with the cytoskeleton, J Am Soc Nephrol: JASN 17(1) (2006) 89-98.

[35] J. Perreau, A. Lilienbaum, M. Vasseur, D. Paulin, Nucleotide sequence of the human vimentin gene and regulation of its transcription in tissues and cultured cells, Gene 62(1) (1988) 7-16.

[36] D.A. Parry, S.V. Strelkov, P. Burkhard, U. Aebi, H. Herrmann, Towards a molecular description of intermediate filament structure and assembly, Exp Cell Res 313(10) (2007) 2204-16.

[37] A. Lupas, M. Van Dyke, J. Stock, Predicting coiled coils from protein sequences, Science 252(5009) (1991) 1162-4.

[38] H. Herrmann, L. Kreplak, U. Aebi, Isolation, characterization, and in vitro assembly of intermediate filaments, Methods Cell Biol 78 (2004) 3-24.

[39] S.V. Strelkov, H. Herrmann, N. Geisler, A. Lustig, S. Ivaninskii, R. Zimbelmann, P. Burkhard, U. Aebi, Divide-and-conquer crystallographic approach towards an atomic structure of intermediate filaments, J Mol Biol 306(4) (2001) 773-81.

[40] S.V. Strelkov, H. Herrmann, N. Geisler, T. Wedig, R. Zimbelmann, U. Aebi, P. Burkhard, Conserved segments 1A and 2B of the intermediate filament dimer: their atomic structures and role in filament assembly, EMBO J 21(6) (2002) 1255-66.

[41] A.A. Chernyatina, S. Nicolet, U. Aebi, H. Herrmann, S.V. Strelkov, Atomic structure of the vimentin central alpha-helical domain and its implications for intermediate filament assembly, Proc Natl Acad Sci U S A 109(34) (2012) 13620-5.

[42] A. Aziz, J.F. Hess, M.S. Budamagunta, J.C. Voss, A.P. Kuzin, Y.J. Huang, R. Xiao, G.T. Montelione, P.G. FitzGerald, J.F. Hunt, The structure of vimentin linker 1 and rod 1B domains characterized by site-directed spin-labeling electron paramagnetic resonance (SDSL-EPR) and X-ray crystallography, J Biol Chem 287(34) (2012) 28349-61.

[43] S. Nicolet, H. Herrmann, U. Aebi, S.V. Strelkov, Atomic structure of vimentin coil 2, J Struct Biol 170(2) (2010) 369-76.

[44] A.A. Chernyatina, S.V. Strelkov, Stabilization of vimentin coil2 fragment via an engineered disulfide, J Struct Biol 177(1) (2012) 46-53.

[45] A.H. Pang, J.M. Obiero, A.W. Kulczyk, V.M. Sviripa, O.V. Tsodikov, A crystal structure of coil 1B of vimentin in the filamentous form provides a model of a high-order assembly of a vimentin filament, FEBS J 285(15) (2018) 2888-2899.

[46] D.D. Gae, M.S. Budamagunta, J.F. Hess, R.M. McCarrick, G.A. Lorigan, P.G. FitzGerald, J.C. Voss, Completion of the Vimentin Rod Domain Structure Using Experimental Restraints: A New Tool for Exploring Intermediate Filament Assembly and Mutations, Structure (2019) (https://doi.org/10.1016/j.str.2019.07.011).

[47] J.F. Hess, M.S. Budamagunta, J.C. Voss, P.G. FitzGerald, Structural characterization of human vimentin rod 1 and the sequencing of assembly steps in intermediate filament formation in vitro using site-directed spin labeling and electron paramagnetic resonance, J Biol Chem 279(43) (2004) 44841-6.

[48] H. Herrmann, M. Haner, M. Brettel, S.A. Muller, K.N. Goldie, B. Fedtke, A. Lustig, W.W. Franke, U. Aebi, Structure and assembly properties of the intermediate filament protein vimentin: the role of its head, rod and tail domains, J Mol Biol 264(5) (1996) 933-53.

[49] L. Kreplak, K. Richter, U. Aebi, H. Herrmann, Electron microscopy of intermediate filaments: teaming up with atomic force and confocal laser scanning microscopy, Methods Cell Biol 88 (2008) 273-97.

[50] M.L. Steinert P., Parry D., Diversity of Intermediate Filament Structure, J Biol Chem 268(33) (1993) 16-25.

[51] N. Mucke, T. Wedig, A. Burer, L.N. Marekov, P.M. Steinert, J. Langowski, U. Aebi, H. Herrmann, Molecular and biophysical characterization of assembly-starter units of human vimentin, J Mol Biol 340(1) (2004) 97-114.

[52] J.F. Hess, J.C. Voss, P.G. FitzGerald, Real-time observation of coiled-coil domains and subunit assembly in intermediate filaments, J Biol Chem 277(38) (2002) 35516-22.

[53] A. Premchandar, N. Mucke, J. Poznanski, T. Wedig, M. Kaus-Drobek, H. Herrmann, M. Dadlez, Structural Dynamics of the Vimentin Coiled-coil Contact Regions Involved in Filament Assembly as Revealed by Hydrogen-Deuterium Exchange, J Biol Chem 291(48) (2016) 24931-24950.

[54] H. Herrmann, M. Haner, M. Brettel, N.O. Ku, U. Aebi, Characterization of distinct early assembly units of different intermediate filament proteins, J Mol Biol 286(5) (1999) 1403-20.

[55] A.V. Sokolova, L. Kreplak, T. Wedig, N. Mucke, D.I. Svergun, H. Herrmann, U. Aebi, S.V. Strelkov, Monitoring intermediate filament assembly by small-angle x-ray scattering reveals the molecular architecture of assembly intermediates, Proc Natl Acad Sci U S A 103(44) (2006) 16206-11.

[56] N. Mucke, L. Kammerer, S. Winheim, R. Kirmse, J. Krieger, M. Mildenberger, J. Bassler, E. Hurt, W.H. Goldmann, U. Aebi, K. Toth, J. Langowski, H. Herrmann, Assembly Kinetics of Vimentin Tetramers to Unit-Length Filaments: A Stopped-Flow Study, Biophys J 114(10) (2018) 2408-2418.

[57] C.G. Lopez, O. Saldanha, K. Huber, S. Koster, Lateral association and elongation of vimentin intermediate filament proteins: A time-resolved light-scattering study, Proc Natl Acad Sci U S A 113(40) (2016) 11152-11157.

[58] R. Kirmse, C. Bouchet-Marquis, C. Page, A. Hoenger, Three-dimensional cryo-electron microscopy on intermediate filaments, Methods Cell Biol 96 (2010) 565-89.

[59] R. Kirmse, S. Portet, N. Mucke, U. Aebi, H. Herrmann, J. Langowski, A quantitative kinetic model for the in vitro assembly of intermediate filaments from tetrameric vimentin, J Biol Chem 282(25) (2007) 18563-72.

[60] S. Winheim, A.R. Hieb, M. Silbermann, E.M. Surmann, T. Wedig, H. Herrmann, J. Langowski, N. Mucke, Deconstructing the late phase of vimentin assembly by total internal reflection fluorescence microscopy (TIRFM), PLoS One 6(4) (2011) e19202.

[61] H. Herrmann, A. Eckelt, M. Brettel, C. Grund, W.W. Franke, Temperature-sensitive intermediate filament assembly. Alternative structures of Xenopus laevis vimentin in vitro and in vivo, J Mol Biol 234(1) (1993) 99-113.

[62] M.E. Brennich, S. Bauch, U. Vainio, T. Wedig, H. Herrmann, S. Koster, Impact of ion valency on the assembly of vimentin studied by quantitative small angle X-ray scattering, Soft Matter 10(12) (2014) 2059-68.

[63] G. Colakoglu, A. Brown, Intermediate filaments exchange subunits along their length and elongate by end-to-end annealing, J Cell Biol 185(5) (2009) 769-77.

[64] A. Robert, M.J. Rossow, C. Hookway, S.A. Adam, V.I. Gelfand, Vimentin filament precursors exchange subunits in an ATP-dependent manner, Proc Natl Acad Sci U S A 112(27) (2015) E3505-14.

[65] J.E. Eriksson, T. He, A.V. Trejo-Skalli, A.S. Harmala-Brasken, J. Hellman, Y.H. Chou, R.D. Goldman, Specific in vivo phosphorylation sites determine the assembly dynamics of vimentin intermediate filaments, J Cell Sci 117(Pt 6) (2004) 919-32.

[66] Y.H. Chou, P. Opal, R.A. Quinlan, R.D. Goldman, The relative roles of specific N- and C-terminal phosphorylation sites in the disassembly of intermediate filament in mitotic BHK-21 cells, J Cell Sci 109 (Pt 4) (1996) 817-26.

[67] Á.V.-P. S. Duarte, E. Navarro, A.E. Martínez, M.A. Pajares, D. Pérez-Sala, Vimentin filaments interact with the mitotic cortex allowing normal cell division, BioRxiv (2018) (https://doi.org/10.1101/356642).

[68] E. Colucci-Guyon, M.M. Portier, I. Dunia, D. Paulin, S. Pournin, C. Babinet, Mice lacking vimentin develop and reproduce without an obvious phenotype, Cell 79(4) (1994) 679-94.

[69] R.M. Evans, Vimentin: the conundrum of the intermediate filament gene family, Bioessays 20(1) (1998) 79-86.

[70] E. Colucci-Guyon, Y.R.M. Gimenez, T. Maurice, C. Babinet, A. Privat, Cerebellar defect and impaired motor coordination in mice lacking vimentin, Glia 25(1) (1999) 33-43.

[71] F. Cheng, Y. Shen, P. Mohanasundaram, M. Lindstrom, J. Ivaska, T. Ny, J.E. Eriksson, Vimentin coordinates fibroblast proliferation and keratinocyte differentiation in wound healing via TGF-beta-Slug signaling, Proc Natl Acad Sci U S A 113(30) (2016) E4320-7.

[72] M. Nieminen, T. Henttinen, M. Merinen, F. Marttila-Ichihara, J.E. Eriksson, S. Jalkanen, Vimentin function in lymphocyte adhesion and transcellular migration, Nat Cell Biol 8(2) (2006) 156-62.

[73] B. Langlois, E. Belozertseva, A. Parlakian, M. Bourhim, J. Gao-Li, J. Blanc, L. Tian, D. Coletti, C. Labat, Z. Ramdame-Cherif, P. Challande, V. Regnault, P. Lacolley, Z. Li, Vimentin knockout results in increased expression of sub-endothelial basement membrane components and carotid stiffness in mice, Sci Rep 7(1): 11628 (2017).

[74] O.E. Nekrasova, M.G. Mendez, I.S. Chernoivanenko, P.A. Tyurin-Kuzmin, E.R. Kuczmarski, V.I. Gelfand, R.D. Goldman, A.A. Minin, Vimentin intermediate filaments modulate the motility of mitochondria, Mol Biol Cell 22(13) (2011) 2282-9.

[75] M.L. Styers, G. Salazar, R. Love, A.A. Peden, A.P. Kowalczyk, V. Faundez, The endo-lysosomal sorting machinery interacts with the intermediate filament cytoskeleton, Mol Biol Cell 15(12) (2004) 5369-82.

[76] Y. Gao, E. Sztul, A novel interaction of the Golgi complex with the vimentin intermediate filament cytoskeleton, J Cell Biol 152(5) (2001) 877-94.

[77] W.W. Franke, M. Hergt, C. Grund, Rearrangement of the vimentin cytoskeleton during adipose conversion: formation of an intermediate filament cage around lipid globules, Cell 49(1) (1987) 131-41.

[78] J.A. Olzmann, L. Li, L.S. Chin, Aggresome formation and neurodegenerative diseases: therapeutic implications, Curr Med Chem 15(1) (2008) 47-60.

[79] J.A. Johnston, C.L. Ward, R.R. Kopito, Aggresomes: a cellular response to misfolded proteins, J Cell Biol 143(7) (1998) 1883-98.

[80] I. Dupin, S. Etienne-Manneville, Nuclear positioning: mechanisms and functions, Int J Biochem Cell Biol 43(12) (2011) 1698-707.

[81] M.G. Mendez, D. Restle, P.A. Janmey, Vimentin enhances cell elastic behavior and protects against compressive stress, Biophys J 107(2) (2014) 314-323.

[82] R.A. Battaglia, S. Delic, H. Herrmann, N.T. Snider, Vimentin on the move: new developments in cell migration, F1000Res 7 (2018) (10.12688/f1000research.15967.1).

[83] V. Das, S. Bhattacharya, C. Chikkaputtaiah, S. Hazra, M. Pal, The basics of epithelial-mesenchymal transition (EMT): A study from a structure, dynamics, and functional perspective, J Cell Physiol (2019) (doi: 10.1002/jcp.28160).

[84] J. Ivaska, Vimentin: Central hub in EMT induction?, Small GTPases 2(1) (2011) 51-53.

[85] S. Kreis, H.J. Schonfeld, C. Melchior, B. Steiner, N. Kieffer, The intermediate filament protein vimentin binds specifically to a recombinant integrin alpha2/beta1 cytoplasmic tail complex and co-localizes with native alpha2/beta1 in endothelial cell focal adhesions, Exp Cell Res 305(1) (2005) 110-21.

[86] J. Kim, J. Jang, C. Yang, E.J. Kim, H. Jung, C. Kim, Vimentin filament controls integrin alpha5beta1-mediated cell adhesion by binding to integrin through its Ser38 residue, FEBS Lett 590(20) (2016) 3517-3525.

[87] J. Kim, C. Yang, E.J. Kim, J. Jang, S.J. Kim, S.M. Kang, M.G. Kim, H. Jung, D. Park, C. Kim, Vimentin filaments regulate integrin-ligand interactions by binding to the cytoplasmic tail of integrin beta3, J Cell Sci 129(10) (2016) 2030-42.

[88] G. Burgstaller, M. Gregor, L. Winter, G. Wiche, Keeping the vimentin network under control: cell-matrix adhesion-associated plectin 1f affects cell shape and polarity of fibroblasts, Mol Biol Cell 21(19) (2010) 3362-75.

[89] H. Kim, F. Nakamura, W. Lee, Y. Shifrin, P. Arora, C.A. McCulloch, Filamin A is required for vimentin-mediated cell adhesion and spreading, Am J Physiol Cell Physiol 298(2) (2010) C221-36.

[90] I. Correia, D. Chu, Y.H. Chou, R.D. Goldman, P. Matsudaira, Integrating the actin and vimentin cytoskeletons. adhesion-dependent formation of fimbrin-vimentin complexes in macrophages, J Cell Biol 146(4) (1999) 831-42.

[91] D. Tsuruta, J.C. Jones, The vimentin cytoskeleton regulates focal contact size and adhesion of endothelial cells subjected to shear stress, J Cell Sci 116(Pt 24) (2003) 4977-84.

[92] G. Tzivion, Z.J. Luo, J. Avruch, Calyculin A-induced vimentin phosphorylation sequesters 14-3-3 and displaces other 14-3-3 partners in vivo, J Biol Chem 275(38) (2000) 29772-8.

[93] M.E. Kidd, D.K. Shumaker, K.M. Ridge, The role of vimentin intermediate filaments in the progression of lung cancer, Am J Respir Cell Mol Biol 50(1) (2014) 1-6.

[94] M. Muller, S.S. Bhattacharya, T. Moore, Q. Prescott, T. Wedig, H. Herrmann, T.M. Magin, Dominant cataract formation in association with a vimentin assembly disrupting mutation, Hum Mol Genet 18(6) (2009) 1052-7.

[95] F. Richardson, G.D. Young, R. Sennello, J. Wolf, G.M. Argast, P. Mercado, A. Davies, D.M. Epstein, B. Wacker, The evaluation of E-Cadherin and vimentin as biomarkers of clinical outcomes among patients with non-small cell lung cancer treated with erlotinib as second- or third-line therapy, Anticancer Res 32(2) (2012) 537-52.

[96] S. Al-Saad, K. Al-Shibli, T. Donnem, M. Persson, R.M. Bremnes, L.T. Busund, The prognostic impact of NF-kappaB p105, vimentin, E-cadherin and Par6 expression in epithelial and stromal compartment in non-small-cell lung cancer, Br J Cancer 99(9) (2008) 1476-83.

[97] M.I. Kokkinos, R. Wafai, M.K. Wong, D.F. Newgreen, E.W. Thompson, M. Waltham, Vimentin and epithelial-mesenchymal transition in human breast cancer--observations in vitro and in vivo, Cells Tissues Organs 185(1-3) (2007) 191-203.

[98] J. Wei, G. Xu, M. Wu, Y. Zhang, Q. Li, P. Liu, T. Zhu, A. Song, L. Zhao, Z. Han, G. Chen, S. Wang, L. Meng, J. Zhou, Y. Lu, S. Wang, D. Ma, Overexpression of vimentin contributes to prostate cancer invasion and metastasis via src regulation, Anticancer Res 28(1A) (2008) 327-34.

[99] M. Brzozowa, G. Wyrobiec, I. Kolodziej, M. Sitarski, N. Matysiak, E. Reichman-Warmusz, M. Zaba, R. Wojnicz, The aberrant overexpression of vimentin is linked to a more aggressive status in tumours of the gastrointestinal tract, Prz Gastroenterol 10(1) (2015) 7-11.

[100] M. Li, B. Zhang, B. Sun, X. Wang, X. Ban, T. Sun, Z. Liu, X. Zhao, A novel function for vimentin: the potential biomarker for predicting melanoma hematogenous metastasis, J Exp Clin Cancer Res 29:109 (2010).

[101] M. Scharl, N. Huber, S. Lang, A. Furst, E. Jehle, G. Rogler, Hallmarks of epithelial to mesenchymal transition are detectable in Crohn's disease associated intestinal fibrosis, Clin Transl Med 4: 1 (2015).

[102] M.M. Steenvoorden, T.C. Tolboom, G. van der Pluijm, C. Lowik, C.P. Visser, J. DeGroot, A.C. Gittenberger-DeGroot, M.C. DeRuiter, B.J. Wisse, T.W. Huizinga, R.E. Toes, Transition of healthy to diseased synovial tissue in rheumatoid arthritis is associated with gain of mesenchymal/fibrotic characteristics, Arthritis Res Ther 8(6): R165 (2006).

[103] S.M. Evrard, L. Lecce, K.C. Michelis, A. Nomura-Kitabayashi, G. Pandey, K.R. Purushothaman, V. d'Escamard, J.R. Li, L. Hadri, K. Fujitani, P.R. Moreno, L. Benard, P. Rimmele, A. Cohain, B. Mecham, G.J. Randolph, E.G. Nabel, R. Hajjar, V. Fuster, M. Boehm, J.C. Kovacic, Endothelial to mesenchymal transition is common in atherosclerotic lesions and is associated with plaque instability, Nat Commun 7: 11853 (2016).

[104] R. Surolia, F.J. Li, Z. Wang, H. Li, K. Dsouza, V. Thomas, S. Mirov, D. Perez-Sala, M. Athar, V.J. Thannickal, V.B. Antony, Vimentin intermediate filament assembly regulates fibroblast invasion in fibrogenic lung injury, JCI Insight 4(7) (2019).

[105] H.J. Tarbet, L. Dolat, T.J. Smith, B.M. Condon, E.T. O'Brien, 3rd, R.H. Valdivia, M. Boyce, Site-specific glycosylation regulates the form and function of the intermediate filament cytoskeleton, Elife 7: e31807 (2018).

[106] A. Musaelyan, S. Lapin, V. Nazarov, O. Tkachenko, B. Gilburd, A. Mazing, L. Mikhailova, Y. Shoenfeld, Vimentin as antigenic target in autoimmunity: A comprehensive review, Autoimmun Rev 17(9) (2018) 926-934.

[107] P. Nicaise Roland, S. Grootenboer Mignot, A. Bruns, M. Hurtado, E. Palazzo, G. Hayem, P. Dieude, O. Meyer, S. Chollet Martin, Antibodies to mutated citrullinated vimentin for diagnosing rheumatoid arthritis in anti-CCP-negative patients and for monitoring infliximab therapy, Arthritis Res Ther 10(6): R142 (2008).

[108] D. Frescas, C.M. Roux, S. Aygun-Sunar, A.S. Gleiberman, P. Krasnov, O.V. Kurnasov, E. Strom, L.P. Virtuoso, M. Wrobel, A.L. Osterman, M.P. Antoch, V. Mett, O.B. Chernova, A.V. Gudkov, Senescent cells expose and secrete an oxidized form of membrane-bound vimentin as revealed by a natural polyreactive antibody, Proc Natl Acad Sci U S A 114(9) (2017) E1668-E1677.

[109] T. Kueper, T. Grune, S. Prahl, H. Lenz, V. Welge, T. Biernoth, Y. Vogt, G.M. Muhr, A. Gaemlich, T. Jung, G. Boemke, H.P. Elsasser, K.P. Wittern, H. Wenck, F. Stab, T. Blatt, Vimentin is the specific target in skin glycation. Structural prerequisites, functional consequences, and role in skin aging, J Biol Chem 282(32) (2007) 23427-36.

[110] P. Turowski, T. Myles, B.A. Hemmings, A. Fernandez, N.J. Lamb, Vimentin dephosphorylation by protein phosphatase 2A is modulated by the targeting subunit B55, Mol Biol Cell 10(6) (1999) 1997-2015.

[111] J. Li, R. Wang, D.D. Tang, Vimentin dephosphorylation at ser-56 is regulated by type 1 protein phosphatase in smooth muscle, Respir Res 17(1) (2016) 91.

[112] M. Meriane, S. Mary, F. Comunale, E. Vignal, P. Fort, C. Gauthier-Rouviere, Cdc42Hs and Rac1 GTPases induce the collapse of the vimentin intermediate filament network, J Biol Chem 275(42) (2000) 33046-52.

[113] J.E. Eriksson, D.L. Brautigan, R. Vallee, J. Olmsted, H. Fujiki, R.D. Goldman, Cytoskeletal integrity in interphase cells requires protein phosphatase activity, Proc Natl Acad Sci U S A 89(22) (1992) 11093-7.

[114] J.E. Eriksson, P. Opal, R.D. Goldman, Intermediate filament dynamics, Curr Opin Cell Biol 4(1) (1992) 99-104.

[115] Y. Takai, M. Ogawara, Y. Tomono, C. Moritoh, S. Imajoh-Ohmi, O. Tsutsumi, Y. Taketani, M. Inagaki, Mitosis-specific phosphorylation of vimentin by protein kinase C coupled with reorganization of intracellular membranes, J Cell Biol 133(1) (1996) 141-9.

[116] R.C. Wang, Y. Wei, Z. An, Z. Zou, G. Xiao, G. Bhagat, M. White, J. Reichelt, B. Levine, Akt-mediated regulation of autophagy and tumorigenesis through Beclin 1 phosphorylation, Science 338(6109) (2012) 956-9.

[117] J. Ivaska, K. Vuoriluoto, T. Huovinen, I. Izawa, M. Inagaki, P.J. Parker, PKCepsilon-mediated phosphorylation of vimentin controls integrin recycling and motility, EMBO J 24(22) (2005) 3834-45.

[118] J. Ivaska, H.M. Pallari, J. Nevo, J.E. Eriksson, Novel functions of vimentin in cell adhesion, migration, and signaling, Exp Cell Res 313(10) (2007) 2050-62.

[119] A.M. Shi, Z.Q. Tao, R. Li, Y.Q. Wang, X. Wang, J. Zhao, Vimentin and post-translational modifications in cell motility during cancer - a review, Eur Rev Med Pharmacol Sci 20(12) (2016) 2603-6.

[120] D. Guo, X. Song, T. Guo, S. Gu, X. Chang, T. Su, X. Yang, B. Liang, D. Huang, Vimentin acetylation is involved in SIRT5-mediated hepatocellular carcinoma migration, Am J Cancer Res 8(12) (2018) 2453-2466.

[121] Y. Zhu, Y. Zhang, Z. Sui, Y. Zhang, M. Liu, H. Tang, USP14 de-ubiquitinates vimentin and miR-320a modulates USP14 and vimentin to contribute to malignancy in gastric cancer cells, Oncotarget 8(30) (2017) 48725-48736.

[122] C. Slawson, T. Lakshmanan, S. Knapp, G.W. Hart, A mitotic GlcNAcylation/phosphorylation signaling complex alters the posttranslational state of the cytoskeletal protein vimentin, Mol Biol Cell 19(10) (2008) 4130-40.

[123] N.T. Snider, N.O. Ku, M.B. Omary, The sweet side of vimentin, Elife 7 : e35336 (2018).

[124] N.T. Snider, M.B. Omary, Post-translational modifications of intermediate filament proteins: mechanisms and functions, Nat Rev Mol Cell Biol 15(3) (2014) 163-77.

[125] H. Sies, C. Berndt, D.P. Jones, Oxidative Stress, Annu Rev Biochem 86 (2017) 715-748.

[126] H. Sies, Oxidative stress: a concept in redox biology and medicine, Redox Biol 4 (2015) 180-3.

[127] Y.M. Go, D.P. Jones, Thiol/disulfide redox states in signaling and sensing, Crit Rev Biochem Mol Biol 48(2) (2013) 173-81.

[128] R.M. Domingues, P. Domingues, T. Melo, D. Perez-Sala, A. Reis, C.M. Spickett, Lipoxidation adducts with peptides and proteins: deleterious modifications or signaling mechanisms?, J Proteomics 92 (2013) 110-31.

[129] C.M. Spickett, A.R. Pitt, Oxidative lipidomics coming of age: advances in analysis of oxidized phospholipids in physiology and pathology, Antioxid Redox Signal 22(18) (2015) 1646-66.

[130] J. Schroter, J. Schiller, Chlorinated Phospholipids and Fatty Acids: (Patho)physiological Relevance, Potential Toxicity, and Analysis of Lipid Chlorohydrins, Oxid Med Cell Longev 2016 (2016) 8386362.

[131] T. Melo, J.F. Montero-Bullon, P. Domingues, M.R. Domingues, Discovery of bioactive nitrated lipids and nitro-lipid-protein adducts using mass spectrometry-based approaches, Redox Biol (2019) (doi: 10.1016/j.redox.2019.101106).

[132] E. Gianazza, M. Brioschi, A.M. Fernandez, C. Banfi, Lipoxidation in cardiovascular diseases, Redox Biol (2019) (doi: 10.1016/j.redox.2019.101119).

[133] C.B. Afonso, C.M. Spickett, Lipoproteins as targets and markers of lipoxidation, Redox Biol (2018) (doi: 10.1016/j.redox.2018.101066).

[134] C. Martin-Sierra, P. Laranjeira, M.R. Domingues, A. Paiva, Lipoxidation and cancer immunity, Redox Biol (2019) (doi: 10.1016/j.redox.2019.101103).

[135] M. Jove, I. Pradas, M. Dominguez-Gonzalez, I. Ferrer, R. Pamplona, Lipids and lipoxidation in human brain aging. Mitochondrial ATP-synthase as a key lipoxidation target, Redox Biol (2018) (doi: 10.1016/j.redox.2018.101082).

[136] T. Patinen, S. Adinolfi, C.C. Cortes, J. Harkonen, A. Jawahar Deen, A.L. Levonen, Regulation of stress signaling pathways by protein lipoxidation, Redox Biol (2019) (doi: 10.1016/j.redox.2019.101114).

[137] V. Bochkov, B. Gesslbauer, C. Mauerhofer, M. Philippova, P. Erne, O.V. Oskolkova, Pleiotropic effects of oxidized phospholipids, Free Radic Biol Med 111 (2017) 6-24.

[138] G. Vistoli, D. De Maddis, A. Cipak, N. Zarkovic, M. Carini, G. Aldini, Advanced glycoxidation and lipoxidation end products (AGEs and ALEs): an overview of their mechanisms of formation, Free Radic Res 47 Suppl 1 (2013) 3-27.

[139] F. Gueraud, M. Atalay, N. Bresgen, A. Cipak, P.M. Eckl, L. Huc, I. Jouanin, W. Siems, K. Uchida, Chemistry and biochemistry of lipid peroxidation products, Free Radic Res 44(10) (2010) 1098-124.

[140] A. Reis, C.M. Spickett, Chemistry of phospholipid oxidation, Biochim Biophys Acta 1818(10) (2012) 2374-87.

[141] D. Perez-Sala, Electrophilic eicosanoids: Signaling and targets, Chem Biol Interact 192(1-2) (2011) 96-100.

[142] Y.V. Vasil'ev, S.C. Tzeng, L. Huang, C.S. Maier, Protein modifications by electrophilic lipoxidation products: adduct formation, chemical strategies and tandem mass spectrometry for their detection and identification, Mass Spectrom Rev 33(3) (2014) 157-82.

[143] S. Zorrilla, A. Monico, S. Duarte, G. Rivas, D. Perez-Sala, M.A. Pajares, Integrated approaches to unravel the impact of protein lipoxidation on macromolecular interactions, Free Radic Biol Med (2019) (doi: 10.1016/j.freeradbiomed.2019.04.011).

[144] M. Csala, T. Kardon, B. Legeza, B. Lizak, J. Mandl, E. Margittai, F. Puskas, P. Szaraz, P. Szelenyi, G. Banhegyi, On the role of 4-hydroxynonenal in health and disease, Biochim Biophys Acta 1852(5) (2015) 826-38.

[145] P.I. Homem de Bittencourt, Jr., D.J. Lagranha, A. Maslinkiewicz, S.M. Senna, A.M. Tavares, L.P. Baldissera, D.R. Janner, J.S. Peralta, P.M. Bock, L.L. Gutierrez, G. Scola, T.G. Heck, M.S. Krause, L.A. Cruz, D.S. Abdalla, C.J. Lagranha, T. Lima, R. Curi, LipoCardium: endothelium-directed cyclopentenone prostaglandin-based liposome formulation that completely reverses atherosclerotic lesions, Atherosclerosis 193(2) (2007) 245-58.

[146] J. Korbecki, R. Bobinski, M. Dutka, Self-regulation of the inflammatory response by peroxisome proliferator-activated receptors, Inflamm Res 68(6) (2019) 443-458.

[147] C.L. Oeste, D. Perez-Sala, Modification of cysteine residues by cyclopentenone prostaglandins: interplay with redox regulation of protein function, Mass Spectrom Rev 33(2) (2014) 110-25.

[148] B. Diez-Dacal, D. Perez-Sala, Anti-inflammatory prostanoids: focus on the interactions between electrophile signaling and resolution of inflammation, ScientificWorldJournal 10 (2010) 655-75.

[149] J.Y. Lee, J.H. Je, K.J. Jung, B.P. Yu, H.Y. Chung, Induction of endothelial iNOS by 4-hydroxyhexenal through NF-kappaB activation, Free Radic Biol Med 37(4) (2004) 539-48.

[150] T. Kumagai, N. Matsukawa, Y. Kaneko, Y. Kusumi, M. Mitsumata, K. Uchida, A lipid peroxidation-derived inflammatory mediator: identification of 4-hydroxy-2-nonenal as a potential inducer of cyclooxygenase-2 in macrophages, J Biol Chem 279(46) (2004) 48389-96.

[151] B.T. Kurien, K. Hensley, M. Bachmann, R.H. Scofield, Oxidatively modified autoantigens in autoimmune diseases, Free Radic Biol Med 41(4) (2006) 549-56.

[152] F.J. Sanchez-Gomez, B. Diez-Dacal, M.A. Pajares, O. Llorca, D. Perez-Sala, Cyclopentenone prostaglandins with dienone structure promote cross-linking of the chemoresistance-inducing enzyme glutathione transferase P1-1, Mol Pharmacol 78(4) (2010) 723-33.

[153] F.J. Sanchez-Gomez, J. Gayarre, M.I. Avellano, D. Perez-Sala, Direct evidence for the covalent modification of glutathione-S-transferase P1-1 by electrophilic prostaglandins: implications for enzyme inactivation and cell survival, Arch Biochem Biophys 457(2) (2007) 150-9.

[154] R. Sultana, M. Perluigi, D.A. Butterfield, Lipid peroxidation triggers neurodegeneration: a redox proteomics view into the Alzheimer disease brain, Free Radic Biol Med 62 (2013) 157-169.

[155] A. Viedma-Poyatos, Y. de Pablo, M. Pekny, D. Perez-Sala, The cysteine residue of glial fibrillary acidic protein is a critical target for lipoxidation and required for efficient network organization, Free Radic Biol Med 120 (2018) 380-394.

[156] M.A. Baraibar, B. Friguet, Oxidative proteome modifications target specific cellular pathways during oxidative stress, cellular senescence and aging, Exp Gerontol 48(7) (2013) 620-5.

[157] E.A. Perry, R.J. Castellani, P.I. Moreira, A. Nunomura, Q. Lui, P.L. Harris, L.M. Sayre, P.A. Szweda, L.I. Szweda, X. Zhu, M.A. Smith, G. Perry, Neurofilaments are the major neuronal target of hydroxynonenal-mediated protein cross-links, Free Radic Res 47(6-7) (2013) 507-10.

[158] G. Aldini, M. Carini, G. Vistoli, T. Shibata, Y. Kusano, L. Gamberoni, I. Dalle-Donne, A. Milzani, K. Uchida, Identification of actin as a 15-deoxy-Delta12,14-prostaglandin J2 target in neuroblastoma cells: mass spectrometric, computational, and functional approaches to investigate the effect on cytoskeletal derangement, Biochemistry 46(10) (2007) 2707-18.

[159] G. Aldini, I. Dalle-Donne, G. Vistoli, R. Maffei Facino, M. Carini, Covalent modification of actin by 4-hydroxy-trans-2-nonenal (HNE): LC-ESI-MS/MS evidence for Cys374 Michael adduction, J Mass Spectrom 40(7) (2005) 946-54.

[160] I. Dalle-Donne, M. Carini, G. Vistoli, L. Gamberoni, D. Giustarini, R. Colombo, R. Maffei Facino, R. Rossi, A. Milzani, G. Aldini, Actin Cys374 as a nucleophilic target of alpha,beta-unsaturated aldehydes, Free Radic Biol Med 42(5) (2007) 583-98.

[161] B. Huang, S.C. Chen, D.L. Wang, Shear flow increases S-nitrosylation of proteins in endothelial cells, Cardiovasc Res 83(3) (2009) 536-46.

[162] S.B. Wall, J.Y. Oh, A.R. Diers, A. Landar, Oxidative modification of proteins: an emerging mechanism of cell signaling, Front Physiol 3: 369 (2012).

[163] K.R. Rogers, C.J. Morris, D.R. Blake, Oxidation of thiol in the vimentin cytoskeleton, Biochem J 275 (Pt 3) (1991) 789-91.

[164] S. Gharbi, B. Garzon, J. Gayarre, J. Timms, D. Perez-Sala, Study of protein targets for covalent modification by the antitumoral and anti-inflammatory prostaglandin PGA1: focus on vimentin, J Mass Spectrom 42(11) (2007) 1474-84.

[165] I.S.C. E. A. Matveeva, A. A. Minin, Vimentin Intermediate Filaments Protect Mitochondria from Oxidative Stress, Biochem (Mosc) Suppl Ser A Membr Cell Biol 4:321 (2010).

[166] C. Ospelt, H. Bang, E. Feist, G. Camici, S. Keller, J. Detert, A. Kramer, S. Gay, K. Ghannam, G.R. Burmester, Carbamylation of vimentin is inducible by smoking and represents an independent autoantigen in rheumatoid arthritis, Ann Rheum Dis 76(7) (2017) 1176-1183.

[167] J. Chavez, W.G. Chung, C.L. Miranda, M. Singhal, J.F. Stevens, C.S. Maier, Site-specific protein adducts of 4-hydroxy-2(E)-nonenal in human THP-1 monocytic cells: protein carbonylation is diminished by ascorbic acid, Chem Res Toxicol 23(1) (2010) 37-47.

[168] C. Gronwall, K. Amara, U. Hardt, A. Krishnamurthy, J. Steen, M. Engstrom, M. Sun, A.J. Ytterberg, R.A. Zubarev, D. Scheel-Toellner, J.D. Greenberg, L. Klareskog, A.I. Catrina, V. Malmstrom, G.J. Silverman, Autoreactivity to malondialdehyde-modifications in rheumatoid arthritis is linked to disease activity and synovial pathogenesis, J Autoimmun 84 (2017) 29-45.

[169] C.T. Shearn, D.J. Orlicky, L.M. Saba, A.H. Shearn, D.R. Petersen, Increased hepatocellular protein carbonylation in human end-stage alcoholic cirrhosis, Free Radic Biol Med 89 (2015) 1144-53.

[170] E. Griesser, V. Vemula, N. Raulien, U. Wagner, S. Reeg, T. Grune, M. Fedorova, Cross-talk between lipid and protein carbonylation in a dynamic cardiomyocyte model of mild nitroxidative stress, Redox Biol 11 (2017) 438-455.

[171] G. Aldini, M.R. Domingues, C.M. Spickett, P. Domingues, A. Altomare, F.J. Sanchez-Gomez, C.L. Oeste, D. Perez-Sala, Protein lipoxidation: Detection strategies and challenges, Redox Biol 5 (2015) 253-266.

[172] C.B. Afonso, B.C. Sousa, A.R. Pitt, C.M. Spickett, A mass spectrometry approach for the identification and localization of small aldehyde modifications of proteins, Arch Biochem Biophys 646 (2018) 38-45.

[173] I. Verrastro, S. Pasha, K.T. Jensen, A.R. Pitt, C.M. Spickett, Mass spectrometry-based methods for identifying oxidized proteins in disease: advances and challenges, Biomolecules 5(2) (2015) 378-411.

[174] S.B. Wall, J.Y. Oh, L. Mitchell, A.H. Laube, S.L. Campbell, M.B. Renfrow, A. Landar, Rac1 modification by an electrophilic 15-deoxy Delta(12,14)-prostaglandin J2 analog, Redox Biol 4 (2015) 346-54.

[175] K. Uchida, K. Itakura, S. Kawakishi, H. Hiai, S. Toyokuni, E.R. Stadtman, Characterization of epitopes recognized by 4-hydroxy-2-nonenal specific antibodies, Arch Biochem Biophys 324(2) (1995) 241-8.

[176] N. Tanaka, S. Tajima, A. Ishibashi, K. Uchida, T. Shigematsu, Immunohistochemical detection of lipid peroxidation products, protein-bound acrolein and 4-hydroxynonenal protein adducts, in actinic elastosis of photodamaged skin, Arch Dermatol Res 293(7) (2001) 363-7.

[177] K. Uchida, K. Sakai, K. Itakura, T. Osawa, S. Toyokuni, Protein modification by lipid peroxidation products: formation of malondialdehyde-derived N(epsilon)-(2-propenol)lysine in proteins, Arch Biochem Biophys 346(1) (1997) 45-52.

[178] B. Monterroso, C. Alfonso, S. Zorrilla, G. Rivas, Combined analytical ultracentrifugation, light scattering and fluorescence spectroscopy studies on the functional associations of the bacterial division FtsZ protein, Methods 59(3) (2013) 349-62.

[179] J. Gayarre, D. Sanchez, F.J. Sanchez-Gomez, M.C. Terron, O. Llorca, D. Perez-Sala, Addition of electrophilic lipids to actin alters filament structure, Biochem Biophys Res Commun 349(4) (2006) 1387-93.

[180] M. Sardar Sinha, A.M. Villamil Giraldo, K. Ollinger, M. Hallbeck, L. Civitelli, Lipid vesicles affect the aggregation of 4-hydroxy-2-nonenal-modified alpha-synuclein oligomers, Biochim Biophys Acta Mol Basis Dis 1864(9 Pt B) (2018) 3060-3068.

[181] M. Georgieva, D.I. Cattoni, J.B. Fiche, T. Mutin, D. Chamousset, M. Nollmann, Nanometer resolved single-molecule colocalization of nuclear factors by two-color super resolution microscopy imaging, Methods 105 (2016) 44-55.

[182] A.N. Higdon, B.P. Dranka, B.G. Hill, J.Y. Oh, M.S. Johnson, A. Landar, V.M. Darley-Usmar, Methods for imaging and detecting modification of proteins by reactive lipid species, Free Radic Biol Med 47(3) (2009) 201-12.

[183] C. Andreini, L. Banci, I. Bertini, A. Rosato, Counting the zinc-proteins encoded in the human genome, J Proteome Res 5(1) (2006) 196-201.

[184] R.J. Cousins, A role of zinc in the regulation of gene expression, Proc Nutr Soc 57(2) (1998) 307-11.

[185] B.L. Vallee, A. Galdes, The metallobiochemistry of zinc enzymes, Adv Enzymol Relat Areas Mol Biol 56 (1984) 283-430.

[186] Jackson M.J. (1989) Physiology of Zinc: General Aspects. In: Mills C.F. (eds) Zinc in Human Biology. ILSI Human Nutrition Reviews. Springer, London (1989) (ISBN: 978-1-4471-3881-5).

[187] T. Kambe, T. Tsuji, A. Hashimoto, N. Itsumura, The Physiological, Biochemical, and Molecular Roles of Zinc Transporters in Zinc Homeostasis and Metabolism, Physiol Rev 95(3) (2015) 749-84.

[188] J.L. Vinkenborg, T.J. Nicolson, E.A. Bellomo, M.S. Koay, G.A. Rutter, M. Merkx, Genetically encoded FRET sensors to monitor intracellular Zn2+ homeostasis, Nat Methods 6(10) (2009) 737-40.

[189] K. Vogt, J. Mellor, G. Tong, R. Nicoll, The actions of synaptically released zinc at hippocampal mossy fiber synapses, Neuron 26(1) (2000) 187-96.

[190] W. Maret, Zinc in Cellular Regulation: The Nature and Significance of "Zinc Signals", Int J Mol Sci 18(11) (2017).

[191] W. Maret, The redox biology of redox-inert zinc ions, Free Radic Biol Med 134 (2019) 311-326.

[192] M.H. Salter, Jr., J.H. Reibenspies, S.B. Jones, R.D. Hancock, Lewis acid properties of zinc(II) in Its cyclen complex. The structure of [Zn(cyclen)(S=C(NH2)2](ClO4)2 and the bonding of thiourea to metal ions. Some implications for zinc metalloenzymes, Inorg Chem 44(8) (2005) 2791-7.

[193] W. Maret, New perspectives of zinc coordination environments in proteins, J Inorg Biochem 111 (2012) 110-6.

[194] M. Cassandri, A. Smirnov, F. Novelli, C. Pitolli, M. Agostini, M. Malewicz, G. Melino, G. Raschella, Zinc-finger proteins in health and disease, Cell Death Discov 3: 17071 (2017).

[195] W. Maret, Zinc biochemistry: from a single zinc enzyme to a key element of life, Adv Nutr 4(1) (2013) 82-91.

[196] T.M. D. Keilin, Carbonic anhydrase, Nature 144 (1939) 442-443.

[197] C. Andreini, I. Bertini, A bioinformatics view of zinc enzymes, J Inorg Biochem 111 (2012) 150-6.

[198] S.L. Sensi, P. Paoletti, A.I. Bush, I. Sekler, Zinc in the physiology and pathology of the CNS, Nat Rev Neurosci 10(11) (2009) 780-91.

[199] S. Yamasaki, K. Sakata-Sogawa, A. Hasegawa, T. Suzuki, K. Kabu, E. Sato, T. Kurosaki, S. Yamashita, M. Tokunaga, K. Nishida, T. Hirano, Zinc is a novel intracellular second messenger, J Cell Biol 177(4) (2007) 637-45.

[200] G.R. Eagle, R.R. Zombola, R.H. Himes, Tubulin-zinc interactions: binding and polymerization studies, Biochemistry 22(1) (1983) 221-8.

[201] Y. Kress, F. Gaskin, C.F. Brosnan, S. Levine, Effects of zinc on the cytoskeletal proteins in the central nervous system of the rat, Brain Res 220(1) (1981) 139-49.

[202] L. Perrin, S. Roudeau, A. Carmona, F. Domart, J.D. Petersen, S. Bohic, Y. Yang, P. Cloetens, R. Ortega, Zinc and Copper Effects on Stability of Tubulin and Actin Networks in Dendrites and Spines of Hippocampal Neurons, ACS Chem Neurosci 8(7) (2017) 1490-1499.

[203] J.W. Mills, J.H. Zhou, L. Cardoza, V.H. Ferm, Zinc alters actin filaments in Madin-Darby canine kidney cells, Toxicol Appl Pharmacol 116(1) (1992) 92-100.

[204] C. Bjorkdahl, M.J. Sjogren, B. Winblad, J.J. Pei, Zinc induces neurofilament phosphorylation independent of p70 S6 kinase in N2a cells, Neuroreport 16(6) (2005) 591-5.

[205] E. Rudolf, L. Klvacova, S. John, M. Cervinka, Zinc alters cytoskeletal integrity and migration in colon cancer cells, Acta Medica (Hradec Kralove) 51(1) (2008) 51-7.

[206] W. Maret, B.L. Vallee, Thiolate ligands in metallothionein confer redox activity on zinc clusters, Proc Natl Acad Sci U S A 95(7) (1998) 3478-82.

[207] W. Maret, Molecular aspects of human cellular zinc homeostasis: redox control of zinc potentials and zinc signals, Biometals 22(1) (2009) 149-57.

[208] S.R. Lee, Critical Role of Zinc as Either an Antioxidant or a Prooxidant in Cellular Systems, Oxid Med Cell Longev 2018: 9156285 (2018).

[209] T. Fukai, M. Ushio-Fukai, Superoxide dismutases: role in redox signaling, vascular function, and diseases, Antioxid Redox Signal 15(6) (2011) 1583-606.

[210] D.D. Marreiro, K.J. Cruz, J.B. Morais, J.B. Beserra, J.S. Severo, A.R. de Oliveira, Zinc and Oxidative Stress: Current Mechanisms, Antioxidants (Basel) 6(2) (2017).

[211] V. Gunther, U. Lindert, W. Schaffner, The taste of heavy metals: gene regulation by MTF-1, Biochim Biophys Acta 1823(9) (2012) 1416-25.

[212] A.T. Dinkova-Kostova, W.D. Holtzclaw, N. Wakabayashi, Keap1, the sensor for electrophiles and oxidants that regulates the phase 2 response, is a zinc metalloprotein, Biochemistry 44(18) (2005) 6889-99.

[213] W. Maret, The function of zinc metallothionein: a link between cellular zinc and redox state, J Nutr 130(5S Suppl) (2000) 1455S-8S.

[214] E. Ho, B.N. Ames, Low intracellular zinc induces oxidative DNA damage, disrupts p53, NFkappa B, and AP1 DNA binding, and affects DNA repair in a rat glioma cell line, Proc Natl Acad Sci U S A 99(26) (2002) 16770-5.

[215] V. Duzguner, S. Kaya, Effect of zinc on the lipid peroxidation and the antioxidant defense systems of the alloxan-induced diabetic rabbits, Free Radic Biol Med 42(10) (2007) 1481-6.

[216] L.M. Plum, L. Rink, H. Haase, The essential toxin: impact of zinc on human health, Int J Environ Res Public Health 7(4) (2010) 1342-65.

[217] C. Garnier, F. Devred, D. Byrne, R. Puppo, A.Y. Roman, S. Malesinski, A.V. Golovin, R. Lebrun, N.N. Ninkina, P.O. Tsvetkov, Zinc binding to RNA recognition motif of TDP-43 induces the formation of amyloid-like aggregates, Sci Rep 7(1): 6812 (2017).

[218] J. Lemire, R. Mailloux, V.D. Appanna, Zinc toxicity alters mitochondrial metabolism and leads to decreased ATP production in hepatocytes, J Appl Toxicol 28(2) (2008) 175-82.

[219] S.G. Ji, Y.V. Medvedeva, H.L. Wang, H.Z. Yin, J.H. Weiss, Mitochondrial Zn(2+) Accumulation: A Potential Trigger of Hippocampal Ischemic Injury, Neuroscientist 25(2) (2019) 126-138.

[220] J.J. Hwang, S.J. Lee, T.Y. Kim, J.H. Cho, J.Y. Koh, Zinc and 4-hydroxy-2-nonenal mediate lysosomal membrane permeabilization induced by H2O2 in cultured hippocampal neurons, J Neurosci 28(12) (2008) 3114-22.

[221] A.S. Prasad, A. Miale, Jr., Z. Farid, H.H. Sandstead, A.R. Schulert, Zinc metabolism in patients with the syndrome of iron deficiency anemia, hepatosplenomegaly, dwarfism, and hypognadism, J Lab Clin Med 61 (1963) 537-49.

[222] N. Roohani, R. Hurrell, R. Kelishadi, R. Schulin, Zinc and its importance for human health: An integrative review, J Res Med Sci 18(2) (2013) 144-57.

[223] K.H. Brown, J.M. Peerson, J. Rivera, L.H. Allen, Effect of supplemental zinc on the growth and serum zinc concentrations of prepubertal children: a meta-analysis of randomized controlled trials, Am J Clin Nutr 75(6) (2002) 1062-71.

[224] S.D. Gower-Winter, C.W. Levenson, Zinc in the central nervous system: From molecules to behavior, Biofactors 38(3) (2012) 186-93.

[225] P. Bonaventura, G. Benedetti, F. Albarede, P. Miossec, Zinc and its role in immunity and inflammation, Autoimmun Rev 14(4) (2015) 277-85.

[226] B.X. Hoang, B. Han, D.G. Shaw, M. Nimni, Zinc as a possible preventive and therapeutic agent in pancreatic, prostate, and breast cancer, Eur J Cancer Prev 25(5) (2016) 457-61.

[227] N.F. Krebs, Overview of zinc absorption and excretion in the human gastrointestinal tract, J Nutr 130(5S Suppl) (2000) 1374S-7S.

[228] S. Kasana, J. Din, W. Maret, Genetic causes and gene-nutrient interactions in mammalian zinc deficiencies: acrodermatitis enteropathica and transient neonatal zinc deficiency as examples, J Trace Elem Med Biol 29 (2015) 47-62.

[229] E. Maverakis, M.A. Fung, P.J. Lynch, M. Draznin, D.J. Michael, B. Ruben, N. Fazel, Acrodermatitis enteropathica and an overview of zinc metabolism, J Am Acad Dermatol 56(1) (2007) 116-24.

[230] K.R. Jat, R.K. Marwaha, I. Panigrahi, S. Kaur, Fulminant candida infection in an infant with Acrodermatitis Enteropathica, Indian J Pediatr 76(9) (2009) 941-2.

[231] K.H. Neldner, K.M. Hambidge, Zinc therapy of acrodermatitis enteropathica, N Engl J Med 292(17) (1975) 879-82.

[232] A. Grider, Y.F. Lin, S.J. Muga, Differences in the cellular zinc content and 5'-nucleotidase activity of normal and acrodermatitis enteropathica (AE) fibroblasts, Biol Trace Elem Res 61(1) (1998) 1-8.

[233] H. Herrmann, I. Hofmann, W.W. Franke, Identification of a nonapeptide motif in the vimentin head domain involved in intermediate filament assembly, J Mol Biol 223(3) (1992) 637-50.

[234] A. Kocyla, A. Pomorski, A. Krezel, Molar absorption coefficients and stability constants of metal complexes of 4-(2-pyridylazo)resorcinol (PAR): Revisiting common chelating probe for the study of metalloproteins, J Inorg Biochem 152 (2015) 82-92.

[235] M. Koch, S. Bhattacharya, T. Kehl, M. Gimona, M. Vasak, W. Chazin, C.W. Heizmann, P.M. Kroneck, G. Fritz, Implications on zinc binding to S100A2, Biochim Biophys Acta 1773(3) (2007) 457-70.

[236] A. Krezel, W. Maret, The biological inorganic chemistry of zinc ions, Arch Biochem Biophys 611 (2016) 3-19.

[237] B. Reija, B. Monterroso, M. Jimenez, M. Vicente, G. Rivas, S. Zorrilla, Development of a homogeneous fluorescence anisotropy assay to monitor and measure FtsZ assembly in solution, Anal Biochem 418(1) (2011) 89-96.

[238] A.J. Sarria, J.G. Lieber, S.K. Nordeen, R.M. Evans, The presence or absence of a vimentin-type intermediate filament network affects the shape of the nucleus in human SW-13 cells, J Cell Sci 107 (Pt 6) (1994) 1593-607.

[239] L. Chang, K. Barlan, Y.H. Chou, B. Grin, M. Lakonishok, A.S. Serpinskaya, D.K. Shumaker, H. Herrmann, V.I. Gelfand, R.D. Goldman, The dynamic properties of intermediate filaments during organelle transport, J Cell Sci 122(Pt 16) (2009) 2914-23.

[240] M.M. Bradford, A rapid and sensitive method for the quantitation of microgram quantities of protein utilizing the principle of protein-dye binding, Anal Biochem 72 (1976) 248-54.

[241] R.H. Barton, D. Waterman, F.W. Bonner, E. Holmes, R. Clarke, C. Procardis, J.K. Nicholson, J.C. Lindon, The influence of EDTA and citrate anticoagulant addition to human plasma on information recovery from NMR-based metabolic profiling studies, Mol Biosyst 6(1) (2010) 215-24.

[242] J.K. Nicholson, High resolution 1H n.m.r. studies of vertebrate blood and plasma, Biochem J 211 (3) (1983) 605-615.

[243] A. Monico, E. Martinez-Senra, F.J. Canada, S. Zorrilla, D. Perez-Sala, Drawbacks of Dialysis Procedures for Removal of EDTA, PloS one 12(1): e0169843 (2017).

[244] S. Georgakopoulou, D. Moller, N. Sachs, H. Herrmann, U. Aebi, Near-UV circular dichroism reveals structural transitions of vimentin subunits during intermediate filament assembly, J Mol Biol 386(2) (2009) 544-53.

[245] J. Fu, P.A. Guerette, A. Miserez, Self-Assembly of Recombinant Hagfish Thread Keratins Amenable to a Strain-Induced alpha-Helix to beta-Sheet Transition, Biomacromolecules 16(8) (2015) 2327-39.

[246] T.M. Cooper, R.W. Woody, The effect of conformation on the CD of interacting helices: a theoretical study of tropomyosin, Biopolymers 30(7-8) (1990) 657-76.

[247] Y.E. Quax-Jeuken, W.J. Quax, H. Bloemendal, Primary and secondary structure of hamster vimentin predicted from the nucleotide sequence, Proc Natl Acad Sci U S A 80(12) (1983) 3548-52.

[248] A. Ariza, M.I. Montanez, D. Perez-Sala, Proteomics in immunological reactions to drugs, Curr Opin Allergy Clin Immunol 11(4) (2011) 305-12.

[249] P.L.N. Fox, Kosower EM, Formation of disulfides with diamide, Methods Enzymol 143 (1987) 264-70.

[250] S.L. Uchida K, Chae HZ, Stadtman ER, Immunochemical detection of 4-hydroxynonenal protein adducts in oxidized hepatocytes, Proc Natl Acad Sci USA 90(18) (1993) 8742-6.

[251] A.G. Yamaguchi S, Ito S, Morishita N, Shibata T, Vistoli G, Delta(12)-Prostaglandin J(2) as a Product and Ligand of Human Serum Albumin: Formation of an Unusual Covalent Adduct at His146, J Am Chem Soc 132 (2010) 824-32.

[252] Z.K. Papanyan, Interaction of L-cysteine with dimethyl sulfoxide in mild conditions, Proc Yerevan State Univ 2 (2013) 11-14.

[253] J.L. Gilge, M. Fisher, Y.C. Chai, The effect of oxidant and the non-oxidant alteration of cellular thiol concentration on the formation of protein mixed-disulfides in HEK 293 cells, PloS one 3(12): e4015 (2008).

[254] M.S. Benz R. , The molecular mechanism of action of the proton ionophore FCCP (carbonylcyanide p-trifluoromethoxyphenylhydrazone), Biophys J 41 (3) (1983) 381-98.

[255] B. Maro, M. Bornens, Reorganization of HeLa cell cytoskeleton induced by an uncoupler of oxidative phosphorylation, Nature 295(5847) (1982) 334-6.

[256] J.N. Stannard, B.L. Horecker, The in vitro inhibition of cytochrome oxidase by azide and cyanide, J Biol Chem 172(2) (1948) 599-608.

[257] A.B. Nowakowski, D.H. Petering, Reactions of the fluorescent sensor, Zinquin, with the zinc-proteome: adduct formation and ligand substitution, Inorg Chem 50(20) (2011) 10124-33.

[258] M.E. Brennich, S. Bauch, U. Vainio, T. Wedig, H. Herrmann, S. Köster, Impact of ion valency on the assembly of vimentin studied by quantitative small angle X-ray scattering, Soft Matter 10(12) (2014) 2059-2068.

[259] C.L. Oeste, B. Diez-Dacal, F. Bray, M. Garcia de Lacoba, B.G. de la Torre, D. Andreu, A.J. Ruiz-Sanchez, E. Perez-Inestrosa, C.A. Garcia-Dominguez, J.M. Rojas, D. Perez-Sala, The C-terminus of H-Ras as a target for the covalent binding of reactive compounds modulating Ras-dependent pathways, PloS one 6(1): e15866 (2011).

[260] J.S. Kim, R.T. Raines, Dibromobimane as a fluorescent crosslinking reagent, Anal Biochem 225(1) (1995) 174-6.

[261] W. Huang da, B.T. Sherman, R.A. Lempicki, Systematic and integrative analysis of large gene lists using DAVID bioinformatics resources, Nat Protoc 4(1) (2009) 44-57.

[262] W. Huang da, B.T. Sherman, R.A. Lempicki, Bioinformatics enrichment tools: paths toward the comprehensive functional analysis of large gene lists, Nucleic Acids Res 37(1) (2009) 1-13.

[263] F.I. Malik Zibouche, Jesus Ayala-Sanmartin, Annexin A2 expression and partners during epithelial cell differentiation, Biochem Cell Biol (2019) (doi: 10.1139/bcb-2018-0393).

[264] S. Yonemura, Actin filament association at adherens junctions, J Med Invest 64 (2017) 14-19.

[265] A.C. Grabski, Advances in preparation of biological extracts for protein purification, Methods Enzymol 463 (2009) 285-303.

[266] J.R. Wright, D.F. Zlogar, J.C. Taylor, T.M. Zlogar, C.I. Restrepo, Effects of endotoxin on surfactant protein A and D stimulation of NO production by alveolar macrophages, Am J Physiol 276(4) (1999) L650-8.

[267] E.R. Stadtman, Metal ion-catalyzed oxidation of proteins: biochemical mechanism and biological consequences, Free Radic Biol Med 9(4) (1990) 315-25.

[268] J.K. Nyborg, O.B. Peersen, That zincing feeling: the effects of EDTA on the behaviour of zinc-binding transcriptional regulators, Biochem J 381(Pt 3) (2004) e3-4.

[269] M. Muller, A. Haeberli, pH-dependent formation of ethylenediaminetetraacetic acid supramolecular aggregates, FEBS letters 340(1-2) (1994) 17-21.

[270] A.I. Kuzmenko, H. Wu, J.P. Bridges, F.X. McCormack, Surfactant lipid peroxidation damages surfactant protein A and inhibits interactions with phospholipid vesicles, J Lipid Res 45(6) (2004) 1061-8.

[271] C. Dammann, S. Koster, Dynamics of counterion-induced attraction between vimentin filaments followed in microfluidic drops, Lab Chip 14(15) (2014) 2681-7.

[272] D.G. Searcy, L. Greif, Apparent thermal destabilization of Escherichia coli nucleoprotein due to the incomplete dialysis of EDTA, Biochim Biophys Acta 418(1) (1976) 133-6.

[273] J.C. Sharpe, E. London, Inadvertent concentrating of EDTA by ion exchange chromatography: avoiding artifacts that can interfere with protein purification, Anal Biochem 250(1) (1997) 124-5.

[274] A.S. Kord, I. Tumanova, W.L. Matier, A novel HPLC method for determination of EDTA in a cataract inhibiting ophthalmic drug, J Pharm Biomed Anal 13(4-5) (1995) 575-80.

[275] B. Kratochvil, M.C. White, Spectrophotometric Determination of Microgram Quantities of (Ethylenedinitrilo)Tetraacetic Acid with Bis(2,4,6-Tripyridyl-S-Triazine)Iron(Ii), Anal Chem 37 (1965) 111-3.

[276] H.X. Zhou, X. Pang, Electrostatic Interactions in Protein Structure, Folding, Binding, and Condensation, Chem Rev 118(4) (2018) 1691-1741.

[277] B. Noding, H. Herrmann, S. Koster, Direct observation of subunit exchange along mature vimentin intermediate filaments, Biophys J 107(12) (2014) 2923-2931.

[278] B.P. Helmke, R.D. Goldman, P.F. Davies, Rapid displacement of vimentin intermediate filaments in living endothelial cells exposed to flow, Circ Res 86(7) (2000) 745-52.

[279] C. Rodriguez-Burford, D.K. Oelschlager, L.I. Talley, M.N. Barnes, E.E. Partridge, W.E. Grizzle, The use of dimethylsulfoxide as a vehicle in cell culture experiments using ovarian carcinoma cell lines, Biotech Histochem 78(1) (2003) 17-21.

[280] L. Misuri, M. Cappiello, F. Balestri, R. Moschini, V. Barracco, U. Mura, A. Del-Corso, The use of dimethylsulfoxide as a solvent in enzyme inhibition studies: the case of aldose reductase, J Enzyme Inhib Med Chem 32(1) (2017) 1152-1158.

[281] N.Z. Homer, J. Reglinski, C.M. Spickett, R. Wilson, J.J. Walker, Sowden Dimethylsulfoxide oxidizes glutathione in vitro and in human erythrocytes: kinetic analysis by 1H NMR. Cryobiology 50(3) (2005): 317-24.

[282] K. Uchida, 4-Hydroxy-2-nonenal: a product and mediator of oxidative stress, Prog Lipid Res 42(4) (2003) 318-43.

[283] C.H. Kaschula, R. Tuveri, E. Ngarande, K. Dzobo, C. Barnett, D.A. Kusza, L.M. Graham, A.A. Katz, M.S. Rafudeen, M.I. Parker, R. Hunter, G. Schafer, The garlic compound ajoene covalently binds vimentin, disrupts the vimentin network and exerts anti-metastatic activity in cancer cells, BMC Cancer 19(1): 248 (2019).

[284] M. Fratelli, H. Demol, M. Puype, S. Casagrande, I. Eberini, M. Salmona, V. Bonetto, M. Mengozzi, F. Duffieux, E. Miclet, A. Bachi, J. Vandekerckhove, E.

Gianazza, P. Ghezzi, Identification by redox proteomics of glutathionylated proteins in oxidatively stressed human T lymphocytes, Proc Natl Acad Sci U S A 99(6) (2002) 3505-10.

[285] J. Jia, A. Arif, F. Terenzi, B. Willard, E.F. Plow, S.L. Hazen, P.L. Fox, Target-selective protein S-nitrosylation by sequence motif recognition, Cell 159(3) (2014) 623-34.

[286] Y. Xiong, J.D. Uys, K.D. Tew, D.M. Townsend, S-glutathionylation: from molecular mechanisms to health outcomes, Antioxid Redox Signal 15(1) (2011) 233-70.

[287] D.C. Pother, M. Liebeke, F. Hochgrafe, H. Antelmann, D. Becher, M. Lalk, U. Lindequist, I. Borovok, G. Cohen, Y. Aharonowitz, M. Hecker, Diamide triggers mainly S Thiolations in the cytoplasmic proteomes of Bacillus subtilis and Staphylococcus aureus, J Bacteriol 191(24) (2009) 7520-30.

[288] J.M. Held, S.R. Danielson, J.B. Behring, C. Atsriku, D.J. Britton, R.L. Puckett, B. Schilling, J. Campisi, C.C. Benz, B.W. Gibson, Targeted quantitation of site-specific cysteine oxidation in endogenous proteins using a differential alkylation and multiple reaction monitoring mass spectrometry approach, Mol Cell Proteomics 9(7) (2010) 1400-10.

[289] K.M. Humphries, J.K. Pennypacker, S.S. Taylor, Redox regulation of cAMP-dependent protein kinase signaling: kinase versus phosphatase inactivation, J Biol Chem 282(30) (2007) 22072-9.

[290] M. Yoon, R.D. Moir, V. Prahlad, R.D. Goldman, Motile properties of vimentin intermediate filament networks in living cells, J Cell Biol 143(1) (1998) 147-57.

[291] S.F. Sousa, A.B. Lopes, P.A. Fernandes, M.J. Ramos, The Zinc proteome: a tale of stability and functionality, Dalton Trans (38) (2009) 7946-56.

[292] J.S. Butler, S.N. Loh, Zn(2+)-dependent misfolding of the p53 DNA binding domain, Biochemistry 46(10) (2007) 2630-9.

[293] B. Alies, P.L. Solari, C. Hureau, P. Faller, Dynamics of Zn(II) binding as a key feature in the formation of amyloid fibrils by Abeta11-28, Inorg Chem 51(1) (2012) 701-8.

[294] A. Krezel, W. Maret, Dual nanomolar and picomolar Zn(II) binding properties of metallothionein, J Am Chem Soc 129(35) (2007) 10911-21.

[295] J.E. Hesketh, Zinc binding to tubulin, Int J Biochem 15(5) (1983) 743-6.

[296] M. Dudev, C. Lim, Discovering structural motifs using a structural alphabet: application to magnesium-binding sites, BMC Bioinformatics 8: 106 (2007).

[297] H. Zheng, M. Chruszcz, P. Lasota, L. Lebioda, W. Minor, Data mining of metal ion environments present in protein structures, J Inorg Biochem 102(9) (2008) 1765-76.

[298] A.G. Daniel, N.P. Farrell, The dynamics of zinc sites in proteins: electronic basis for coordination sphere expansion at structural sites, Metallomics 6(12) (2014) 2230-41.

[299] I. Lengyel, J.M. Flinn, T. Peto, D.H. Linkous, K. Cano, A.C. Bird, A. Lanzirotti, C.J. Frederickson, F.J. van Kuijk, High concentration of zinc in sub-retinal pigment epithelial deposits, Exp Eye Res 84(4) (2007) 772-80.

[300] R.B. Thompson, V. Reffatto, J.G. Bundy, E. Kortvely, J.M. Flinn, A. Lanzirotti, E.A. Jones, D.S. McPhail, S. Fearn, K. Boldt, M. Ueffing, S.G. Ratu, L. Pauleikhoff, A.C. Bird, I. Lengyel, Identification of hydroxyapatite spherules provides new insight into subretinal pigment epithelial deposit formation in the aging eye, Proc Natl Acad Sci U S A 112(5) (2015) 1565-70.

[301] L.B. Poole, The basics of thiols and cysteines in redox biology and chemistry, Free Radic Biol Med 80 (2015) 148-57.

[302] A.L. Cai, G.J. Zipfel, C.T. Sheline, Zinc neurotoxicity is dependent on intracellular NAD levels and the sirtuin pathway, Eur J Neurosci 24(8) (2006) 2169-76.

[303] K. Kohama, L.H. Ye, K. Hayakawa, T. Okagaki, Myosin light chain kinase: an actin-binding protein that regulates an ATP-dependent interaction with myosin, Trends Pharmacol Sci 17(8) (1996) 284-7.

[304] Z. Li, E.S. Kim, E.L. Bearer, Arp2/3 complex is required for actin polymerization during platelet shape change, Blood 99(12) (2002) 4466-74.

[305] K.J. Chalut, E.K. Paluch, The Actin Cortex: A Bridge between Cell Shape and Function, Dev Cell 38(6) (2016) 571-3.

[306] F. Huber, A. Boire, M.P. Lopez, G.H. Koenderink, Cytoskeletal crosstalk: when three different personalities team up, Curr Opin Cell Biol 32 (2015) 39-47.

[307] Y. Jiu, J. Lehtimaki, S. Tojkander, F. Cheng, H. Jaalinoja, X. Liu, M. Varjosalo, J.E. Eriksson, P. Lappalainen, Bidirectional Interplay between Vimentin Intermediate Filaments and Contractile Actin Stress Fibers, Cell Rep 11(10) (2015) 1511-8.

[308] I. Ferjani, A. Fattoum, S.K. Maciver, M. Manai, Y. Benyamin, C. Roustan, Calponin binds G-actin and F-actin with similar affinity, FEBS letters 580(20) (2006) 4801-6.

[309] A.M. Lopez-Colome, I. Lee-Rivera, R. Benavides-Hidalgo, E. Lopez, Paxillin: a crossroad in pathological cell migration, J Hematol Oncol 10(1): 50 (2017).

[310] A.A. Birukova, N. Zebda, P. Fu, V. Poroyko, I. Cokic, K.G. Birukov, Association between adherens junctions and tight junctions via Rap1 promotes barrier protective effects of oxidized phospholipids, J Cell Physiol 226(8) (2011) 2052-62.

[311] O. Oskolkova, G. Gawlak, Y. Tian, Y. Ke, N. Sarich, S. Son, K. Andreasson, V.N. Bochkov, A.A. Birukova, K.G. Birukov, Prostaglandin E receptor-4 receptor mediates endothelial barrier-enhancing and anti-inflammatory effects of oxidized phospholipids, FASEB J 31(9) (2017) 4187-4202.

[312] D. Zhang, M.J. Sweredoski, R.L. Graham, S. Hess, S.O. Shan, Novel proteomic tools reveal essential roles of SRP and importance of proper membrane protein biogenesis, Mol Cell Proteomics 11(2): M111.011585 (2012).

[313] R. Plumb, Z.R. Zhang, S. Appathurai, M. Mariappan, A functional link between the co-translational protein translocation pathway and the UPR, Elife 4: e07426 (2015).

[314] C. Ninsontia, P.P. Phiboonchaiyanan, P. Chanvorachote, Zinc induces epithelial to mesenchymal transition in human lung cancer H460 cells via superoxide anion-dependent mechanism, Cancer Cell Int 16: 48 (2016).

[315] X. Zhang, D. Liang, Z.H. Chi, Q. Chu, C. Zhao, R.Z. Ma, Y. Zhao, H. Li, Effect of zinc on high glucose-induced epithelial-to-mesenchymal transition in renal tubular epithelial cells, Int J Mol Med 35(6) (2015) 1747-54.

[316] E.K. Ahmed, A. Rogowska-Wrzesinska, P. Roepstorff, A.L. Bulteau, B. Friguet, Protein modification and replicative senescence of WI-38 human embryonic fibroblasts, Aging Cell 9(2) (2010) 252-72.

LIST OF PUBLICATIONS

The following publications have resulted from this Thesis:

1. Mónico A., Martínez-Senra E., Cañada J., Zorrilla S. Pérez-Sala D. Drawbacks of Dialysis Procedures for Removal of EDTA. Plos ONE 12(1): e0169843.

2. Mónico A., Duarte S., Pajares MA., Perez-Sala D. Vimentin disruption by lipoxidation and electrophiles: Role of the cysteine residue and filament dynamics. Redox Biol 2019:101098.

3. Zorrilla S., Mónico A., Duarte S., Rivas G., Pérez-Sala D., Pajares MA. Integrated approaches to unravel the impact of protein lipoxidation on macromolecular interactions. Free Radical Biology and Medicine 2019 (In press). (https://doi.org/10.1016/j.freeradbiomed.2019.04.011).